MEASUREMENTS VERSUS PREDICTIONS FOR THE STATIC AND DYNAMIC CHARACTERISTICS OF A FOUR-PAD, ROCKER-PIVOT, TILTING-PAD JOURNAL BEARING

A Thesis

by

DAVID PATRICK TSCHOEPE

Submitted to the Office of Graduate Studies of
Texas A&M University
in partial fulfillment of the requirements for the degree of

MASTER OF SCIENCE

Approved by:

Chair of Committee,	Dara W. Childs
Committee Members,	Alan Palazzolo
	Lynn Beason
Head of Department,	Jerald A. Caton

December 2012

Major Subject: Mechanical Engineering

ABSTRACT

Measured and predicted static and dynamic characteristics are provided for a four-pad, rocker-pivot, tilting-pad journal bearing in the load-on-pad and load-between-pad orientations. The bearing has the following characteristics: 4 pads, .57 pad pivot offset, 0.6 *L/D* ratio, 60.33 mm (2.375in) pad axial length, 0.08255 mm (0.00325 in) radial clearance in the load-on-pad orientation, and 0.1189 mm (0.00468 in) radial clearance in the load-between-pad orientation. Tests were conducted on a *floating* test bearing design with unit loads ranging from 0 to 2903 kPa (421.1 psi) and speeds from 6.8 to 13.2 krpm.

For all rotor speeds, hot-clearance measurements were taken to show the reduction in bearing clearance due to thermal expansion of the shaft and pads during testing. As the testing conditions get hotter, the rotor, pads, and bearing expand, decreasing radial bearing clearance. Hot-clearance measurements showed a 16-25% decrease in clearance compared to a clearance measurement at room temperature.

For all test conditions, dynamic tests were performed over a range of excitation frequencies to obtain complex dynamic stiffness coefficients as a function of frequency. The direct real dynamic stiffness coefficients were then fitted with a quadratic function with respect to frequency. From the curve fit, the frequency dependence was captured by including a virtual-mass matrix [M] to produce a frequency independent [K][C][M] model.

The direct dynamic stiffness coefficients for the load-on-pad orientation showed significant orthotropy, while the load-between-pad did not. The load-between-pad showed slight orthotropy as load increased. Experimental cross-coupled stiffness coefficients were measured in both load orientations, but were of the same sign and significantly less than direct stiffness coefficients.

In both orientations the imaginary part of the measured dynamic stiffness increased linearly with increasing frequency, allowing for frequency independent direct damping coefficients.

Rotordynamic coefficients presented were compared to predictions from two different Reynolds-based models. Both models showed the importance of taking into

account pivot flexibility and different pad geometries (due to the reduction in bearing clearance during testing) in predicting rotordynamic coefficients. If either of these two inputs were incorrect, then predictions for the bearings impedance coefficients were very inaccurate. The main difference between prediction codes is that one of the codes incorporates pad flexibility in predicting the impedance coefficients for a tilting-pad journal bearing.

To look at the effects that pad flexibility has on predicting the impedance coefficients, a series of predictions were created by changing the magnitude of the pad's bending stiffness. Increasing the bending stiffness used in predictions by a factor of 10 typically caused a 3-11% increase in predicted K_{xx} and K_{yy}, and a 10-24% increase in predicted C_{xx} and C_{yy}. In all cases, increasing the calculated bending stiffness from ten to a hundred times the calculated value caused slight if any change in K_{xx}, K_{yy}, C_{xx}, and C_{yy}. For a flexible pad an increase in bending stiffness can have a large effect on predictions; however, for a more rigid pad an increase in pad bending stiffness will have a much lesser effect.

Results showed that the pad's structural bending stiffness can be an important factor in predicting impedance coefficients. Even though the pads tested in this thesis are extremely stiff, changes are still seen in predictions when the magnitude of the pad's bending stiffness is increased, especially in C_{xx}, and C_{yy}. The code without pad flexibility predicted K_{xx} and K_{yy} much more accurately than the code with pad flexibility. The code with pad flexibility predicts C_{xx} more accurately, while the code without pad flexibility predicted C_{yy} more accurately. Regardless of prediction Code used, the K_{xx} and K_{yy} were over-predicted at low loads, but predicted more accurately as load increased. C_{xx}, and C_{yy} were modeled very well in the load-on-pad orientation, while slightly overpredicted in the load-between-pad orientation. For solid pads, like the ones tested here, both codes do a decent job at predicting impedance coefficients.

DEDICATION

For my family,

You don't choose your family. They are God's gift to you, as you are to them.

~Desmond Tutu

ACKNOWLEDGEMENTS

First I would like to express my thanks to Dr. Dara Childs for this opportunity to work at the Turbomachinery Laboratory. What I have learned will stay with me for the rest of my engineering career.

I would like to thank Dr. Alan Palazzolo and Dr. Lynn Beason for serving on my committee.

My sincere thanks to Dr. Jason Wilkes for all of his guidance and support through my time at Texas A&M. Without Jason, the tests rig would not have been in its current condition, and my research would not have been possible.

I would like to thank all of the other students out at the Turbomachinery Laboratory - Michael Murphey, David Coghlan, Stephen Arthur, and Naitik Mehta, - who made working at the lab enjoyable.

I would like to graciously thank my parents, Phil and Helen Tschoepe, for their constant love and support. They have given me so much in life and have never asked for anything in return. I would also like to thank my sisters: Elizabeth, Mary, and Rebecca. You will always be my best friends.

Lastly I would like to thank God for all that he has given me. Without Him, nothing is possible.

NOMENCLATURE

$\boldsymbol{A_{ij}}$	Fourier transforms for the measured stator acceleration. (e.g. A_{ij} is the acceleration in the "j" direction, due to an excitation force in the "i" direction) [L/t^2]
C_{ij}	Direct and cross-coupled damping coefficients [F.t/L]
ΔC_{ij}	Uncertainty of direct and cross-coupled damping coefficients [F.t/L]
C_b	Radial bearing clearance [L]
C_p	Radial pad clearance [L]
c_p	Lubricant specific heat [FL/(M.t)]
D	Bearing diameter [L]
$\boldsymbol{D_{ij}}$	Fourier transforms for the measured stator relative motion [L]
e_{xo} e_{yo}	Bearing equilibrium position in the *x*, *y* directions [L]
$\boldsymbol{F_{ij}}$	Fourier transforms for the measured stator force [F]
F_s	Static force applied by pneumatic loader [F]
f_{bx} f_{by}	Bearing reaction force component in the *x*, *y* directions [F]
f_x f_y	Measured excitation force component in the *x*, *y* directions [F]
$\boldsymbol{H_{ij}}$	Direct and cross-coupled dynamic stiffness [F/L]
$\Delta\, \boldsymbol{H_{ij}}$	Uncertainty of direct and cross-coupled dynamic stiffness [F/L]
$\boldsymbol{j}$	Imaginary unit, $\sqrt{-1}$ [-]
k_{c_p}	Pad's structural bending stiffness [N]
K_{ij}	Direct and cross-coupled stiffness coefficients [F/L]
ΔK_{ij}	Uncertainty of direct and cross-coupled stiffness coefficients [F/L]
L	Pad length [L]
M_s	Mass of the stator [M]
M_{ij}	Direct and cross-coupled virtual-mass coefficients [M]
ΔM_{ij}	Uncertainty of virtual-mass coefficients [M]
P	Bearing unit load, $\left(\frac{F_S}{LD}\right)$ [F/L^2]

$\dot{Q}$	Bearing oil supply flow rate [L^3/t]
R	Bearing radius [L]
Re	Reynolds number, $Re = \frac{\rho C_b R \omega}{\mu}$ [-]
r^2_{ij}	Square of the correlation coefficient [-]
S	Sommerfeld number, $S = \frac{\mu N L D}{W} \left(\frac{R}{C_b}\right)^2$ [-]
T_{in}	Oil inlet temperature [T]
T_{out}	Oil outlet temperature (non-drive end) [T]
$\ddot{x}_s$ $\ddot{y}_s$	Absolute acceleration of the stator in the *x*, *y* directions [L/t^2]]
Δx Δy	Relative motion between the rotor and the stator in the *x*, *y* directions [L]
ε_o	Static eccentricity ratio [-]
ϕ	Attitude angle measured from the +*y* axis to the +*x* axis [Angle]
Λ	Square of the excitation frequency, Ω^2 [(1/t)^2]
ρ	Lubricant density [M/L^3]
μ	Lubricant viscosity [F.t /L^2]
ω	Running speed of rotor [1/t]
Ω	Excitation frequency of stator [1/t]

Subscripts

x,y	x and y direction
i,j	x,y

Abbreviations

DE, NDE	Drive end, non-drive end
LBP	Load-between-pad
LOP	Load-on-pad
rpm	Revolutions per minute
TPJB	Tilting-pad journal bearing
WFR	Whirl frequency ratio

TABLE OF CONTENTS

Page

Page

LIST OF FIGURES

Page

Page

Page

Page

Page

LIST OF TABLES

Page

Page

Page

Page

INTRODUCTION

Bearings, which are essential components of most mechanical designs, allow for rotation between objects while transferring reaction forces from one object to another. As a component in rotating machinery, tilting-pad journal bearings (TPJBs) are widely used to increase the limit of stability over fixed-geometry bearings. TPJBs allow for rotor support, by lifting the rotor to avoid contact through the combined actions of the shaft rotation and the lubricant's viscosity. Figure 1 below provides a general rocker-pivot TPJB schematic. For a vertical downward load, a load-between-pad (LBP) orientation is illustrated. A rocker-pivot TPJB frequently uses cylindrical-backed pads inside the curvature of the bearing housing, ideally allowing the pads to roll without slip.

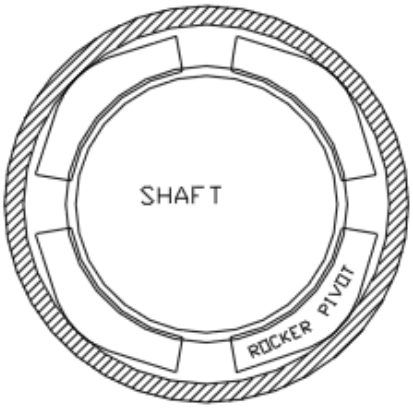

Figure 1: Rocker-Pivot Tilting-Pad Journal Bearing [1]

TPJB performance can be affected by various geometric parameters. The applicable parameters are defined in Table 1 and shown in Figure 2 below. In a vertical downward load, Figure 2 illustrates a load-on-pad (LOP) configuration with a spherical seat support.

Table 1: Definitions of Tilting-Pad Bearing Geometry Parameters

SYMBOL	DEFINITION
R_b	Bearing Radius
R_p	Pad Radius
R_s	Shaft Radius
θ_{pad}	Pad Arc Angle
θ_{pivot}	Pivot Arc Angle
L	Pad Axial Length
L/D	Length to Diameter Ratio
C_b	Radial Bearing Clearance, $C_b = R_b - R_s$
C_p	Radial Pad Clearance, $C_p = R_p - R_s$

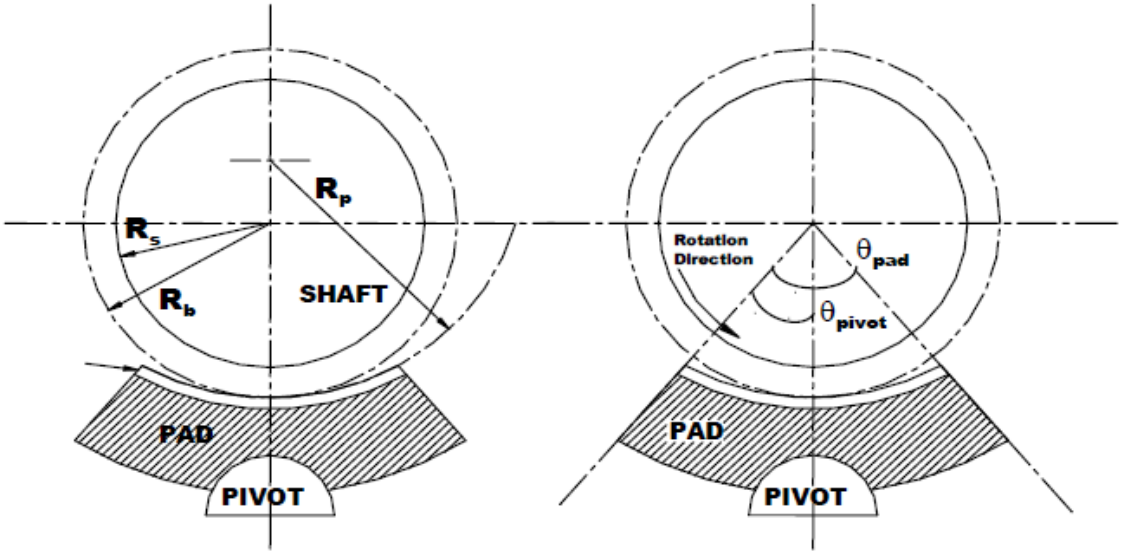

Figure 2: Pad- Shaft Assembly [2]

Figure 2 shows the radius of the pad, bearing, and shaft as well as the pad's pivot offset. Pivot offset is the location of the pivot relative to the leading and trailing edges of the pad, defined by

$$PIVOT\ OFFSET = \frac{\theta_{pivot}}{\theta_{pad}} \tag{1}$$

For a pad with a centered pivot, the offset is 0.5. Pad offsets of 0.5 to 0.6 are commonly used in industrial applications.

Table 1 shows the radial pad and bearing clearance, C_p and C_b respectively. The bearing and pad clearance are commonly related by preload. Preload is a nondimensional parameter quantifying the difference in pad and journal radius defined by

$$PAD\ PRELOAD = 1 - \frac{C_b}{C_p} \tag{2}$$

For a TPJB, a positive preload typically prevents pad flutter. Pad flutter is an instability that can arise during unloaded bearing operation, where the unloaded pads vibrate due to an absence of fluid film forces. Negative preload is typically avoided.

Static external loads are generally applied to a TPJB in either the load-on-pad (LOP) or load-between-pad (LBP) configuration. Typically, the LBP orientation is used to support heavier rotors and is expected to provide more symmetric rotordynamic coefficients. Generally the LOP orientation is expected to provide stiffness orthotropy (to enhance stability), or stiffness asymmetry in that the loaded direction has a larger stiffness.

Using small motions about equilibrium, the dynamic reaction fluid forces acting between a TPJB and rotor can be modeled as a linearized two degree-of-freedom system with stiffness and damping matrices, as shown in Eq. (3).

$$-\begin{Bmatrix} f_x \\ f_y \end{Bmatrix} = \begin{bmatrix} K_{xx} & K_{xy} \\ K_{yx} & K_{yy} \end{bmatrix} \begin{Bmatrix} \Delta x \\ \Delta y \end{Bmatrix} + \begin{bmatrix} C_{xx} & C_{xy} \\ C_{yx} & C_{yy} \end{bmatrix} \begin{Bmatrix} \Delta \dot{x} \\ \Delta \dot{y} \end{Bmatrix} \tag{3}$$

Here, Δx and Δy and their time derivatives define the relative motion between the rotor and the stator. Similar subscripts (*xx*, *yy*) represent direct coefficients while, different subscripts (*xy*, *yx*) represent cross-coupled coefficients. Direct coefficients produce reactions forces against the direction of the displacement or velocity vectors. Cross-coupled terms produce reaction forces perpendicular to the displacement or velocity vectors.

In 1964, Lund [3] pioneered the analysis for predicting dynamic force coefficients of TPJBs. The bearing model is obtained by summing the contribution of each pad to acquire the stiffness and damping in two orthogonal directions. Lund presented a basis used to predict the dynamic performance of TPJBs and was able to present stiffness and damping design curves for numerous bearing configurations.

Following Lund's work, other analytical studies [4]-[6] indicated that TPJB rotordynamic coefficients may be frequency dependent, but experimental data to confirm these predictions were more limited. In 1978, Nicolas, Gunter, and Allaire [4] calculated pad dynamic data with a finite-element method and determined bearing stiffness and damping design curves. In 1983, Parsell et al. [5] derived rotordynamic coefficients for a

5-pad TPJB and predicted that the resulting direct damping coefficients increased with increasing precession frequency while the stiffness coefficients decreased with increasing frequency.

In 1999, Ha and Yang [7] tested a 5-pad, 300 mm (11.8 in) diameter rocker-pivot TPJB in the load-on-pad (LOP) orientation. The rotordynamic coefficients were obtained at a frequency range of 25-60 Hz and a rotor speed of 3,600 rpm. Testing was conducted at a single excitation frequency, ranging from 0.5 to 2 times the running speed. Their results indicated that the stiffness coefficients slightly decreased with increasing excitation frequency, while the damping coefficients slightly increased. Wygant's [8] measurements showed that, when the [K][C] model in Eq. (3) is used, the stiffness and damping coefficients depend slightly on precession frequency.

In 2006, Rodriguez and Childs [9] tested a four-pad, 116.8 mm (4.6 in) diameter, LOP, 0.25 preload, 50% pad pivot offset, flexure-pivot TPJB. Figure 3 shows the flexure-pivot design.

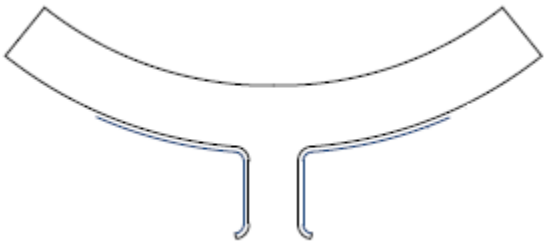

Figure 3: Flexure-Pivot Tilting-Pad Journal Bearing [15]

Through their results, the authors investigated the conventional frequency dependency of TPJB rotordynamic coefficients in more detail by applying a [K][C][M] model.

$$-\begin{Bmatrix} f_x \\ f_y \end{Bmatrix} = \begin{bmatrix} K_{xx} & K_{xy} \\ K_{yx} & K_{yy} \end{bmatrix} \begin{Bmatrix} \Delta x \\ \Delta y \end{Bmatrix} + \begin{bmatrix} C_{xx} & C_{xy} \\ C_{yx} & C_{yy} \end{bmatrix} \begin{Bmatrix} \Delta \dot{x} \\ \Delta \dot{y} \end{Bmatrix} + \begin{bmatrix} M_{xx} & M_{xy} \\ M_{yx} & M_{yy} \end{bmatrix} \begin{Bmatrix} \Delta \ddot{x} \\ \Delta \ddot{y} \end{Bmatrix} \quad (4)$$

The [K][C][M] model, described in Eq. (4), uses a virtual-mass matrix to capture the frequency dependency of the stiffness in a [K][C] model. When the real dynamic-stiffness coefficients were curve fitted as a quadratic function of excitation frequency, frequency-independent stiffness and virtual-mass coefficients arose. Rodriguez and Childs used multi-frequency excitation ranging from 20 to 300 Hz in 20 Hz increments. Results showed that a [K][C][M] model correlated closely with the data. In particular, the measured damping coefficients were independent of excitation frequency. The validity of the frequency-independent [K][C][M] model was further verified by Al-Ghasem and Childs [1] and Hensley and Childs [10] for flexure-pivot TPJBs.

In 2008, Carter and Childs [11] tested a 5-pad, 60% pivot offset, rocker-pivot TPJB in the LBP and LOP configurations. The bearing included a half-flooded design with one seal preventing axial leakage in one direction. Experimental results showed direct damping coefficients to be independent of frequency with very little change with respect to load and speed. Reviewers of their paper suggested that pads with a 50% pivot offset were more likely to exhibit frequency dependence than pads with a 60% pivot offset in the rocker-pivot TPJB design.

In 2010, Delgado et al. [12] tested both a 5-pad LOP, and 4-pad LBP rocker-

pivot tilting-pad journal bearing to study the frequency dependency of the rotordynamic coefficients. Both bearings had a 109 mm (4.29 in) diameter, 50% and 60% pad pivot offset, and 0.4 L/D ratio. Testing was performed at 7.5, 10, and 17 krpm with a static unit load of 300 kPa (44 psi). Through utilizing a multi-frequency excitation, dynamic stiffness coefficients were acquired. When using a [K][C][M] model, the data showed that all rotordynamic coefficients exhibit slight or no dependency regarding excitation frequency.

In 2010, Kulhanek and Childs [13] tested a five-pad, LBP, 0.3 preload, rocker-pivot TPJB with 50% and 60% pad offsets. Testing was performed with static unit loads from zero to 3,101 kPa (450 psi). Using a virtual-mass coefficient they accounted for an increasing direct dynamic stiffness that occurred with an increasing excitation frequency in both pivot offsets tested. Overall, using the same [K][C][M] model, Kulhanek produced rotordynamic coefficients and dynamic stiffness results that agreed with the findings by Delgado et al. [12].

In 2012, Wilkes and Childs [14] tested a five-pad, LOP, 0.44 preload, 50% offset, rocker-pivot TPJB. Through the authors' study, a new bearing perturbation model was proposed allowing for both journal and bearing motion, including pad rotation, pad compliance, and radial pivot flexibility. A Reynolds-equation finite-difference code was used producing real and imaginary dynamic stiffness coefficients. The model shows the importance of pivot and pad flexibility in predicting the impedance coefficients for a tilting-pad journal bearing. The pivot stiffness, or pivot flexibility, refers to the flexibility of the pad relative to the bearing housing and partially results from Hertzian

contact stiffness [15]. As shown in Figure 4, the pad flexibility refers to the change in pad curvature resulting from an applied moment at the end of the pad from the fluid film pressure.

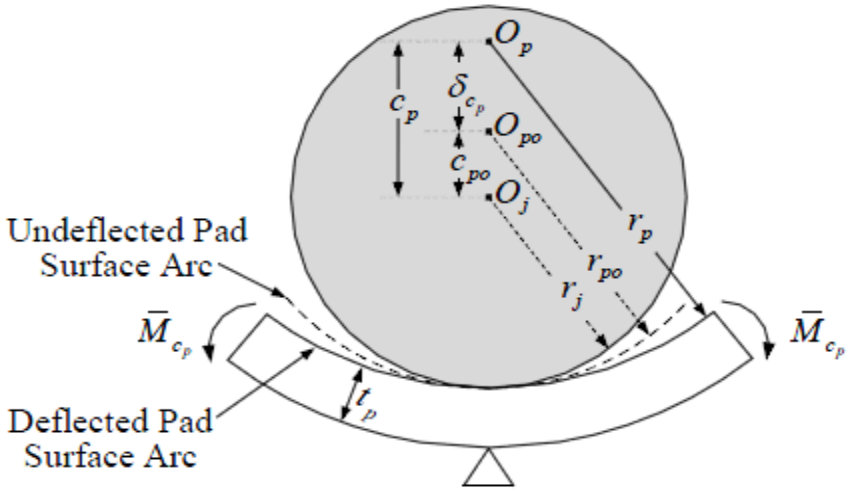

Figure 4: Change in Pad Curvature Resulting from Applied End Moments [14]

where O_j and O_p represent the centers of the journal and bearing respectively and δ_{c_p} is the change in pad radius resulting from the applied pressure field.

From Figure 4, the deflected pad surface resulting from the applied end moments has a radius r_p, defined by

$$r_p = r_{po} + \delta_{c_p} \tag{5}$$

In taking a modified version of Branagan and Barrett [16], Wilkes obtained the following model for pad stiffness

$$\delta_{c_p} = \frac{M_{c_p}}{k_{c_p}} \tag{6}$$

where M_{c_p} is the average applied fluid-film moment and k_{c_p} represents the pad's structural bending stiffness that relates the moment to the change in pad clearance. Overall, the model by Wilkes and Childs showed significant improvements in predicted direct stiffness and damping coefficients when pivot and pad flexibility were included.

This thesis presents the measured and predicted dynamic and static characteristics for a 4-pad rocker-pivot tilting-pad journal bearing in the load-on-pad and load-between-pad orientations. This work focuses on the frequency dependence of the rotordynamic coefficients at a pivot offset and *L*/*D* ratio not typically tested: .57 and 0.6, respectively.

In addition to testing a different offset and *L/D* ratio, this thesis will explore unit loads greater than that of Delgado et al. [12]. Test results include static unit loads from zero to 2903 kPa (421.1 psi). Test results will also be delivered in both the LOP and LBP orientation. Delgado only presented results for a 4-pad bearing in the LBP orientation.

To study the radial temperature gradient experienced during testing, pad metal temperatures were taken with thermocouples embedded just below the surface of the loaded pad as well as, near the bearing housing. In 1988, Branagan and Barrett [16] studied the thermal deflection associated with a TPJB pad during operation, but pad temperatures at the back of the pad (bearing housing side of the pad) were not measured. The bearing housing side of the pad was modeled to be dominated by a stagnant sump region behind the pad, and was characterized to be fixed at the inlet oil temperature to the bearing. Through a finite-element (FE) analysis, Branagan found that the thermal

deformed pad showed a radial growth of 0.0034-0.0059 mm (0.00013-0.00023 in), increasing the radial pad clearance. Branagan found that the sharp drop in bearing clearance had a greater effect on pad preload and was not counteracted by the slight increase in radial pad clearance. He established that taking into account all pad and especially pivot deformations resulted in dramatic changes in predicting dynamic coefficients.

Static results and rotordynamic coefficients presented will be compared to predictions from a new rotordynamic bearing code, "Code A" developed by Tao and San Andrés at the Texas A&M Turbomachinery Laboratory. The predictions come from the first version of this code to be published in the near future. A full description of Code A can be found in the Predictions section. Code A takes into account pivot flexibility with a user-defined load-versus-deflection approximation, and if needed, different pad geometries (preloads and clearances) to predict the static and dynamic behavior of a TPJB.

Dynamic stiffness results presented will be compared to the model of Wilkes and Childs [14][17][18], "Code B". Wilkes dissertation [15] uses a Reynolds-based model to predict dynamic results, utilizing pivot and pad flexibility. A full description of Wilkes code can be found in the Predictions section. In taking into account pad and contact flexibility, Wilkes was able to substantially improve predictions for the direct stiffness and damping coefficients for a five-pad, rocker-pivot TPJB.

DESCRIPTION OF THE TEST RIG

Testing Apparatus

Figure 5 shows the bearing test rig used to measure the static and dynamic performance of the high-speed TPJB. Kaul [19] presents a detailed account of the floating test rig design and facility at the Texas A&M Turbomachinery Laboratory. Similar to Glienicke' approach [20], the main features of the test rig are described below.

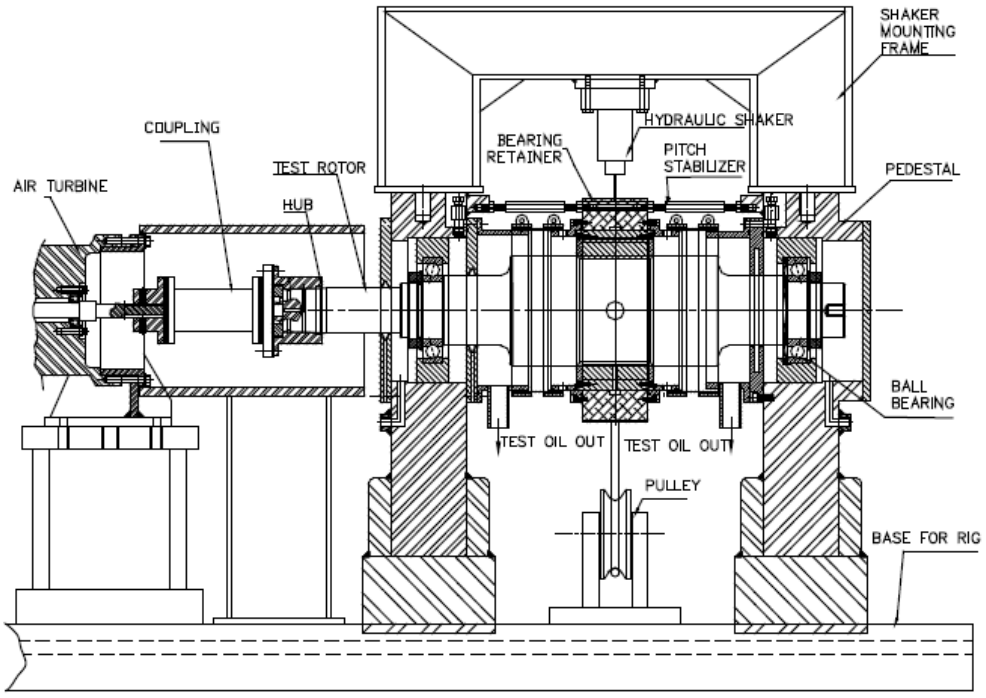

Figure 5: Test Rig Main Section [19]

The rig consists of a steel base that supports the main test section and the air turbine that drives the shaft. A 65 kW-power air turbine with a high-speed flexible disc coupling can run up to 17,000 rpm. The test shaft is made of 4140 steel and machined to a precise diameter of 101.59 mm (3.9997 in) at the bearing. The balanced shaft is supported at the pedestals by two hybrid-ceramic angular contact ball bearings. An oil-mist lubrication system lubricates the ball bearings, and pressurized buffer air seals are used to prevent oil from the outlet chambers entering the ball bearing section. As shown in Figure 5, six pitch stabilizers provide angular alignment between the bearing and the shaft.

ISO VG32 turbine oil is delivered to the test bearing from an oil supply system. The supply system can deliver oil at up to 82.7 bars supply pressure and a volumetric flow rate of 75 liters per minute. A heat exchanger and a set of pneumatically driven valves allow for control of the test-oil temperature.

A stator holds the test bearing and all the associated instruments, specifically the accelerometers, non-contacting eddy-current proximity sensors, and pressure transducers. In combination with a press fit, an anti-rotation pin hole secures the bearing from rotating within the stator. A pneumatic loader and two hydraulic shakers apply static and dynamic loads to the bearing stator.

The stator-shaker-stinger arrangement is shown in Figure 6, as observed from the non-drive end. The shaker in the x direction can excite the stator with dynamic loads up to 4450 N in tension and compression, while the shaker in the y-direction can excite the stator with dynamic loads up to 4450 N in tension and 11125 N in compression. Both

shakers can provide excitation frequencies up to 1000 Hz. Stingers isolate the test structure from the dynamics of the shakers structure.

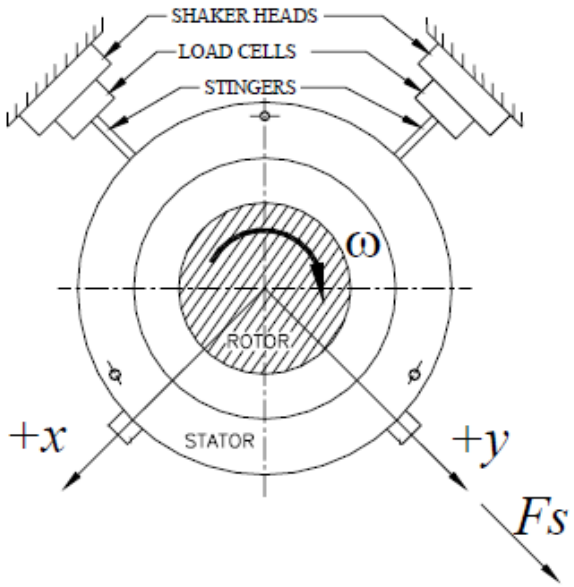

Figure 6: Shaker-Stinger Arrangement (Adapted from [13])

The pneumatic loader applies a static tensile load to the stator in the $+y$ direction. As shown in Figure 7, a cable connects the stator assembly to the loader through a pulley and a yoke with a maximum available load of 22,240 N (5,000 lbf).

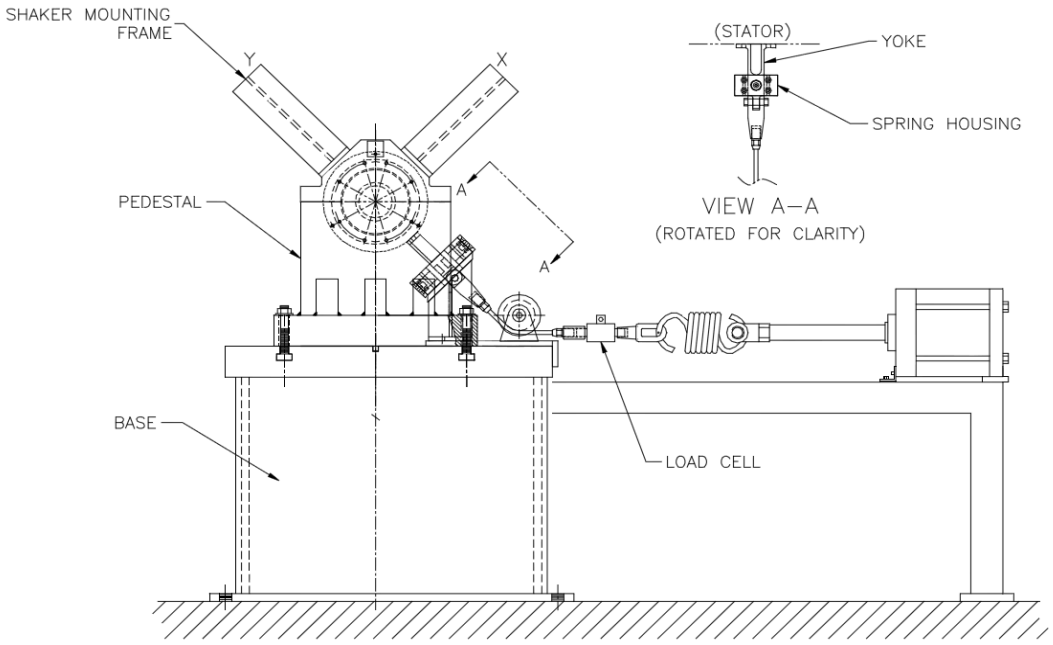

Figure 7: Static Loader Arrangement [1]

Instrumentation

To record the relative motion of the stator with respect to the rotor for each direction of excitation, two proximity probes are placed in a plane at the non-drive end (NDE), and two proximity probes are placed in a parallel plane at the drive end (DE). As shown in Figure 8, to measure the stator's acceleration, two accelerometers are positioned in the *x* and *y* directions. Four proximity probes, positioned in the stator end caps, define an average test bearing location and allow for monitoring of the stator's pitch.

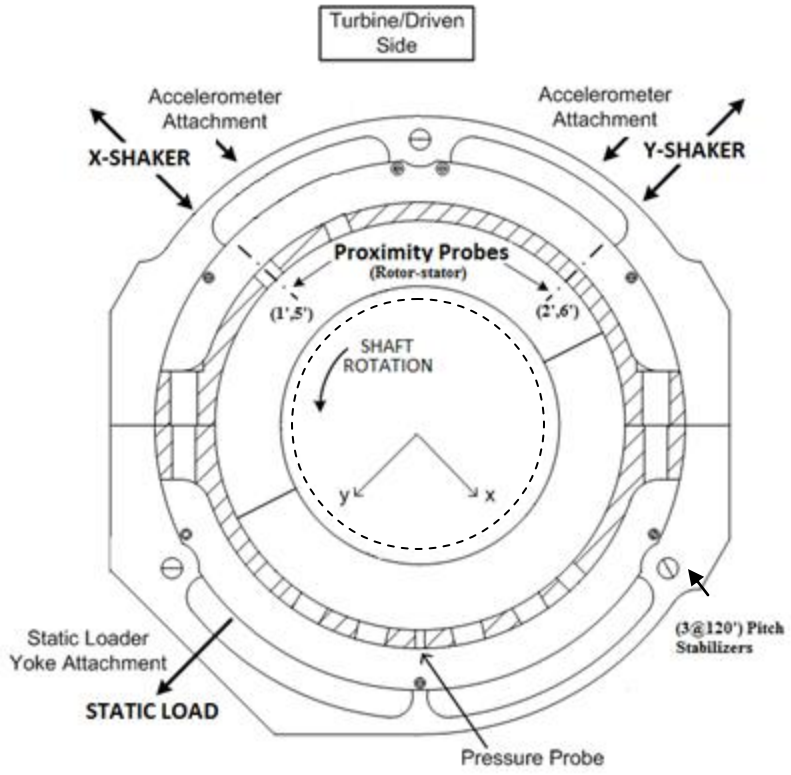

Figure 8: Bearing Configuration and Instrumentation (Adapted from [13])

Static pressure probes are used to measure the oil pressure at the inlet and outlet locations. Thermocouples are located in the oil-inlet chambers, downstream end caps, and ball bearing cartridges.

Bearing Description

As illustrated in Figure 9, the bearing is a 4-pad, rocker-pivot, tilting-pad journal bearing manufactured by Bearings Plus Inc. The bearing assembly uses a flooded configuration and contains pads with a pad pivot offset of 0.57.

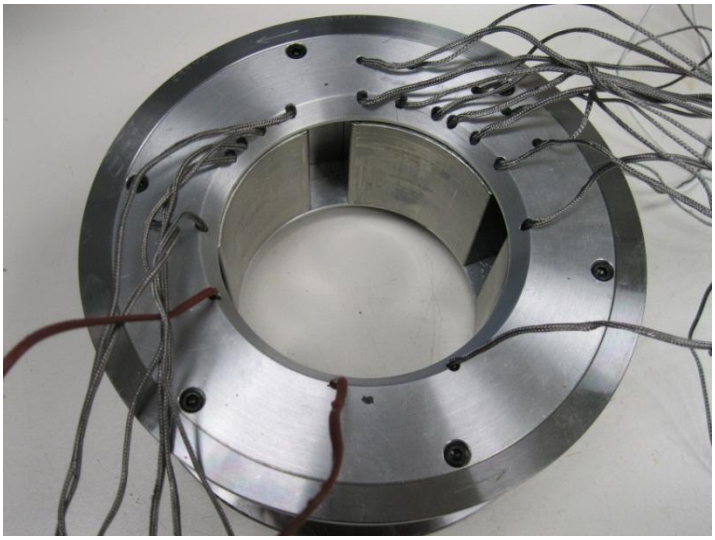

Figure 9: Test Bearing from Drive End

Figure 10 below is a picture of the test bearing pad, and details of the test bearing's geometry, loading style, and lubricant type are presented in Table 2.

Figure 10: Test Bearing Pad

Table 2: Bearing Parameters

Rotor Diameter	101.5238 mm (3.997 in)
Number of Pads	4
Configuration	LOP/LBP
Bearing (Bore) Diameter	101.7575 mm (4.0062 in)
Radial Pad Clearance, C_p	0.1118 mm (0.0044 in)
Radial Bearing Clearance	0.0826 mm (0.00325 in)
Pad Axial Length	60.33 mm (2.375 in)
Pad Arc Angle	72°
Pivot Offset	0.57
Measured Preload	0.3
Pad Mass	0.96 kg (2.12 lbm)
Lubricant Type	ISO VG 32
Oil Inlet Temperature	110 °F

Pad Instrumentation

Embedded thermocouples provide pad metal temperature just below the bearing's surface. The twenty-one thermocouples help define the temperatures experienced by the bearing pads during testing. In the loaded pad, embedded thermocouples were introduced near the bearing housing, radially opposite from the thermocouples below the Babbitt surface. These thermocouples, along with the near-surface thermocouples define the radial temperature gradient experienced during testing. The remaining thermocouples are embedded in the other pads to give an idea of the circumferential temperature distribution.

Three radial probes (M_{11}-M_{13}) in Figure 11, were added in the LOP orientation to the loaded pad similar to the procedure performed in Wilkes and Childs [17]. These three radial probes, pad-stator probes, were added in a triangular pattern to measure the back of the loaded pad while a force is applied directly through the pivot, to more

closely show the stiffness of the pad relative to the housing (see Predictions).

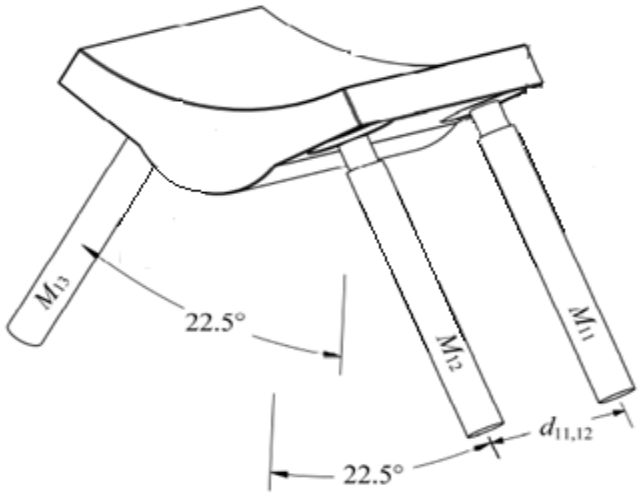

Figure 11: Proximity Probe Orientation on Loaded Pad (Adapted from [17])

EXPERIMENTAL PROCEDURE

The general testing procedure includes achieving steady state operating conditions. To attain steady state conditions, the rotor is held at a constant rotational speed, oil inlet temperature, and static load. Testing conditions include four running speeds varying from 6800 to 13200 rpm and five static loads from 0 kPa to 2903 kPa (421.1 psi). Table 3 presents the test matrix for nominal test conditions.

Table 3: Matrix of Nominal Test Conditions

Static Load	Speed [RPM], (Flow-rate [L/min] @ 110°F)			
kPa (psi)	6800, (22.7)	9000, (26.5)	10800, (30.3)	13200, (34.1)
0	x	x	x	x
725 (105.3)	x	x	x	x
1452 (210.5)	x	x	x	x
2178 (315.8)	x	x	x	x
2903 (421.1)	x	x	x	x

After achieving steady state conditions, the bearing stator is alternately excited in the *x* and *y* directions using the hydraulic shakers with a pre-specified pseudo-random dynamic excitation waveform. The excitation waveform has frequencies from 10 Hz to 320 Hz in 10 Hz increments in two orthogonal directions, the *x*-direction and the *y*-direction (static load direction). To avoid noise at 60 Hz and its multipliers, the actual excitation frequencies are slightly offset from the nominal values.

Dynamic Stiffness-Coefficients

Rotordynamic coefficients are obtained through the parameter identification model adapted from Childs and Hale [21]. Their approach uses an equation of motion for the

stator mass M_s that can be written as:

$$M_s \begin{Bmatrix} \ddot{x}_s \\ \ddot{y}_s \end{Bmatrix} = \begin{Bmatrix} f_x \\ f_y \end{Bmatrix} - \begin{Bmatrix} f_{bx} \\ f_{by} \end{Bmatrix} \tag{7}$$

In this equation, $\ddot{x}_s$ and $\ddot{y}_s$ are measured components of the stator's acceleration, f_x and f_y are the measured excitation forces, and f_{bx} and f_{by} are the bearing reaction force components.

Substituting the [K][C][M] model from Eq. (4) into the equation above, the bearing reaction force as a function of the rotordynamic coefficients becomes:

$$\begin{Bmatrix} f_x - M_s\ddot{x}_s \\ f_y - M_s\ddot{y}_s \end{Bmatrix} = -\begin{bmatrix} K_{xx} & K_{xy} \\ K_{yx} & K_{yy} \end{bmatrix} \begin{Bmatrix} \Delta x \\ \Delta y \end{Bmatrix} - \begin{bmatrix} C_{xx} & C_{xy} \\ C_{yx} & C_{yy} \end{bmatrix} \begin{Bmatrix} \Delta\dot{x} \\ \Delta\dot{y} \end{Bmatrix} - \begin{bmatrix} M_{xx} & M_{xy} \\ M_{yx} & M_{yy} \end{bmatrix} \begin{Bmatrix} \Delta\ddot{x} \\ \Delta\ddot{y} \end{Bmatrix} \tag{8}$$

Here, Δx and Δy define the relative motion between the rotor and the stator, and K_{ij}, C_{ij}, and M_{ij} are stiffness, damping, and virtual-mass coefficients, respectively. Both the left-hand vector of Eq. (8) and Δx and Δy are measured functions of time.

Using a fast Fourier transform, the rotordynamic coefficients are determined in the frequency domain:

$$\begin{Bmatrix} \boldsymbol{F_x} - M_s\boldsymbol{A_x} \\ \boldsymbol{F_y} - M_s\boldsymbol{A_y} \end{Bmatrix} = -\begin{bmatrix} \boldsymbol{H_{xx}} & \boldsymbol{H_{xy}} \\ \boldsymbol{H_{yx}} & \boldsymbol{H_{yy}} \end{bmatrix} \begin{Bmatrix} \boldsymbol{D_x} \\ \boldsymbol{D_y} \end{Bmatrix} \tag{9}$$

$\boldsymbol{F_i}$, $\boldsymbol{A_i}$, and $\boldsymbol{D_i}$ are the Fourier transforms of the excitation force, the stators acceleration, and the relative stator to rotor motion in x and y directions. The elements of the bearing dynamic stiffness function $\boldsymbol{H_{ij}}$ are related to the coefficients defined by:

$$\boldsymbol{H_{ij}} = \left(K_{ij} - \Omega^2 \mathrm{M_{ij}}\right) + \boldsymbol{j}\left(\Omega C_{ij}\right) \tag{10}$$

$\boldsymbol{H_{ij}}$ is the complex dynamic stiffness that relates the force in the "i" direction due to the motion in the "j" direction. The real and imaginary components yield,

$$Re\left(\boldsymbol{H_{ij}}\right) = K_{ij} - \Omega^2 \mathrm{M_{ij}} \tag{11}$$

$$Im\left(\boldsymbol{H_{ij}}\right) = \Omega C_{ij} \tag{12}$$

Ω represents the excitation frequency.

If Re($\boldsymbol{H_{ij}}$) can be fitted as a quadratic function of Ω, Eq. (11) exhibits how the stiffness and virtual-mass coefficients can be estimated. K_{ij} represents the zero-frequency intercept and M_{ij} represents the curvature. From Eq. (12), the damping coefficients can be defined as the slope of the Im($\boldsymbol{H_{ij}}$) with respect to Ω.

Looking back, Eq. (9) provides only two equations for four unknowns $\boldsymbol{H_{xx}}$, $\boldsymbol{H_{xy}}$, $\boldsymbol{H_{yx}}$, and $\boldsymbol{H_{yy}}$. To obtain four independent equations, alternate shakes at a given steady-state rotor position are conducted in the *X* and *Y* directions while measuring the response in both directions. The equations are given by:

$$\begin{bmatrix} \boldsymbol{F}_{xx} - M_s \boldsymbol{A}_{xx} & \boldsymbol{F}_{xy} - M_s \boldsymbol{A}_{xy} \\ \boldsymbol{F}_{yx} - M_s \boldsymbol{A}_{yx} & \boldsymbol{F}_{yy} - M_s \boldsymbol{A}_{yy} \end{bmatrix} = -\begin{bmatrix} \boldsymbol{H}_{xx} & \boldsymbol{H}_{xy} \\ \boldsymbol{H}_{yx} & \boldsymbol{H}_{yy} \end{bmatrix} \begin{bmatrix} \boldsymbol{D}_{xx} & \boldsymbol{D}_{xy} \\ \boldsymbol{D}_{yx} & \boldsymbol{D}_{yy} \end{bmatrix} \tag{13}$$

One set of frequency-dependent dynamic stiffness coefficients, ($\boldsymbol{H_{xx}}$, $\boldsymbol{H_{xy}}$, $\boldsymbol{H_{yx}}$, and $\boldsymbol{H_{yy}}$) is obtained from a simultaneous excitation that is applied through a frequency range of 10 Hz to 320 Hz in increments of 10 Hz. The dynamic waveform takes less than a second to execute and is applied along each the *X* and *Y* directions. For each experimental condition, 10 consecutive shakes are conducted in each direction. The measurements in each *X* and *Y* directions are then broken into five groups. The five

groups provide a significant number of averages and a decent resolution from the fast Fourier transform. The five groups of data in the *X* direction are combined alternately with the five groups in the *Y* direction, resulting in a total of 25 complex dynamic stiffness matrices. The dynamic repeatability of an experimental condition is the standard deviation from the 25 complex dynamic stiffness matrices.

To obtain the dynamic stiffness of the fluid film only, a baseline result needs to be subtracted from the dynamic stiffness measured during tests. The baseline result accounts for the stiffness and damping of all the stator attachments (pitch stabilizers, hose connections, etc.). To gather the baseline dynamic stiffness, a dry shake is performed at zero rotor speed with no oil allowed in the bearing. Both loaded and unloaded dynamic-stiffness baseline data are obtained. The dynamic stiffness of the fluid film is found by subtracting the baseline data from the data obtained during a test, shown in Eq. (14).

$$\boldsymbol{H}_{ij} = \boldsymbol{H}_{ij,TEST} - \boldsymbol{H}_{ij,BASELINE} \tag{14}$$

Figure 12 shows the real direct and cross-coupled baseline dynamic stiffness, while Figure 13 shows the imaginary direct and cross-coupled baseline dynamic stiffness for zero loads.

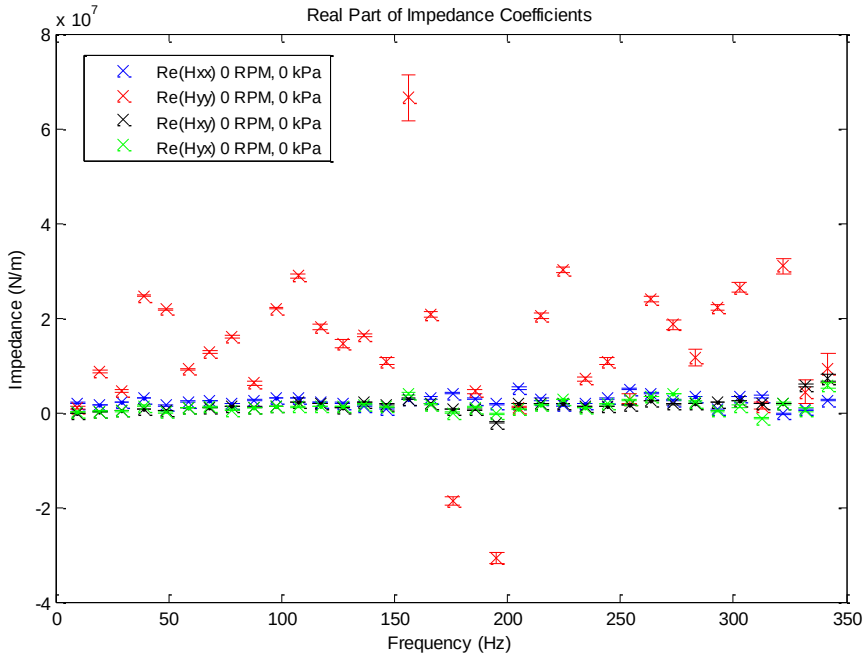

Figure 12: Baseline Real Direct and Cross-coupled Dynamic Stiffness

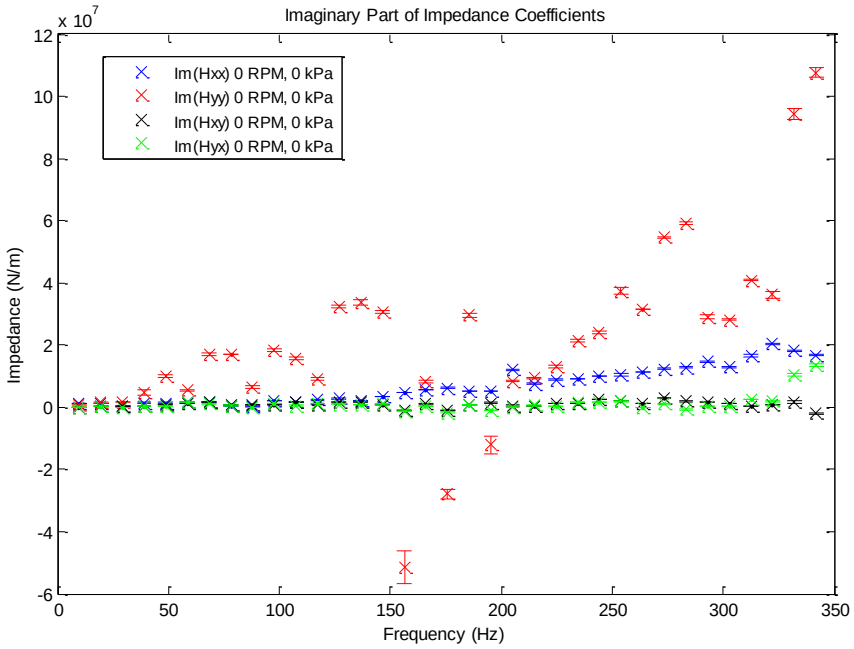

Figure 13: Baseline Imaginary Direct and Cross-coupled Dynamic Stiffness

Curve Fitting and Uncertainty Analysis

As mentioned above, the dynamic repeatability of an experimental condition is the standard deviation from the 25 complex dynamic stiffness matrices. From these shakes, an average dynamic stiffness $\boldsymbol{H_{ij}}$ is obtained at each excitation frequency for each test condition, Eq. (15).

$$\boldsymbol{H_{ij}} = \frac{1}{N}\sum_{k=1}^{N}\left(\boldsymbol{h_{ij}}\right)_k \tag{15}$$

N is the number of shakes and $(\boldsymbol{h_{ij}})_k$ is the dynamic stiffness of each individual shake.

The uncertainty of each dynamic stiffness data point can be described as two times the standard deviation, shown in Eq. (16).

$$\Delta\boldsymbol{H_{ij}} = 2\sigma_{\boldsymbol{H_{ij}}} = 2\sqrt{\frac{\sum_{k=1}^{N}\left[\left(\boldsymbol{h_{ij}}\right) - \boldsymbol{H_{ij}}\right]^2}{N-1}} \tag{16}$$

Eq. (16) is used to calculate the uncertainties for the baseline dynamic stiffness and the tested dynamic stiffness. The uncertainty of $\Delta\boldsymbol{H_{ij}}$ qualifies the repeatability of each test. These uncertainties are shown as error bars in the dynamic stiffness plots.

As shown above in Eq. (11), K_{ij} represents the zero-frequency intercept of Re($\boldsymbol{H_{ij}}$), and M_{ij} represents the curvature of Re($\boldsymbol{H_{ij}}$). By taking Eq. (11), and setting $\Omega^2 = \Lambda,$ the Re($\boldsymbol{H_{ij}}$) becomes a linear function of $\Lambda,$ where K_{ij} is the y-intercept and M_{ij} is the slope, defined by

$$\mathrm{Re}(\boldsymbol{H_{ij}}) = K_{ij} - \Lambda M_{ij} \tag{17}$$

K_{ij} and M_{ij} are then determined from the least squares linear regression, in the form of Eq. (18) that is applied to Re($\boldsymbol{H_{ij}}$) versus Λ data:

$$y = mx + b \tag{18}$$

where, x and y represent the independent and dependent variables respectively.

From Eq. (18), the y-intercept b and slope m of the linear regression are given in Eqs. (19) and (20), respectively.

$$b = \left(\frac{1}{n} \sum_{k=1}^{n} x_k \right) - m \left(\frac{1}{n} \sum_{k=1}^{n} y_k \right) \tag{19}$$

$$m = \frac{n \sum_{k=1}^{n} x_k y_k - \sum_{k=1}^{n} x_k \sum_{k=1}^{n} y_k}{n \sum_{k=1}^{n} x_k^2 - \left(\sum_{k=1}^{n} x_k \right)^2} \tag{20}$$

where, x_k and y_k represent the data points that are fitted and n is the number of data pairs.

The y-intercept b is equal to the stiffness coefficient K_{ij}, and the slope of the line m is equal to the virtual-mass M_{ij}. The linear regression is used for both the direct and cross-coupled coefficients. The frequency independent damping coefficients C_{ij} are the slope of the Im($\boldsymbol{H_{ij}}$) with respect to Ω and are equal to the slope m given in Eq. (20). The y-intercept b has no physical meaning in Im($\boldsymbol{H_{ij}}$).

The uncertainties of the stiffness, damping, and virtual-mass coefficients are determined by the correlation of the linear regression with the dynamic stiffness data. The final coefficient of uncertainty is a function of the mean square error $\left(\hat{\sigma}^2 \right)$ and the quantity S_{xx}, Eqs. (21) and (22) respectively.

$$\hat{\sigma}^2 = \frac{\sum_{k=1}^{n} \left(y_k - \hat{y}_k \right)^2}{n - 2} \tag{21}$$

$$S_{xx} = \sum_{k=1}^{N} \left(x_k^2 - \bar{x}_k^2 \right) \tag{22}$$

where, $\hat{y}_k$ represents the dependent variable fit data, x represent the independent variables, and y represent the dependent variables.

The uncertainties of the y-intercept b are calculated using Eq. (23), and the uncertainties of the slope m are calculated using Eq. (24).

$$\Delta b = t\sqrt{\hat{\sigma}^2\left(\frac{1}{n}+\frac{\bar{x}^2}{S_{xx}}\right)} \tag{23}$$

$$\Delta m = t\sqrt{\frac{\hat{\sigma}^2}{S_{xx}}} \tag{24}$$

Note that t is a multiplicative factor derived by using a 95% confidence interval, and n is the number of fitted data points. For a large number of data points, t = 1.96.

Table 4 shows a summary of the rotordynamic coefficients and uncertainties in the LOP orientation at 13.2 krpm and 2903 kPa (421.1 psi) static load.

Table 4: Experimental Uncertainties for the LOP Orientation at 13.2 krpm and 2903 kPa (421.1 psi) Static Load

Units	Coefficient	Value	Uncert.	%Uncert.
Mn/m	Kxx	293.9	10.6	3.6
	Kxy	-24.7	5.6	22.5
	Kyx	-38.3	2.2	5.6
	Kyy	705.9	24.4	3.5
kN-s/m	Cxx	232.0	8.3	3.6
	Cxy	11.7	4.2	36.0
	Cyx	-5.4	3.6	66.6
	Cyy	210.1	33.2	15.8
MN/m	Mxx	-22.9	9.6	42.1
	Mxy	-34.8	5.0	14.5
	Myx	-15.8	1.9	12.3
	Myy	13.0	22.1	169.3

Note that the uncertainties presented in Table 4 are representative of the majority of the test results. A full list of the rotordynamic uncertainties can be found in Appendix D. Large uncertainties occur when coefficient values are small.

Predictions

Code A

As mentioned earlier, static results and rotordynamic coefficients presented will be compared to predictions from a new rotordynamic bearing code, Code A developed by Tao and San Andrés at the Texas A&M Turbomachinery Laboratory. Code A uses a laminar-flow Reynolds-equation model to predict the static and dynamic behavior of a TPJB, and uses an adiabatic energy transport equation to account for the thermal effects in fluid flow. The lubricant's viscosity is modeled as temperature dependent. Code A takes into account pivot flexibility with a user defined load-versus-deflection curve, and individual geometries for each pad. A multi-frequency option allows for stiffness and damping predictions to be obtained over the range of excitation frequencies (e.g. 0-360 Hz). The output from Code A presents stiffness, and damping coefficients as well as static parameters (journal eccentricity, attitude angle, estimated power loss, and circumferential fluid temperatures). Virtual-mass terms are obtained by curve fitting the frequency-dependent stiffness coefficients. Figure 14 provides the input and output screen for Code A.

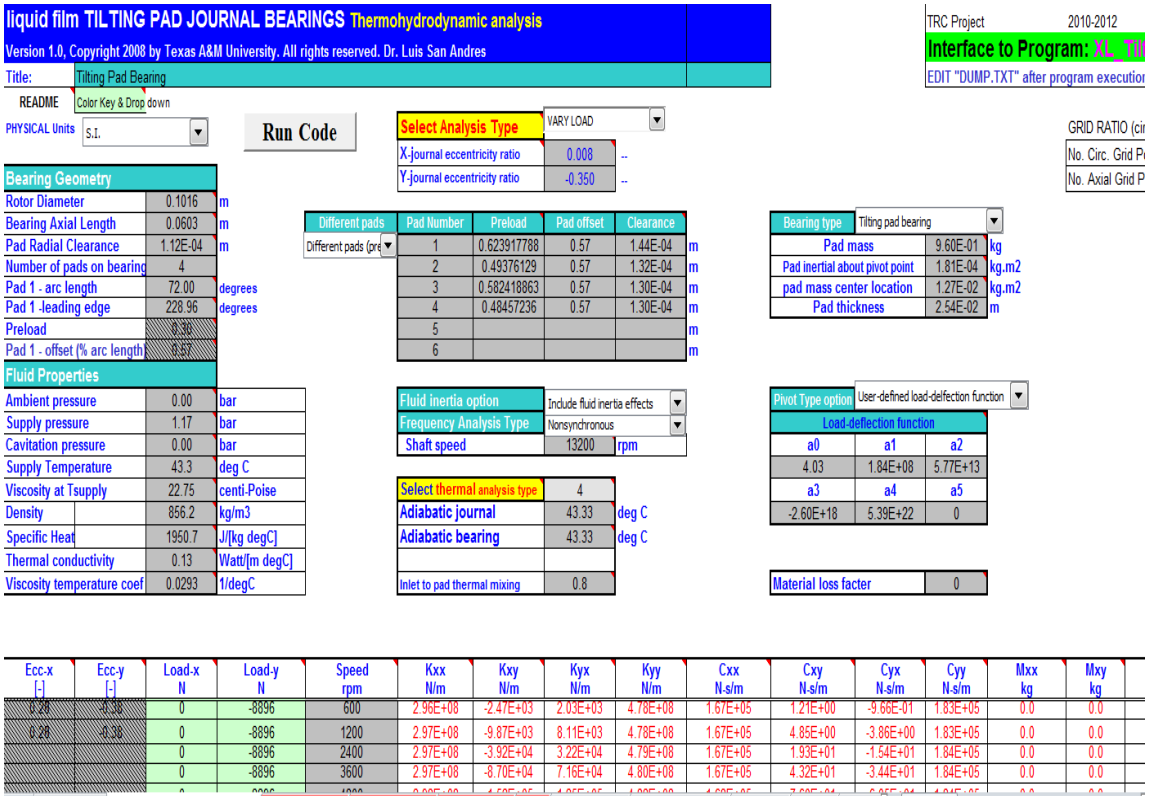

Figure 14: Code A Input and Output Screen

Figure 14 shows that a value of 0.8 is used as the input for the inlet to pad thermal mixing. This value represents the fraction of hot oil carry from trailing the edge of a pad to the leading edge of the preceding pad. Increasing the inlet to pad thermal mixing value, increases the influence that the trailing edge of the one pad has on the preceding pad, and results in higher circumferential temperature predictions.

Code B

Dynamic stiffness results presented will be compared to predictions from the model of Wilkes and Childs [14][17][18], which will be referenced as Code B. Wilkes dissertation [15] uses a laminar-flow Reynolds-based model to predict dynamic results,

utilizing pivot and pad flexibility in predicting the impedance coefficients for a tilting-pad journal bearing. Code B takes into account different pad geometries. It does not include an energy equation to calculate temperature and viscosity distributions, but experimental temperature measurements are used to estimate the lubricant's viscosity distribution. The output from Code B presents plots of the impedance coefficients. Since experimental temperature measurements are used in the model, circumferential fluid temperatures are not predicted. Static parameters (journal eccentricity and attitude angles) are also predicted by Code B. Code B utilizes a MATLAB interface that will not be shown in this thesis.

Table 5 below shows the main features and differences between prediction codes.

Table 5: Difference Between Predictions

Code Developer	Tao and San Andrés	Wilkes
Code Name	Code A	Code B
Model Type	Reynolds-based	Reynolds-based
Pad Geometry	User-defined	User-defined
Thermal Analysis	Adiabatic Energy Transport Equation	Experimental Temperature Measurements
Pivot Stiffness	User-defined Load-versus-Deflection Curve	User-defined Load-versus-Deflection Curve
Pad Flexibility	Assumed Rigid	User Defined Flexibility
Static Outputs	Journal Eccentricity, Attitude Angle, Estimated Power Loss, and Circumferential Fluid Temperatures	Journal Eccentricity and Attitude Angle
Dynamic Outputs	Dynamic Stiffness Coefficients	Plots of Impedance Coefficients

Input Parameters for Prediction Codes

Hot Clearance

A bearing clearance measurement is taken by slowly precessing the stator around the non-rotating shaft with a sufficiently small circular force to prevent significant pivot deflection. A clearance measurement is the boundary of the bearing when the pads have not deflected radially due to the fluid film loads. “Cold clearance” refers to the measurement taken at room temperature prior to testing, while “Hot clearance” refers to the measurement taken immediately after shutting down the test rig after tests. Hot clearance measurements occur approximately 10 seconds after shutting down the test rig from steady state conditions.

Figure 15 shows the bearing’s rectangular cold clearance. The static load is applied in the $+Y$ direction. As can be seen, the bearing tested shows non-symmetry in that two of the parallel pad clearances are larger.

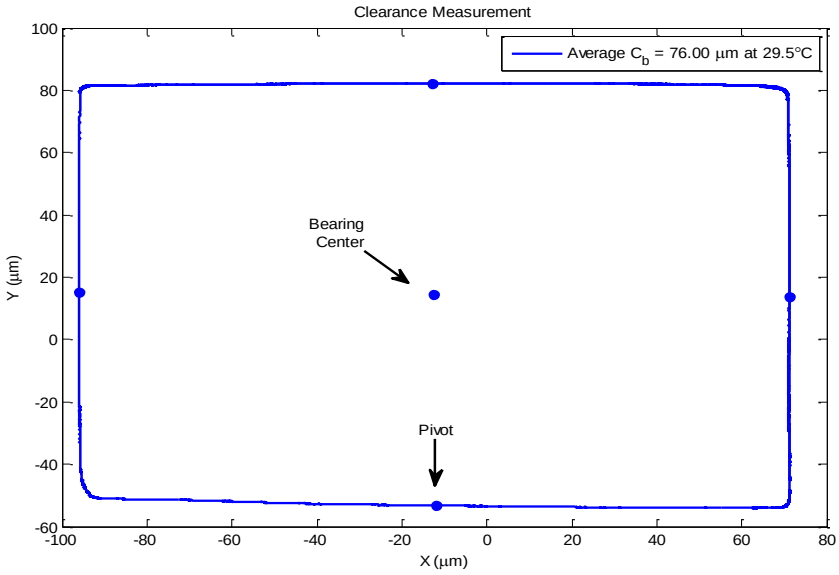

(A) LOP Orientation

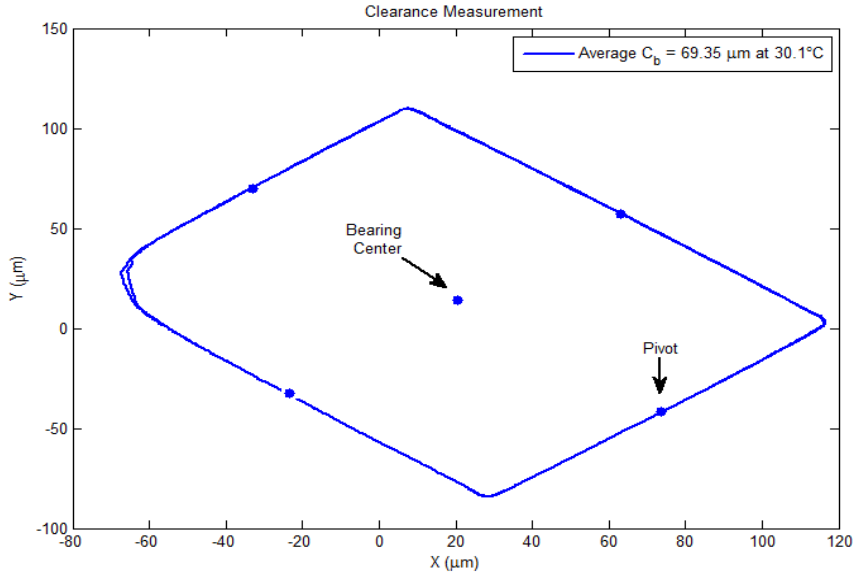

(B) LBP Orientation

Figure 15: Measured Clearance at Room Temperature

In comparing Figure 15 to the manufactured bearing clearance previously shown in Table 2, different results are obtained. The manufactured cold bearing clearance for each pad was averaged to be 82.55 μm. Table 6 gives a summary of the cold bearing clearance for each pad.

Table 6: Radial Cold Clearance Measurements

Cold Clearance (μm)				
Orientation	3 (Loaded Pad)	4	1	2
LOP	68.4	83.6	68.4	83.6
LBP	69.4	75.7	69.4	75.7

Figure 16 shows the bearings LOP hot and cold clearances. The figure shows a clearance measurement taken corresponding to each running speed. The temperature of the clearance measurement is the mean pad surface temperature experienced at the time of the clearance measurement. The colored dots in the middle show each measured bearing center in reference to the clearance measurement taken.

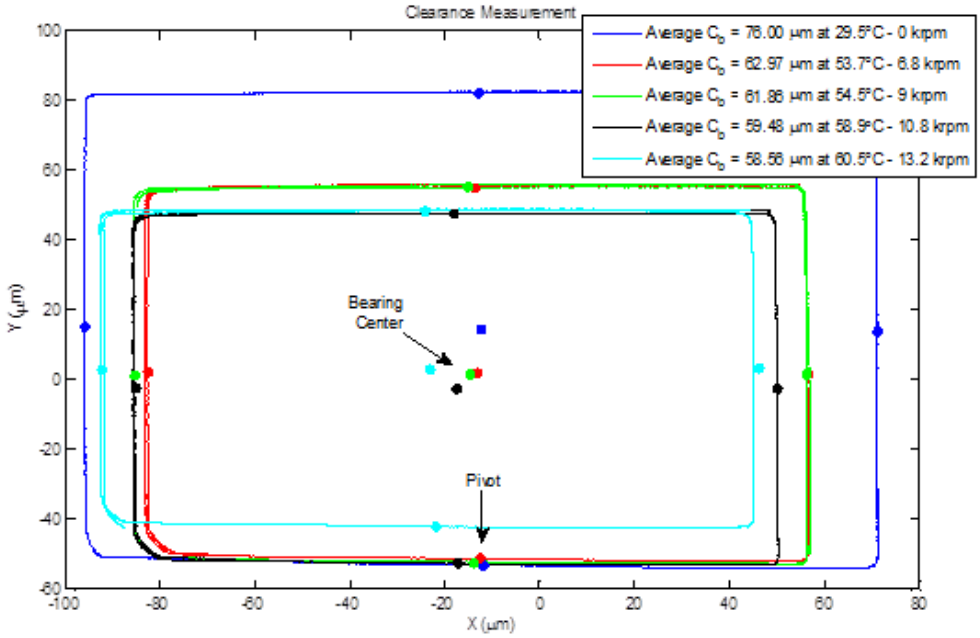

(A) LOP Orientation

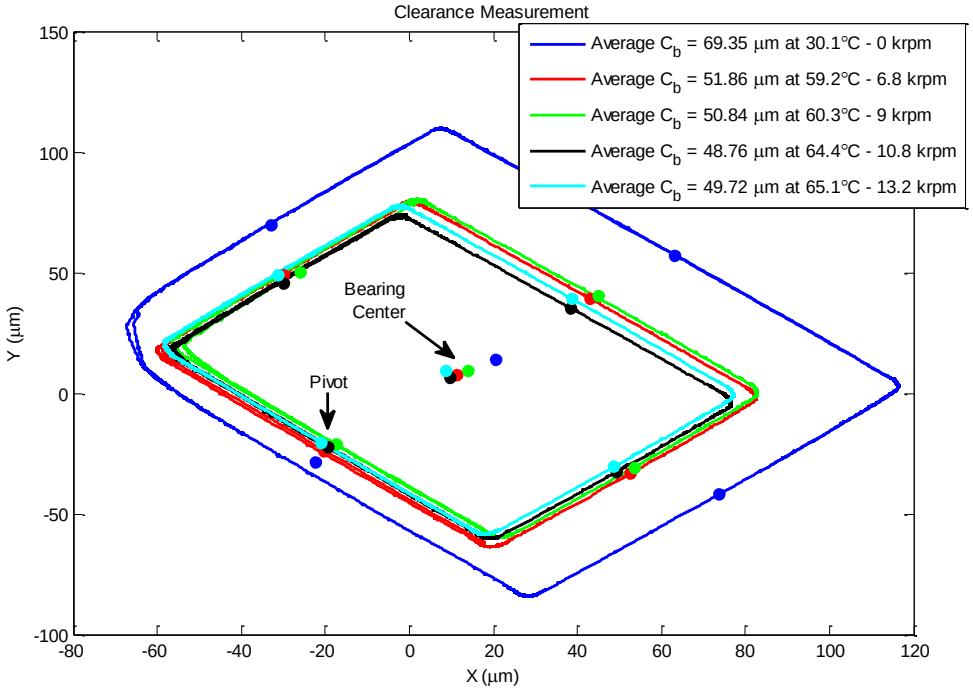

(B) LBP Orientation

Figure 16: Measured Clearance for All Speeds

The hot-clearance measurements of Figure 16 show the reduction in bearing clearance due to thermal expansion of the shaft and pads during testing. As testing conditions get hotter radial bearing clearances decrease. Except for one clearance measurement above, all measurements show this outcome. The clearance measurement at 13.2 krpm in the LBP orientation increases compared to the 10.8 krpm case. Similar to the cold clearance measurement, the hot clearances show that the clearances of adjacent pads are different. The measured hot clearance for each pad will be used in modeling predictions to give the most accurate representation of the bearing clearance during testing. Table 7 and Table 8 give a summary of the LOP and LBP hot bearing clearance used for prediction calculations.

Table 7: LOP Radial Hot Clearance Measurements

Hot Clearance (μm)					
Orientation	Speed (rpm)	3 (Loaded Pad)	4	1	2
LOP	6800	56.6	69.3	56.6	69.3
	9000	56.1	68.8	56.1	68.8
	10800	55.1	67.8	55.1	67.8
	13200	54.2	66.9	54.2	66.9

Table 8: LBP Radial Hot Clearance Measurements

Hot Clearance (μm)					
Orientation	Speed (rpm)	3	4	1	2
LBP	6800	52.6	50.2	52.6	50.2
	9000	50.4	49.8	50.4	49.8
	10800	47.6	47.4	47.6	47.4
	13200	48.9	48.4	48.9	48.4

Loaded Pad's Radial Temperature Gradient

In 1988, Branagan and Barrett [16] studied the thermal deflection associated with a TPJB pad during operation. They looked into the differential heating of a pad and its effects on pad clearance. To model the differential heating associated with the front of the pad (rotor side of the pad) Branagan used the circumferential temperatures along the Babbitt surface. To model the back of the pad (bearing housing side of the pad), Branagan assumed the heat transfer would be dominated by a stagnant sump region behind the pad. This sump region temperature was set at the inlet oil temperature to the bearing. The model was created by assuming the entire pad was initially at the sump temperature, and then the higher temperatures were applied along the Babbitt surface. Through a finite-element (FE) analysis, Branagan found that the thermal deformed pad showed a radial growth of 0.0034-0.0059 mm (0.00013-0.00023 in), increasing the curvature of the pad and thus the radial pad clearance and preload. The increase in pad clearance due to thermal deflection alone was found to have little impact on the static and dynamic bearing characteristics.

In the present study, the thermal gradient in the loaded pad was defined by embedded thermocouples inserted inside the bearing pad near the bearing housing. In combination with measurements on the rotor side of the pad these thermocouples define the radial temperature difference experienced during tests. Figure 17 details the 11 thermocouples in the loaded pad. All pad-temperature data are given in Appendix B.

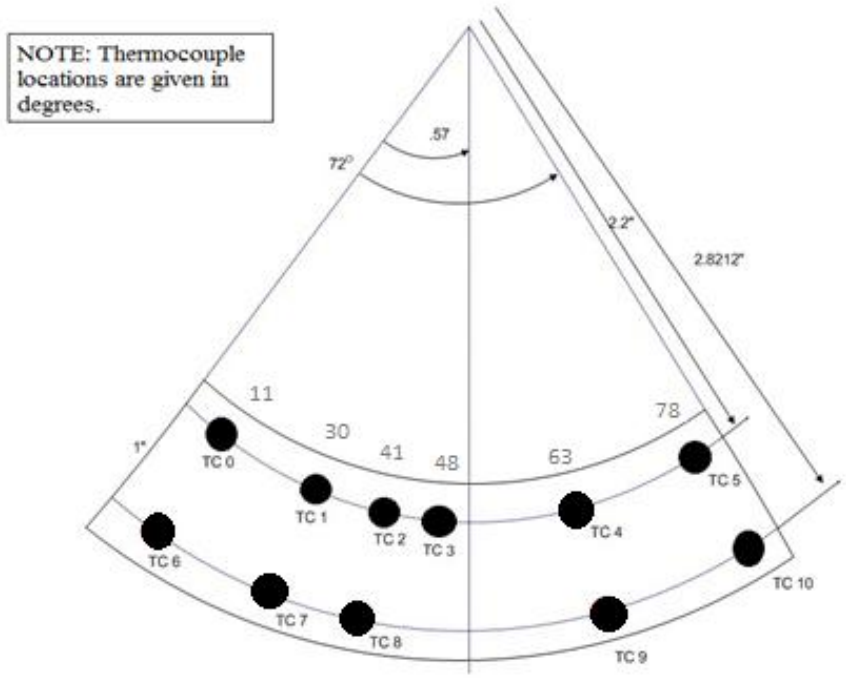

Figure 17: Loaded Pad Thermocouple Diagram

Figure 18 shows the loaded pad's radial temperature difference (pad surface temperature minus back-side temperatures) measured during the 6.8 and 13.2 krpm cases. Note that a negative temperature represents a higher temperature measurement at the bearing housing side of the pad.

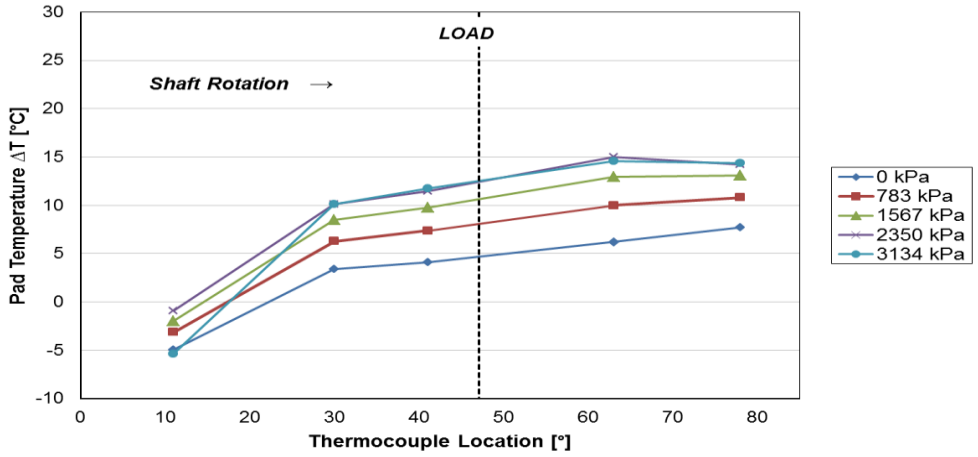

(A) 6.8 krpm

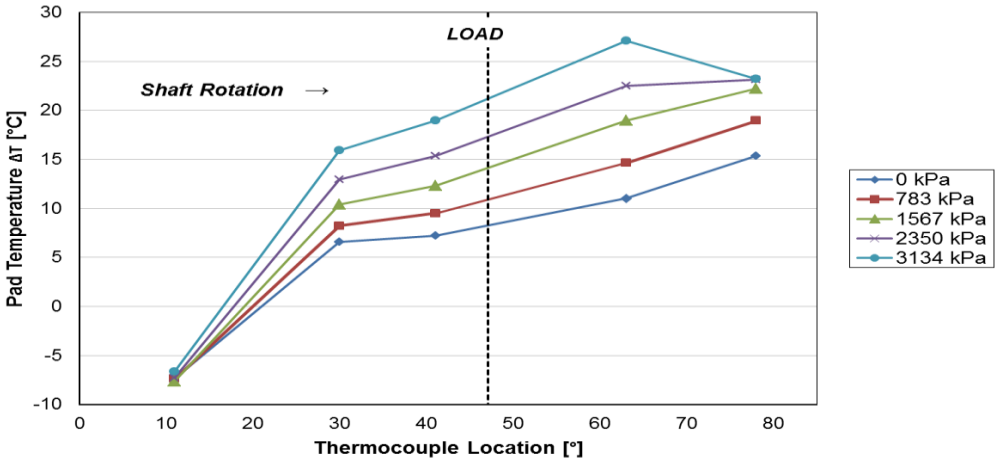

(B) 13.2 krpm

Figure 18: Loaded Pad Radial Temperature Difference

The thermal gradient in the loaded pad generally shows a radial temperature decrease from the rotor side of the pad to the bearing housing. Only the thermocouples on the leading edge of the pad showed a radial temperature increase. This temperature increase can be attributed to the thermocouple location; being located in the proximity of the oil inlet to the bearing. Overall, the radial temperature difference from the rotor side of

the pad to the bearing housing increases with increasing load and speed. The radial temperature difference increases across the face of the pad in the direction of rotation.

An FEA model was created to look at the thermal gradients present in the pads during dynamic tests. As seen above, the temperature increases experienced along the pad, is not uniform. The temperature of the rotor side of the pad is usually greater than the temperature near the bearing housing. This radial temperature gradient will cause an uneven thermal deflection in the pad, changing the pad's radius of curvature. From Eq. (2), the change in pad radius will affect the preload of the pad. Note that thermal effects on the radial bearing clearance were taken into account using the measured hot clearance.

Using measured temperatures a thermal model in ANSYS was created. Thermal conditions were modeled by assuming the whole pad is at room temperature and then applying the measured temperatures to the Babbitt surface and back of the pad. Oil inlet temperatures were applied to the sides of the pad. The line of contact at the pad pivot was constrained to allow zero translation in the *x*, *y*, and *z* axes to prevent pad rotation, allowing for the thermal deflection to be studied. Figure 19 shows the thermal distribution obtained for the FEA analysis, for the 13.2 krpm dynamic test. Note that the temperature does not change axially across the face of the pad.

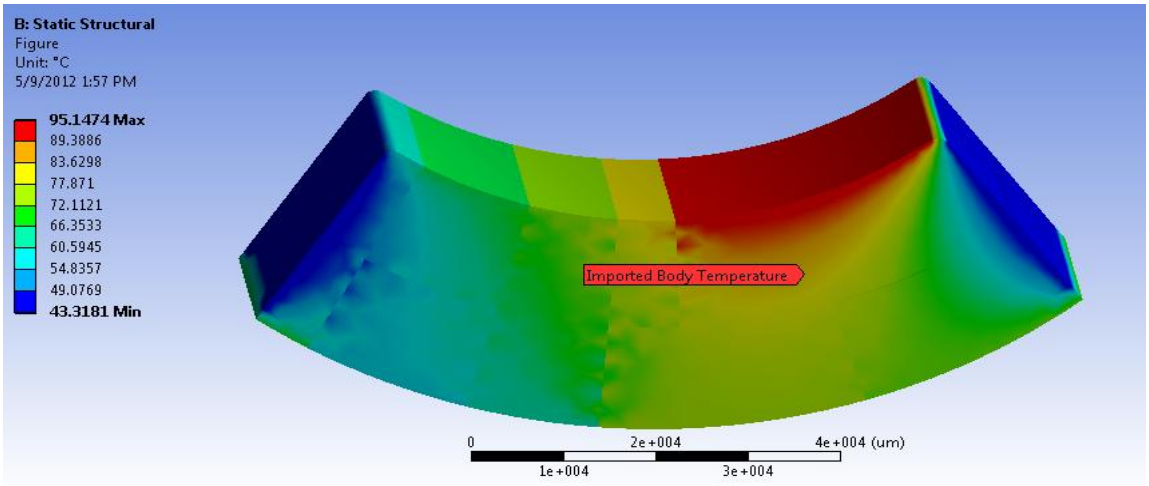

Figure 19: FEA Temperature Distribution for LOP Orientation 13.2 krpm with 1452 kPa (210.5 psi) Static Load

In supplying the thermal load above, Figure 20 shows the thermal deflection results from the FEA analysis.

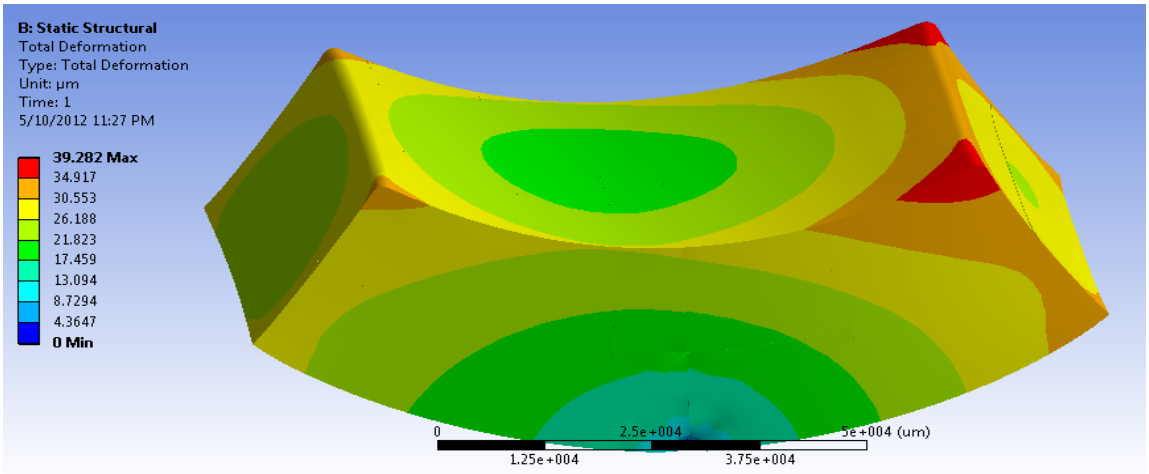

Figure 20: FEA Thermal Deflection for LOP Orientation 13.2 krpm with 1452 kPa (210.5 psi) Static Load

Figure 20 shows an increase in thermal deflection circumferentially across the face of the pad. These results seem reasonable since the trailing edge of the pad is where

the larger thermal loads are applied. In obtaining the thermal deflection for multiple points across the mid-axial location of the pad, the resulting change in radius of curvature was established. The FEA results showed a 0.016-0.036 mm (0.00063-0.0014 in) increase in the loaded pad's radius depending on running speed and load.

To model the other pads, the same procedure was performed using the specific pad's metal temperatures. Since radial temperatures were not recorded for the other pads, the temperature near the bearing housing was modeled as the measured bearing inlet oil temperature. In the LBP orientation, pad 4 supports more of the unit load and resulted in higher temperature measurements than pad 3. The radial temperatures from pad 3 were modeled as the temperatures near the bearing housing for pad 4. Due to similar temperature measurements, pads 1 and 2 were modeled only once, resulting in the same change in pad radius. Table 9 shows the predicted change in radius of curvature for the 13.2 krpm LOP orientation.

Table 9: Pad Radius and Preload for LOP 13.2 krpm

Pad Number	Machined Pad Radius (mm)	Preload	Thermal Change in Pad Radius (mm)	Resulting Preload
3 (Loaded Pad)	0.112	0.516	0.034	0.628
4	0.112	0.403	0.021	0.497
1	0.112	0.516	0.020	0.588
2	0.112	0.403	0.020	0.492

Using Eq. (2) for preload, Table 9 shows that, as the radius of curvature increases, the resulting preload of the pad's increase by 0.065-0.136. Overall, the change in preload slightly affected the predicted bearing impedance coefficients. A higher preload per pad resulted in lowered predictions for the impedance coefficients (see

DYNAMIC RESULTS). Including the change in pad's radius resulted in slightly poorer predictions, but gives a more accurate representation of the pad's radial clearance during testing. Appendix C shows the complete FEA results for the change in pad radius of curvature and preload for 6.8 and 13.3 krpm in the LOP and LBP orientations.

Pivot Stiffness

Both codes use a polynomial load-versus-deflection curve that describes the static nonlinear stiffness of the pivot. The pivot stiffness, or pivot flexibility, refers to the flexibility of the pad relative to the bearing housing (partially from Hertzian-contact), Wilkes and Childs [14]. The Hertzian-contact flexibility arises from the localized strains that develop between elastically curved bodies distorted from imposed loads. Pivot flexibility characteristics are obtained by pressing the rotor into the pad while increasing the force applied directly through the pivot (LOP orientation) with the static loader, similar to the approach taken by Harris and Childs [22]. Figure 21 compares the measured load-versus-deflection curves for the pivot. In Figure 21, the blue crosses represent the pivot displacement as seen by the relative rotor-stator probes, shown in Figure 8, while the black crosses represent the pivot deflection as seen by the pad-stator probes, shown in Figure 11.

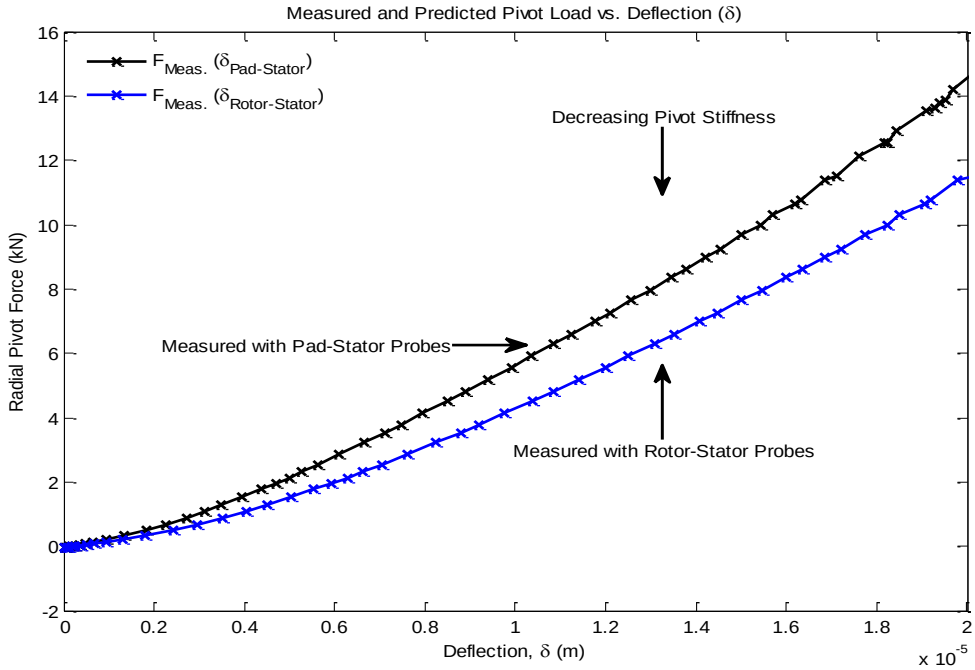

Figure 21: Comparison of Measured Pivot Load-Versus-Deflection

The pad-stator load-deflection curve shows the pivot to be significantly stiffer than the rotor-stator load-deflection curve. This observation agrees with Wilkes and suggests that the rotor-stator probes include the pivot, pad, rotor, and *Babbitt* stiffness. The pad-stator probes measure the back of the loaded pad while a force is applied directly through the pivot and more closely show the stiffness of the pad relative to the housing. The load-versus-deflection curve from the pad-stator probes will be used in both bearing prediction codes. A fourth-order approximation fits the measured load-versus-deflection curve and will be used as a numerical input for the pivot stiffness. This polynomial is given by:

$$f_c = 4.03 + 1.836\times10^{8}\delta + 5.771\times10^{13}\delta^2 - 2.598\times10^{18}\delta^3 + 5.393\times10^{22}\delta^4 \qquad (25)$$

where f_c is in Newton's, and δ is in meters.

Pad Flexibility

In addition to pivot stiffness, Code B also incorporates pad flexibility. Pad flexibility is the change in pad curvature resulting from an applied moment at the end of the pad from the fluid film pressure, Figure 4 and Eq. (6) from Wilkes and Childs [14].

In 1988 Branagan and Barrett [16] studied the mechanical pad deflection experienced in a TPJB during operation. This mechanical deflection is found by characterizing the pad as a curved beam with uniform thickness and an applied moment at the ends of the pad. The beam was considered to have a free-free boundary condition (extending from leading to trailing edge of the pad) or to have clamped-free boundary conditions (extending from the pivot to the trailing edge). Branagan analyzed the accuracy of several analytical bending stiffness formulas, comparing them with a finite-element prediction. In regards to k_{c_p} in Eq. (6), Deutschman et al.'s [23] formula was found to be the most accurate equation.

$$k_{c_p} = \frac{E_p L_p t_p}{\Theta - 1} \frac{\left(\Theta^2 - 1\right)^2 - \left[2\Theta \ln\left(\Theta\right)\right]^2}{4\left\{1 - \Theta^2\left[1 - 2\ln\left(\Theta\right)\right]\right\}} \tag{26}$$

Eq. (26) determines the change in radius using the analytically determined stress field of a curved beam with end moments [15]. Where $\Theta = \left(r_p + t_p\right)/r_p$ is the ratio of outer to inner pad radii, t_p is the thickness of the pad, L_p is the length of the pad, and E_p is the elastic modulus of the pad.

From Eq. (26) the following constant bending stiffness will be used as a numerical input for Code B, in Eq. (6).

$$k_{c_p} = 22.049 \text{ MN } (4.957 \times 10^6 \text{lbf}) \quad (27)$$

Note that the bearing tested in Wilkes consisted of pads with a hardened pivot insert to reduce wear, different from the pads tested in this thesis. Figure 22 shows a typical tilting-pad with pivot insert and is similar to the pads used in the tests by Wilkes [15].

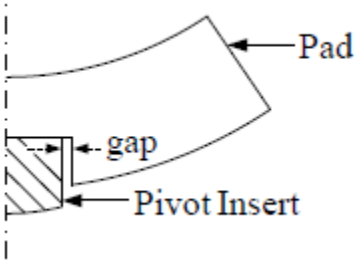

Figure 22: Illustration of Pad with a Pivot Insert [14]

The cut-out slot shown in Figure 22 greatly affected the pad's ability to resist bending moments, invalidating Deutschman et al.'s formula. For this reason, Wilkes predictions used a bending stiffness from measured load-defection results.

STATIC RESULTS

The static results include the measured journal eccentricity, bearing loci, attitude angle, estimated power loss, and circumferential pad metal temperatures in both the LOP and LBP configuration. As stated, Code B does not include an energy equation to calculate temperature and viscosity distributions, and experimental temperature measurements were used in predictions. To be consistent, all static results will be compared to predictions from Code A.

Eccentricity and Attitude Angle

The position of the bearing at operating conditions may be described with the static eccentricity ε_o and the attitude angle ϕ_o. Eccentricity provides the distance between the bearing center and the shaft center. ε_o and ϕ_o are defined by:

$$\begin{aligned} \varepsilon_{ox} &= e_{ox} \\ \varepsilon_{oy} &= e_{oy} \end{aligned} \tag{28}$$

$$\varepsilon_o = \sqrt{\left(\varepsilon_{ox}\right)^2 + \left(\varepsilon_{oy}\right)^2} \tag{29}$$

$$\phi_o = tan^{(-1)}\left(\frac{\varepsilon_{ox}}{\varepsilon_{oy}}\right)\frac{180}{\pi}[deg] \tag{30}$$

An eccentricity of zero indicates a centered bearing. An eccentricity of one would suggest contact between the shaft and bearing. The attitude angle indicates the relative transverse displacement of the shaft from the load-axis.

Figure 23 show the measured static ε_o and attitude angle ϕ_o results for the LOP orientation. Results are generated by increasing the unit load applied to the bearing from zero to 2903 kPa (421.1 psi), while keeping a constant rotor speed. This figure shows the measured static eccentricity vector within the cold and hottest LOP bearing clearance.

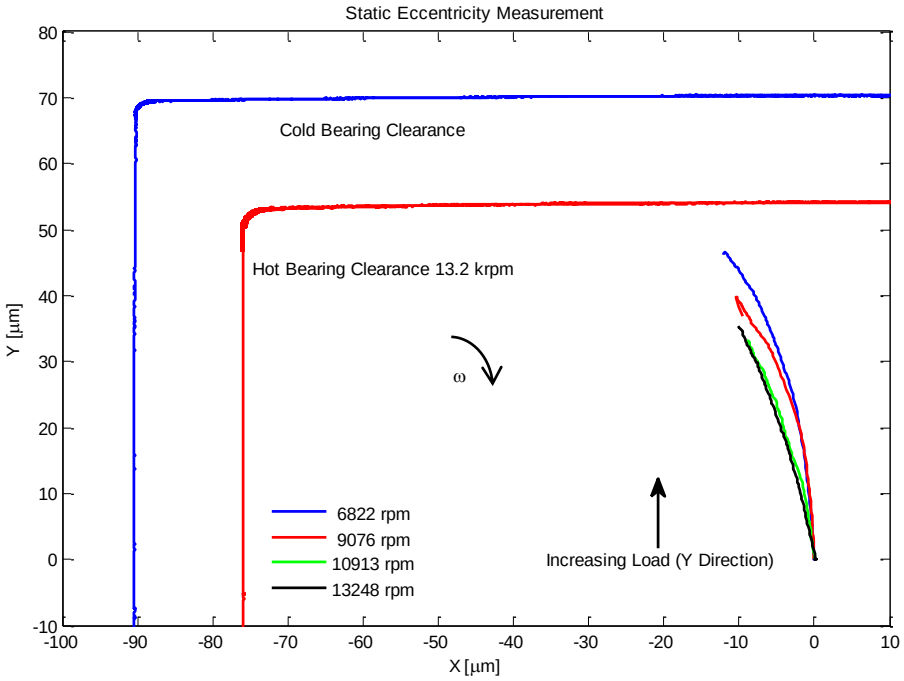

Figure 23: LOP Measured Static Eccentricity at Various Speeds with Unit Loads in the Y-Direction from 0-2903 kPa

Figure 23 shows that the measured static eccentricity vector changes with increasing load and speed. As speed increases, the static eccentricity vector decreases. In looking at the 13.2 krpm case and the hot bearing clearance shown, Figure 23 supports the notion of using the hot bearing clearance in predicting journal eccentricity. Using a cold clearance measurement for predictions would greatly under predict ε_o in Eq. (28).

Figure 24 show the measured static ε_o and attitude angle ϕ_o results for the LBP orientation. Similar to the LOP orientation, this figure shows the measured static eccentricity vector within the cold and hottest LBP bearing clearance.

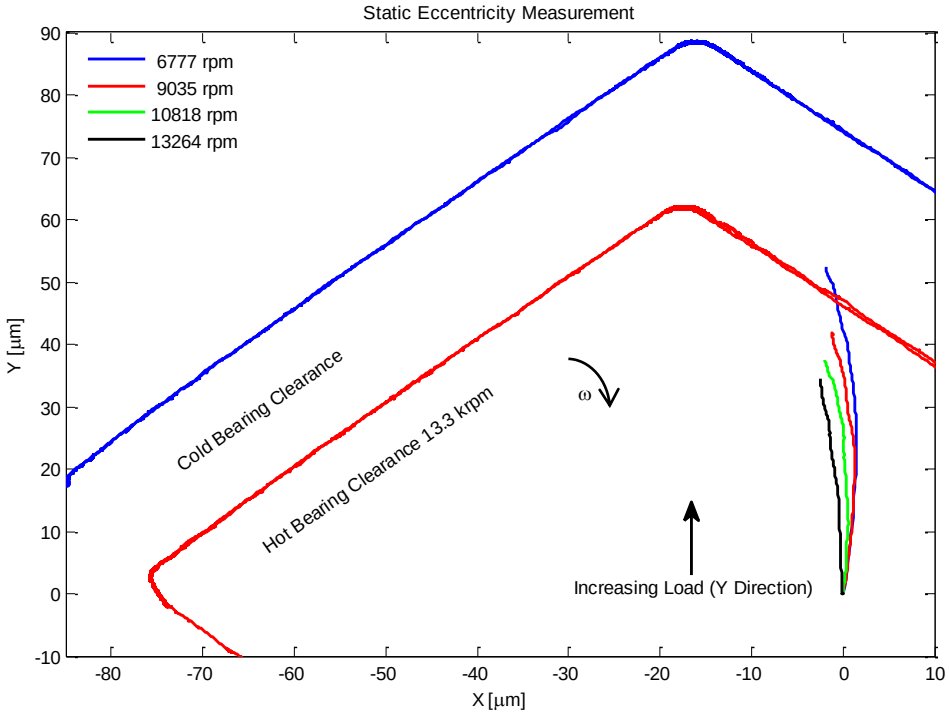

Figure 24: LBP Measured Static Eccentricity at Various Speeds with Unit Loads in the Y-Direction from 0-2903 kPa

Similar to the LOP orientation, Figure 24 shows that the measured static eccentricity vector changes with increasing load and speed in the LBP orientation. As speed increases, the static eccentricity vector decreases. The static data shows that for high static loads at low speeds the journal exceeds the measured hottest bearing clearance. The static eccentricity of 13.2 krpm is not as close to this measured bearing

clearance. Figure 24 supports using the hot bearing clearance in predicting journal eccentricity in the LBP orientation.

Figure 25 provides the measured and predicted loci plots to Code A for the LOP orientation. Each data point represents a static load condition, and the point furthest from the origin signifies the highest load condition, 2903 kPa (421.1 psi).

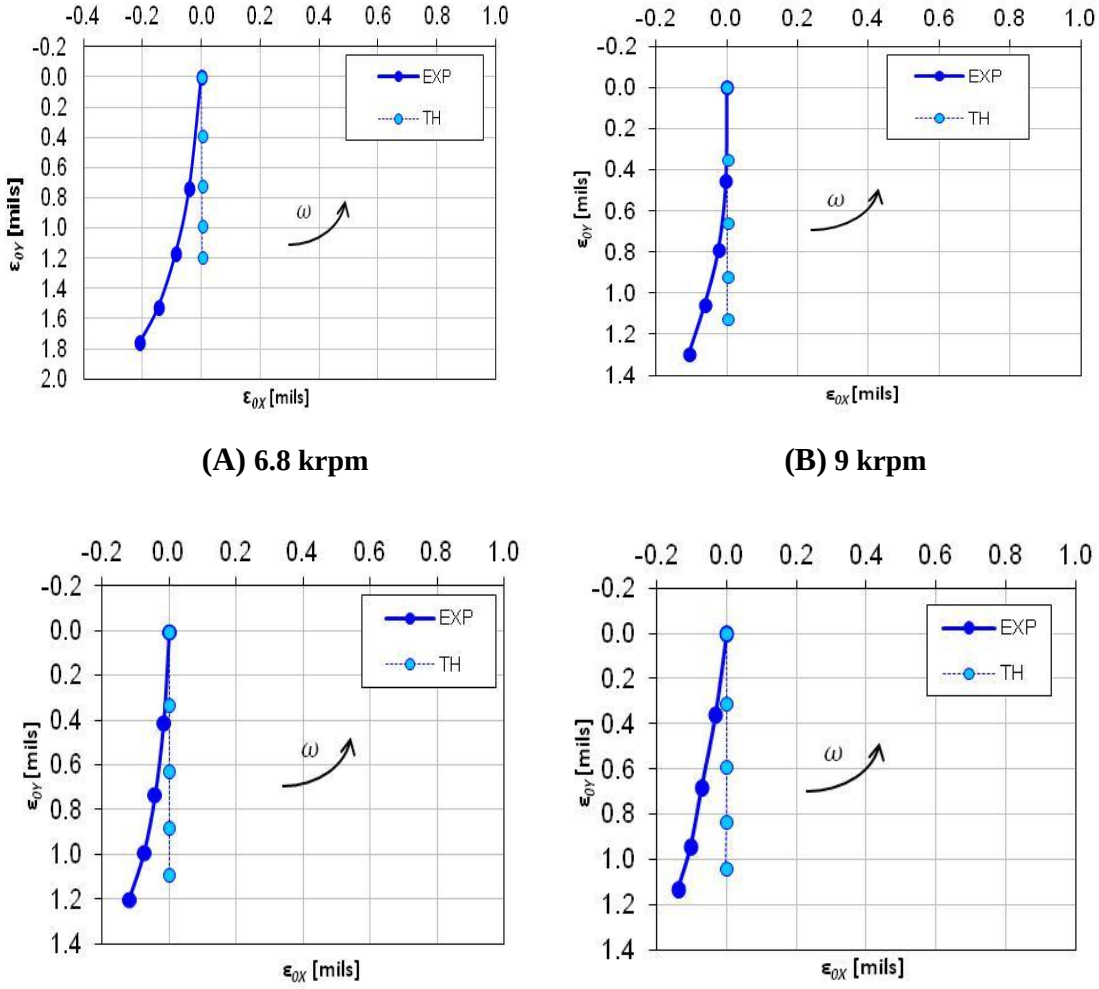

(A) 6.8 krpm **(B) 9 krpm**

(C) 10.8 krpm **(D) 13.2 krpm**

Figure 25: LOP Bearing Loci

At low speeds, the ε_o predictions are less than measured values. At higher speeds, the ε_o predictions are more accurate. The predicted bearing loci plots show less movement in the ε_{oy} direction than measurements, predicting a stiffer bearing. Comparing these predictions to the measured load-versus-deflection curve in Figure 21 showed that the loci predictions were in fact more flexible than the measured load-versus-deflection curve from the pad-stator probes. The measured load-versus-deflection curve from the pad-stator probes was used as a numerical input for the pivot stiffness of Code A. At all speeds, the unpredicted lateral displacement ε_{ox} is substantial. Note that a change in ε_o and ϕ_o can be attributed to a change in probe length due to temperature, suggested by Wilkes and Childs [15]. In ideal conditions, a lateral displacement from the loaded *y* axis indicates cross-coupled stiffness.

The LBP loci plots are presented in Figure 26.

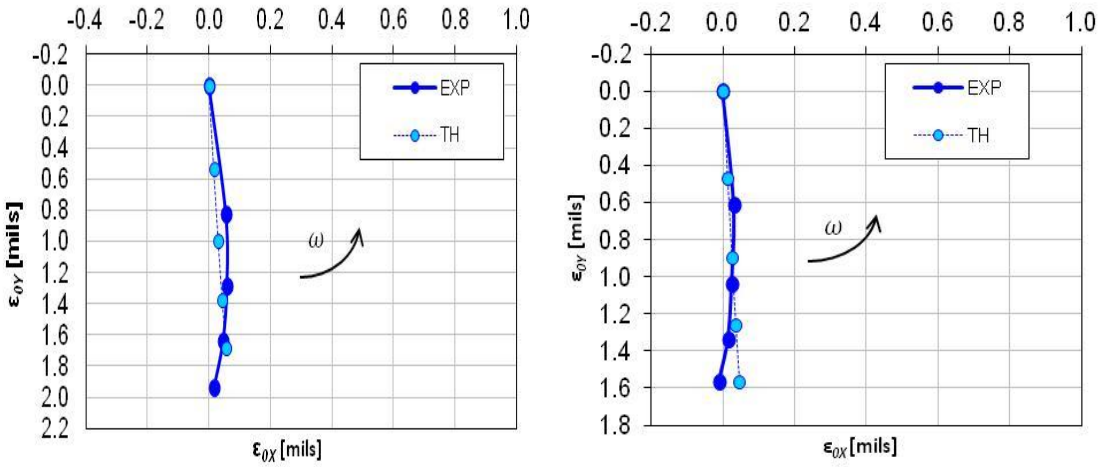

(A) 6.8 krpm **(B) 9 krpm**

Figure 26: LBP Bearing Loci

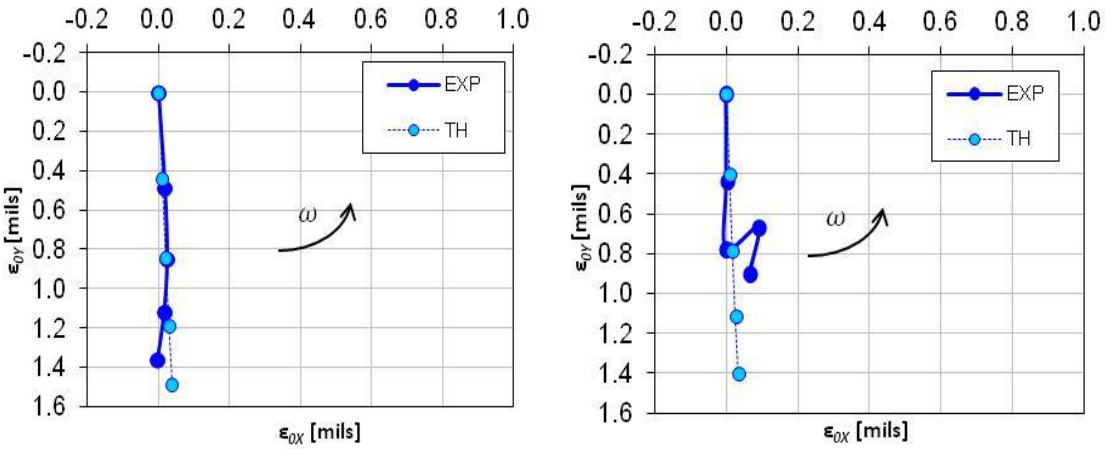

(C) 10.8 krpm **(D) 13.2 krpm**

Figure 26: Continued

For high speeds, the eccentricity is predicted well and better than the LOP plots. Except for the deviation experienced in Figure 26(D), the eccentricity predictions are more accurate for LBP than LOP. Overall, the lateral displacement from the loaded *y* axis or cross-coupling is less significant in the LBP orientation.

The measured and predicted attitude angles for the LOP configuration are presented in Figure 27.

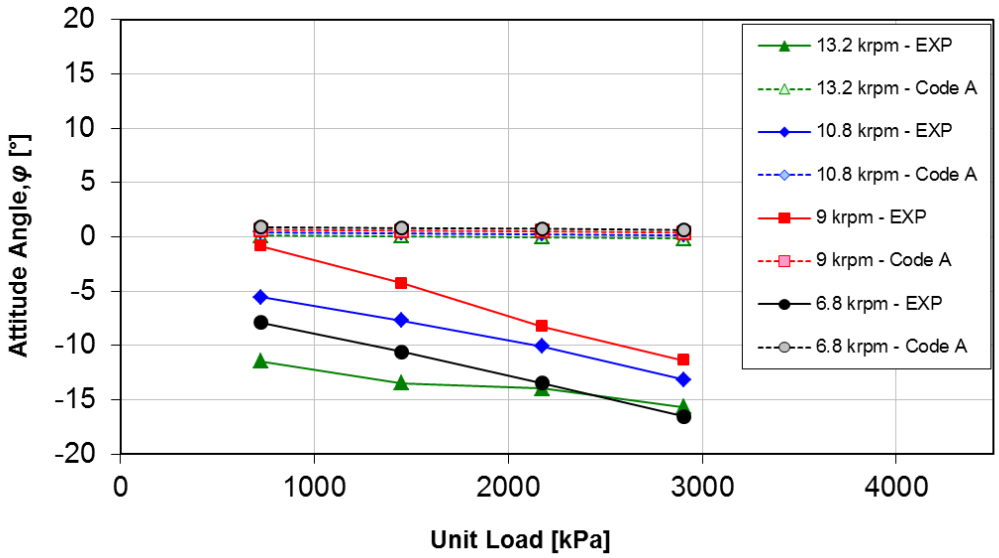

Figure 27: Measured and Predicted Attitude Angles LOP Orientation

For the most part, the measured attitude angle in the LOP orientation decreases (is more negative) with increasing load. The measured values are considerably different from the predicted attitude angles by Code A, which are approximately zero. From fluid rotation, typical attitude angles in fixed-arc bearings are expected to be positive and result from rotor movement in the same transverse direction as shaft rotation. Appendix D shows that all experimental K_{xy} and K_{yx} coefficients are negative (same sign), and thus do not promote instability.

The measured and predicted attitude angles for the LBP configuration are presented in Figure 28.

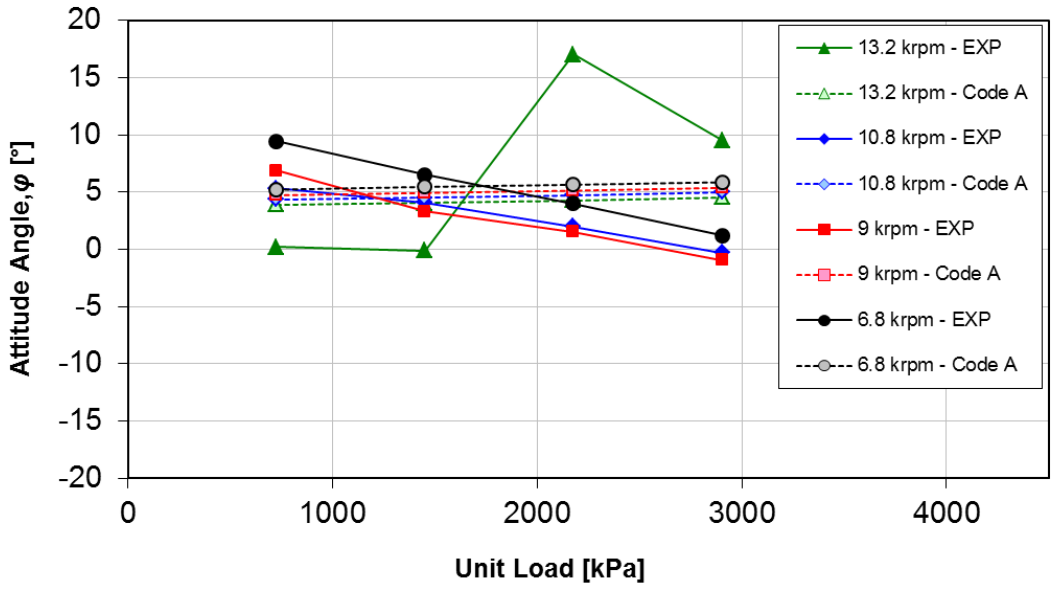

Figure 28: Measured and Predicted Attitude Angles LBP Orientation

In the LBP orientation, the measured attitude angle decreases (more negative) with speed and load, except at 13.2 krpm. The predicted values slightly increase as load increases. The measured values decrease through the predicted values. Code A's LBP predicted values are more accurate than the LOP. Overall, both conditions show that the measured cross-coupling effects between the *x* and *y* direction are significant.

Pad Metal Temperatures

Embedded thermocouples provide pad metal temperature just below the surface of the Babbitt. Measured surface temperatures provide an idea of the lubricant temperatures experienced during testing. Figure 29 shows the 21 thermocouples used during testing. All pad temperature data are given in Appendix B.

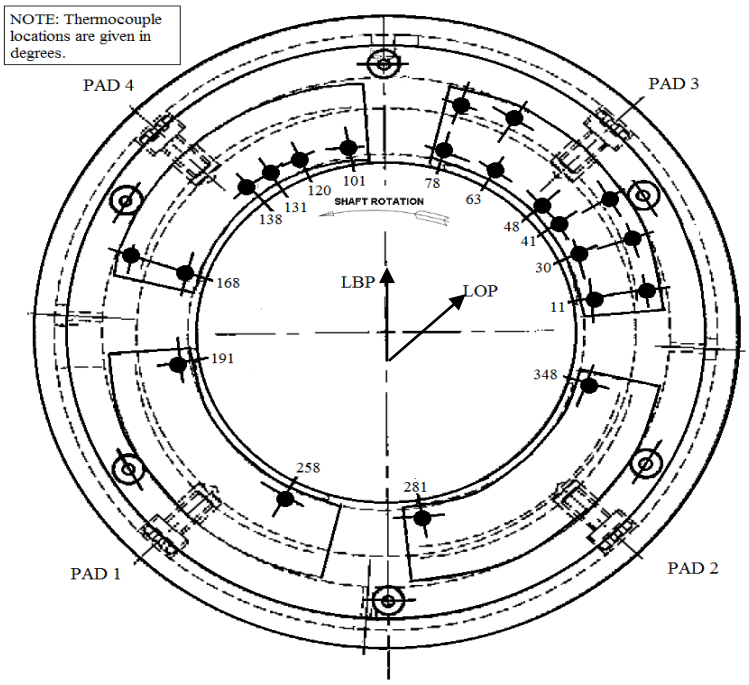

Figure 29: Pad Thermocouple Diagram

LOP Circumferential Temperature Gradient

Figure 30 shows all of the thermocouple readings in the LOP orientation at a rotor speed of 6.8 krpm and 13.2 krpm.

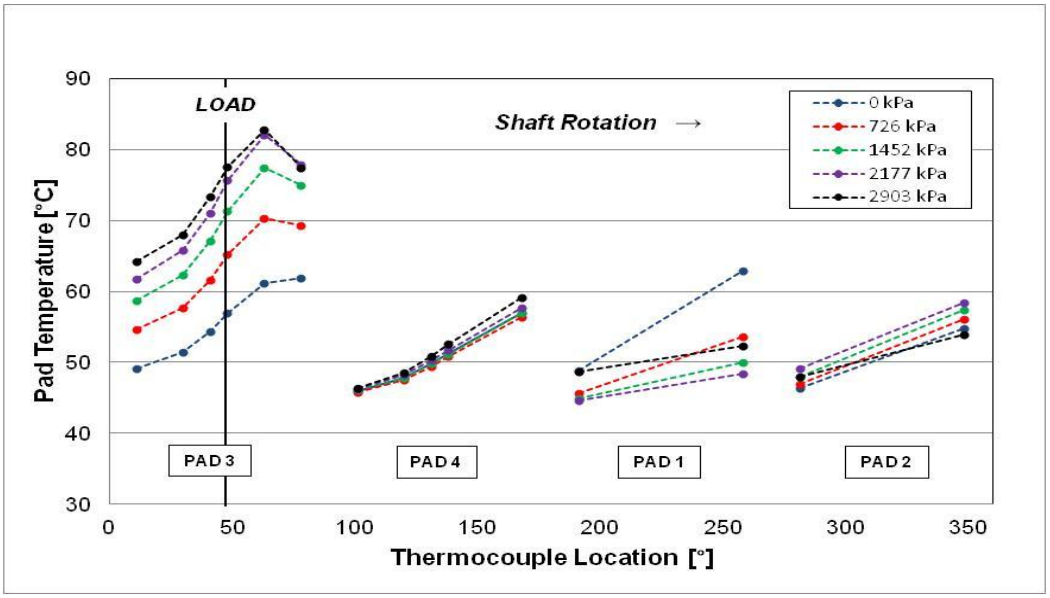

(A) 6.8 krpm

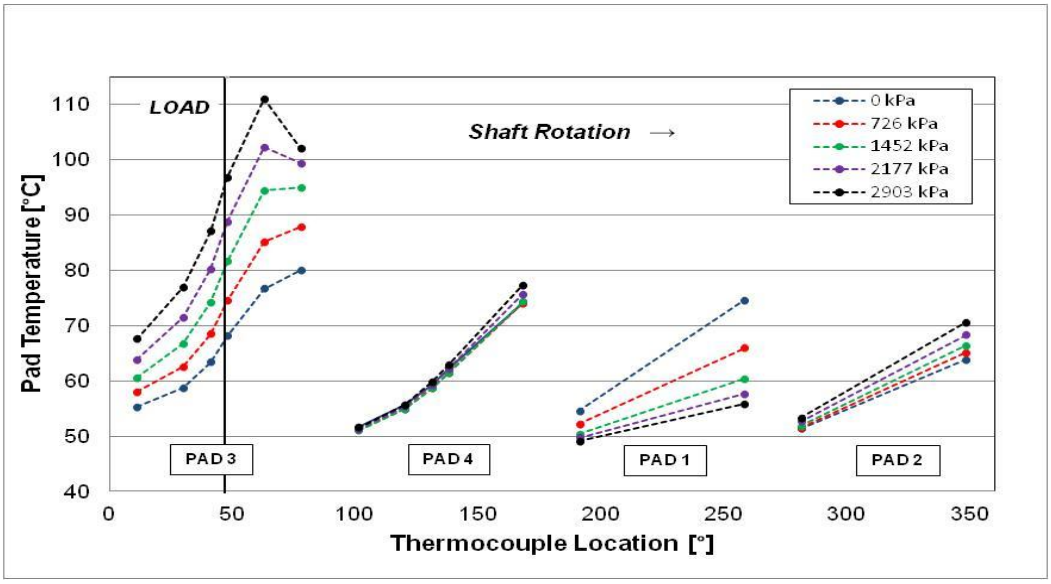

(B) 13.2 krpm

Figure 30: LOP Measured Pad Bearing Temperatures

The loaded pad has higher temperatures than the remaining three pads (supporting more of the static unit load), and the temperature increases circumferentially

across the pad with shaft rotation (from leading to trailing edge of the pads). The remaining 3 pads experienced similar temperature measurements for a certain rotor speed or load.

To compare measured temperatures to predictions, Code A predicts the temperature distribution for the lubricant at a circumferential angle. Code A accounts for the thermal effects in fluid flow via the energy transport equation. Note that Code A predicts the *lubricant's* temperature, but *pad* metal temperatures are measured. Input for Code A can be found in Table 2 for bearing parameters, Table 7 and Table 8 for hot bearing clearances, and the Predictions section for pivot flexibility.

Figure 31 shows the measured and predicted pad temperatures at 6.8 krpm.

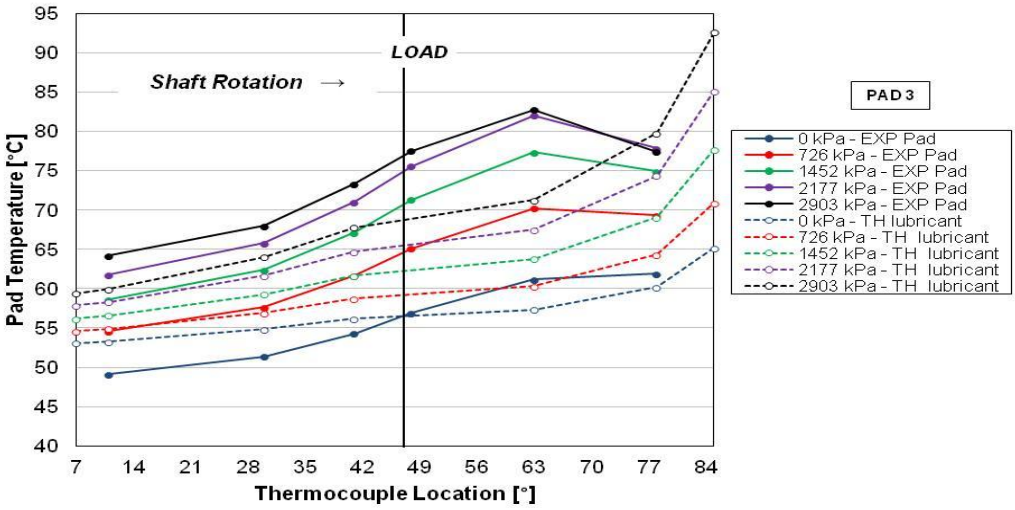

(A) Pad 3 (Loaded Pad)

Figure 31: LOP Measured Pad and Predicted Lubricant Temperatures at 6.8 krpm

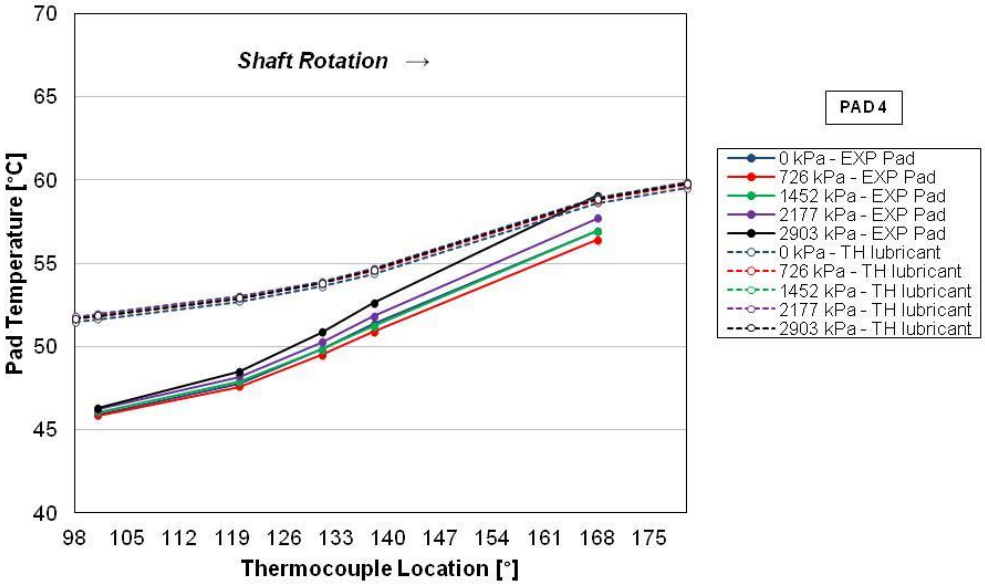

(B) Pad 4 (Following Loaded Pad)

Figure 31: Continued

The code also predicts a circumferential temperature increases with increasing load. For the loaded pad, all pad temperatures are slightly lower than predicted lubricant temperatures, except the unloaded case. Predicted lubricants temperature should be slightly greater that the pad's metal temperatures.

Thermocouple readings from pad 4 (following the loaded pad) show similar results in that measurements and predictions both show a circumferential temperature increase. Measured temperatures for pad 4 were over-predicted regardless of load or location. Temperatures for pads one and two are given in Appendix B.

Figure 32 shows the measured and predicted pad temperatures at 13.2 krpm.

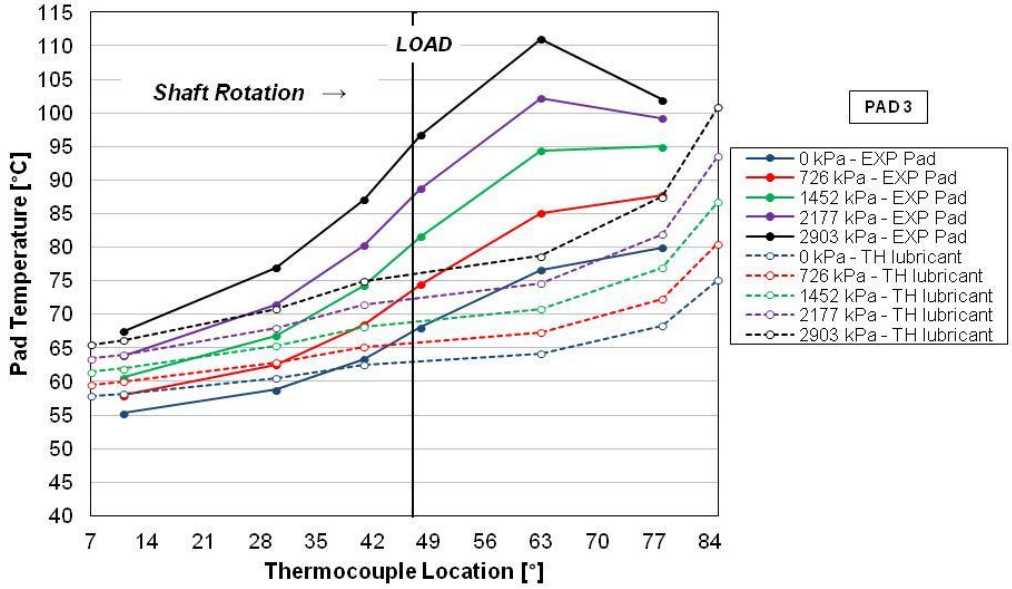

(A) Pad 3 (Loaded Pad)

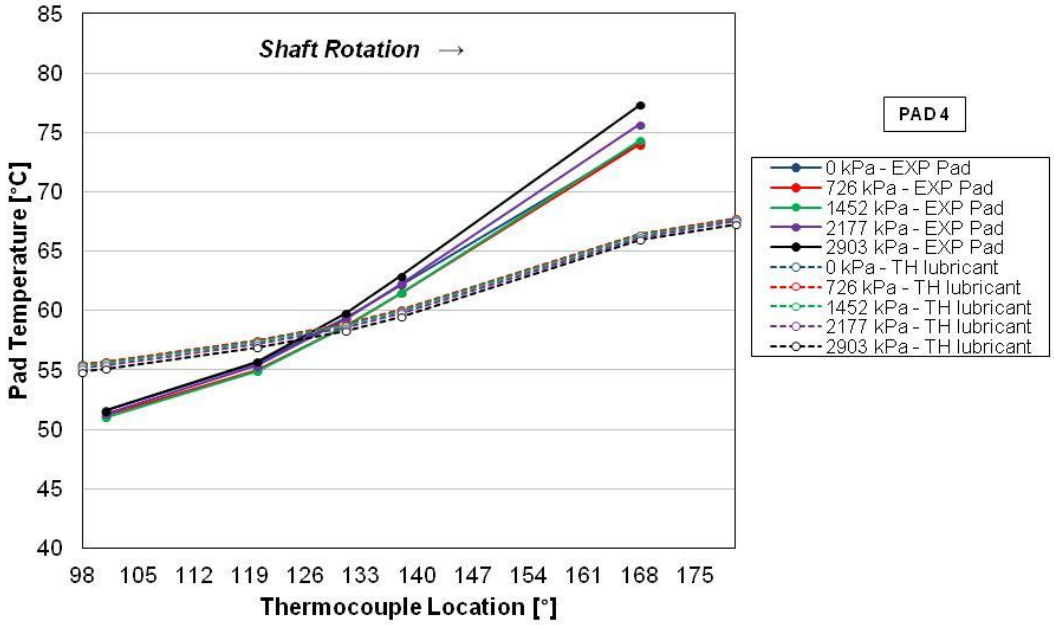

(B) Pad 4 (Following Loaded Pad)

Figure 32: LOP Measured Pad and Predicted Lubricant Temperatures at 13.2 krpm

Similar to the 6.8 krpm case, the code predicts that pad temperature increases circumferentially in the direction of shaft rotation. The measured and predicted temperatures increase with increasing load. For the loaded pad, all temperatures are under-predicted except for the thermocouple at the leading edge of the pad. In pad 4, the temperatures are over-predicted at the leading edge of the pad and under predicted at the trailing edge of the pad. Predictions at 13.2 krpm are more accurate than predictions at 6.8 krpm.

LBP Circumferential Temperature Gradient

Figure 33 shows the circumferential temperature gradient at 6.8 krpm and 13.2 krpm in the LBP orientation. The static load is applied between pad 3, (loaded pad in LOP orientation) and pad 4. In looking back, Figure 15 shows that since the bearing is non-symmetric, pad 4 supports more of the unit load in the LBP configuration and may result in higher temperature measurements. Note that in Figure 33(A), the temperature at the leading edge of pad 3 is greater than the temperature at the leading edge of pad 4. This finding is interesting since the temperature at the leading edge of the pad is typically controlled by the oil inlet temperature, and results in similar temperature measurements at the leading edge between pads. The LBP 6.8 krpm test, is the only condition where these findings were made.

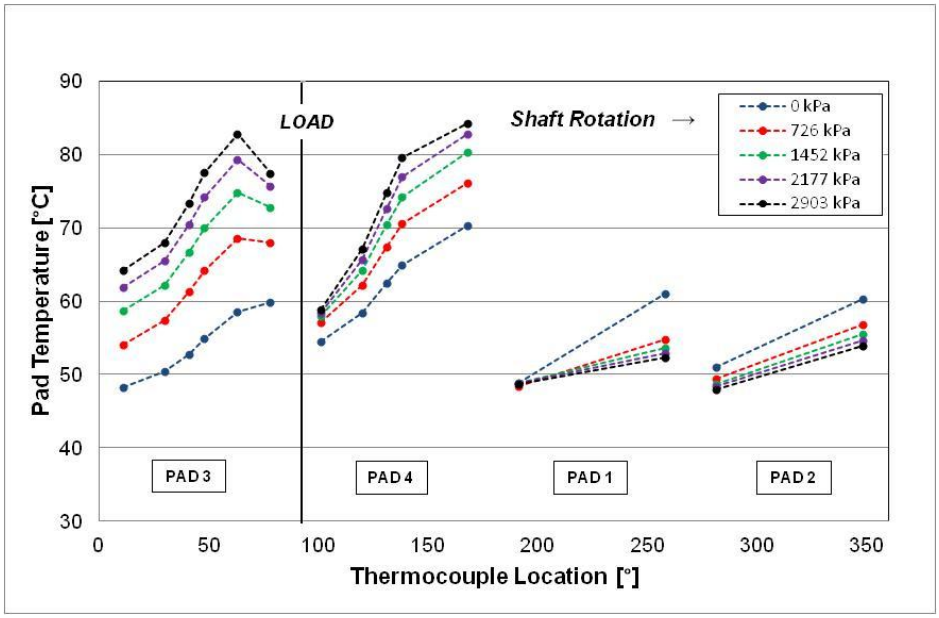

(A) 6.8 krpm

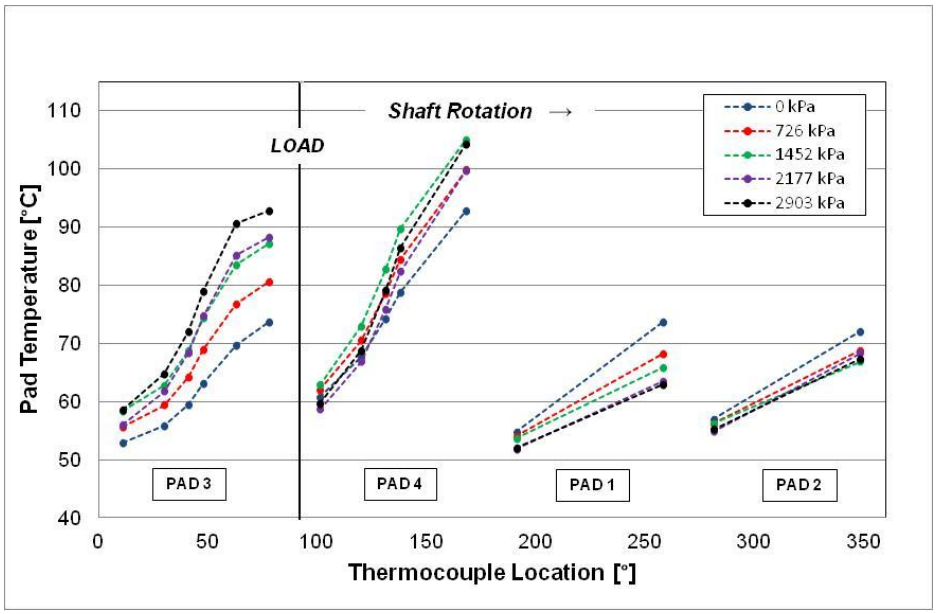

(B) 13.2 krpm

Figure 33: LBP Measured Pad Bearing Temperatures

Similar to the LOP orientation, the temperature increases circumferentially along the pad with shaft rotation (from leading to trailing edge of the pads). Pad 4 does have slightly higher temperature measurements than pad 3, showing that pad 4 did support more of the applied load in the LBP orientation.

Figure 34 shows the LBP measured and predicted pad temperatures at 6.8 krpm.

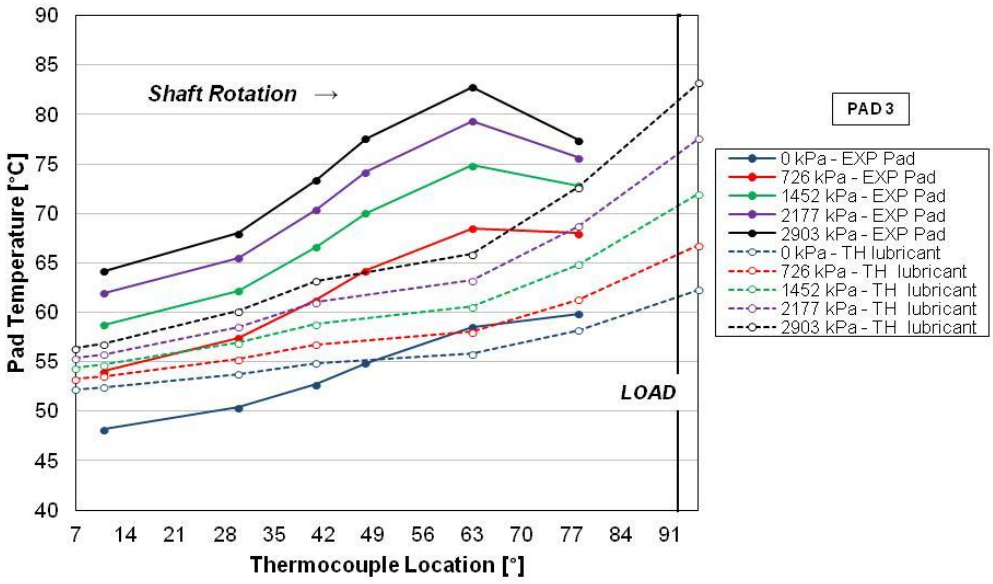

(A) Pad 3

Figure 34: LBP Measured Pad and Predicted Lubricant Temperatures at 6.8 krpm

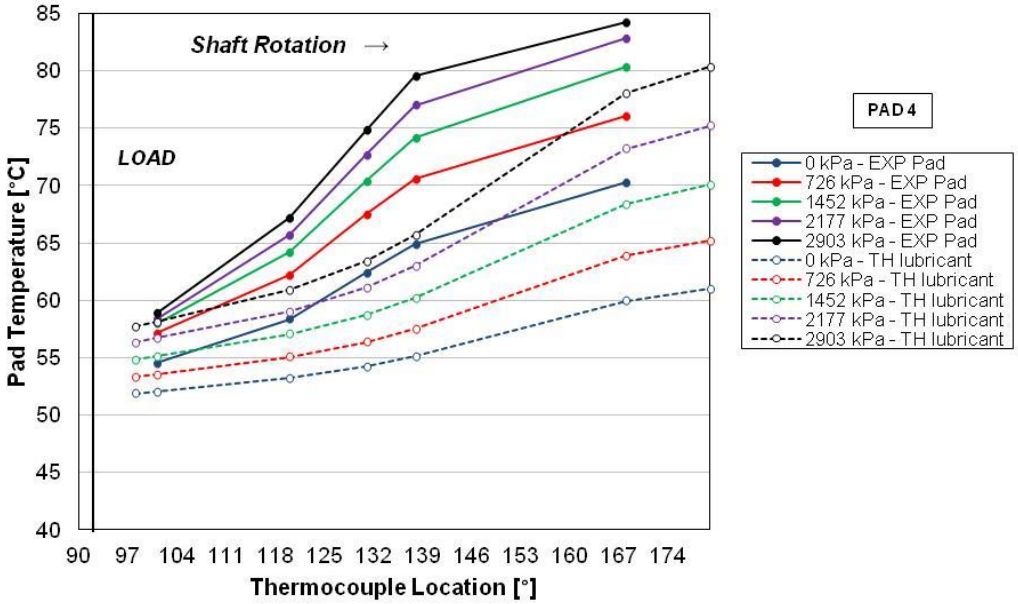

(B) Pad 4

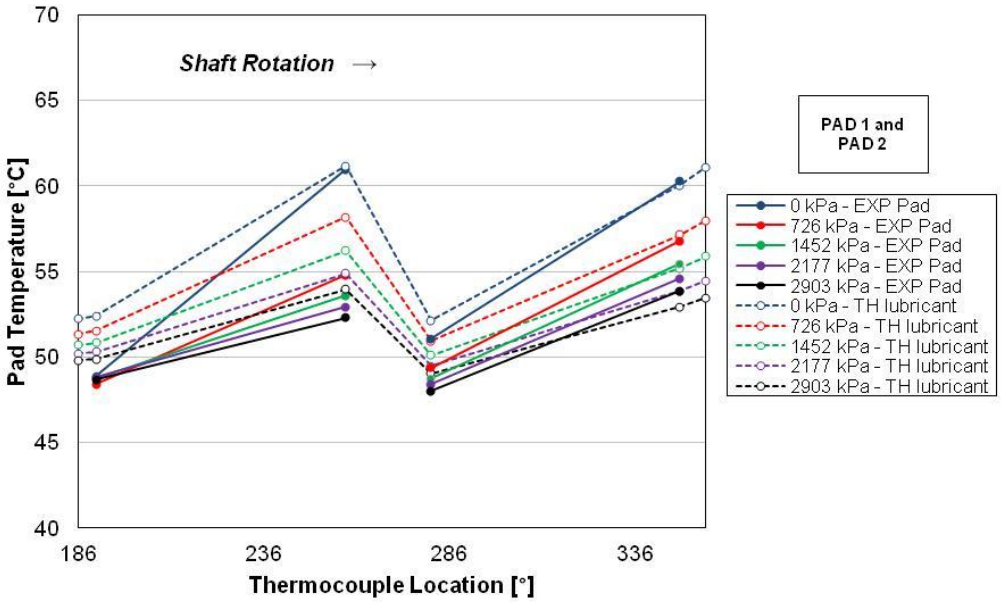

(C) Pad 1 and Pad 2

Figure 34: Continued

Except for pads 1 and 2, most measured pad metal temperatures are lower than predicted. Pad 4 shows the largest difference from measurements to predictions. Agreeing with measurements, predictions showed pad 4 to experience greater temperatures than pad 3. Figure 34(C) shows the temperature drop from the trailing edge of pad 1, to the leading edge of pad 2. Pads 1 and 2 were generally predicted higher than measurements.

Figur shows the LBP measured and predicted pad temperatures at 13.2 krpm.

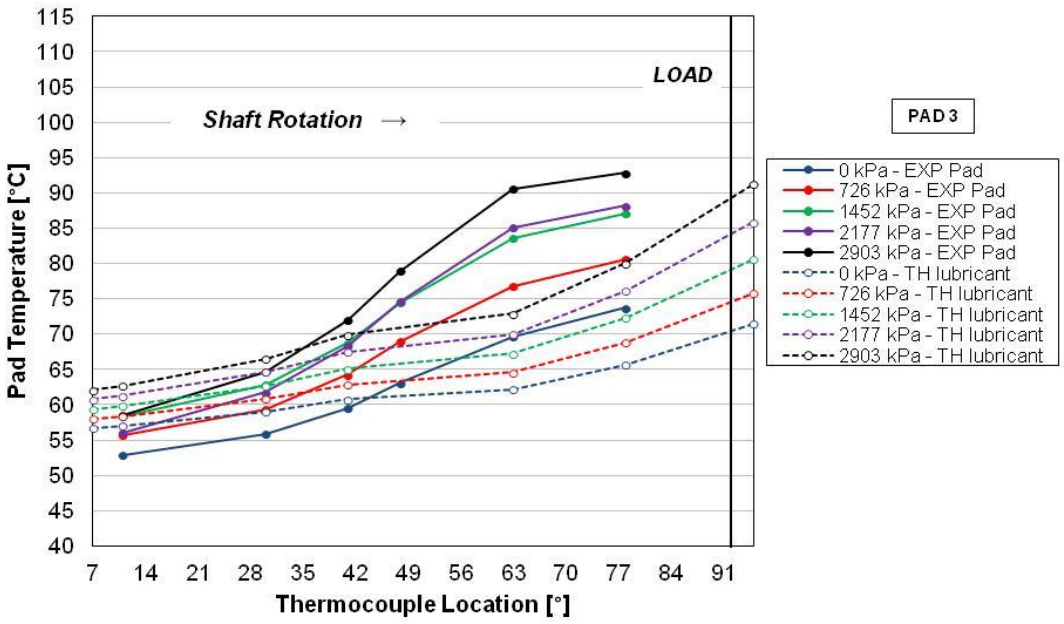

(A) Pad 3

Figure 35: LBP Measured Pad and Predicted Lubricant Temperatures at 13.2 krpm

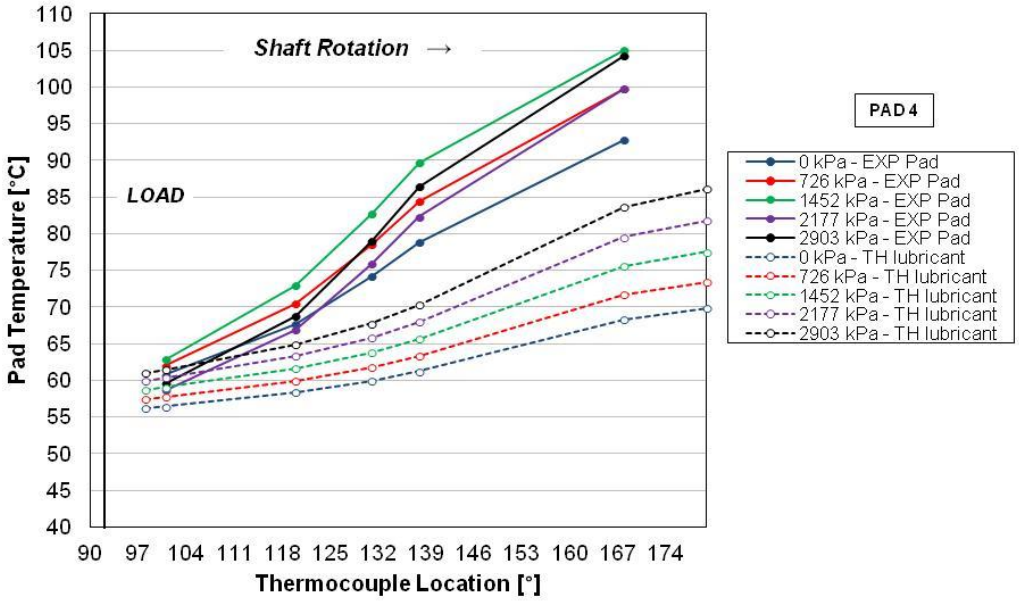

(B) Pad 4

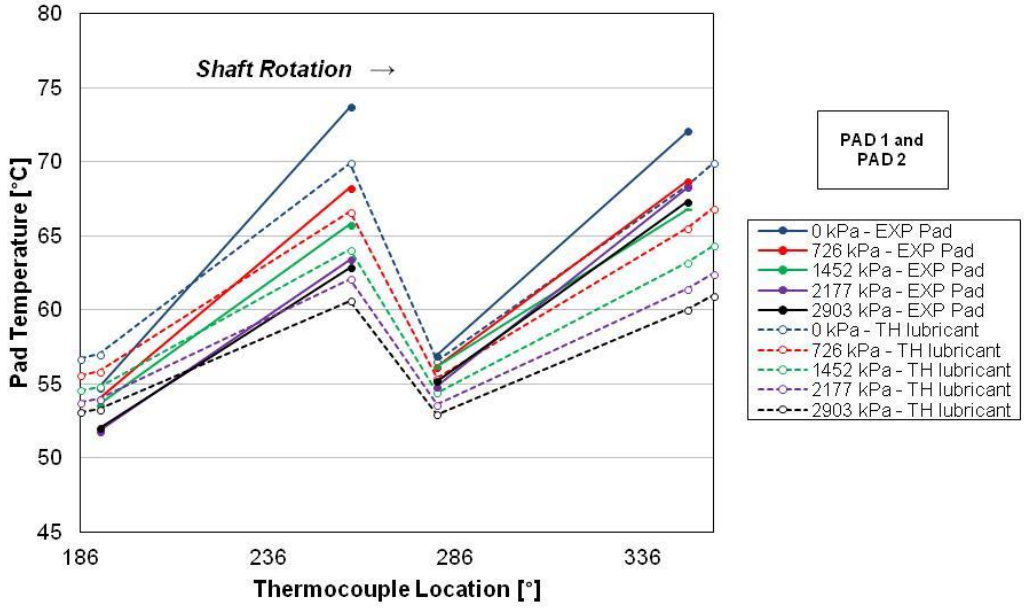

(C) Pad 1 and Pad 2

Figure 35: Continued

As with the 6.8 krpm case, the code predicts that pad temperature increases circumferentially in the shaft rotation direction in the loaded pad and increases with increasing load. The figure also shows that pad 4 supports more of the static load, and as speed increases, there is more of a temperature difference in measurements between pad 3 and 4. Predictions are more accurate at the leading edge of the pads. Figur(C) shows the temperature drop from the trailing edge of pad 1, to the leading edge of pad 2. Pads 1 and 2 were predicted well.

Estimated Power Loss

Estimated power loss values are obtained from an energy-balanced equation assuming adiabatic conditions, Eq. (31)

$$Power_{Loss} = Q_{ave}(T_{out}\rho_{out}c_{p,out} - T_{in}\rho_{in}c_{p,in}) \tag{31}$$

where Q_{ave}, ρ, $c_{p,}$ and T are the mass flow rate (m^3/s), the oil density(kg/m^3), the specific heat (J/(kg-K)), and the oil temperature (K), respectively [13]. Figure 36 shows the estimated and predicted power loss from Code A, using temperature measurements for the LOP and LBP orientations.

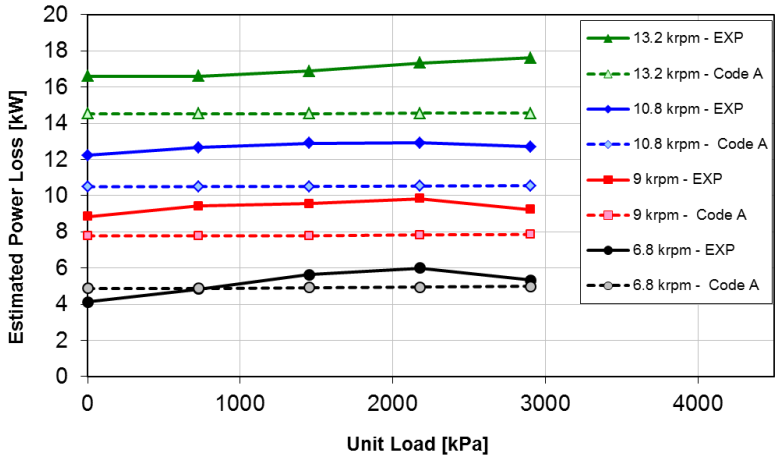

(A) LOP

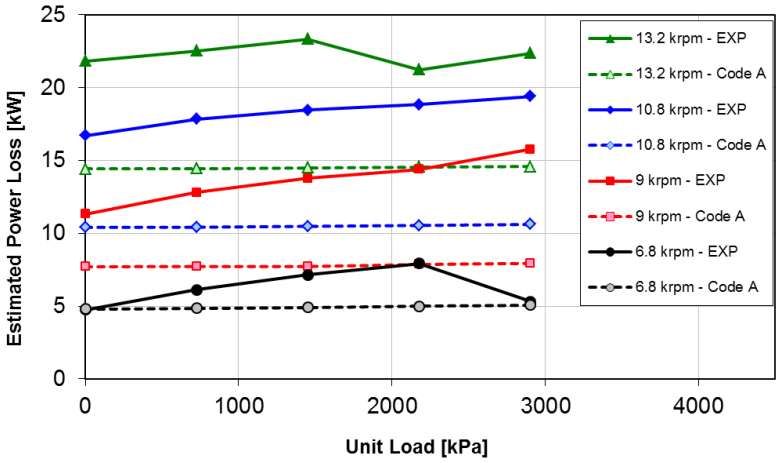

(B) LBP

Figure 36: Estimated and Predicted Power Loss

As can be seen, the power loss predictions are lower than the estimated power loss in both the LOP and LBP orientation. The predictions are modeled independently from load. For the most part, the LOP power loss is independent of load while the LBP power loss shows a slight increase as load increases. Similar to measurements, Code A predicts that power loss increases with speed.

DYNAMIC RESULTS

The following sections provide the experimental and theoretical stiffness, damping, and virtual-mass data for the 4-pad, rocker-pivot TPJB in LOP and LBP configuration. Appendix D presents the rotordynamic coefficients for all tested speeds and loads, while Appendix H presents the dynamic data used to determine the rotordynamic coefficients. The predicted values in the dynamic stiffness sections were obtained from the perturbation model created in Wilkes and Childs [18]. Predictions from both Code A and Code B for stiffness and damping coefficients will be compared to measurements. Input parameters to prediction codes can be found in the Prediction section. A major difference between codes is that Code B incorporates *pad* flexibility in predicting the impedance coefficients for a tilting-pad journal bearing. The effects that *pad* flexibility has on predictions will be discussed in the following sections.

Looking back to EXPERIMENTAL PROCEDURES, the dynamic stiffness functions are written in terms of the rotordynamic coefficients:

$$\boldsymbol{H_{ij}} = \left(K_{ij} - \Omega^2 \mathrm{M_{ij}}\right) + \boldsymbol{j}\left(\Omega C_{ij}\right) \tag{10}$$

$$Re\left(\boldsymbol{H_{ij}}\right) = K_{ij} - \Omega^2 \mathrm{M_{ij}} \tag{11}$$

$$Im\left(\boldsymbol{H_{ij}}\right) = \Omega C_{ij} \tag{12}$$

Dynamic Stiffness

The following section presents the measured and predicted dynamic stiffness functions for the LOP orientation. The conditions shown include rotor speeds of 6.8 and

13.2 krpm with a light static load of 725 kPa (105.3 psi) and a large unit load of 2903 kPa (421.1 psi). Predictions are generated using Code B. For the best curve fit and to obtain the most precise predictions, erratic data especially at high frequencies (>250 Hz) were discarded. This is mainly true for lightly loaded cases. The baseline results, shown in Figure 12 and Figure 13, were subtracted from the dynamic stiffness to obtain the dynamic response of the fluid-film only. Input for Code B can be found in Table 2 for bearing parameters, Table 7 and

for hot bearing clearances, and the Predictions section for pivot stiffness and pad flexibility. For brevity, the results for the LBP dynamic stiffness can be found in Appendix F.

LOP Dynamic Stiffness

Figure 37 presents the experimental and predicted dynamic stiffness functions for the LOP orientation at 6.8 krpm with a 725 kPa unit load. Figure 37 (A) shows the real dynamic stiffness functions, while Figure 37 (B) shows the imaginary dynamic stiffness functions. Both figures depict the direct and cross-coupled dynamic stiffness functions. Note that the impedances shown in the following figures represent complex numbers, and that the static load is being applied in the *y*-direction. The running speed for each test condition is represented by ω, and is shown by a black vertical line.

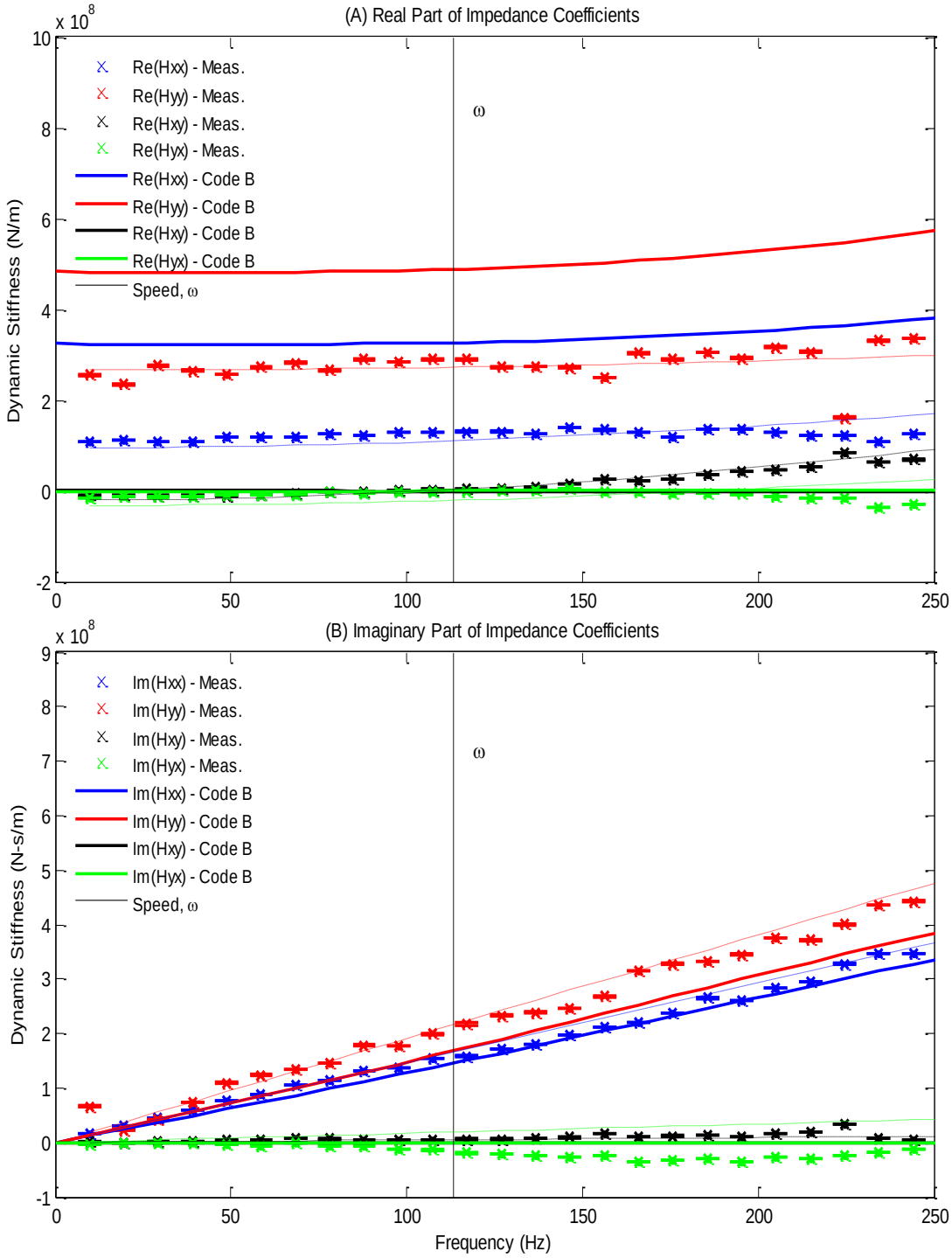

Figure 37: LOP Components of Measurements and Predicted (Code B) Bearing Impedance Coefficients at 6.8 krpm with 725 kPa (105.3 psi) Static Load

In Figure 37(A), measured Re($\boldsymbol{H_{yy}}$) is larger than measured Re($\boldsymbol{H_{xx}}$) and shows stiffness orthotropy. The measured dynamic stiffness shows a very slight dependence on Ω. At around running speed (150 Hz), Re($\boldsymbol{H_{xy}}$) becomes slightly larger than Re($\boldsymbol{H_{yx}}$). At larger frequencies Re($\boldsymbol{H_{xy}}$) and Re($\boldsymbol{H_{yx}}$) have opposite signs, suggesting different signs for M_{xy} and M_{yx} with a possible impact on stability (See Whirl Frequency Ratio).

Figure 37(B) shows that the direct imaginary dynamic stiffness functions increases linearly with increasing frequency, resulting in frequency-independent direct damping coefficients. Measured Im($\boldsymbol{H_{yy}}$) is larger than measured Im($\boldsymbol{H_{xx}}$). Im($\boldsymbol{H_{xy}}$) is slightly larger than Im($\boldsymbol{H_{yx}}$), and both terms are negative.

Figure 37 shows that the model does well at predicting damping, but over-predicts stiffness. Measured stiffness coefficients are smaller than predicted at all frequencies, while damping is modestly larger than predicted at high frequencies. The over-predicted Re($\boldsymbol{H_{xx}}$) and Re($\boldsymbol{H_{yy}}$) values agree with the under-predicted bearing loci plots, shown in Figure 25(A). The predicted bearing loci plots show less movement in the ε_{oy} than measurements, typically resulting in greater Re($\boldsymbol{H_{xx}}$) and Re($\boldsymbol{H_{yy}}$) predictions. The magnitude differences between Re($\boldsymbol{H_{xx}}$) and Re($\boldsymbol{H_{yy}}$) is predicted well. At around 100 Hz (close to running speed) the stiffness predictions begin to increase as Ω increases. Im($\boldsymbol{H_{xx}}$) is predicted very accurately and Im($\boldsymbol{H_{yy}}$) is slightly predicted under measurements. The code predicts real and imaginary cross-coupled dynamic stiffness to be zero, which does not match measured results at high frequencies.

Figure 38 presents the experimental and predicted dynamic stiffness functions for the LOP orientation 6.8 krpm and 2903 kPa unit load

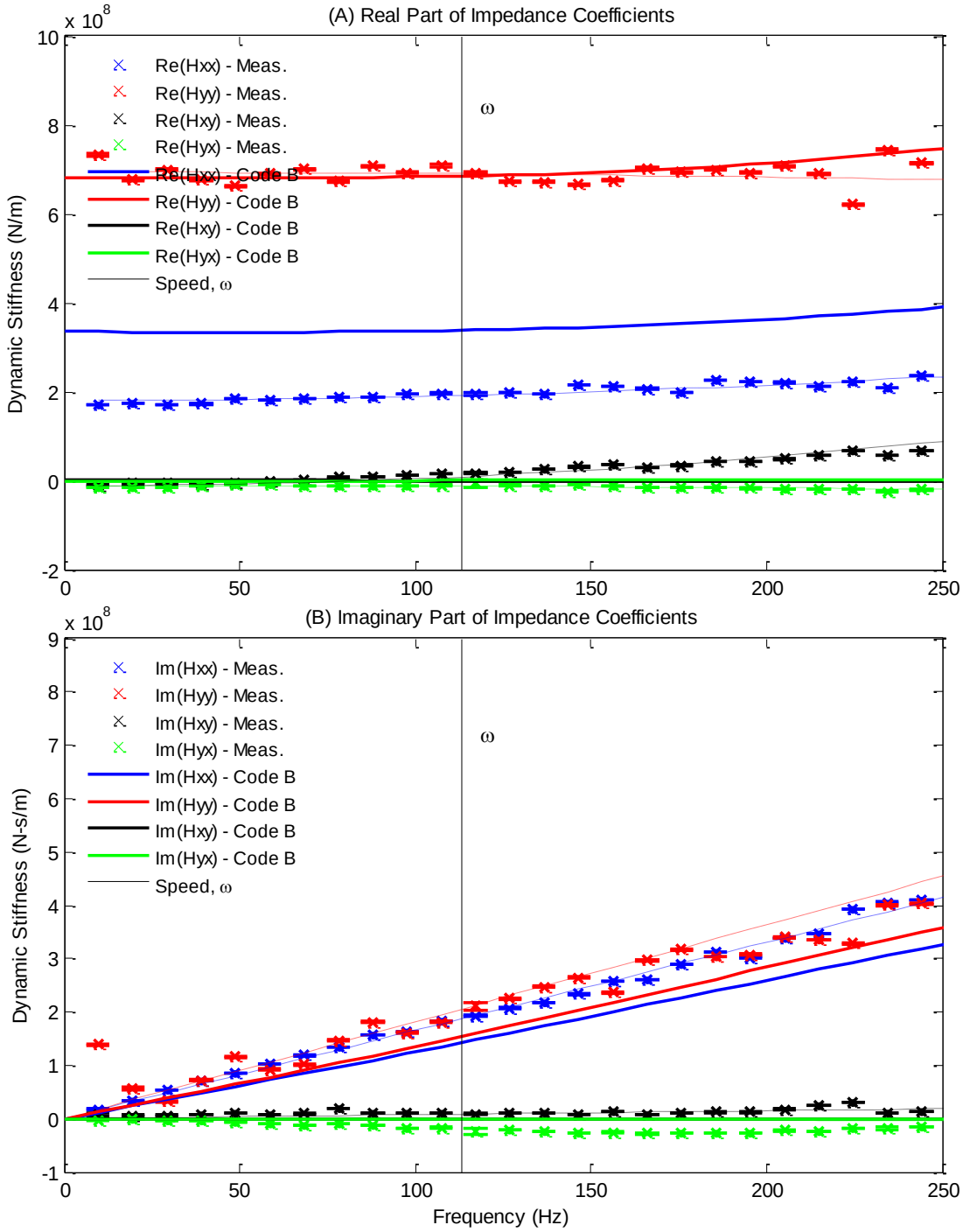

Figure 38: LOP Components of Measurements and Predicted (Code B) Bearing Impedance Coefficients at 6.8 krpm with 2903 kPa (421.1 psi) Static Load

Similar to the lightly loaded case but to a larger degree, measured Re($\boldsymbol{H}_{yy}$) is larger than measured Re($\boldsymbol{H}_{xx}$), showing significant stiffness orthotropy. Measured Re($\boldsymbol{H}_{xx}$) and Re($\boldsymbol{H}_{yy}$) have no dependency on Ω. Similar to the lightly loaded case, around running speed (113.3 Hz), Re($\boldsymbol{H}_{xy}$) becomes slightly larger than Re($\boldsymbol{H}_{yx}$). At larger frequencies Re($\boldsymbol{H}_{xy}$) and Re($\boldsymbol{H}_{yx}$) have opposite signs. Im($\boldsymbol{H}_{xx}$) and Im($\boldsymbol{H}_{yy}$) are measured to be the same. The cross-coupled damping terms are approximately zero. At higher frequencies, Im($\boldsymbol{H}_{xy}$) and Im($\boldsymbol{H}_{yx}$) have opposite signs.

Figure 38 shows that the model more accurately predicts dynamic stiffness at the higher loaded case. Re($\boldsymbol{H}_{yy}$) is predicted very accurately, while Re($\boldsymbol{H}_{xx}$) is predicted higher than measurements. The predicted Re($\boldsymbol{H}_{xx}$) and Re($\boldsymbol{H}_{yy}$) values are more accurate than the under-predicted bearing loci plots, shown in Figure 25(A). The difference in magnitudes between Re($\boldsymbol{H}_{xx}$) and Re($\boldsymbol{H}_{yy}$) is predicted well. The code predicts Re($\boldsymbol{H}_{xy}$) and Re($\boldsymbol{H}_{yx}$) to be zero which does not match measurements at high frequencies. Im($\boldsymbol{H}_{yy}$) and Im($\boldsymbol{H}_{xx}$) are slightly under-predicted.

Figure 39 and Figure 40 show that the model follows the same trend with increasing speed, but with a better accuracy.

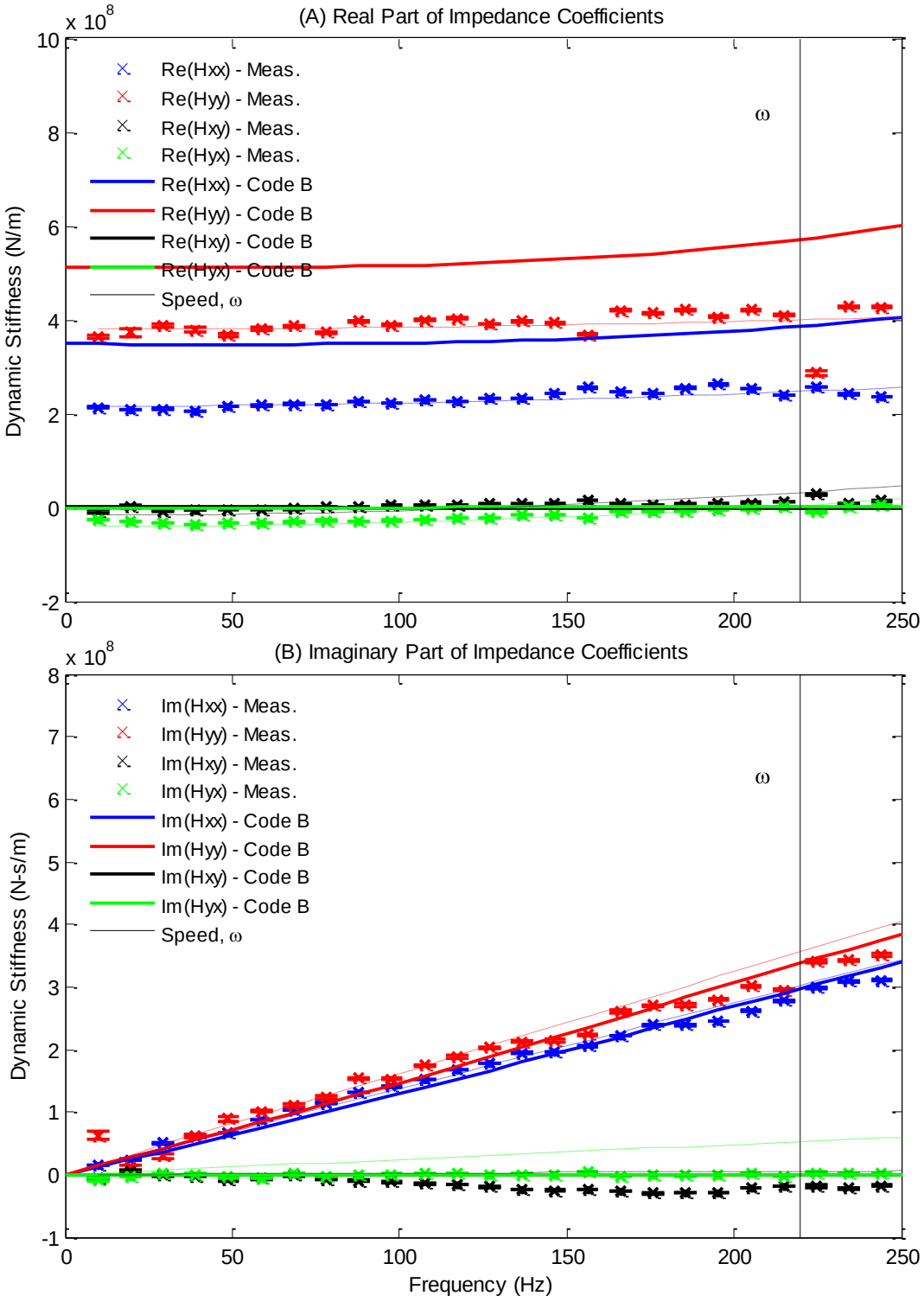

Figure 39: LOP Components of Measurements and Predicted (Code B) Bearing Impedance Coefficients at 13.2 krpm with 725 kPa (105.3 psi) Static Load

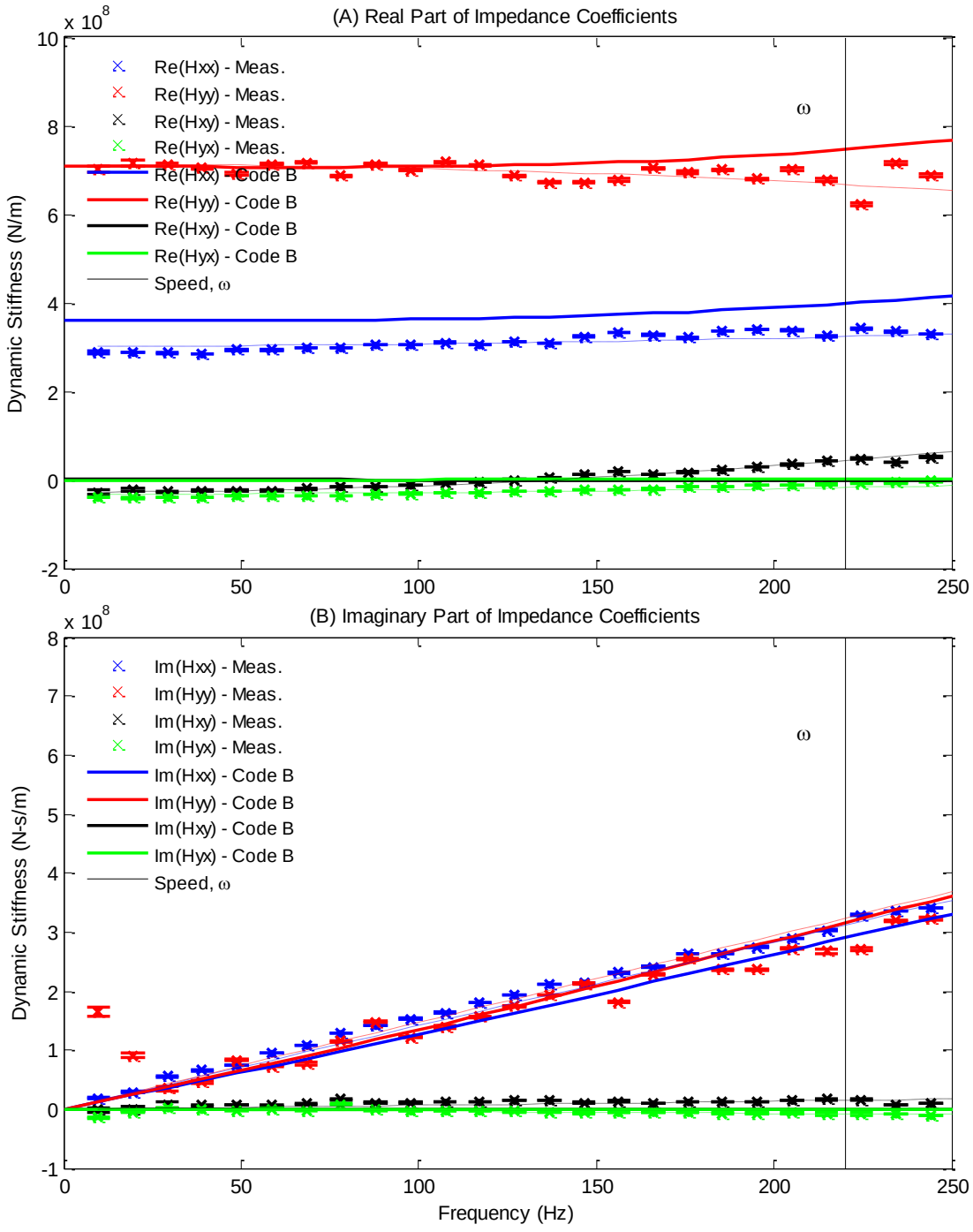

Figure 40: LOP Components of Measurements and Predicted (Code B) Bearing Impedance Coefficients at 13.2 krpm with 2903 kPa (421.1 psi) Static Load

Similar to 6.8 krpm results (Figure 37 and Figure 38), at 13.2 krpm Re($\boldsymbol{H}_{yy}$) is measured to be larger than Re($\boldsymbol{H}_{xx}$) and show stiffness orthotropy. In the lightly loaded case, the measured dynamic stiffness coefficients show a slight dependence on Ω, while the loaded dynamic stiffness shows no dependence. Re($\boldsymbol{H}_{xy}$) is slightly larger than Re($\boldsymbol{H}_{yx}$) in the heavily loaded case. At larger frequencies Re($\boldsymbol{H}_{xy}$) and Re($\boldsymbol{H}_{yx}$) have opposite signs.

Both figures show that Im($\boldsymbol{H}_{xx}$) and Im($\boldsymbol{H}_{yy}$) increase linearly with increasing frequency, resulting in frequency-independent direct damping coefficients. In the unloaded case, Im($\boldsymbol{H}_{yy}$) is slightly larger than Im($\boldsymbol{H}_{xx}$) while the opposite is true in the loaded case. In the lightly loaded case, Im($\boldsymbol{H}_{yx}$) is slightly larger than Im($\boldsymbol{H}_{xy}$).

At low loads, the model predicts damping well, but over-predicts stiffness. Stiffness is predicted much more accurately at the higher speed and load combination. Re($\boldsymbol{H}_{yy}$) is predicted very accurately, while Re($\boldsymbol{H}_{xx}$) is slightly smaller than predicted. Similar to 6.8 krpm at low loads, the over-predicted Re($\boldsymbol{H}_{xx}$) and Re($\boldsymbol{H}_{yy}$) values agree with the under-predicted bearing loci plots, shown in Figure 25(D). At low static loads the predicted bearing loci plots show less movement in the ε_{oy} than measurements, typically resulting in greater Re($\boldsymbol{H}_{xx}$) and Re($\boldsymbol{H}_{yy}$) predictions. The magnitude differences between Re($\boldsymbol{H}_{xx}$) and Re($\boldsymbol{H}_{yy}$) is predicted well. Orthotropy is predicted reasonably well at the higher rotor speed. Again, at around 100 Hz, Re($\boldsymbol{H}_{xx}$) and Re($\boldsymbol{H}_{yy}$) begin to increase with frequency. Im($\boldsymbol{H}_{yy}$) and Im($\boldsymbol{H}_{xx}$) predictions are very accurate. In both cases the code predicts Re($\boldsymbol{H}_{xy}$) and Re($\boldsymbol{H}_{yx}$) to be zero which does not match results at high frequencies.

Results for the LBP dynamic stiffness are not shown for brevity, and can be found in Appendix F. For LOP and LBP cases, the Re($\boldsymbol{H}_{xx}$), Re($\boldsymbol{H}_{yy}$), Re($\boldsymbol{H}_{xy}$), and Re($\boldsymbol{H}_{yx}$) functions showed a dependence on excitation frequency that could be accounted for with virtual-mass coefficients, producing frequency-independent stiffness and virtual-mass coefficients. In both orientations, Im($\boldsymbol{H}_{yy}$) and Im($\boldsymbol{H}_{xx}$) increase linearly with Ω, allowing for frequency independent damping coefficients. Overall, both the LOP and LBP orientations show that the frequency dependency of the test bearing was modeled well with a [K][C][M] model.

Importance of Pad Flexibility in Predictions

As previously mentioned, the main difference between codes A and B is that Code B incorporates pad flexibility in predicting the impedance coefficients for a tilting-pad journal bearing, while Code A generates predictions assuming an infinitely rigid pad. The *pad* flexibility refers to the change in pad curvature resulting from an applied moment at the end of the pad from the fluid film pressure (see Predictions). Both codes account for pivot flexibility with the same user-defined load-versus-deflection model, and allow for different pad geometry (clearances and preloads) entries. Code B does not include an energy equation to calculate temperature and viscosity distributions, but experimental temperature measurements were used to estimate the lubricant's viscosity.

To look at the effects that *pad* flexibility has on predicting the impedance coefficients, a series of predictions were created with Code B by changing the magnitude of the pad's calculated bending stiffness from Eq. (27). Figure 41 presents the measured

and predicted K_{xx} and K_{yy} predictions for Code A and Code B in the LOP configuration. Results for the LBP orientation can be found in Appendix G. Measured values are shown here for reference, but will be discussed in the following sections.

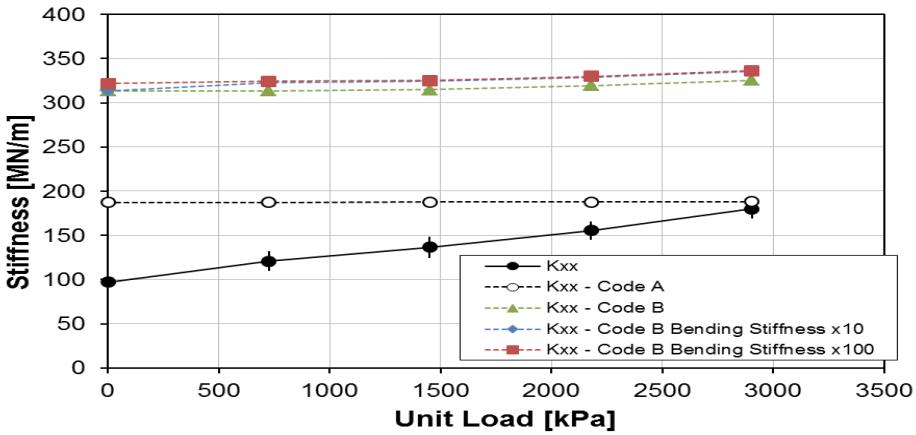

(A) K_{xx} at 6.8 krpm

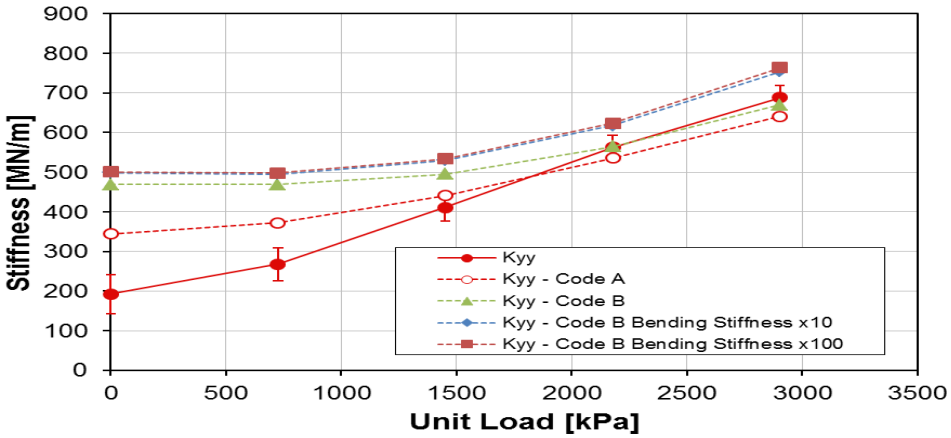

(B) K_{yy} at 6.8 krpm

Figure 41: Measured and Predicted Direct Stiffness Coefficients for LOP Orientation

As seen from Figure 41, Code B predicted higher K_{xx} and K_{yy} values than Code A. Code A predicts K_{xx} and K_{yy} much more accurately than Code B. Both predictions are

more accurate as load increases. Changing the bending stiffness from its actual value by a factor of 10 or by a factor of 100 in Code B, showed a 3% increase in predictions for K_{xx} and an 11% increase in predictions for K_{yy}.

Figure 42 presents measured and predicted K_{xx} and K_{yy} values for Code A and Code B in the LOP configuration at 13.2 krpm.

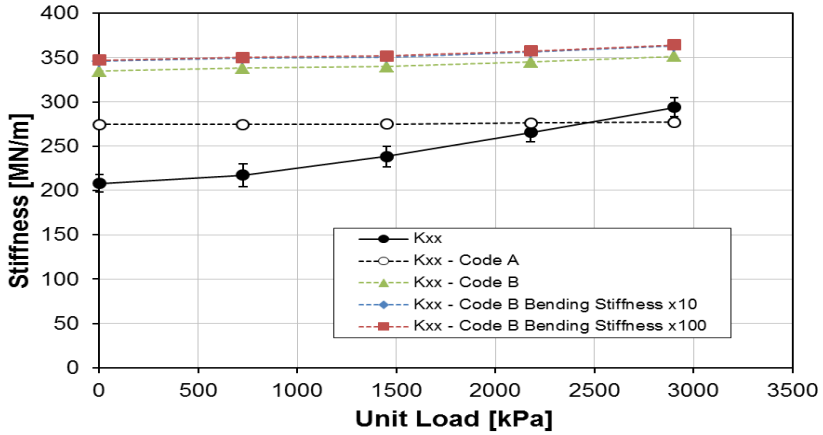

(A) K_{xx} at 13.2 krpm

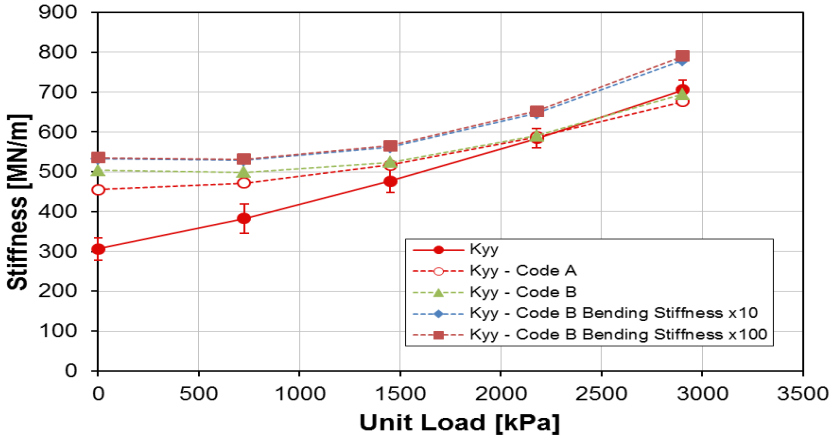

(B) K_{yy} at 13.2 krpm

Figure 42: Measured and Predicted Direct Stiffness Coefficients for LOP Orientation

As with the 6.8 krpm case, Code B predicted higher K_{xx} and K_{yy} values than Code A, and Code A predicts K_{xx} and K_{yy} more accurately than Code B

Changing the bending stiffness from its actual value by a factor of 10 or by a factor of 100 in Code B showed a 3% increase in predictions for K_{xx} and an 11% increase in predictions for K_{yy}. For a flexible pad an increase in bending stiffness can have a large effect on predictions; however, for a more rigid pad an increase in pad bending stiffness will have a much lesser effect. When the bending stiffness was increased by a factor of 10 to a factor of 100, no changes in predictions resulted. These findings suggest that if the calculated bending stiffness of 22MN was 10 times greater, then the pads would be effectively rigid.

Figure presents the measured and predicted direct damping coefficients for Code A and Code B in the LOP configuration.

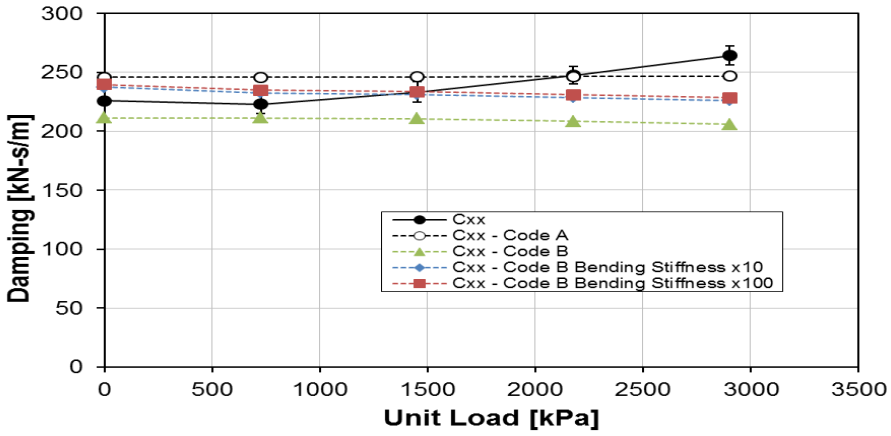

(A) C_{xx} at 6.8 krpm

Figure 43: Measured and Predicted Direct Stiffness Coefficients for LOP Orientation

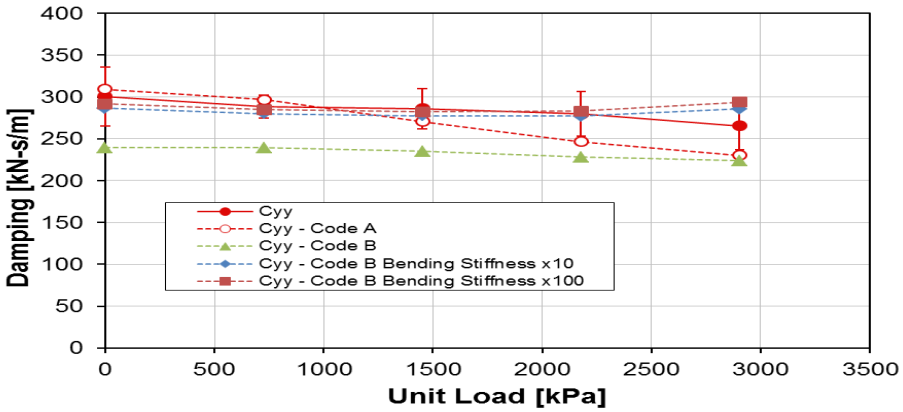

(B) C_{yy} at 6.8 krpm

Figure 43: Continued

Figure, shows that both codes predict C_{xx} and C_{yy} fairly accurately. Changing the bending stiffness from its actual value by a factor of 10 in Code B showed a 10% increase in predictions for C_{xx} and a 22% increase in predictions for C_{yy}. When the bending stiffness was increased from a factor of 10 to a factor of 100, very slight changes in predictions were made.

Figure 44 presents the measured and predicted C_{xx} and C_{yy} for Code A and Code B in the LOP configuration at 13.2 krpm.

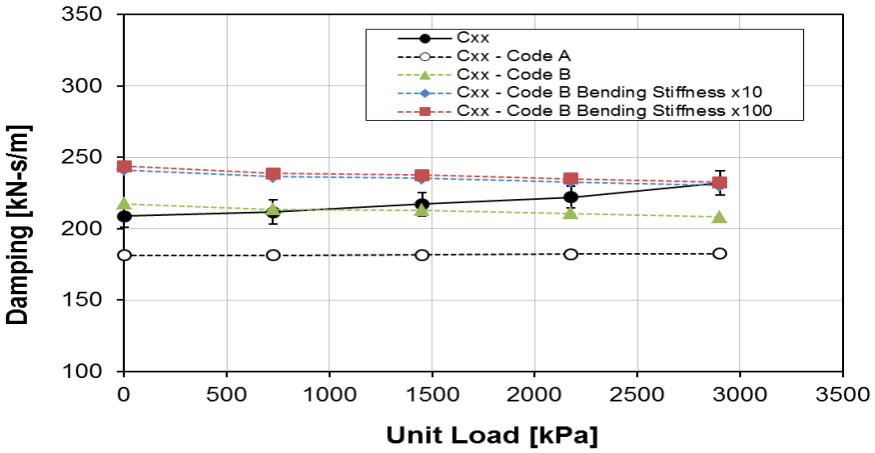

(A) C_{xx} at 13.2 krpm

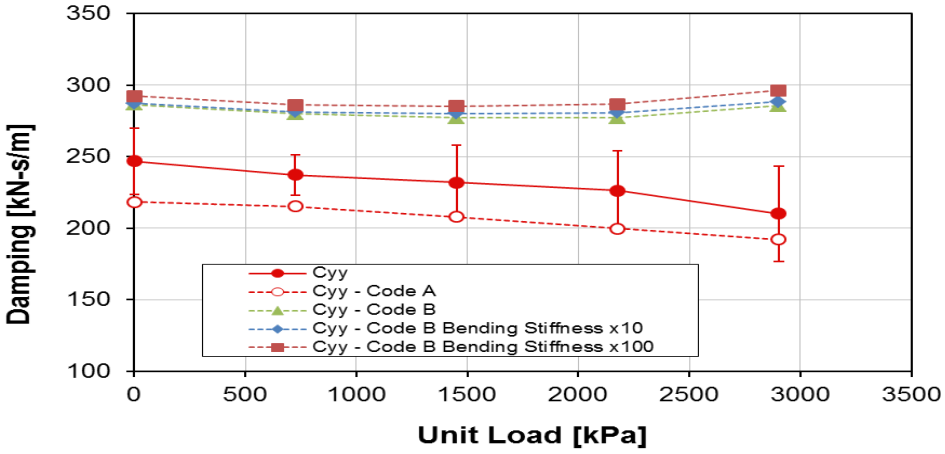

(B) C_{yy} at 13.2 krpm

Figure 44: Measured and Predicted Direct Stiffness Coefficients for LOP Orientation

At 13.2 krpm Code B predicts C_{xx} and C_{yy} to be greater than Code A. As speed increases, Code B predicts C_{xx} much more accurately, while Code A predicts C_{yy} more accurately. Code B shows relatively no increase in C_{yy} when the pad bending stiffness is increased, but shows a 24% increase in C_{xx} when the pad bending stiffness is increased.

In an attempt to obtain identical predictions from both codes, predicted lubricant

temperature from Code A and a calculated bending stiffness of 100 times greater were used as an input to Code B to assume that both codes were using an infinitely rigid pad, allowing for all input parameters to be identical between prediction codes.

Table 10: Prediction Comparisons of 13.2 krpm with 2903 kPa Static Load

Coefficient	Code A	Code B Bending stiffness x100	Code B Bending stiffness x100 (Temperature Change)	Larger Difference
Kxx	277.1	364.3	383.2	5%
Kyy	676.8	790.1	809.8	2%
Cxx	182.6	232.4	245.4	5%
Cyy	192.2	296.3	320.0	7%

Table 10 shows that when the temperatures are changed to match between codes, the difference between the two codes predictions increase. As shown in the Pad Metal Temperatures section, the predicted circumferential temperature gradient from Code A is lower than measured values. Decreasing the temperature input to Code B, increases the fluid viscosity, increasing the stiffness and damping coefficients, causing a greater difference between prediction codes. These results raise and interesting question, why do the two prediction codes still generate different rotordynamic coefficients when all input parameters are identical?

Overall, increasing the bending stiffness used in Code B typically caused a 3-11% increase in K_{xx} and K_{yy}, and a 10-24% increase in C_{xx} and C_{yy} in the LOP orientation. In all cases, increasing the calculated bending stiffness, given in Eq. (27) by a factor of ten to hundred times caused slight if any change in K_{xx}, K_{yy}, C_{xx}, and C_{yy}. For a more flexible pad, an increase in bending stiffness can have a large effect on predictions; however, for a nearly rigid pad, an increase in pad bending stiffness will

have much less effect. These findings suggest that if the calculated bending stiffness of 22MN were 10 times greater, then the pads could be considered rigid.

Results from Code B show that the pad's structural bending stiffness can be an important factor in predicting impedance coefficients. Even though the pads tested in this thesis are extremely stiff, changes are still seen in Code B's predictions when the magnitude of the pad's bending stiffness is increased, especially in C_{xx} and C_{yy}. Overall, Code A predicts K_{xx} and K_{yy} more accurately than Code B in both load orientations. In the LOP orientation, Code B predicts C_{xx} more accurately, while Code A predicts C_{yy} more accurately. For solid pads, like the ones tested in this thesis, both codes do a decent job at predicting dynamic stiffness coefficients.

Stiffness Coefficients

For brevity, predictions for stiffness, damping, and virtual-mass coefficients will be generated using only Code A. Code A predicted K_{xx} and K_{yy} much more accurately than Code B. Input for Code A can be found in Table 2 for bearing parameters, Table 7 and Table 8 for hot bearing clearances, and the Predictions section for pivot flexibility.

LOP Orientation

Figure 45 presents the experimental and predicted direct stiffness coefficients in the LOP configuration.

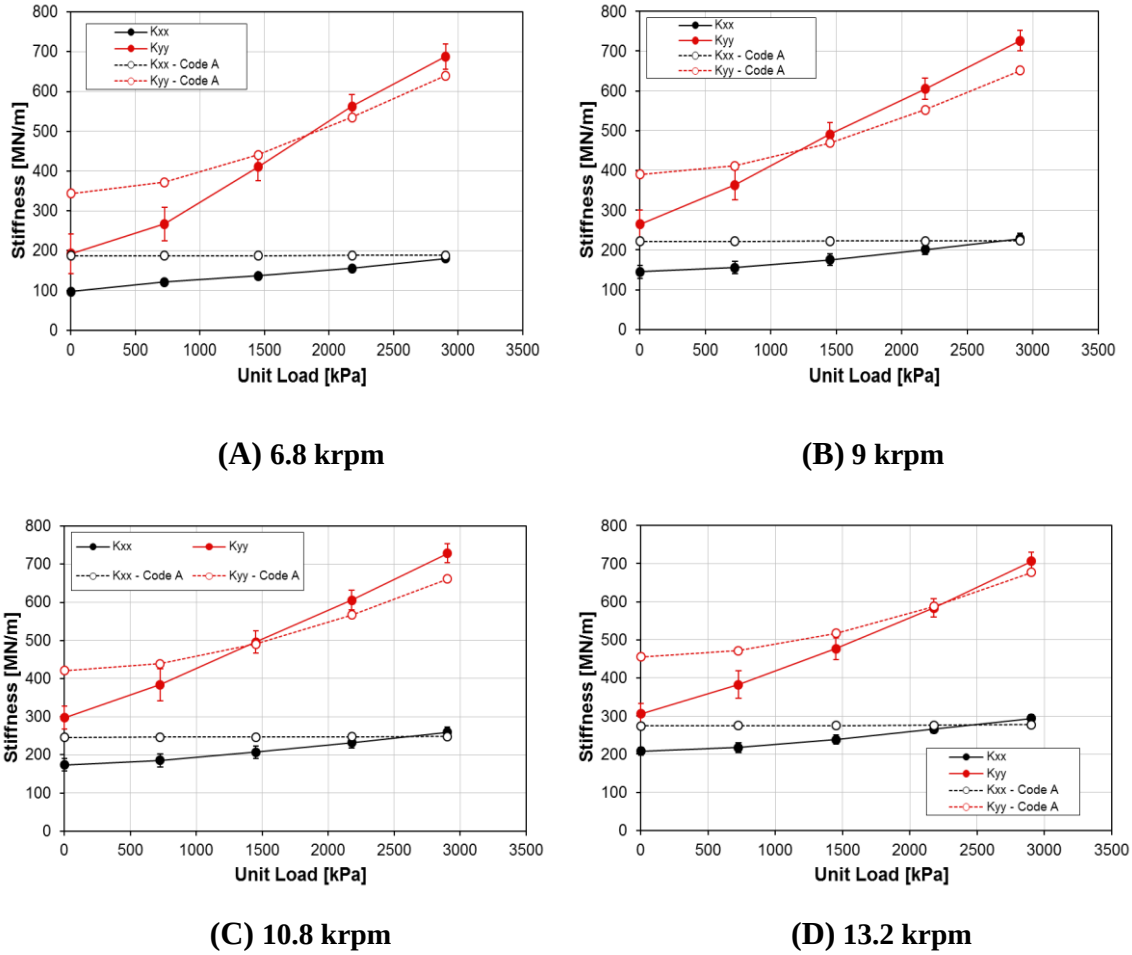

Figure 45: LOP Measured and Predicted K_{xx} and K_{yy} (A) 6.8 krpm, (B) 9 krpm, (C) 10.8 krpm, (D) 13.2 krpm

Figure 45 shows measured K_{xx} and K_{yy} increasing with increasing static unit load, and K_{yy} increases at a considerably greater rate than K_{xx}. At high loads, the loaded direction, K_{yy} was ~70% greater than K_{xx}. K_{xx} increases with increasing rotor speed while K_{yy} stays relatively independent (slight increase). K_{yy} shows a larger dependency on unit load and rotor speed. At all conditions, the direct stiffness coefficients are predicted well at high unit loads, but are larger than predicted at light unit loads. Measured K_{xx}

increases slightly due to static unit loads, while the predicted K_{xx} remains constant relative to unit loads. The bearing orthotropy is predicted well at high unit loads.

Figure 46 presents the measured and predicted cross-coupled stiffness coefficients in the LOP configuration.

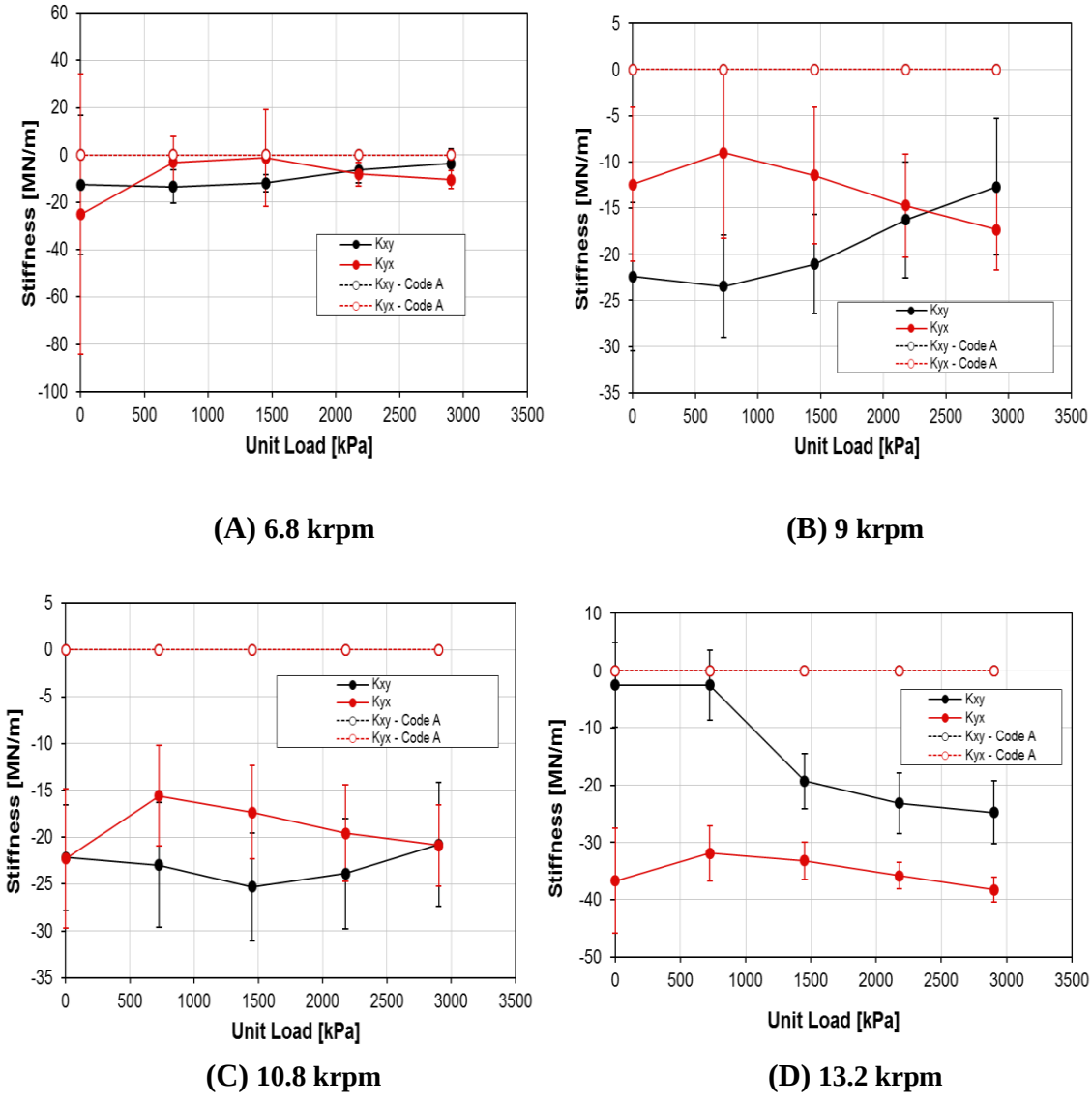

(A) 6.8 krpm **(B) 9 krpm**

(C) 10.8 krpm **(D) 13.2 krpm**

Figure 46: LOP Measured and Predicted K_{xy} and K_{yx} (A) 6.8 krpm, (B) 9 krpm, (C) 10.8 krpm, (D) 13.2 krpm

Figure 46 shows that significant measured cross-coupled stiffness coefficients were obtained at all rotor speeds. All K_{xy} and K_{yx} coefficients are negative (have the same sign), and do not promote instability. No trend in cross-coupled stiffness terms can be seen in regards to changes in either load or speed. At all conditions, the cross-coupled stiffness coefficients are predicted to be zero. Only at 6.8 krpm are the K_{xy} and K_{yx} predictions similar to the experimental results. Measured negative K_{xy} and K_{yx} have a much smaller magnitude than the direct stiffness coefficients.

Experimental results shown above agree with the trends of the LOP loci plots and attitude angles of Figure 25 and Figure 27 that suggest cross-coupled stiffness. Note that a change in ε_o and ϕ_o can be attributed to a change in probe length due to temperature, suggested by Wilkes [15]. All K_{xy} and K_{yx} coefficients are negative and do not promote instability. Testing was performed twice in the LOP orientation, and both times negative cross-coupled stiffness results were found.

LBP Orientation

Figure 47 presents the experimental and predicted direct stiffness coefficients in the LBP configuration.

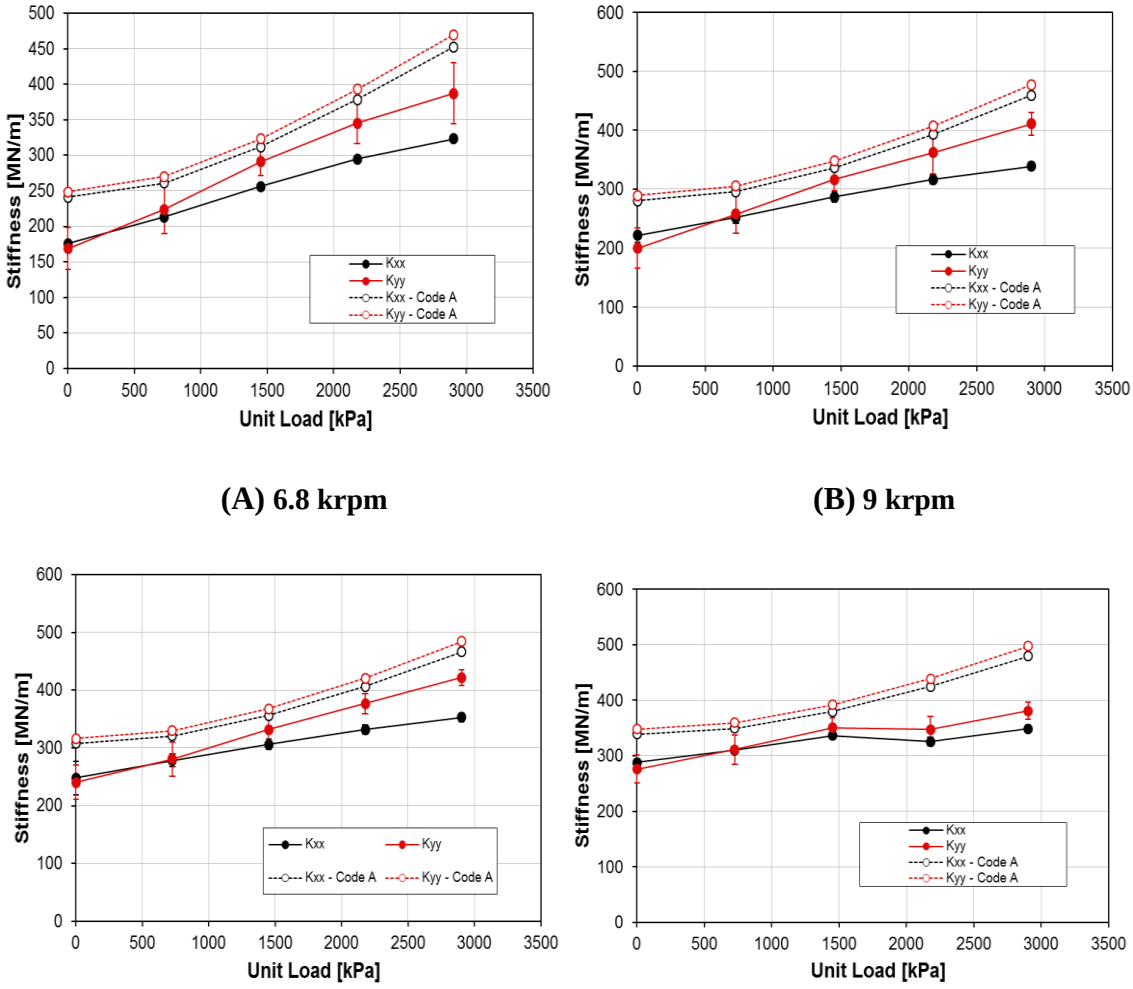

Figure 47: LBP Measured and Predicted K_{xx} and K_{yy} (A) 6.8 krpm, (B) 9 krpm, (C) 10.8 krpm, (D) 13.2 krpm

In the LBP orientation, measured K_{xx} and K_{yy} values increase with increasing static unit load, and K_{yy} increases at a rate slightly greater than K_{xx}. Both K_{xx} and K_{yy} increase with increasing rotor speed. At all conditions, K_{xx} and K_{yy} are predicted well and follow similar trends to predictions. In comparison to the LOP configuration, K_{yy} coefficients are smaller in the LBP orientation, and the K_{xx} coefficients are greater. The

lack of orthotropy in the LBP orientation is predicted well.

Figure 48 presents the measured and predicted K_{xy} and K_{yx} in the LBP configuration.

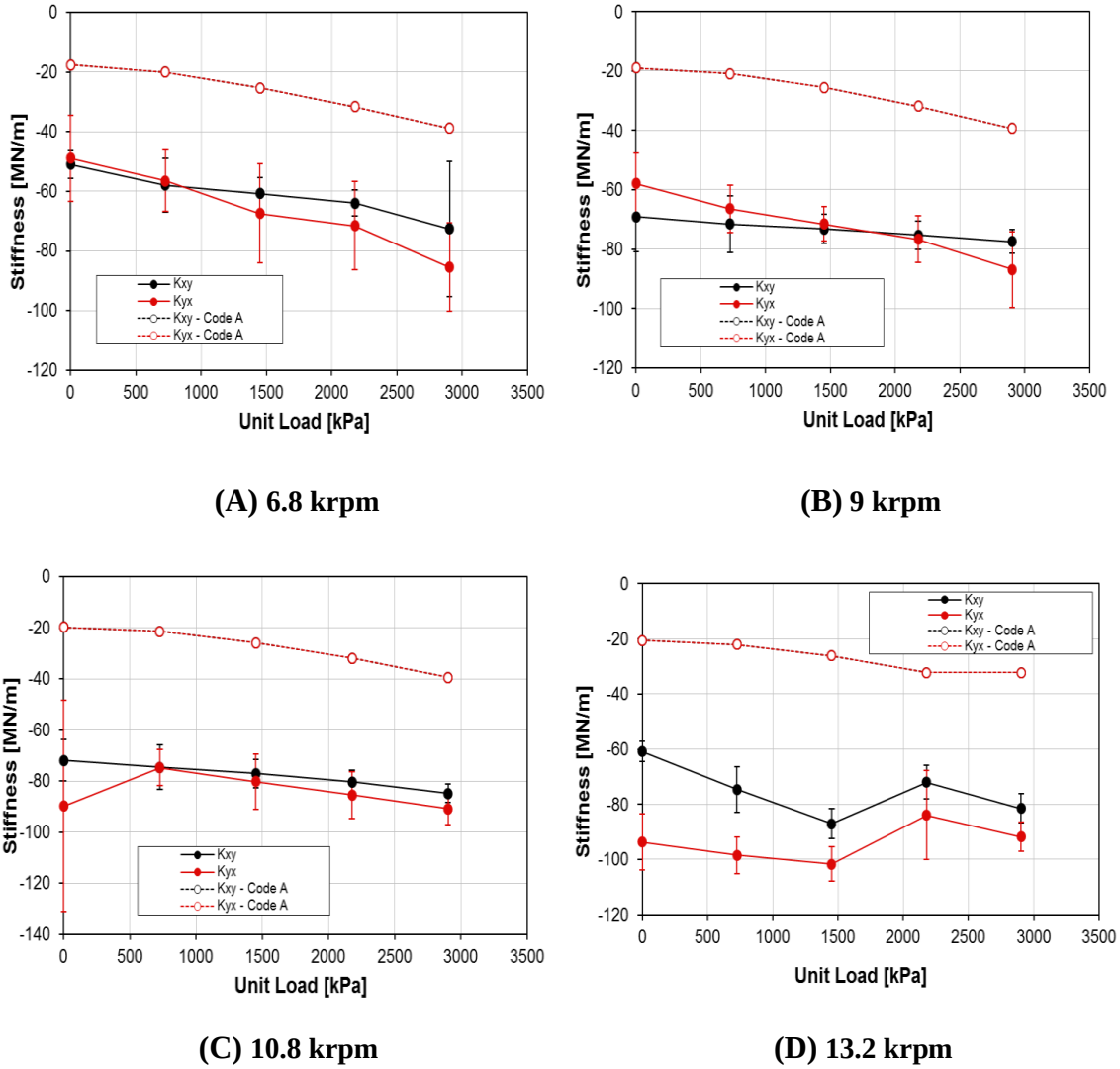

(A) 6.8 krpm **(B) 9 krpm**

(C) 10.8 krpm **(D) 13.2 krpm**

Figure 48: LBP Measured and Predicted K_{xy} and K_{yx} (A) 6.8 krpm, (B) 9 krpm, (C) 10.8 krpm, (D) 13.2 krpm

As with the LOP configuration, the bearing experienced cross-coupled stiffness at all rotor speeds in the LBP orientation. All measured K_{xy} and K_{yx} coefficients are negative, and generally K_{yx} has a larger magnitude than K_{xy}. Because all K_{xy} and K_{yx}

coefficients have the same signs they do not promote instability. At all conditions, the predicted K_{xy} and K_{yx} have similar trends to measured results, but are much closer to zero. Measured and predicted values become more negative as load increases. Experimental results shown above agree with the trends of the LOP loci plots and attitude angles of Figure 26 and Figure 28 that suggest cross-coupled stiffness.

The bearing tested showed significant orthotropy in the LOP orientation and slight orthotropy in the heavier load cases in the LBP orientation. In 2010, Delgado et al. [12] tested both a 5-pad LOP, and 4-pad LBP rocker-pivot tilting-pad journal bearing with 50% and 60% pad pivot offset and a 0.4 L/D ratio with much lower static unit loads than the one in this thesis. Delgado reported (~25%) orthotropy in the loaded direction for the LOP orientation when testing a 5-pad TPJB. Delgado did not test the 4-pad TPJB in the LOP orientation. The bearing in this thesis showed much larger coefficients (~70%) in the loaded direction when testing at large static unit load.

In the LBP orientation, Delgado experience similar coefficients in both the loaded and orthogonal direction. At low static loads, similar orthotropy to Delgado was shown in this thesis, but with much greater K_{xx} and K_{yy} values. Note that Delgado tested with much lower static unit loads. The present findings support Zeidan and Herbage [2] predictions that much higher levels of stiffness orthotropy will be experienced in the LOP configuration than the LBP orientation for a 4-pad TPJB.

Damping Coefficients

The following section presents measured and predicted C_{xx}, C_{yy}, C_{xy}, and C_{yx} values at all speeds and static unit loads for both the LOP or LBP orientation.

LOP Orientation

Figure 49 presents measured and predicted C_{xx} and C_{yy} in the LOP configuration.

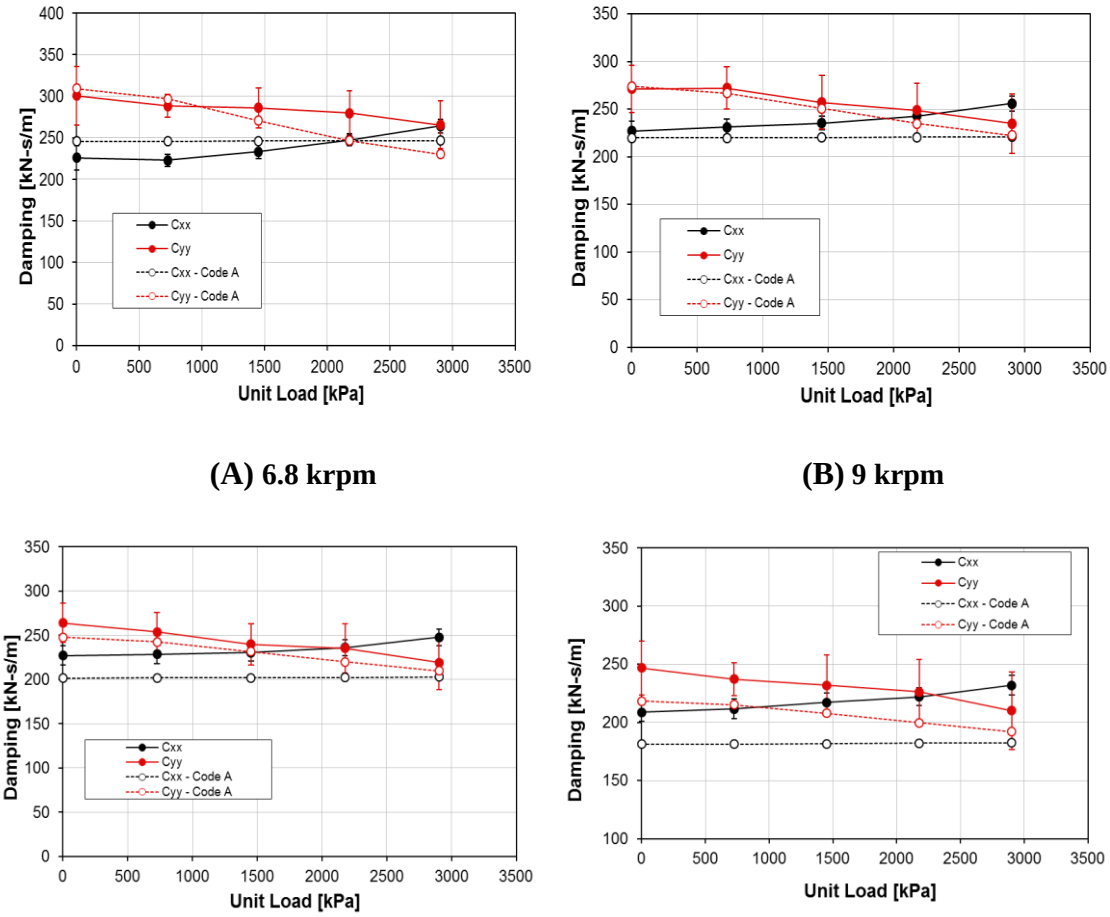

Figure 49: LOP Measured and Predicted C_{xx} and C_{yy} (A) 6.8 krpm, (B) 9 krpm, (C) 10.8 krpm, (D) 13.2 krpm

C_{xx} slightly increase with increasing unit load, while C_{yy} slightly decreases. Both measured C_{xx} and C_{yy} slightly decrease as rotor speed increases. For the most part, measured C_{yy} values are greater than measured C_{xx} values, except for the highest loaded case. All predicted C_{yy} values are greater than C_{xx}. Both coefficients are predicted well. Measured values are slightly smaller than predicted as unit load and speed increase. The damping predictions match the experimental results best at 9 krpm.

Figure 50 below presents the experimental and theoretical cross-coupled damping coefficients in the LOP configuration.

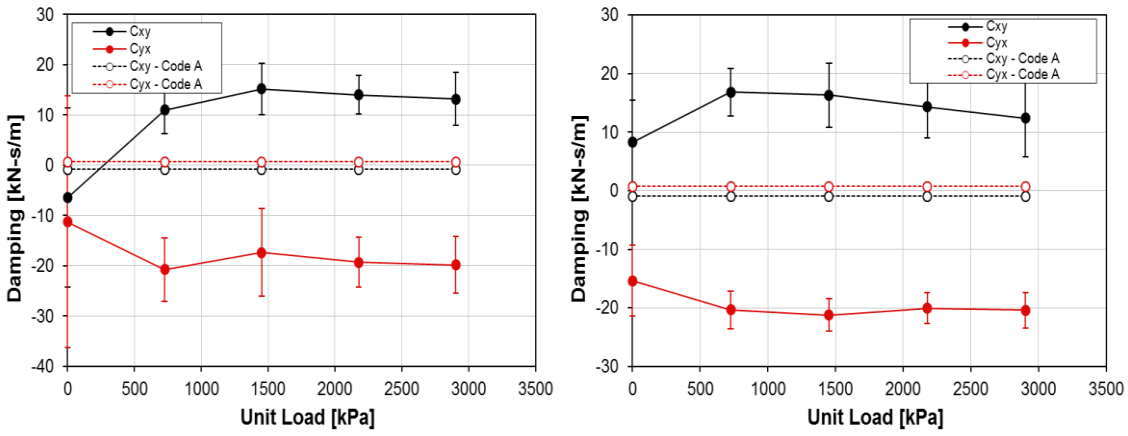

(A) 6.8 krpm **(B) 9 krpm**

Figure 50: LOP Measured and Predicted C_{xy} and C_{yx} (A) 6.8 krpm, (B) 9 krpm, (C) 10.8 krpm, (D) 13.2 krpm

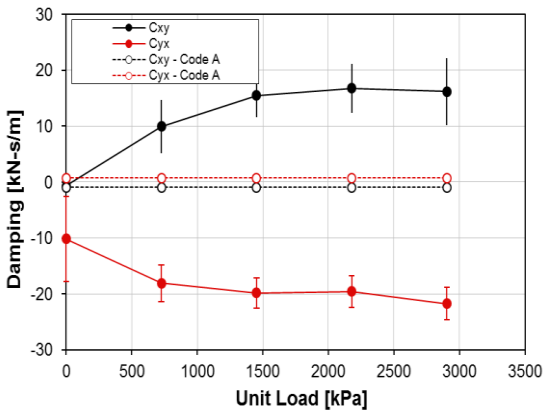

(C) 10.8 krpm

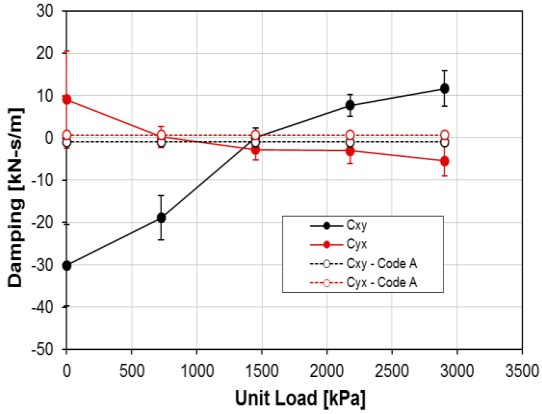

(D) 13.2 krpm

Figure 50: Continued

Significant measured C_{xy} and C_{yx} values were obtained at all rotor speeds. Measured C_{xy} and C_{yx} values have opposite signs. At all rotor speeds, C_{xy} is positive while C_{yx} is negative, signifying gyroscopic (not dissipative) damping. Only at 13.2 krpm do the signs of the C_{xy} and C_{yx} change with increasing unit load. The cross-coupled damping coefficients are much smaller than the direct damping terms shown in Figure 49. At all conditions, C_{xy} and C_{yx} are predicted to be zero.

LBP Orientation

Figure 51 presents measured and predicted C_{xx} and C_{yy} values in the LBP configuration.

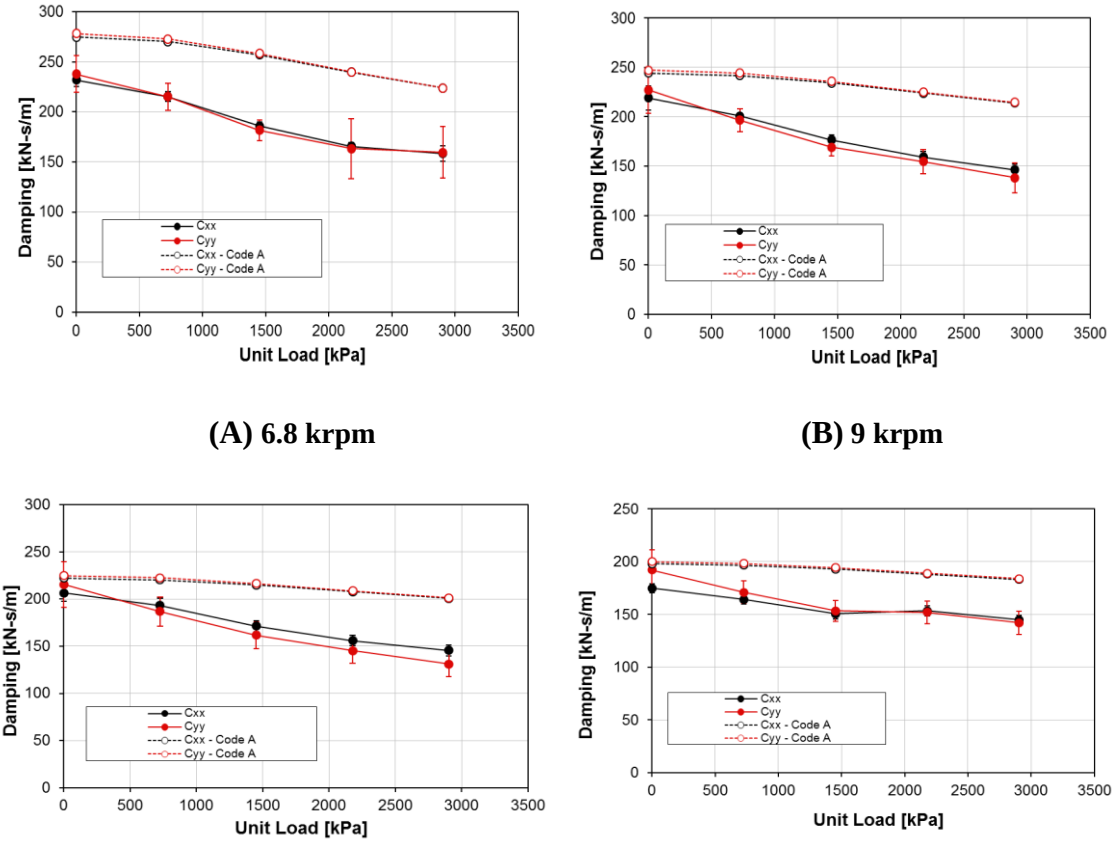

Figure 51: LBP Measured and Predicted C_{xx} and C_{yy} (A) 6.8 krpm, (B) 9 krpm, (C) 10.8 krpm, (D) 13.2 krpm

At all speeds, C_{xx} and C_{yy} decrease with increasing unit load. C_{xx} and C_{yy} slightly decrease with increasing rotor speed. At all conditions, C_{xx} and C_{yy} are smaller than predicted. In looking at all the predictions, the damping predictions match the experimental results best at 13.2 krpm. Predictions became more accurate as rotor speed increased. Predictions from Code A follow similar trends to measured results; specifically with a slight decrease with increasing load.

By comparing Figure 49 and Figure 51, C_{xx} and C_{yy} are lower in the LBP orientation than the LOP orientation. C_{xx} and C_{yy} in the LBP orientation are greater than Delgado et al. [12] for a 4-pad TPJB. The bearing tested by Delgado had different pivot offsets, different *L/D* ratios, and experienced much lower static unit loads than the one in this thesis.

Figure 52 below presents the measured and predicted C_{xy} and C_{yx} values in the LBP configuration.

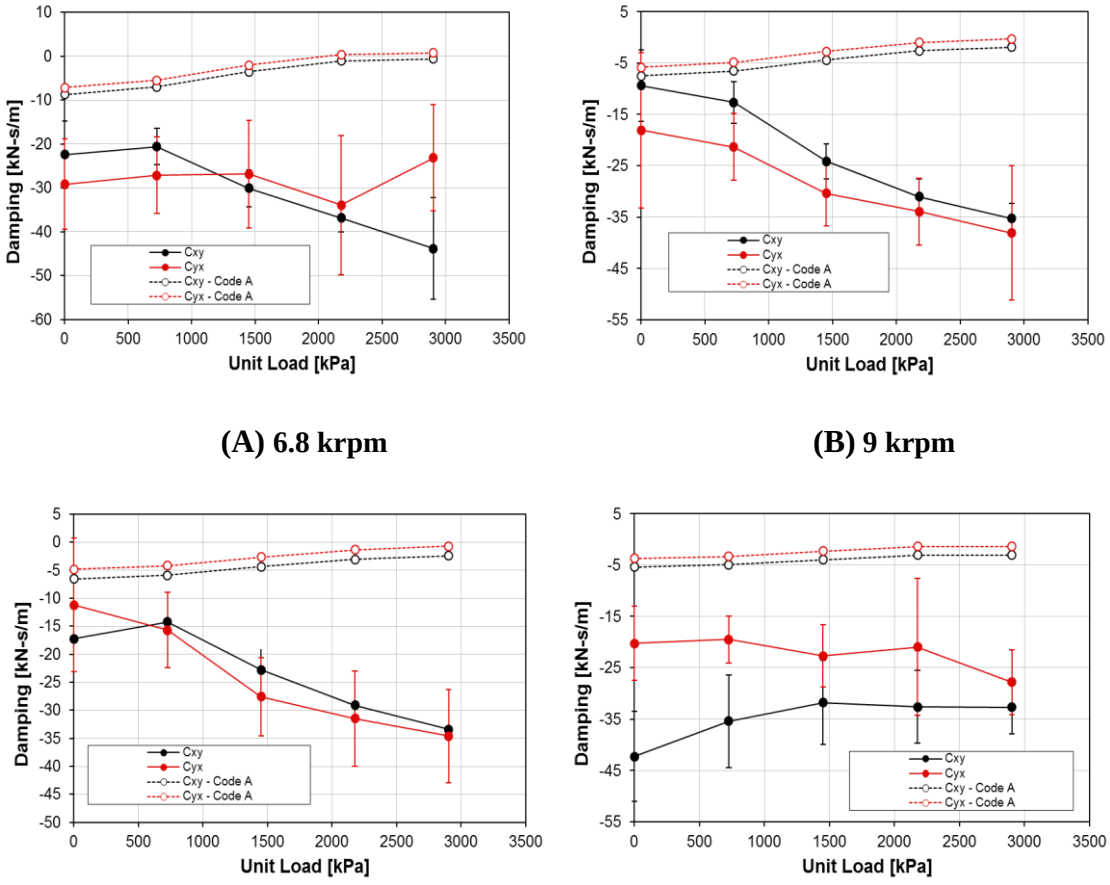

Figure 52: LBP Measured and Predicted C_{xy} and C_{yx} (A) 6.8 krpm, (B) 9 krpm, (C) 10.8 krpm, (D) 13.2 krpm

In the LBP orientation, all measured C_{xy} and C_{yx} values are negative regardless of unit load or rotor speed. Predicted values for C_{xy} and C_{yx} follow different trends from measurements. Measured C_{xy} and C_{yx} values tend to decrease with increasing unit load, versus a predicted increase. Measured C_{xy} and C_{yx} magnitudes are much larger than predicted. The C_{xy} and C_{yx} are much smaller than the C_{xx} and C_{yy} terms in Figure 51. Unlike the LOP orientation, C_{xy} and C_{yx} have the same sign in the LBP orientation, signifying physical damping.

Virtual-mass Coefficients

This section presents the measured and predicted M_{xx}, M_{yy}, M_{xy}, and M_{yx} virtual-mass coefficients at all speeds and static loads tested for either the LOP or LBP orientation. A positive M_{ij} represents a negative curvature and acts like a real physical mass.

LOP Orientation

The experimental and predicted virtual-mass coefficients are given in Figure 53 below.

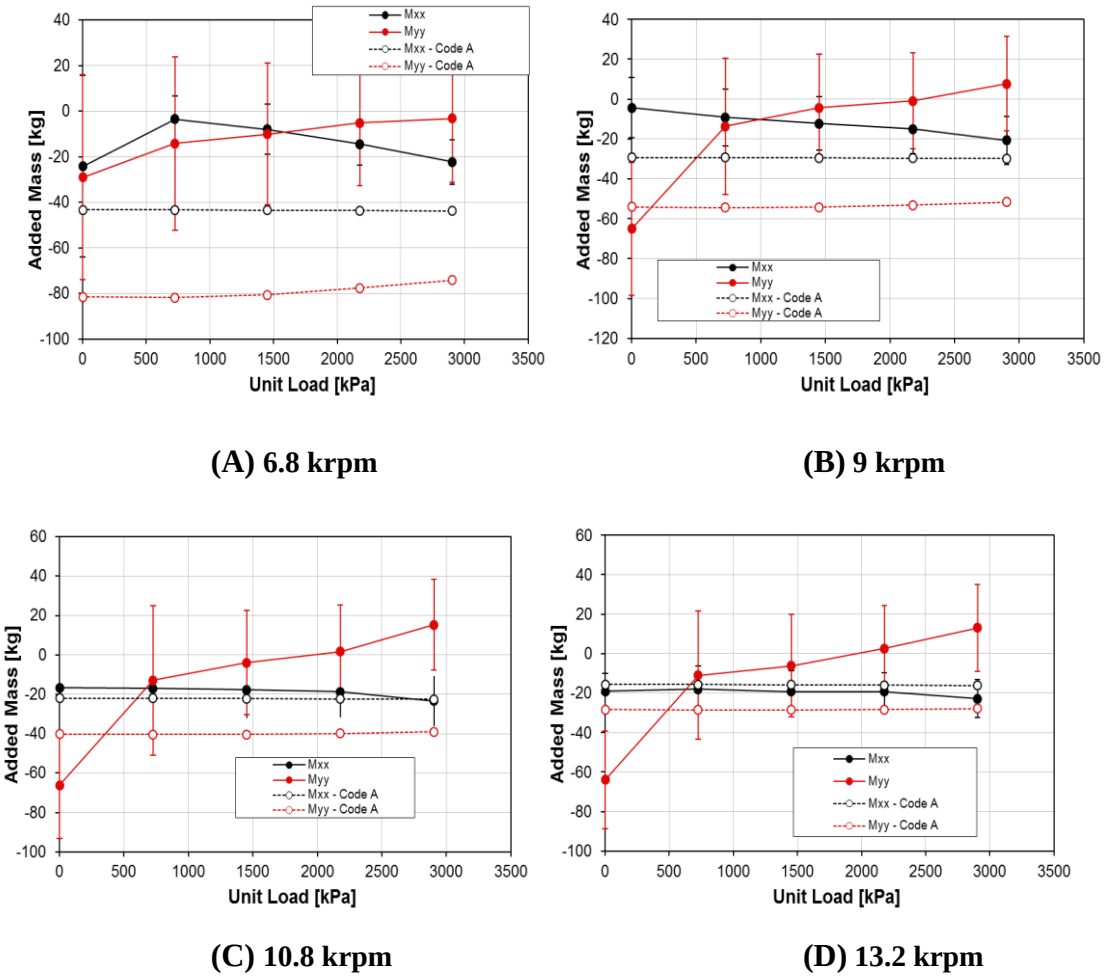

Figure 53: LOP Measured and Predicted M_{xx} and M_{yy} (A) 6.8 krpm, (B) 9 krpm, (C) 10.8 krpm, (D) 13.2 krpm

Measured M_{yy} values increase with increasing static unit load. The increasing curvature of Re($\boldsymbol{H_{ij}}$) led to all of the M_{xx} coefficients being negative, while the M_{yy} coefficients sign changes as load increases, agreeing with the dynamic stiffness plots of Figure 37 - Figure 40. At low speeds, the predicted virtual-mass coefficients are much larger than measured values. M_{xx} coefficients are predicted more accurately as speed

increases, even though neither coefficient is predicted well. All measured M_{yy} values have large uncertainties.

Figure 54 shows the measured and predicted M_{xy} and M_{yx} coefficients in the LOP configuration.

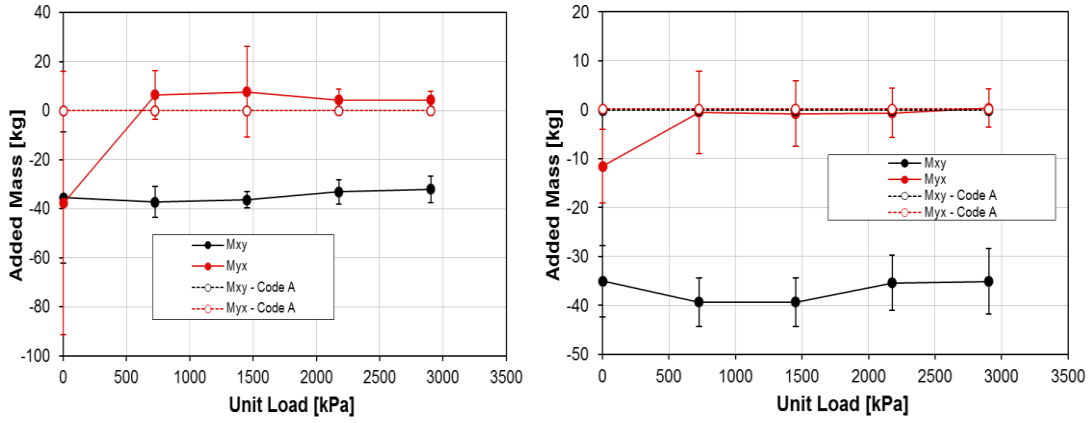

(A) 6.8 krpm **(B) 9 krpm**

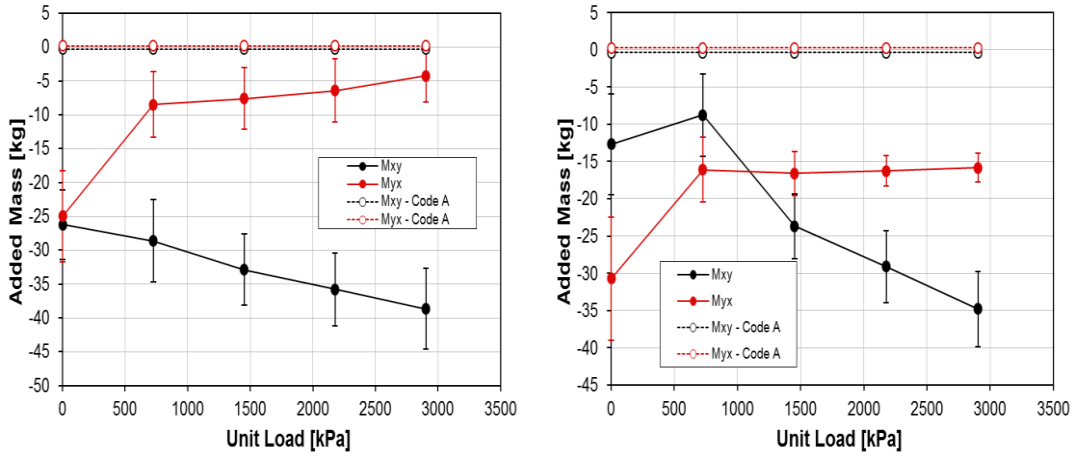

(C) 10.8 krpm **(D) 13.2 krpm**

Figure 54: LOP Measured and Predicted M_{xy} and M_{yx} (A) 6.8 krpm, (B) 9 krpm, (C) 10.8 krpm, (D) 13.2 krpm

M_{xy} and M_{yx} are mostly negative, except at 6.8 krpm. For higher rotor speeds, M_{xy} and M_{yx} are both negative. The virtual-mass coefficients at 6.8 krpm have opposite signs, suggesting an impact on stability (See Whirl Frequency Ratio). At all test conditions, M_{xy} and M_{yx} are predicted to be zero. At low speeds, M_{yx} values are similar to predicted values. Most cross-coupled virtual mass coefficients in the LOP orientation have large uncertainties.

LBP Orientation

Measured and predicted virtual-mass coefficients are given in Figure 55 for the LBP configuration.

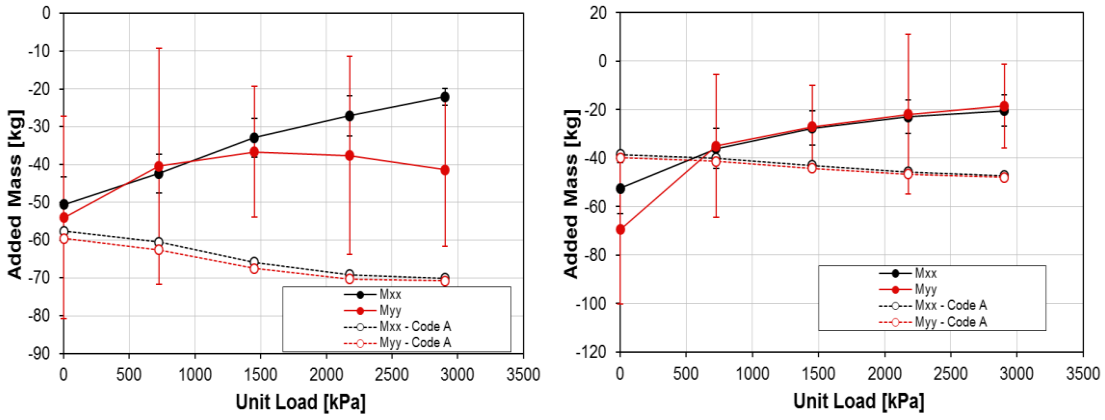

(A) 6.8 krpm **(B) 9 krpm**

Figure 55: LBP Measured and Predicted M_{xx} and M_{yy} (A) 6.8 krpm, (B) 9 krpm, (C) 10.8 krpm, (D) 13.2 krpm

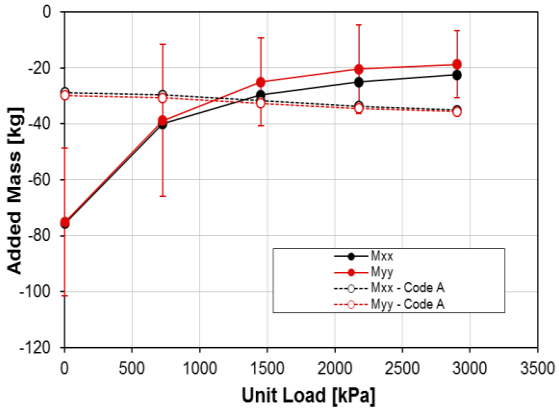

(C) 10.8 krpm

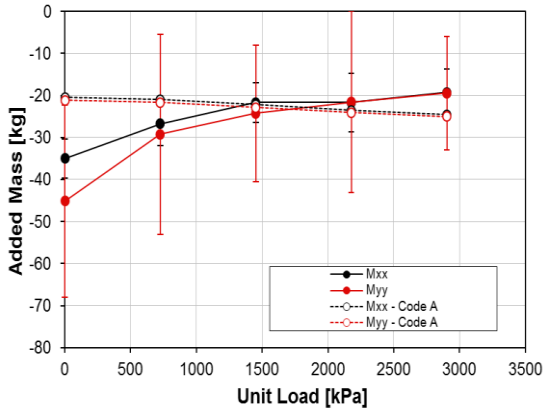

(D) 13.2 krpm

Figure 55: Continued

M_{yy} and M_{xx} coefficients follow similar trends with respect to changing rotor speed and loads. All of the M_{xx} and M_{yy} coefficients are negative with the zero-load case having the largest magnitudes, agreeing with the dynamic stiffness plots of Figure 57 - Figure 60. M_{xx} and M_{yy} coefficients are predicted more accurately as speed increases, even though neither coefficient is predicted well. The predicted values show a slight decrease with respect to increasing unit load and speed. For the most part, the experimental results show the opposite trends. Results are comparable to the LOP orientation. All measured M_{yy} coefficients have large uncertainties.

Figure 56 shows measured and predicted M_{xy} and M_{yx} coefficient's for the LBP configuration.

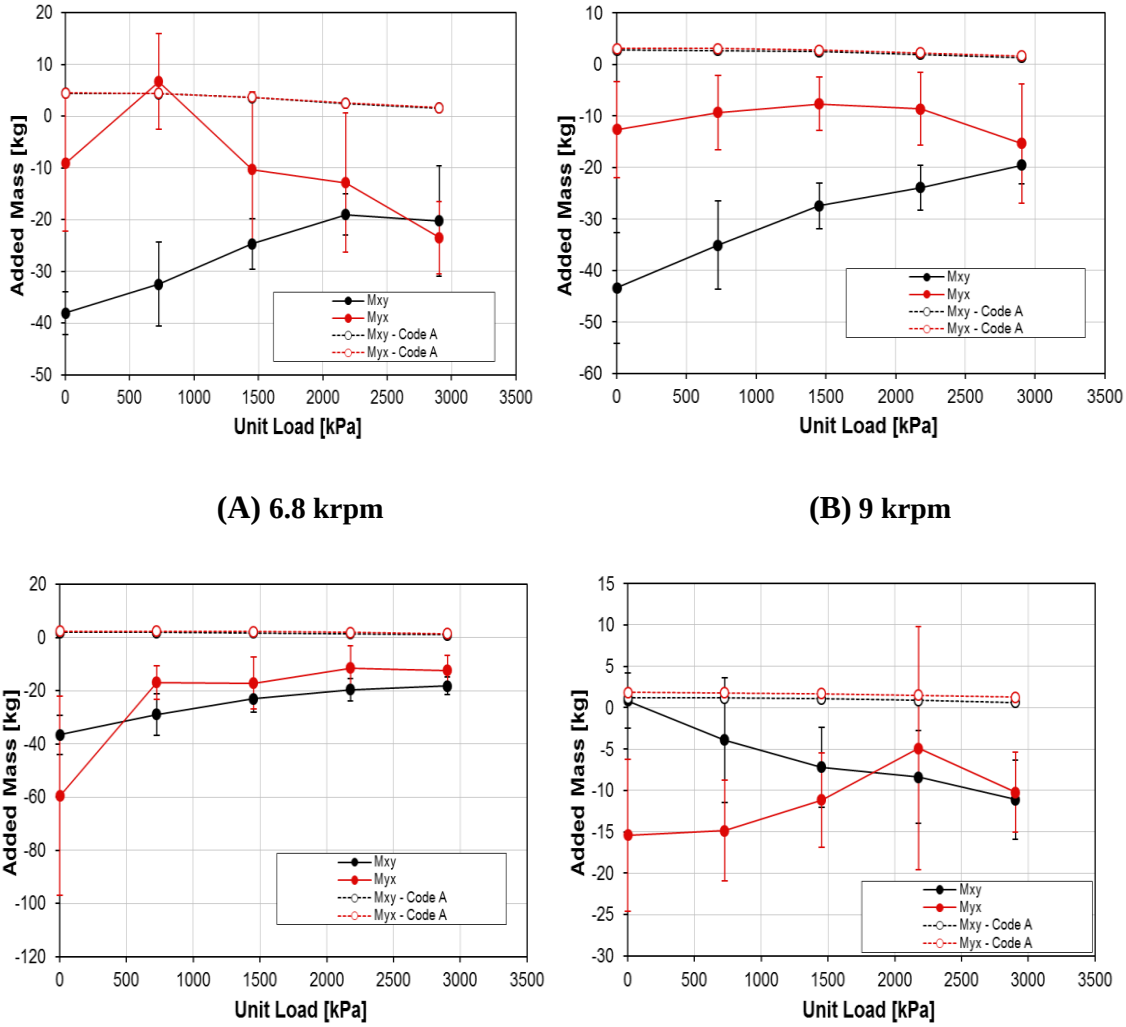

(A) 6.8 krpm **(B) 9 krpm**

(C) 10.8 krpm **(D) 13.2 krpm**

Figure 56: LBP Measured and Predicted M_{xy} and M_{yx} (A) 6.8 krpm, (B) 9 krpm, (C) 10.8 krpm, (D) 13.2 krpm

M_{xy} and M_{yx} are generally negative, except for the rotor speed of 6.8 krpm. At 6.8 krpm and 725kPa (105.3 psi) M_{xy} is negative and M_{yx} is positive, implying an effect on stability (See Whirl Frequency Ratio). M_{xy} increases with increasing unit load except for a rotor speed of 13.2 krpm. At low rotor speeds both M_{xy} and M_{yx} slightly decrease with increasing load.

Whirl Frequency Ratio

In Figure 54(A) and Figure 56(A) above, the virtual-mass coefficients for Re($\boldsymbol{H_{xy}}$) and Re($\boldsymbol{H_{yx}}$) have approximately equal but opposite signs, suggesting an impact on stability. The whirl frequency ratio (WFR) defines the stability characteristics of a bearing. If a bearing has zero cross-coupling effects than the whirl frequency ratio would be zero. The whirl frequency ratio is defined as the ratio of the rotor whirl or precessional frequency to the rotor's onset speed of instability. San Andrés [24] extended Lund's [25] definition of WFR to include the impact of cross-couples mass terms. The formulas used to calculate WFR can be found in Appendix E and are from San Andrés [24]. A small WFR will raise the onset speed of instability and thus produce a more stable system. For a typical journal bearing, the whirl frequency ratio is 0.5. At all conditions in both the LOP and LBP orientations the WFR was negative or zero, showing no impact on stability.

SUMMARY, DISCUSSION, AND CONCLUSIONS

Measured and predicted static and dynamic characteristics are presented for a 4-pad, rocker-pivot, tilting-pad journal bearing (TPJB) in load-on-pad (LOP) and load-between-pad (LBP) orientations. The bearing has the following characteristics: 4 pads, .57 pad pivot offset, 0.6 L/D ratio, and 60.33 mm (2.375in) pad axial length. Tests were conducted on a *floating* bearing test rig with unit loads ranging from 0 to 2903 kPa (421.1 psi) and speeds from 6.8 to 13.2 krpm.

Two newly developed prediction codes utilizing slightly different variables were used to compare to measured results. Static results and rotordynamic coefficients presented will be compared to predictions from a new rotordynamic bearing code, "Code A," developed by Tao and San Andrés at the Texas A&M Turbomachinery Laboratory. The predictions come from the first version of this code to be published in the near future. A full description of Code A can be found in the Predictions section. Code A takes into account pivot flexibility with a user-defined load-versus-deflection approximation, and if needed, different pad geometries (preloads and clearances for each pad) to predict the static and dynamic behavior of a TPJB.

Dynamic stiffness results presented will be compared to the model of Wilkes and Childs [14][17][18], "Code B". Wilkes dissertation [15] uses a Reynolds-based model to predict dynamic results, utilizing pivot *and* pad flexibility. Experimental temperature measurements are used to model the lubricant's viscosity. A full description of Code B can be found in the Predictions section.

Static Characteristics

The static results presented include the measured cold and hot clearance differences, bearing loci plots, journal eccentricity ratios, attitude angle, estimated power loss, and pad metal temperatures. Both cold and the hot clearance measurements show that the clearance of adjacent pads are different. Hot-clearance measurements showed a 16-25% decrease in clearance compared to a clearance measurement at room temperature. Because of this difference, measured hot clearances were used in predictions; giving a more accurate representation of the bearing clearances.

The measured attitude angle and eccentricity loci plots show that cross-coupled effects (lateral displacement) between the *x* displacement and *y* load direction are significant. However, the deviation from the loaded *y* axis and *x* axis motion was less significant in the LBP orientation. Wilkes and Childs [18] suggest that some observed change in eccentricity and attitude angle can be attributed to a change in probe length due to temperature, and not necessarily true cross-coupling effects. In comparison, Code A's LOP loci plots predicted no cross-coupling effects due to fluid rotation. The predicted bearing loci plots showed less movement in the ε_{oy} direction than measurements, predicting a stiffer bearing. LOP attitude angles were predicted to be zero while measured values were negative. Code A predicted small positive attitude angles in the LBP configuration, matching measured values.

Embedded thermocouples provide pad metal temperature just below the surface of the Babbitt. The circumferentially-spaced thermocouples showed a temperature increase along the faces of the pad in the shaft-rotation direction that increases with increasing

running speed. In the LOP orientation, temperatures at the trailing edge of the pad were much greater than temperatures at the leading edge of the pad (in some cases +40°C). Due to the difference in bearing clearances, in the LBP orientation, one of the loaded pads experienced greater temperatures because it was supporting more of the static load. Code A predictions showed an increase in temperature circumferentially across the pad with shaft rotation, agreeing with measurements. In the LOP orientation, all circumferential temperatures in the loaded pad were under predicted by Code A except for the temperature at the leading edge of the pad. In some cases, Code A under-predicted temperature measurements by 30°C at the trailing edge of the pad. In the unloaded pads, the leading edge of the pads are all over predicted by Code A, and the trailing edge of the pads are under predicted (±10°C). Overall, Code A did not predict the temperatures of trailing edge of the loaded pads well, but reasonable prediction results for rotordynamic coefficients were still obtained.

In the loaded pad, not only were thermocouples installed just below the surface of the Babbitt (rotor side of the pad), but thermocouples were also installed near the bearing housing. The thermocouples in the loaded pad showed a radial temperature decrease from the rotor side of the pad to the bearing-housing side. A finite-element (FE) analysis in ANSYS predicted that the measured radial temperature gradient caused an uneven thermal deflection in the pad, changing the pad's radius of curvature. The FEA predictions showed a 0.019-0.032 mm (0.00077-0.00126 in) increase in the loaded pad's radius depending on running speed and load. As the radius of curvature increased, the resulting preload of the pad's increased by 0.065-0.136. Overall, the change in radius of

curvature and preload only slightly affected the predicted bearing impedance coefficients, leading to slightly poorer predictions.

Estimated power loss values were obtained from an energy-balance equation assuming adiabatic conditions. Code-A power loss predictions were lower than the estimated power loss in the LBP orientation, but higher than the estimated power loss values for the LOP orientation. The LOP estimated power loss values were modeled well. Consistent with the measurements, Code A predicts that power loss is independent of load but increases with increasing speed.

Dynamic Characteristics

Rotordynamic coefficients including stiffness, damping, and virtual-mass coefficients were determined from measured $\boldsymbol{H_{ij}}$ dynamic-stiffness functions. For LOP and LBP cases, the Re($\boldsymbol{H_{xx}}$), Re($\boldsymbol{H_{yy}}$), Re($\boldsymbol{H_{xy}}$), and Re($\boldsymbol{H_{yx}}$) functions showed a dependence on excitation frequency that could be accounted for with virtual-mass coefficients, producing frequency-independent stiffness and virtual-mass coefficients.

In both orientations, Im($\boldsymbol{H_{xx}}$), Im($\boldsymbol{H_{yy}}$), Im($\boldsymbol{H_{xy}}$), and Im($\boldsymbol{H_{yx}}$) increased linearly with increasing Ω, allowing for frequency independent damping coefficients. Overall, for all test conditions the frequency dependency of the test bearing was modeled well with a [K][C][M] model. Similar results were obtained by Delgado et al. [12] for a 4-pad TPJB.

Except for some unloaded cases, measured K_{yy} was larger than K_{xx} regardless of orientation. In the LOP orientation, K_{yy} was much greater than K_{xx} (~70% with large

static loads). In the LBP orientation, K_{yy} was slightly greater than K_{xx} when testing with low static loads, but greater than K_{xx} when testing with heavier loads (~17%). In both orientations, measured K_{xy} and K_{yx} coefficients were negative and considerably smaller than the K_{yy} and K_{xx} coefficients. All measured K_{xy} and K_{yx} coefficients were the same sign (negative), and do not promote instability. Measured rotordynamic coefficients were compared to predictions from Code A. For both orientations K_{xx} and K_{yy} were smaller than Code A's predictions at light loads, but were more accurately predicted as load increased.

Measured C_{xx} and C_{yy} coefficients were mostly constant with respect to unit load in the LOP orientation, but decreased slightly with increasing unit load in the LBP orientation. Both orientations showed C_{xx} and C_{yy} decreasing slightly with increasing rotor speed. C_{yy} and C_{xx} predictions by Code A were very accurate in the LOP orientation. In the LBP orientation, Code A predicted higher C_{xx} and C_{yy} values than were measured. The measured C_{xy} and C_{yx} coefficients were considerably smaller than the C_{xx} and C_{yy}.

The main difference between prediction codes is that Code B incorporates pad flexibility in predicting the impedance coefficients for a tilting-pad journal bearing. The *pad* flexibility refers to the change in pad curvature resulting from an applied moment at the end of the pad from the fluid film pressure. To look at the effects that *pad* flexibility has on predicting the impedance coefficients, a series of predictions were created with Code B by changing the magnitude of the pad's bending stiffness. Increasing the bending stiffness used in Code B by a factor of 10 typically caused a 3-11% increase in

predicted K_{xx} and K_{yy}, and a 10-24% increase in predicted C_{xx} and C_{yy}. In all cases, increasing the calculated bending stiffness from ten to a hundred times the calculated value caused slight if any change in K_{xx}, K_{yy}, C_{xx}, and C_{yy}. For a flexible pad an increase in bending stiffness can have a large effect on predictions; however, for a more rigid pad an increase in pad bending stiffness will have a much lesser effect.

Overall, Code B's predictions showed that the pad's structural bending stiffness can be an important factor in predicting impedance coefficients. Even though the pads tested in this thesis are extremely stiff, changes are still seen in Code B's predictions when the magnitude of the pad's bending stiffness is increased, especially in C_{xx}, and C_{yy}. For the most part, Code A predicted K_{xx} and K_{yy} much more accurately than Code B showing that pad flexibility may not be as large of a factor in predicting K_{xx} and K_{yy} coefficients. Code B predicts C_{xx} more accurately, while Code A predicted C_{yy} more accurately.

For solid pads, like the ones tested here, both codes did a decent job at predicting the impedance coefficients. That said, both codes show the importance of including pivot-flexibility and the reduction of bearing clearance due to thermal expansion in predicting the impedance coefficients of a TPJB with solid pads. If either of these two inputs were incorrect, then predictions for the bearings impedance coefficients were very inaccurate.

Virtual-mass coefficients for both orientations were able to capture the frequency dependence of the measured Re($\boldsymbol{H}_{ij}$) values at all test conditions. For the most part, all M_{xx} and M_{yy} coefficients were negative regardless of orientation. Uncertainties for most

virtual-mass coefficients were significant. Delgado et al. and Kulhanek obtained M_{yy} and M_{xx} coefficients comparable to this thesis.

For the LOP and LBP 6.8 krpm case, the cross-coupled virtual-mass coefficients had approximately equal but opposite signs, suggesting an impact on stability. The whirl frequency ratio (WFR) was used to examine the stability characteristics of the bearing. At all conditions in both the LOP and LBP orientations the WFR was negative or zero, showing no impact on stability.

Overall, the measured dynamic stiffness and rotordynamic coefficients in the thesis were larger, but comparable to the test results of Delgado et al. [12]. The bearing tested have displayed significant orthotropy in the LOP orientation and slight orthotropy in the heavier load cases in the LBP orientation. Delgado reported (~25%) orthotropy in the loaded direction for the LOP orientation when testing a 5-pad TPJB. Delgado did not test the 4-pad TPJB in the LOP orientation. The bearing tested has showed much larger coefficients (~70%) in the loaded direction when testing at large static unit load. In the LBP orientation, Delgado experience similar coefficients in both the loaded and orthogonal direction. At low static loads, similar orthotropy was shown in this thesis, but with much greater K_{xx} and K_{yy} values. Delgado tested with much lower static unit loads. The present findings supported Zeidan and Herbage's [2] predictions that much higher levels of stiffness orthotropy will be experienced in the LOP configuration than the LBP orientation for a 4-pad TPJB.

REFERENCES

[1] Al-Ghasem, A., and Childs, D., 2006, "Rotordynamic Coefficients Measurement Versus Predictions for a High-Speed Flexure-Pivot Tilting-Pad Bearing (Load-between-Pad Configuration)," ASME J. Tribol., **128**, pp. 896-906.

[2] Zeidan, F., and Herbage B., 1991, "Fluid Film Bearing Fundamentals and Failure Analysis," *Proceedings of the 20th Turbomachinery Symposium*, pp. 161-186, June 17-19, Dallas, Texas.

[3] Lund, J.W., "Spring and Damping Coefficients for the Tilting-Pad Journal Bearing," ASLE Trans., **7** (3), pp. 342-352.

[4] Nicholas, J.C., Gunter, E.J., Allaire, P.E., 1979, "Stiffness and Damping Coefficients for the Five Pad Tilting Pad Bearing," ASLE Trans., **22** (2), pp. 112-124.

[5] Parsell, J.K., Allaire, P.E., and Wilson, B.W., 1988, "The Eigenvalue Dependence of Reduced Tilting Pad Bearing Stiffness and Damping Coefficients," ASLE Trans., **31**, pp. 411-419.

[6] White M. F., and Chan S. H., 1992, "The Subsynchronous Dynamic Behavior of Tilting-Pad Journal Bearings," J. Tribol., **114** (1) pp. 167-174.

[7] Ha, H., and Yang, S., 1999, "Excitation Frequency Effects on the Stiffness and Damping Coefficients of a Five-Pad Tilting Pad Journal Bearing," ASME J. Tribol., **121**, pp. 517-522.

[8] Wygant, K. D., 2001 "The Influence of Negative Preload and Nonsynchronous Excitation on the Performance of Tilting Pad Journal Bearings," Ph.D. Dissertation, Univ. of Virginia, Charlottesville, Virginia.

[9] Rodriguez, L., and Childs, D., 2006, "l Frequency-Dependency of Measured and Predicted Rotordynamic Coefficients for a Load-on-Pad, Flexible-Pivot Tilting-Pad Bearing," ASME J. Tribol., **128** (2), pp. 388-395.

[10] Hensley, E. J., and Childs, D., 2008, "Measurements versus Predictions for the Rotordynamic Characteristics of a Flexure Pivot-Pad Tilting Pad Bearing in an LBP Condition at Higher Unit Loads," *Proceedings of the ASME Turbo Expo 2008*, Paper GT2008-50069, June 9-13, Berlin, Germany.

[11] Carter, C., and Childs, D., 2008 "Measurements versus Predictions for the Rotordynamic Characteristics of a 5-pad, Rocker-Pivot, Tilting-Pad Bearing in the Load Between Pad Configuration, " *Proceedings of ASME Turbo Expo 2008*, Paper GT2008-50069, June 9-13, Berlin, Germany.

[12] Delgado, A., Ertas, B., Drexel M., Naldi, L., and Vannini, G., 2010, "A Component Level Test Rig for Dynamic Characterization of Oil Lubricated Bearing Using Different Input Excitations," *Proceedings of ISROMAC Thirteenth International Symposium on Transport Phenomena and Dynamics of Rotating Machinery*, April 4-9, Honolulu, Hawaii.

[13] Kulhanek, C., 2010, "Dynamic and Static Characteristics of a Rocker-Pivot, Tilting-Pad Bearing with 50% and 60% Offsets," M.S. thesis, Texas A&M University, College Station, TX.

[14] Wilkes, J., and Childs, D., 2012, "Improving Tilting-Pad Journal Bearing Predictions: Part I – Model Development and Impact of Rotor Excited Versus Bearing Excited Impedance Coefficients," *Proceedings of ASME Turbo Expo 2012*, Paper GT2012-69804, June 11-15, Copenhagen, Denmark.

[15] Wilkes, J., 2011, "Measured and Predicted Rotor-pad Transfer Functions for a Rocker-pivot Tilting-pad Journal Bearing," Doctoral Dissertation, Texas A&M University, College Station, TX.

[16] Branagan, L., and Barrett, L., 1988, "Thermal Analysis of Fixed and Tilting Pad Journal bearings Including Cross-Field Viscosity Variations and Deformation," ROMAC Report No. 276, UVA Report No. UVA/643092/MAE88/376.

[17] Wilkes, J., and Childs, D., 2012, "Improving Tilting-Pad Journal Bearing Predictions: Part II – Comparison of Measured and Predicted Rotor-Pad Transfer Functions for a Rocker-Pivot Tilting-Pad Journal Bearing,"

Proceedings of ASME Turbo Expo 2012, Paper GT2012-69808, June 11-15, Copenhagen, Denmark.

[18] Wilkes, J., and Childs, D., 2012, "Tilting Pad Journal Bearings – A Discussion on Stability Calculation, Frequency Dependence, and Pad and Pivot Flexibility," *Proceedings of ASME Turbo Expo 2012*, Paper GT2012-69809, June 11-15, Copenhagen, Denmark.

[19] Kaul, A., 1999, "Design and Development of a Test Setup for the Experimental Determination of the Rotordynamic and Leakage Characteristics of Annular Bushing Oil Seals," M.S. Thesis, Mechanical Engineering, Texas A&M University.

[20] Glienicke, J., 1966, "Experimental Investigation of the Stiffness and Damping Coefficients of Turbine Bearings and Their Application to Instability Predictions," *Proceedings of the International Mech. E.*, **181** (3B), pp. 116-129.

[21] Childs, D., and Hale, K., 1994, "A Test Apparatus and Facility to Identify the Rotordynamic Coefficients of High-Speed Hydrostatic Bearings," ASME Journal of Tribology, **116**, pp. 337-344.

[22] Harris, J., and Childs, D., 2008, "Static Performance Characteristics and Rotordynamic Coefficients for a Four-Pad Ball-In-Socket Tilting Pad Journal Bearing," *Proc. Of ASME Turbo Expo 2008*, Paper GT2008-50063, June 9-13, Berlin, Germany.

[23] Deutschman, A., Michaels, W., and Wilson, C., 1975, Machine Design, Macmillan Publishing Co., Inc., New York, pp. 862-863.

[24] San Andrés, L. A., 1991, "Effect of Eccentricity on the Force Response of a Hybrid Bearing," STLE Tribology Transactions, **34**, 4, pp. 537- 544.

[25] Lund, J.W., "The Stability of an elastic Rotor in Journal Bearings with Flexible, Damped Supports," *ASME Jour. of Applied Mechanics*, pp. 911-920 (1965).

APPENDIX A: MEASURED ECCENTRICITY

Table 11: LOP Measured Attitude Angle and Eccentricity

Running Speed [rpm]	Unit Loading [kPa]	Unit Loading [psi]	*US Customary Units*						*Metric Units*									
			X_{NTS} [mils]	Y_{NTS} [mils]	X_{TS} [mils]	Y_{TS} [mils]	$e_{X,ave}$ [mils]	$e_{Y,ave}$ [mils]	X_{NTS} [μm]	Y_{NTS} [μm]	X_{TS} [μm]	Y_{TS} [μm]	$e_{X,ave}$ [μm]	$e_{Y,ave}$ [μm]	ε_X [-]	ε_Y [-]	ε_o [-]	φ [deg]
6800	0	0.0	-0.64	0.20	-0.36	0.05	0.50	0.12	-16.20	5.08	-9.02	1.18	-12.61	3.13	0.00	0.00	0.00	-
	726	105.3	-0.55	1.05	-0.23	0.67	0.39	0.86	-14.07	26.68	-5.96	16.97	-10.02	21.83	-0.03	0.23	0.23	-7.90
	1452	210.5	-0.45	1.48	-0.10	1.11	0.28	1.30	-11.43	37.65	-2.67	28.14	-7.05	32.89	-0.07	0.36	0.37	-10.59
	2177	315.8	-0.32	1.85	0.05	1.45	0.13	1.65	-8.02	46.87	1.33	36.80	-3.34	41.84	-0.11	0.47	0.48	-13.47
	2903	421.1	-0.18	2.10	0.23	1.67	-0.03	1.88	-4.46	53.27	5.75	42.32	0.64	47.80	-0.16	0.54	0.56	-16.53
9000	0	0.0	-0.28	0.48	0.14	0.22	0.07	0.35	-7.17	12.27	3.61	5.70	-1.78	8.98	0.00	0.00	0.00	-
	726	105.3	-0.32	0.94	0.20	0.68	0.06	0.81	-8.17	23.88	4.95	17.19	-1.61	20.53	0.00	0.14	0.14	-0.84
	1452	210.5	-0.28	1.27	0.26	1.02	0.01	1.15	-7.18	32.31	6.64	25.90	-0.27	29.10	-0.02	0.24	0.24	-4.28
	2177	315.8	-0.19	1.54	0.36	1.28	-0.08	1.41	-4.84	39.21	9.09	32.56	2.13	35.89	-0.05	0.33	0.33	-8.26
	2903	421.1	-0.09	1.78	0.47	1.51	-0.19	1.65	-2.20	45.31	11.88	38.47	4.84	41.89	-0.08	0.40	0.41	-11.37
10800	0	0.0	-0.42	0.33	0.10	0.16	0.16	0.24	-10.67	8.34	2.58	3.95	-4.04	6.14	0.00	0.00	0.00	-
	726	105.3	-0.42	0.74	0.18	0.56	0.12	0.65	-10.55	18.73	4.47	14.18	-3.04	16.46	-0.01	0.12	0.13	-5.57
	1452	210.5	-0.37	1.05	0.25	0.89	0.06	0.97	-9.35	26.75	6.27	22.62	-1.54	24.68	-0.03	0.22	0.23	-7.68
	2177	315.8	-0.30	1.32	0.33	1.14	-0.02	1.23	-7.62	33.55	8.47	28.98	0.43	31.27	-0.05	0.30	0.31	-10.08
	2903	421.1	-0.20	1.54	0.44	1.33	-0.12	1.44	-5.04	39.23	11.11	33.78	3.03	36.51	-0.09	0.37	0.38	-13.12
13200	0	0.0	-0.67	0.12	-0.01	-0.03	0.34	0.05	-16.90	3.14	-0.25	-0.73	-8.57	1.21	0.00	0.00	0.00	-
	726	105.3	-0.61	0.50	0.08	0.32	0.26	0.41	-15.38	12.73	1.94	8.02	-6.72	10.37	-0.02	0.11	0.11	-11.44
	1452	210.5	-0.52	0.82	0.17	0.64	0.17	0.73	-13.20	20.76	4.32	16.19	-4.44	18.48	-0.05	0.21	0.22	-13.45
	2177	315.8	-0.45	1.07	0.24	0.91	0.10	0.99	-11.34	27.07	6.10	23.20	-2.62	25.13	-0.07	0.29	0.30	-13.98
	2903	421.1	-0.37	1.27	0.33	1.10	0.02	1.18	-9.43	32.19	8.42	27.83	-0.51	30.01	-0.10	0.35	0.36	-15.65

Table 12: LBP Measured Attitude Angle and Eccentricity

Running Speed [rpm]	Unit Loading [kPa]	Unit Loading [psi]	*US Customary Units*						*Metric Units*									
			X_{NTS} [mils]	Y_{NTS} [mils]	X_{TS} [mils]	Y_{TS} [mils]	$e_{X,ave}$ [mils]	$e_{Y,ave}$ [mils]	X_{NTS} [μm]	Y_{NTS} [μm]	X_{TS} [μm]	Y_{TS} [μm]	$e_{X,ave}$ [μm]	$e_{Y,ave}$ [μm]	ε_X [-]	ε_Y [-]	ε_o [-]	φ [deg]
6800	0	0.0	0.50	0.49	0.79	0.60	-0.65	0.54	12.78	12.38	20.16	15.20	16.47	13.79	0.00	0.00	0.00	-
	726	105.3	0.37	1.37	0.65	1.36	-0.51	1.36	9.46	34.85	16.54	34.47	13.00	34.66	0.04	0.25	0.26	9.45
	1452	210.5	0.36	1.82	0.64	1.84	-0.50	1.83	9.26	46.11	16.25	46.70	12.76	46.40	0.05	0.40	0.40	6.50
	2177	315.8	0.41	2.16	0.66	2.21	-0.53	2.18	10.47	54.76	16.67	56.16	13.57	55.46	0.04	0.50	0.51	3.99
	2903	421.1	0.51	2.45	0.71	2.51	-0.61	2.48	12.84	62.13	18.01	63.88	15.42	63.01	0.01	0.60	0.60	1.22
9000	0	0.0	0.44	0.53	0.67	0.58	-0.56	0.55	11.17	13.45	17.03	14.67	14.10	14.06	0.00	0.00	0.00	-
	726	105.3	0.35	1.19	0.61	1.14	-0.48	1.16	8.98	30.21	15.47	28.97	12.23	29.59	0.02	0.19	0.19	6.87
	1452	210.5	0.38	1.60	0.61	1.57	-0.49	1.59	9.60	40.74	15.53	39.97	12.56	40.35	0.02	0.32	0.32	3.34
	2177	315.8	0.41	1.89	0.63	1.89	-0.52	1.89	10.30	47.94	16.10	48.02	13.20	47.98	0.01	0.41	0.41	1.52
	2903	421.1	0.47	2.12	0.69	2.12	-0.58	2.12	11.95	53.81	17.53	53.76	14.74	53.78	-0.01	0.48	0.48	-0.92
10800	0	0.0	0.46	0.57	0.56	0.53	-0.51	0.55	11.75	14.39	14.18	13.41	12.96	13.90	0.00	0.00	0.00	-
	726	105.3	0.36	1.09	0.57	0.98	-0.46	1.04	9.14	27.80	14.47	24.78	11.81	26.29	0.01	0.15	0.15	5.33
	1452	210.5	0.35	1.44	0.55	1.36	-0.45	1.40	8.85	36.48	13.99	34.42	11.42	35.45	0.02	0.26	0.26	4.09
	2177	315.8	0.37	1.69	0.57	1.64	-0.47	1.66	9.47	42.82	14.50	41.68	11.98	42.25	0.01	0.34	0.34	1.98
	2903	421.1	0.43	1.91	0.61	1.89	-0.52	1.90	10.82	48.60	15.47	48.10	13.14	48.35	0.00	0.42	0.42	-0.30
13200	0	0.0	0.38	0.63	0.61	0.39	-0.50	0.51	9.73	16.01	15.48	9.88	12.60	12.94	0.00	0.00	0.00	-
	726	105.3	0.35	1.10	0.64	0.78	-0.49	0.94	8.84	28.01	16.28	19.93	12.56	23.97	0.00	0.13	0.13	0.22
	1452	210.5	0.34	1.48	0.65	1.10	-0.50	1.29	8.66	37.49	16.63	27.86	12.64	32.68	0.00	0.24	0.24	-0.12
	2177	315.8	0.27	1.40	0.31	0.95	-0.29	1.18	6.80	35.68	7.99	24.25	7.39	29.97	0.06	0.21	0.22	17.01
	2903	421.1	0.31	1.64	0.38	1.17	-0.35	1.41	7.76	41.78	9.77	29.81	8.77	35.79	0.05	0.28	0.28	9.53

APPENDIX B: PAD METAL TEMPERATURES

Table 13: LOP Pad Metal Temperatures

Running Speed [rpm]	Unit Loading [kPa]	Unit Loading [psi]	T_{in} [°C]	T_{out} [°C]	*Pad Temperatures (°C)*																			
					Pad 3 [°]											Pad 4 [°]						Pad 1 [°]		Pad 2 [°]	
					0	1	2	3	4	5	6	7	8	9	10	T11	T12	T13	T14	T15	T16	T17	T18	T19	T20
6800	0	0.0	43.9	47.7	49.1	51.4	54.3	56.9	61.2	61.9	54.0	48.0	50.2	54.9	54.1	45.9	47.8	49.8	51.4	57.0	49.1	48.9	62.9	46.3	54.8
	726	105.3	43.8	48.3	54.6	57.7	61.7	65.2	70.3	69.3	57.7	51.4	54.3	60.2	58.5	45.9	47.6	49.5	50.9	56.4	48.9	45.7	53.6	47.0	56.2
	1452	210.5	43.7	49.0	58.6	62.4	67.2	71.4	77.4	75.0	60.6	53.9	57.4	64.5	61.9	46.1	47.9	49.8	51.2	56.9	49.3	44.9	50.0	48.0	57.5
	2177	315.8	43.8	49.4	61.8	65.8	71.0	75.6	82.1	77.9	62.7	55.7	59.6	67.1	63.6	46.3	48.2	50.2	51.8	57.7	50.1	44.6	48.4	49.1	58.4
	2903	421.1	43.8	49.7	64.2	68.0	73.4	77.6	82.8	77.4	69.6	57.8	61.6	68.2	63.0	46.3	48.5	50.8	52.6	59.1	51.3	48.7	52.3	48.0	53.8
9000	0	0.0	43.5	52.4	52.8	56.3	60.9	65.1	72.3	72.4	48.7	50.6	54.0	61.4	59.2	47.1	50.2	53.6	56.2	65.2	53.1	50.4	67.5	47.0	55.1
	726	105.3	43.5	52.9	57.9	62.6	68.5	73.6	82.3	80.2	62.5	54.0	58.3	67.1	63.8	47.3	50.0	53.1	55.3	64.1	52.6	47.8	57.8	47.2	57.3
	1452	210.5	43.5	53.0	62.0	67.6	74.2	79.8	89.6	85.1	65.3	56.6	61.4	71.2	67.0	47.5	50.3	53.2	55.4	64.1	52.9	46.8	53.4	47.9	59.1
	2177	315.8	43.5	53.3	65.2	71.4	78.5	84.6	95.2	87.7	67.6	58.5	63.6	74.0	68.9	48.1	50.9	54.0	56.3	65.6	54.2	46.5	51.7	49.4	60.9
	2903	421.1	43.6	52.8	67.9	74.7	82.2	88.9	99.8	88.6	69.4	60.1	65.5	76.1	69.9	48.3	51.3	54.8	57.2	67.3	55.8	46.0	50.4	50.5	62.4
10800	0	0.0	43.9	54.7	50.6	54.1	57.6	61.0	67.5	70.0	61.8	50.4	53.3	60.7	60.2	57.2	63.5	69.9	73.9	84.6	64.0	52.7	71.0	54.9	72.3
	726	105.3	43.9	54.8	57.0	62.8	69.7	75.9	86.7	85.6	64.1	54.1	59.0	70.0	67.6	48.8	52.0	55.4	57.9	68.6	55.3	49.3	61.2	48.4	60.8
	1452	210.5	43.8	55.0	61.0	68.3	76.1	83.0	93.9	91.2	67.2	56.8	62.3	74.5	71.3	49.1	52.3	55.7	58.1	68.7	56.0	48.1	56.3	49.0	62.5
	2177	315.8	43.9	55.0	64.5	72.7	81.1	88.5	100.6	93.8	69.8	58.9	64.8	77.8	73.6	49.4	52.8	56.2	58.8	69.6	57.1	47.4	53.7	50.2	64.0
	2903	421.1	43.9	54.9	67.7	76.9	85.9	94.0	106.1	95.1	72.0	60.9	67.2	80.5	75.0	49.6	53.1	56.8	59.6	71.4	58.4	46.9	52.2	51.3	65.8
13200	0	0.0	44.7	57.8	55.3	58.8	63.4	68.1	76.7	80.0	62.6	52.2	56.1	65.6	64.7	51.6	55.6	59.4	62.2	74.1	60.3	54.6	74.6	51.4	63.8
	726	105.3	44.7	57.8	57.9	62.5	68.5	74.5	85.1	87.8	65.3	54.3	59.0	70.4	68.9	51.2	55.0	58.7	61.5	74.0	60.1	52.1	65.9	51.4	65.1
	1452	210.5	44.5	57.8	60.6	66.8	74.3	81.6	94.4	95.0	68.2	56.4	61.9	75.4	72.7	51.0	54.9	58.7	61.5	74.3	60.3	50.3	60.4	51.8	66.4
	2177	315.8	44.4	58.1	63.9	71.5	80.2	88.8	102.3	99.3	71.1	58.6	64.9	79.8	76.1	51.3	55.3	59.3	62.2	75.7	61.4	49.7	57.7	52.6	68.3
	2903	421.1	44.4	58.2	67.6	77.0	87.0	96.8	111.0	102.0	74.2	61.0	68.1	84.0	78.8	51.6	55.7	59.8	62.9	77.3	62.3	49.1	55.8	53.3	70.5

Table 14: LBP Pad Metal Temperatures

Running Speed [rpm]	Unit Loading [kPa]	Unit Loading [psi]	T_{in} [°C]	T_{out} [°C]	*Pad Temperatures (°C)*																			
					Pad 3 [°]											Pad 4 [°]						Pad 1 [°]		Pad 2 [°]	
					0	1	2	3	4	5	6	7	8	9	10	T11	T12	T13	T14	T15	T16	T17	T18	T19	T20
6800	0	0.0	130.7	49.2	48.2	50.4	52.7	54.9	58.5	59.9	56.4	48.0	49.8	54.0	53.1	54.5	58.4	62.4	64.9	70.3	56.8	48.9	61.0	51.1	60.3
	726	105.3	130.7	50.7	54.1	57.4	61.2	64.3	68.5	68.0	61.7	51.9	54.7	60.1	57.7	57.1	62.2	67.4	70.6	76.0	60.3	48.4	54.8	49.4	56.8
	1452	210.5	130.7	51.7	58.8	62.2	66.6	70.1	74.9	72.8	65.2	54.5	57.7	63.7	60.2	58.0	64.2	70.4	74.2	80.3	62.9	48.8	53.6	48.8	55.5
	2177	315.8	130.7	52.6	62.0	65.5	70.4	74.2	79.4	75.7	67.6	56.4	59.9	66.2	61.8	58.4	65.7	72.7	77.0	82.8	64.8	48.8	52.9	48.4	54.6
	2903	421.1	130.7	53.4	64.2	68.0	73.4	77.6	82.8	77.4	69.6	57.8	61.6	68.2	63.0	58.9	67.2	74.8	79.5	84.2	66.3	48.7	52.3	48.0	53.8
9000	0	0.0	130.7	54.8	49.7	52.6	55.6	58.4	63.7	65.6	59.4	49.5	51.9	58.0	57.2	55.6	61.1	66.7	70.2	78.4	60.6	51.0	66.6	53.2	67.1
	726	105.3	130.7	56.2	54.1	58.6	63.6	67.9	74.2	74.3	64.6	52.9	56.3	64.2	62.1	57.9	65.0	71.9	76.2	84.9	64.6	50.7	60.0	51.8	63.0
	1452	210.5	130.7	57.1	58.7	63.8	69.8	74.8	81.6	79.8	68.4	55.5	59.6	68.2	64.8	58.8	67.0	75.1	80.2	89.6	68.4	50.6	57.7	50.8	60.3
	2177	315.8	130.7	57.7	62.5	67.8	74.3	79.6	86.9	83.1	71.2	57.5	61.9	70.9	66.0	59.4	68.8	77.9	83.6	92.7	71.6	50.1	56.4	50.2	58.6
	2903	421.1	130.7	59.1	65.6	71.0	78.1	84.0	92.1	86.1	73.7	59.2	64.1	73.8	68.5	59.5	70.1	80.2	86.6	95.0	74.0	50.1	56.0	50.0	57.7
10800	0	0.0	130.7	58.7	50.6	54.1	57.6	61.0	67.5	70.0	61.8	50.4	53.3	60.7	60.2	57.2	63.5	69.9	73.9	84.6	64.0	52.7	71.0	54.9	72.3
	726	105.3	130.7	59.7	53.7	59.0	64.5	69.5	77.4	78.3	66.4	53.1	57.0	66.5	65.0	59.2	67.0	74.7	79.7	91.1	69.0	51.7	63.9	53.4	67.2
	1452	210.5	130.7	60.1	57.2	63.6	70.4	76.4	85.0	84.3	70.2	55.6	60.1	70.9	68.6	60.3	69.4	78.3	84.0	95.8	72.6	51.6	61.0	52.4	64.2
	2177	315.8	130.7	60.5	60.6	67.7	75.3	82.0	91.6	88.7	73.3	57.6	62.7	74.5	71.4	60.9	71.1	81.3	87.8	99.7	75.9	51.7	60.0	52.1	62.4
	2903	421.1	130.7	61.0	64.2	71.7	80.1	87.4	97.8	91.8	76.3	59.7	65.3	77.7	73.4	61.7	73.3	84.6	91.9	102.1	78.7	51.6	59.0	51.7	61.1
13200	0	0.0	130.7	61.7	52.9	55.9	59.5	63.1	69.6	73.7	64.7	51.8	55.0	62.9	62.4	60.8	67.7	74.1	78.8	92.8	70.7	54.8	73.7	56.9	72.1
	726	105.3	130.7	62.3	55.7	59.3	64.3	68.9	76.7	80.6	68.3	53.7	57.5	67.0	65.8	62.0	70.5	78.6	84.4	99.8	75.0	54.0	68.2	56.2	68.7
	1452	210.5	130.7	62.7	58.4	62.8	68.7	74.4	83.5	87.1	71.7	55.6	60.0	71.0	69.2	62.8	72.9	82.7	89.6	105.0	78.2	53.6	65.8	56.2	66.8
	2177	315.8	130.7	60.9	56.0	61.8	68.4	74.7	85.2	88.2	69.5	54.3	59.0	70.9	69.0	58.6	66.8	75.9	82.3	99.7	74.0	51.8	63.4	54.8	68.3
	2903	421.1	130.7	61.8	58.5	64.7	72.0	79.0	90.5	92.8	72.4	56.0	61.1	74.2	71.8	59.7	68.8	79.0	86.4	104.3	77.5	52.0	62.9	55.2	67.3

APPENDIX C: THERMAL PAD DEFLECTION

Orientation	Speed (rpm)	Pad Number	Machined Pad Radius (mm)	Preload	Thermal Change in Pad Radius (mm)	Resulting Preload
LOP	6800	3 (Loaded Pad)	0.112	0.495	0.026	0.589
		4	0.112	0.381	0.016	0.457
		1	0.112	0.495	0.016	0.559
		2	0.112	0.381	0.016	0.460
	13200	3 (Loaded Pad)	0.112	0.516	0.034	0.628
		4	0.112	0.403	0.021	0.497
		1	0.112	0.516	0.020	0.588
		2	0.112	0.403	0.020	0.492
LBP	6800	3	0.112	0.389	0.025	0.500
		4	0.112	0.417	0.027	0.530
		1	0.112	0.389	0.016	0.464
		2	0.112	0.417	0.016	0.489
	13200	3	0.112	0.432	0.030	0.552
		4	0.112	0.438	0.036	0.574
		1	0.112	0.432	0.020	0.518
		2	0.112	0.438	0.020	0.523

APPENDIX D: ROTORDYNAMIC COEFFICIENTS

Table 15: LOP Experimental Rotordynamic Coefficients

Running Speed [rpm]	Unit Loading [kPa]	Unit Loading [psi]	*Rotordynamic Coefficients*												*Uncertainties*											
			Stiffness [MN/m]				Damping [kN-s/m]				Added Mass [kg]				Stiffness [MN/m]				Damping [kN-s/m]				Added Mass [kg]			
			Kxx	Kxy	Kyx	Kyy	Cxx	Cxy	Cyx	Cyy	Mxx	Mxy	Myx	Myy	Kxx	Kxy	Kyx	Kyy	Cxx	Cxy	Cyx	Cyy	Mxx	Mxy	Myx	Myy
6800	0	0.0	97.0	-12.6	-25.1	192.3	225.8	-6.5	-11.3	300.7	-24.2	-35.5	-37.7	-29.1	44.1	29.5	59.2	49.6	14.9	17.8	25.0	35.2	39.9	26.7	53.5	44.9
	726	105.3	120.9	-13.4	-3.1	267.3	222.8	10.9	-20.8	288.4	-3.4	-37.3	6.4	-14.2	11.3	6.9	10.9	42.0	7.6	4.7	6.3	13.5	10.2	6.3	9.9	38.0
	1452	210.5	136.4	-11.9	-1.2	410.8	233.4	15.1	-17.3	286.0	-7.9	-36.4	7.7	-10.0	12.3	3.6	20.5	34.5	8.7	5.1	8.7	23.8	11.1	3.2	18.5	31.2
	2177	315.8	155.3	-6.3	-8.1	562.5	247.5	14.0	-19.3	279.5	-14.5	-33.1	4.3	-5.2	10.1	5.5	5.0	30.3	7.5	3.8	5.0	26.6	9.1	5.0	4.5	27.4
	2903	421.1	180.1	-3.5	-10.5	687.7	264.2	13.2	-19.8	265.6	-22.3	-32.0	4.4	-3.2	10.8	6.0	3.8	31.0	8.3	5.2	5.6	28.9	9.7	5.5	3.4	28.0
9000	0	0.0	144.9	-22.4	-12.5	264.3	227.0	8.3	-15.4	271.2	-4.3	-35.1	-11.6	-65.1	16.7	8.0	8.3	36.7	10.4	7.1	6.1	24.6	15.1	7.3	7.5	33.2
	726	105.3	155.5	-23.5	-9.0	363.6	231.2	16.8	-20.4	272.2	-9.3	-39.4	-0.6	-13.6	15.9	5.5	9.2	37.8	8.4	4.1	3.3	22.1	14.4	5.0	8.4	34.2
	1452	210.5	175.2	-21.1	-11.5	490.3	235.5	16.4	-21.2	257.2	-12.2	-39.4	-0.8	-4.3	14.7	5.4	7.4	29.6	7.5	5.5	2.8	28.3	13.3	4.9	6.7	26.8
	2177	315.8	201.4	-16.3	-14.7	605.0	242.8	14.3	-20.1	248.8	-15.0	-35.4	-0.7	-0.9	13.6	6.3	5.6	26.5	7.4	5.3	2.6	28.4	12.3	5.7	5.0	23.9
	2903	421.1	228.7	-12.7	-17.4	726.1	255.8	12.4	-20.4	234.9	-20.7	-35.1	0.3	7.7	13.3	7.4	4.3	26.3	7.7	6.6	3.0	31.1	12.0	6.7	3.9	23.8
10800	0	0.0	173.8	-22.2	-22.3	297.1	227.1	-0.7	-10.2	264.0	-16.6	-26.2	-24.9	-66.2	16.2	5.6	7.4	30.0	10.9	7.2	7.6	22.1	14.6	5.1	6.7	27.2
	726	105.3	185.2	-23.0	-15.6	383.7	228.5	9.9	-18.1	253.8	-17.0	-28.6	-8.5	-12.9	17.9	6.7	5.4	41.9	10.7	4.8	3.2	21.8	16.2	6.0	4.9	37.9
	1452	210.5	206.9	-25.3	-17.3	496.0	230.6	15.5	-19.8	239.6	-17.7	-32.9	-7.6	-3.9	15.9	5.8	5.0	29.2	9.7	3.9	2.7	23.3	14.4	5.2	4.5	26.4
	2177	315.8	231.8	-23.9	-19.6	605.7	236.1	16.8	-19.6	235.2	-18.7	-35.8	-6.4	1.7	14.2	5.9	5.1	25.9	9.1	4.4	2.8	27.6	12.9	5.3	4.7	23.5
	2903	421.1	259.6	-20.8	-20.9	728.6	247.5	16.2	-21.7	218.9	-23.5	-38.7	-4.2	15.3	13.9	6.6	4.3	25.4	9.4	6.0	2.9	30.6	12.6	6.0	3.9	23.0
13200	0	0.0	208.1	-2.5	-36.7	306.0	208.9	-30.1	9.1	246.9	-19.2	-12.7	-30.7	-64.0	10.2	7.4	9.1	27.4	8.0	9.6	11.5	23.2	9.2	6.7	8.2	24.8
	726	105.3	217.5	-2.5	-31.9	382.5	211.6	-18.9	0.2	237.3	-18.1	-8.8	-16.1	-10.9	12.9	6.1	4.8	36.0	8.4	5.3	2.5	14.3	11.7	5.5	4.3	32.6
	1452	210.5	238.2	-19.3	-33.2	476.7	217.3	0.2	-2.7	231.9	-19.3	-23.7	-16.6	-6.1	11.8	4.8	3.2	28.7	8.3	2.2	2.5	26.3	10.7	4.4	2.9	26.0
	2177	315.8	265.7	-23.2	-35.8	583.4	222.1	7.7	-3.0	226.3	-19.2	-29.1	-16.2	2.5	10.6	5.3	2.3	24.2	7.8	2.6	3.0	27.6	9.6	4.8	2.1	21.9
	2903	421.1	293.9	-24.7	-38.3	705.9	232.0	11.7	-5.4	210.1	-22.9	-34.8	-15.8	13.0	10.6	5.6	2.2	24.4	8.3	4.2	3.6	33.2	9.6	5.0	1.9	22.1

Table 16: LBP Experimental Rotordynamic Coefficients

Running Speed [rpm]	Unit Loading [kPa]	Unit Loading [psi]	*Rotordynamic Coefficients*												*Uncertainties*											
			Stiffness [MN/m]				Damping [kN-s/m]				Added Mass [kg]				Stiffness [MN/m]				Damping [kN-s/m]				Added Mass [kg]			
			Kxx	Kxy	Kyx	Kyy	Cxx	Cxy	Cyx	Cyy	Mxx	Mxy	Myx	Myy	Kxx	Kxy	Kyx	Kyy	Cxx	Cxy	Cyx	Cyy	Mxx	Mxy	Myx	Myy
6800	0	0.0	175.8	-51.0	-48.9	168.7	232.0	-22.4	-29.2	237.9	-50.5	-38.1	-9.1	-54.0	8.1	4.6	14.4	29.6	6.5	7.7	10.3	18.2	7.4	4.1	13.0	26.8
	726	105.3	212.9	-57.9	-56.4	224.0	215.3	-20.6	-27.1	215.1	-42.4	-32.5	6.7	-40.4	5.7	9.0	10.3	34.5	4.6	4.1	8.7	13.6	5.1	8.1	9.3	31.2
	1452	210.5	256.2	-60.8	-67.5	291.0	185.8	-30.1	-26.8	181.6	-32.9	-24.7	-10.3	-36.7	5.6	5.4	16.6	19.1	3.8	4.2	12.2	10.2	5.1	4.9	15.0	17.3
	2177	315.8	294.7	-63.9	-71.6	345.4	165.5	-36.9	-33.9	163.2	-27.1	-19.0	-12.9	-37.6	5.9	4.4	14.8	28.9	4.1	3.1	15.9	29.9	5.3	4.0	13.4	26.2
	2903	421.1	323.2	-72.6	-85.4	387.0	158.4	-43.8	-23.2	159.4	-22.1	-20.2	-23.4	-41.4	4.8	22.8	14.9	43.1	7.6	11.5	12.1	25.7	2.2	10.7	7.0	20.2
9000	0	0.0	221.9	-69.1	-57.9	200.0	219.0	-9.4	-18.1	227.0	-52.4	-43.4	-12.6	-69.5	11.7	11.9	10.3	33.9	12.0	6.9	15.1	23.7	10.6	10.8	9.3	30.6
	726	105.3	251.7	-71.6	-66.4	257.6	200.7	-12.7	-21.4	196.4	-36.1	-35.1	-9.3	-35.0	9.2	9.5	8.0	32.5	7.0	4.1	6.5	11.5	8.3	8.6	7.2	29.4
	1452	210.5	286.6	-73.2	-71.5	316.7	176.4	-24.1	-30.4	169.0	-27.6	-27.5	-7.6	-27.1	7.9	4.9	5.8	19.0	5.2	3.4	6.3	8.9	7.2	4.5	5.2	17.2
	2177	315.8	316.5	-75.3	-76.7	362.0	159.2	-31.1	-33.9	154.6	-23.0	-23.9	-8.6	-22.0	7.6	4.8	7.9	36.4	5.5	3.4	6.5	12.2	6.9	4.3	7.1	33.0
	2903	421.1	339.0	-77.4	-86.9	411.1	146.3	-35.3	-38.1	138.1	-20.4	-19.5	-15.4	-18.5	7.2	4.1	12.8	19.1	5.4	3.0	13.1	15.4	6.5	3.7	11.6	17.3
10800	0	0.0	247.9	-71.8	-89.8	240.4	206.5	-17.2	-11.2	215.4	-75.6	-36.6	-59.5	-75.2	29.2	8.2	41.4	29.2	9.1	19.7	11.9	24.2	26.4	7.5	37.5	26.5
	726	105.3	278.5	-74.5	-74.8	280.7	193.3	-14.2	-15.7	186.8	-40.0	-28.9	-16.9	-38.8	10.5	8.6	7.1	30.0	7.7	4.7	6.8	15.5	9.5	7.8	6.4	27.2
	1452	210.5	306.2	-77.1	-80.2	332.0	171.4	-22.8	-27.6	161.6	-29.7	-23.0	-17.2	-25.0	9.0	5.6	10.8	17.4	5.9	3.8	7.0	14.2	8.2	5.0	9.7	15.7
	2177	315.8	331.9	-80.4	-85.4	376.7	155.9	-29.1	-31.4	145.4	-25.0	-19.6	-11.5	-20.4	8.1	4.8	9.1	17.6	5.5	2.5	8.5	13.3	7.3	4.3	8.3	15.9
	2903	421.1	353.0	-84.8	-90.8	421.8	145.5	-33.4	-34.6	131.1	-22.5	-18.2	-12.4	-18.7	7.5	3.6	6.3	13.3	5.8	2.6	8.3	13.5	6.8	3.3	5.7	12.1
13200	0	0.0	288.3	-60.8	-93.7	275.6	174.8	-42.3	-20.2	192.0	-35.0	0.8	-15.4	-45.2	5.1	3.7	10.1	25.2	4.0	8.7	7.2	19.2	4.6	3.4	9.1	22.8
	726	105.3	310.0	-74.6	-98.5	311.1	164.1	-35.4	-19.5	170.9	-26.8	-3.9	-14.9	-29.3	5.8	8.3	6.7	26.2	4.3	9.0	4.6	10.7	5.3	7.5	6.1	23.7
	1452	210.5	336.3	-87.0	-101.7	350.7	150.5	-31.8	-22.7	153.4	-21.7	-7.2	-11.2	-24.3	5.2	5.4	6.3	18.0	4.6	8.2	6.1	10.0	4.7	4.9	5.7	16.3
	2177	315.8	325.6	-72.0	-83.9	347.5	153.3	-32.6	-21.0	151.9	-21.7	-8.4	-4.9	-21.6	7.6	6.2	16.2	23.8	4.7	7.1	13.3	10.5	6.9	5.6	14.7	21.5
	2903	421.1	348.8	-81.5	-91.8	381.1	144.9	-32.7	-27.8	142.1	-19.3	-11.1	-10.2	-19.4	6.1	5.3	5.3	14.9	3.9	5.2	6.3	11.0	5.5	4.8	4.8	13.5

APPENDIX E: WFR CALCULATION

From the homogeneous solution for the equations of motion of the rotor and bearing supports, the whirl frequency ration ϕ is obtained from the following quartic equations, San Andrés [24]:

$$\frac{M_r}{K_r}\alpha_i\omega_s^4 - \left[1+\alpha_i+\frac{K_{eq}}{K_r}\right]\omega_s^2 + \frac{K_{eq}}{M_r} = 0$$

and,

$$\phi^4 I_4 + \phi^2\left(I_2 - 1\right) + \phi_o^2$$

where,

$$\alpha_i = \frac{\left(M_{xx}+M_{yy}\right)-2I_1}{2M_r}$$

$$K_{eq} = \frac{K_{xx}C_{yy}+C_{xx}K_{yy}-C_{yx}K_{xy}-C_{xy}K_{yx}}{C_{xx}+C_{yy}}$$

$$I_1 = \frac{C_{yx}M_{xy}+C_{xy}M_{yx}}{C_{xx}+C_{yy}}$$

$$I_2 = \frac{K_{xy}M_{yx}+K_{yx}M_{xy}-I_1\left(K_{xx}+K_{yy}\right)+2K_{eq}I_1}{C_{xx}C_{yy}-C_{xy}C_{yx}}$$

$$I_4 = \Omega_s^2\frac{I_1^2-M_{xy}M_{yx}}{C_{xx}C_{yy}-C_{xy}C_{yx}}$$

and,

$$\phi_o^2 = \frac{\left(K_{eq}-K_{xx}\right)\left(K_{eq}-K_{yy}\right)-K_{xy}K_{yx}}{\Omega_s^2\left(C_{xx}C_{yy}-C_{xy}C_{yx}\right)}$$

APPENDIX F: LBP DYNAMIC STIFFNESS

As with predictions generated in the LOP orientation, the hot clearance measurements were used in modeling the predictions; giving a more accurate representation than a cold clearance measurement of the bearing clearance. The baseline results, shown in Figure 12 and Figure 13, were subtracted from the dynamic stiffness to obtain the dynamic response of the fluid-film only.

The following figure presents the measured and predicted dynamic stiffness functions for the LBP orientation at 6.8 krpm. Figure 57 shows the predictions at 725 kPa while Figure 58 shows the predictions at 2903 kPa.

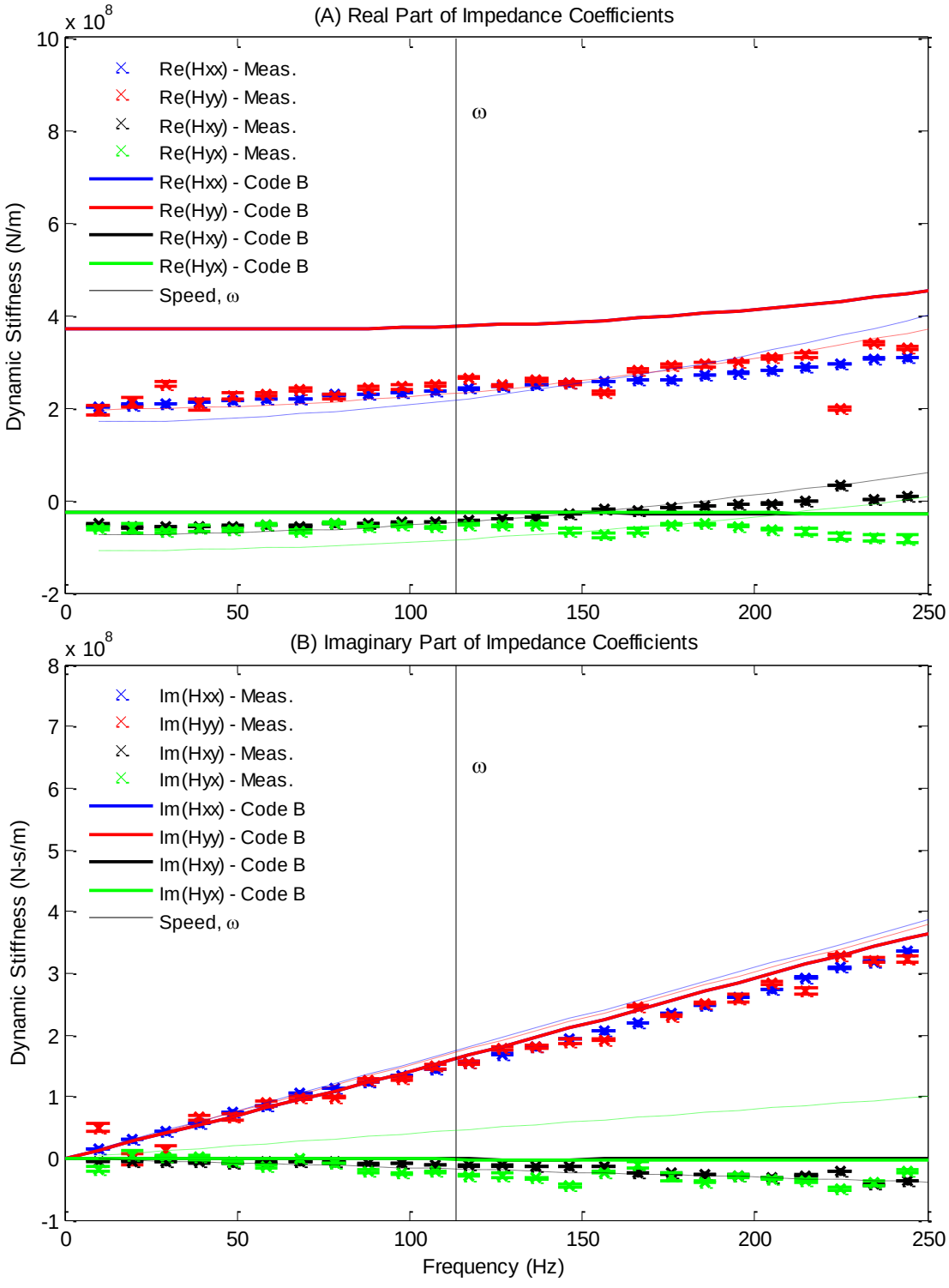

Figure 57: LBP Components of Measurements and Predicted (Code B) Bearing Impedance Coefficients at 6,800 rpm with 725 kPa (105.3 psi) Static Load

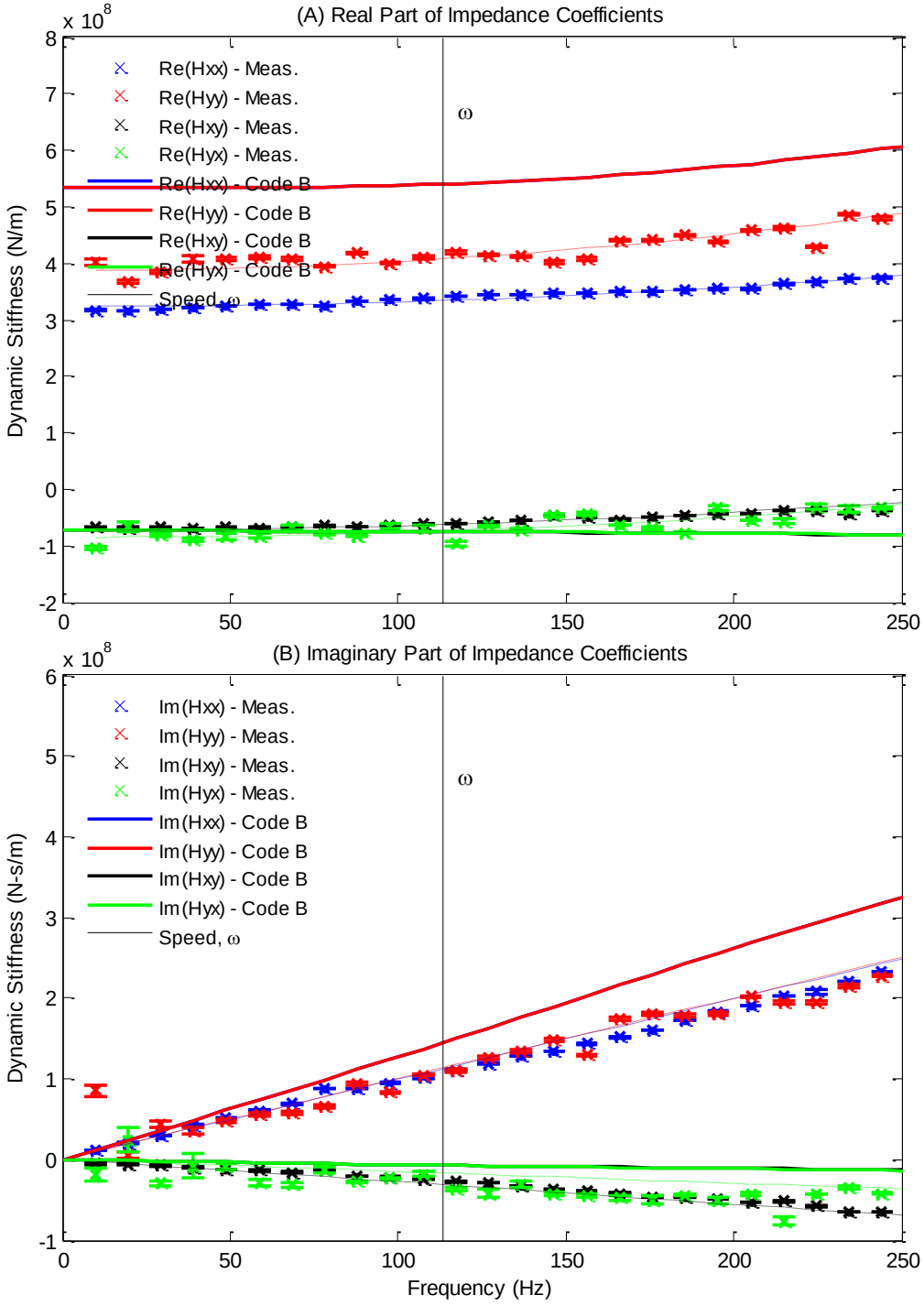

Figure 58: LBP Components of Measurements and Predicted (Code B) Bearing Impedance Coefficients at 6,800 rpm with 2903 kPa (421.1 psi) Static Load

In the unloaded case, Re($\boldsymbol{H_{yy}}$) = Re($\boldsymbol{H_{xx}}$), and in the loaded case Re($\boldsymbol{H_{yy}}$) is greater than Re($\boldsymbol{H_{xx}}$), showing slight orthotropy. In the loaded case, the Re($\boldsymbol{H_{xy}}$) and Re($\boldsymbol{H_{yx}}$) are similar. Similar to the lightly loaded LOP orientation, at larger frequencies Re($\boldsymbol{H_{xy}}$) and Re($\boldsymbol{H_{yx}}$) have opposite signs, suggesting an impact on stability (See Whirl Frequency Ratio). Both figures show frequency-independent direct-damping coefficients. For both cases, measured Im($\boldsymbol{H_{xx}}$) have the same value as Im($\boldsymbol{H_{yy}}$). Im($\boldsymbol{H_{xy}}$) and Im($\boldsymbol{H_{yx}}$) are both negative and become slightly more negative as Ω increases.

Direct dynamic-stiffness predictions are the same [Re($\boldsymbol{H_{xx}}$) = Re($\boldsymbol{H_{yy}}$), Im($\boldsymbol{H_{xx}}$) = Im($\boldsymbol{H_{yy}}$)] regardless of load, while measured values change with load. Re($\boldsymbol{H_{xx}}$) and Re($\boldsymbol{H_{yy}}$) predictions are more accurately predicted at the lightly loaded case. At around 150 Hz the stiffness predictions begin to increase, making predictions worse. Im($\boldsymbol{H_{xx}}$) and Im($\boldsymbol{H_{yy}}$) are predicted very accurately in the lightly loaded case, but become lower than predicted as load increases. For the most part, measured and predicted Im($\boldsymbol{H_{xy}}$) and Im($\boldsymbol{H_{yx}}$) are slightly less than zero, and decrease with increasing Ω.

Figure 59 and Figure 60 show the LBP predictions at 13.2 krpm.

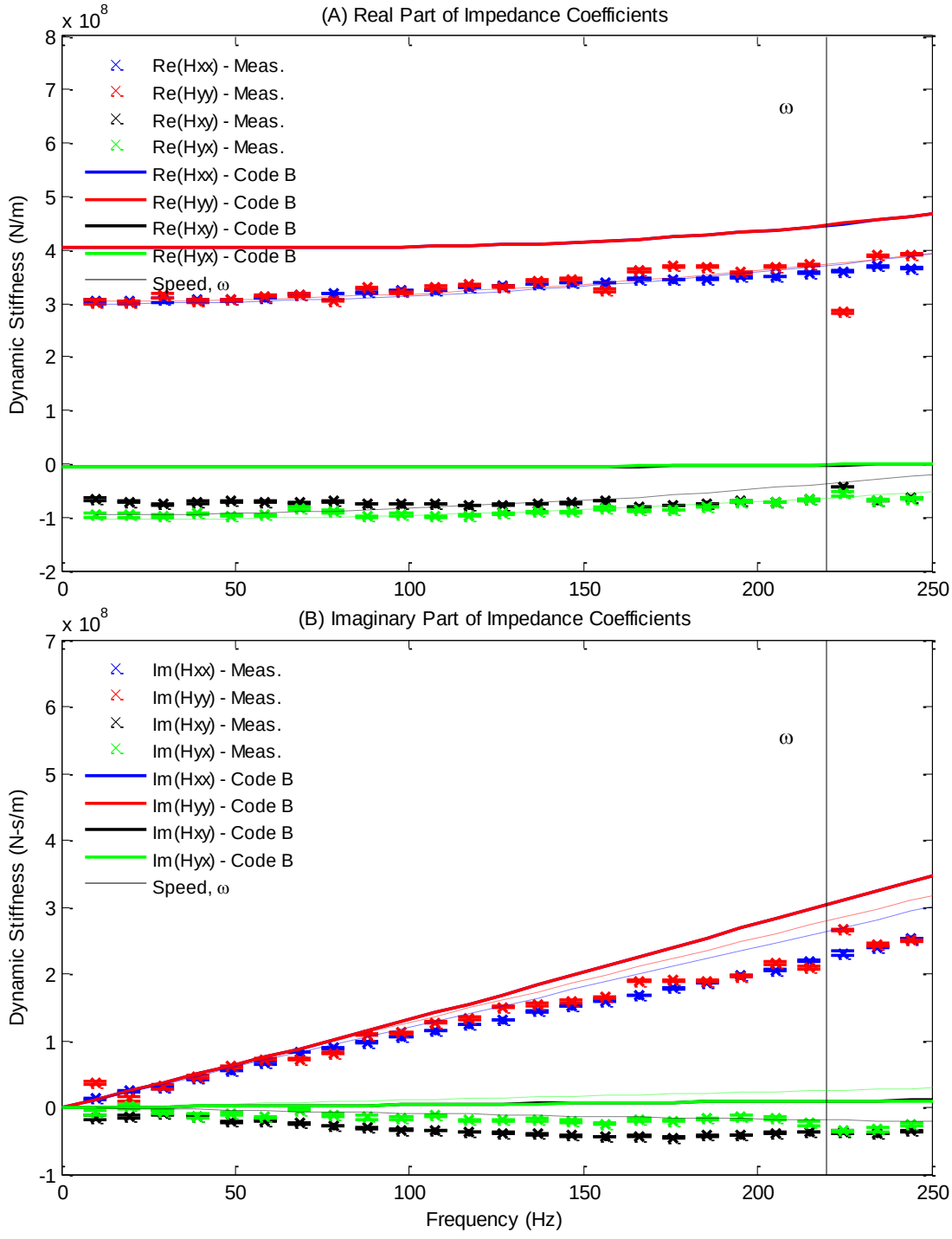

Figure 59: LBP Components of Measurements and Predicted (Code B) Bearing Impedance Coefficients at 13.2 krpm with 725 kPa (105.3 psi) Static Load

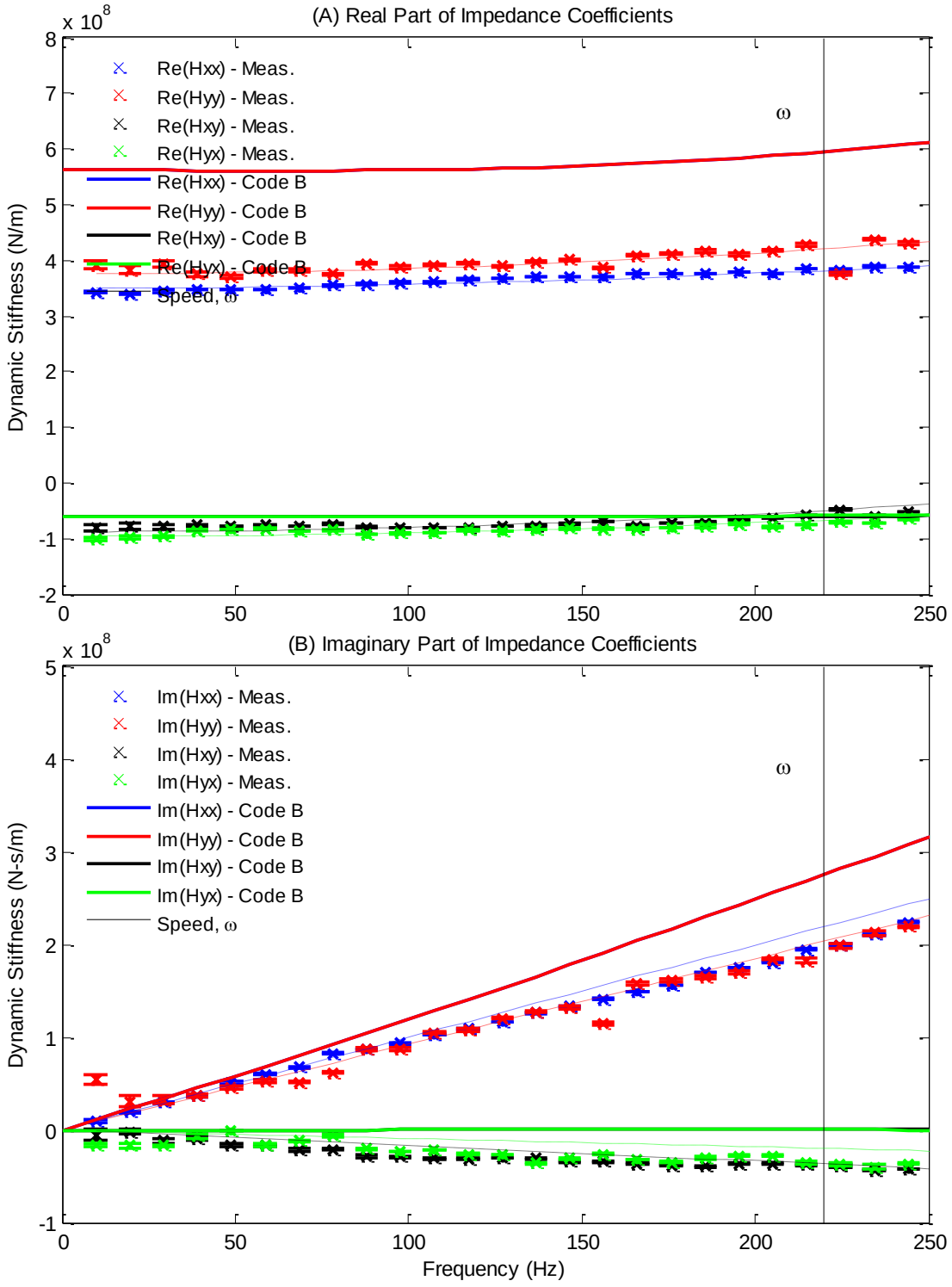

Figure 60: LBP Components of Measurements and Predicted (Code B) Bearing Impedance Coefficients at 13.2 krpm with 2903 kPa (421.1 psi) Static Load

As with the 6.8 krpm case, at 13.2 krpm measured Re($\boldsymbol{H_{yy}}$) = Re($\boldsymbol{H_{xx}}$) in the lightly loaded case. In the loaded case, Re($\boldsymbol{H_{yy}}$) is slightly larger than Re($\boldsymbol{H_{xx}}$), showing slight orthotropy. In the loaded case, measured Re($\boldsymbol{H_{xx}}$) and Re($\boldsymbol{H_{yy}}$) shows no dependency on Ω. In both cases, Re($\boldsymbol{H_{xy}}$) and Re($\boldsymbol{H_{yx}}$) terms are comparable at high frequencies and approximately equal to -1 MN/m.

Both figures show that Im($\boldsymbol{H_{xx}}$) and Im($\boldsymbol{H_{yy}}$) increases linearly with increasing frequency, resulting in frequency-independent direct damping coefficients. Im($\boldsymbol{H_{yy}}$) = Im($\boldsymbol{H_{xx}}$) in both cases. Both Im($\boldsymbol{H_{yy}}$) and Im($\boldsymbol{H_{xx}}$) slightly decrease with increasing frequency.

Predictions for (Re($\boldsymbol{H_{xx}}$) and Re($\boldsymbol{H_{yy}}$)) are the same regardless of load while measured values change with applied static load. Re($\boldsymbol{H_{xx}}$) and Re($\boldsymbol{H_{yy}}$) predictions are more accurate for the lightly loaded case, but are larger than measurements regardless of orientation. At around 150 Hz the Re($\boldsymbol{H_{xx}}$) and Re($\boldsymbol{H_{yy}}$) predictions begin to increase, making predictions worse. The model is more accurate at predicting Im($\boldsymbol{H_{xx}}$) and Im($\boldsymbol{H_{yy}}$) at lower frequencies. Measured Im($\boldsymbol{H_{xx}}$) and Im($\boldsymbol{H_{yy}}$) values are smaller than predicted and become more so as load and speed increase. For the most part, Im($\boldsymbol{H_{xy}}$) and Im($\boldsymbol{H_{yx}}$) predictions are zero or slightly less than zero while measured Im($\boldsymbol{H_{xy}}$) and Im($\boldsymbol{H_{yx}}$) values are less than zero.

In comparing the LBP orientation to the LOP orientation (Figure 40 - Figure 60), very different results were found. The LOP orientation showed significant orthotropy, while the LBP did not. For the lightly loaded case, a comparable Re($\boldsymbol{H_{yy}}$) value was

obtained, but as load increased the difference in Re($\boldsymbol{H_{yy}}$) and Re($\boldsymbol{H_{xx}}$) coefficients became greater.

Overall, both the LOP and LBP orientations show that the frequency dependency of the test bearing was modeled well with a [K][C][M] model. When a static load is applied the Re($\boldsymbol{H_{xx}}$) and Re($\boldsymbol{H_{yy}}$) are not dependent on Ω. In both orientations, Im($\boldsymbol{H_{yy}}$) and Im($\boldsymbol{H_{xx}}$) increase linearly with Ω, allowing for frequency independent damping coefficients.

APPENDIX G: LBP IMPORTANCE OF PAD FLEXIBILITY

To look at the effects that *pad* flexibility has on predicting the impedance coefficients in the LBP orientation, a series of predictions were created with Code B by changing the magnitude of the pad's calculated bending stiffness from Eq. (27). Figure 61 presents the measured and predicted K_{xx} and K_{yy} predictions for Code A and Code B in the LBP configuration.

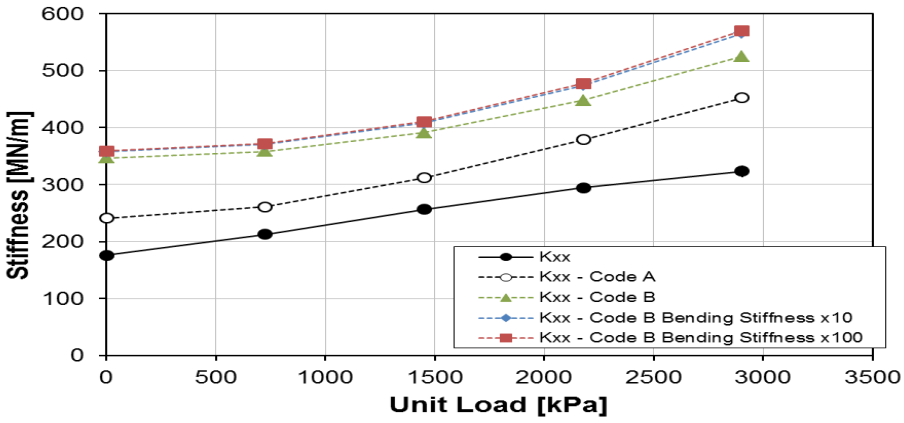

(A) K_{xx} at 6.8 krpm

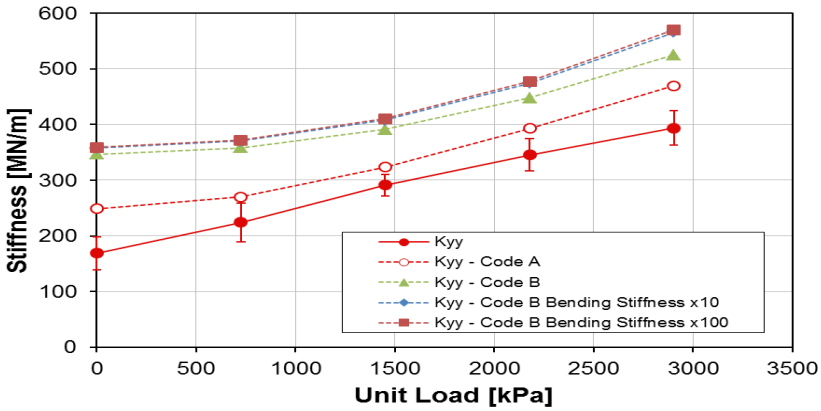

(B) K_{yy} at 6.8 krpm

Figure 61: Measured and Predicted Direct Stiffness Coefficients for LBP Orientation

As seen from Figure 61, Code B predicted higher K_{xx} and K_{yy} values than Code A. Code A predicts K_{xx} and K_{yy} much more accurately than Code B. Changing the bending stiffness from its actual value by a factor of 10 or by a factor of 100 in Code B, showed a 3% increase in predictions for K_{xx} and K_{yy}.

Figure 62 presents measured and predicted K_{xx} and K_{yy} values for Code A and Code B in the LBP configuration at 13.2 krpm.

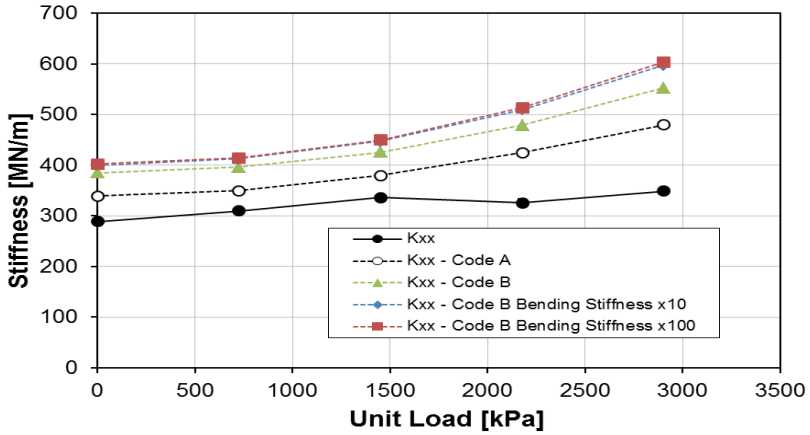

(A) K_{xx} at 13.2 krpm

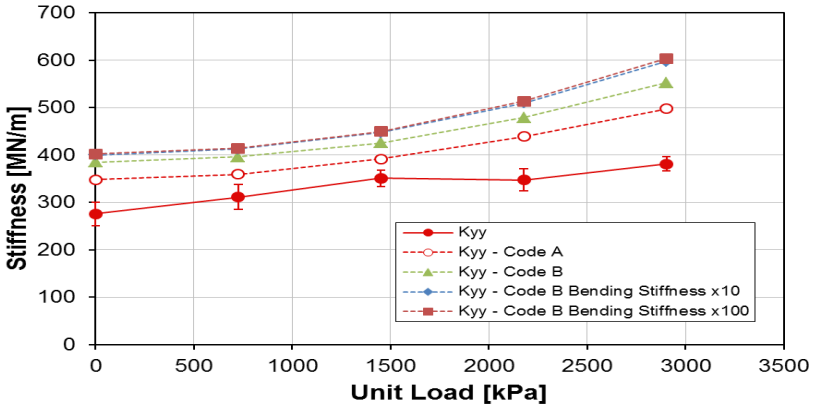

(B) K_{yy} at 13.2 krpm

Figure 62: Measured and Predicted Direct Stiffness Coefficients for LBP Orientation

As with the 6.8 krpm case, Code B predicted higher K_{xx} and K_{yy} values than Code A, and Code A predicts K_{xx} and K_{yy} more accurately than Code B. Changing the bending stiffness from its actual value by a factor of 10 or by a factor of 100 in Code B, showed a 9% increase in predictions for K_{xx} and K_{yy}.

Overall, changing the bending stiffness from its actual value by a factor of 10 or by a factor of 100 in Code B showed a 3-9% increase in predictions for K_{xx} and K_{yy}. Similar to the LOP orientation, for a flexible pad an increase in bending stiffness can have a large effect on predictions; however, for a more rigid pad an increase in pad bending stiffness will have a much lesser effect. When the bending stiffness was increased by a factor of 10 to a factor of 100, no changes in predictions resulted. These findings suggest that if the calculated bending stiffness of 22MN was 10 times greater, then the pads would be effectively rigid.

Figure 63 presents the measured and predicted direct damping coefficients for Code A and Code B in the LBP configuration.

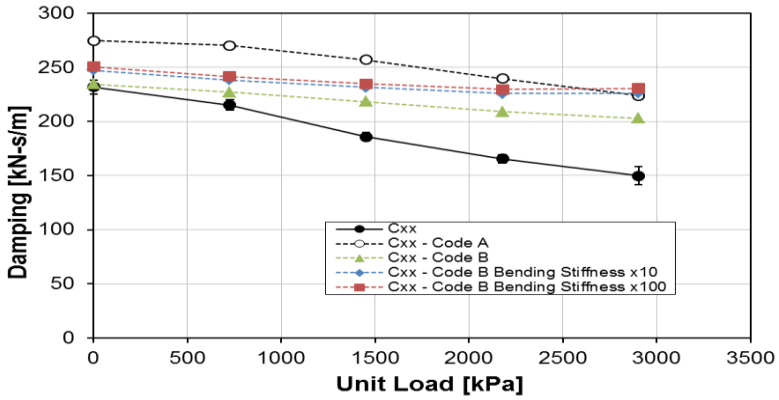

(A) C_{xx} at 6.8 krpm

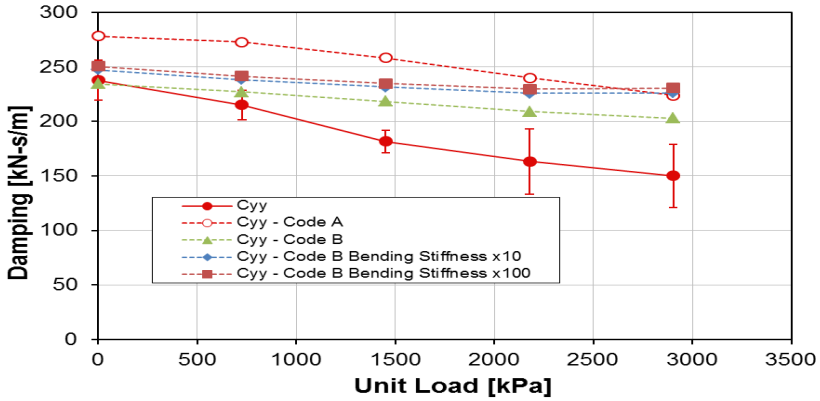

(B) C_{yy} at 6.8 krpm

Figure 63: Measured and Predicted Direct Stiffness Coefficients for LBP Orientation

Figure 63, shows that both codes predict C_{xx} and C_{yy} to be greater than measured values. At 6.8 krpm, Code B predicts C_{xx} and C_{yy} more accurately than Code A. Changing the bending stiffness from its actual value by a factor of 10 in Code B showed a 5% increase in predictions for C_{xx} and C_{yy}. When the bending stiffness was increased from a factor of 10 to a factor of 100, very slight changes in predictions were made.

Figure 64 presents the measured and predicted C_{xx} and C_{yy} for Code A and Code B in the LBP configuration at 13.2 krpm.

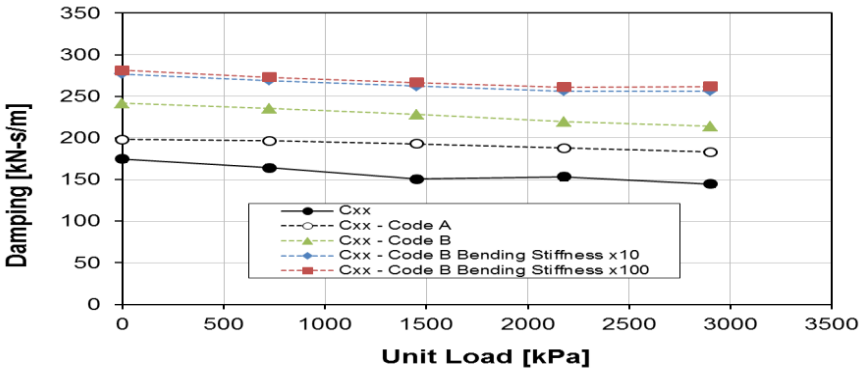

(A) C_{xx} at 13.2 krpm

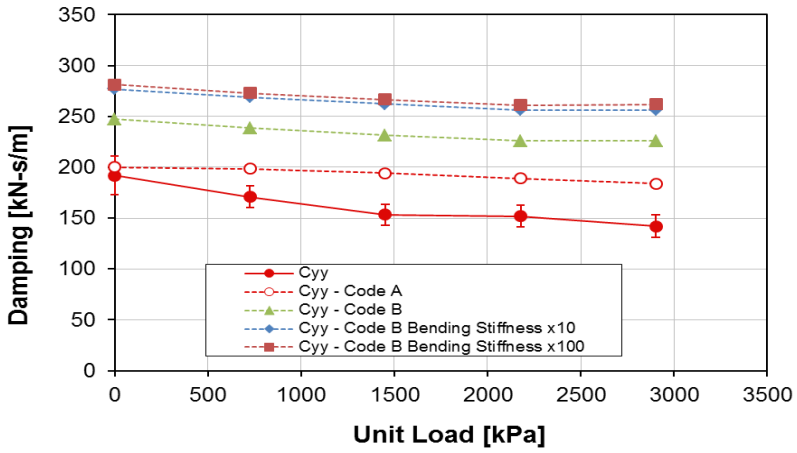

(B) C_{yy} at 13.2 krpm

Figure 64: Measured and Predicted Direct Stiffness Coefficients for LBP Orientation

At 13.2 krpm Code B predicts C_{xx} and C_{yy} to be greater than Code A. As speed increases, Code A predicts C_{xx} and C_{yy} more accurately than Code B. Changing the bending stiffness from its actual value by a factor of 10 in Code B showed an 18% increase in predictions for C_{xx} and C_{yy}.

Overall, increasing the bending stiffness used in Code B typically caused a 3-9% increase in K_{xx} and K_{yy}, and a 5-18% increase in C_{xx} and C_{yy}. In all cases, increasing the calculated bending stiffness, given in Eq. (27) by a factor of ten to hundred times caused slight if any change in K_{xx}, K_{yy}, C_{xx}, and C_{yy}. For a more flexible pad, an increase in bending stiffness can have a large effect on predictions; however, for a nearly rigid pad, an increase in pad bending stiffness will have much less effect. These findings suggest that if the calculated bending stiffness of 22MN were 10 times greater, then the pads could be considered rigid.

Results show that the pad's structural bending stiffness can be an important factor in predicting impedance coefficients. Even though the pads tested in this thesis are extremely stiff, changes are still seen in Code B's predictions when the magnitude of the pad's bending stiffness is increased, especially in C_{xx} and C_{yy}. Overall, Code A predicts K_{xx} and K_{yy} more accurately than Code B in both load orientations. In the LBP orientation, Code B predicts C_{xx} and C_{yy} more accurately at low rotor speeds. Code A predicts C_{xx} and C_{yy} more accurately at high rotor speeds.

APPENDIX H: EXPERIMENTAL DYNAMIC STIFFNESS

Load on Pad

Table 17: Dynamic Stiffness Real and Imaginary Parts at 6800 rpm and 0 kPa (MN/m)

f (Hz)	$R(H_{xx})$	$R(H_{xy})$	$R(H_{yx})$	$R(H_{yy})$	$I(H_{xx})$	$I(H_{xy})$	$I(H_{yx})$	$I(H_{yy})$	$\Delta R(H_{xx})$	$\Delta R(H_{xy})$	$\Delta R(H_{yx})$	$\Delta R(H_{yy})$	$\Delta I(H_{xx})$	$\Delta I(H_{xy})$	$\Delta I(H_{yx})$	$\Delta I(H_{yy})$
9.8	97.4	-13.4	-20.1	193.6	15.7	0.6	-3.4	54.5	-0.2	-1.5	-0.2	-3.9	-0.2	-1.1	-0.3	-2.4
19.5	99.3	-7.1	-16.6	155.8	30.2	0.4	-0.2	42.3	-0.1	-1.0	-0.2	-4.3	-0.1	-0.6	-0.2	-2.1
29.3	100.1	-14.5	-19.9	198.0	47.6	-5.4	-4.9	86.7	-0.1	-1.0	-0.2	-3.7	-0.1	-0.4	-0.1	-1.7
39.1	99.8	-12.3	-16.8	169.9	60.9	-2.1	-1.2	72.3	-0.1	-0.9	-0.2	-3.3	-0.2	-0.3	-0.2	-1.7
48.8	106.1	-17.7	-13.6	172.4	76.0	-2.1	-3.2	97.5	-0.1	-1.0	-0.2	-3.4	-0.2	-0.4	-0.2	-1.9
58.6	109.2	-7.9	-9.4	198.9	88.8	-2.8	-3.3	119.8	-0.1	-0.9	-0.2	-3.2	-0.3	-0.3	-0.2	-1.7
68.4	110.9	-5.7	-10.6	204.2	100.5	-3.7	-8.9	123.7	-0.1	-0.9	-0.2	-3.5	-0.2	-0.3	-0.1	-1.5
78.1	113.7	-3.7	-5.9	206.6	114.4	-5.5	-15.1	148.6	-0.2	-0.8	-0.2	-3.3	-0.2	-0.4	-0.3	-1.7
87.9	111.8	-4.8	-10.1	211.3	127.3	-6.9	-13.4	159.9	-0.2	-0.8	-0.2	-3.2	-0.3	-0.3	-0.1	-1.8
97.7	117.6	-3.0	-3.7	205.5	133.3	-7.9	-17.3	162.7	-0.2	-0.9	-0.2	-3.4	-0.2	-0.4	-0.2	-2.1
107.4	115.9	1.8	-0.4	211.8	151.9	-8.0	-8.9	180.8	-0.3	-1.0	-0.5	-3.5	-0.6	-0.4	-0.7	-2.3
117.2	116.7	3.0	1.6	216.1	155.4	-6.6	-20.7	205.6	-0.6	-1.4	-2.1	-4.5	-1.4	-0.9	-1.7	-2.5
127.0	118.0	6.4	1.0	229.3	168.6	-13.5	-22.5	183.8	-0.3	-0.9	-0.3	-3.4	-0.3	-0.5	-0.6	-1.9
136.7	111.7	6.7	1.4	217.8	179.4	-9.2	-32.2	207.8	-0.2	-0.9	-0.4	-3.5	-0.3	-0.2	-0.5	-1.9
146.5	122.1	12.1	8.6	231.4	190.5	-7.0	-30.4	219.0	-0.2	-0.8	-0.2	-3.5	-0.2	-0.3	-0.4	-1.8
156.3	111.6	22.0	3.0	173.4	202.2	5.9	-28.6	324.9	-0.1	-0.9	-0.6	-3.5	-0.2	-0.3	-0.4	-1.6
166.0	106.5	34.6	3.9	227.0	215.2	0.4	-40.0	281.5	-0.4	-0.9	-0.1	-3.4	-0.2	-0.4	-0.3	-2.0
175.8	97.2	39.5	-6.2	273.7	236.6	-6.4	-40.6	344.8	-0.2	-0.9	-0.3	-3.6	-0.3	-0.3	-0.4	-1.8
185.5	103.1	51.7	-5.7	251.0	237.1	-3.6	-36.7	306.0	-0.3	-1.0	-0.6	-3.3	-0.5	-0.5	-0.3	-2.1
195.3	94.1	68.6	0.7	289.6	257.7	-11.7	-37.2	361.2	-0.5	-0.8	-0.4	-3.4	-0.2	-0.6	-0.4	-1.7
205.1	105.3	46.6	-7.3	239.3	283.0	-25.1	-36.7	370.6	-0.4	-1.0	-0.2	-3.4	-0.5	-1.0	-0.3	-2.3
214.8	91.1	83.0	-35.7	247.5	341.4	-38.2	-2.1	398.8	-1.2	-1.4	-0.5	-3.5	-0.5	-0.8	-1.1	-2.9
224.6	102.1	82.8	-22.4	252.9	341.3	-39.7	17.7	415.9	-0.5	-1.3	-0.9	-4.2	-0.4	-0.5	-1.6	-3.3
234.4	282.4	-32.6	235.5	110.5	370.9	72.8	93.0	570.7	-1.9	-1.9	-6.8	-6.9	-2.5	-2.3	-4.6	-6.2
244.1	186.1	87.1	106.5	323.2	358.2	-20.1	-10.3	513.6	-0.9	-2.0	-1.7	-5.1	-2.1	-1.8	-1.9	-3.3
253.9	134.8	115.6	37.5	346.3	407.5	-61.1	72.6	418.7	-1.1	-1.3	-1.6	-4.6	-0.7	-0.7	-0.8	-2.3
263.7	190.5	62.5	200.3	311.5	367.9	-94.3	12.3	389.6	-1.7	-2.2	-0.8	-4.4	-3.5	-2.7	-7.8	-7.1
273.4	133.3	63.7	72.8	260.7	395.9	-118.8	12.2	326.4	-0.5	-1.4	-1.0	-6.2	-1.5	-1.5	-1.2	-2.0
283.2	259.4	35.3	351.6	217.8	410.7	-208.9	-108.8	245.3	-5.4	-7.1	-12.1	-13.1	-5.0	-3.5	-6.9	-7.3
293.0	148.9	73.2	189.6	270.1	383.8	-99.3	-44.4	485.3	-1.4	-1.8	-4.7	-7.3	-1.9	-2.4	-3.4	-5.0
302.7	84.7	117.5	114.0	331.6	403.6	-131.8	-52.3	436.5	-1.0	-2.4	-3.0	-5.2	-0.9	-0.8	-1.2	-4.1
312.5	110.6	122.0	53.6	435.2	450.7	-92.0	-94.8	512.5	-2.0	-2.0	-1.5	-5.6	-1.0	-0.8	-2.1	-3.9
322.3	163.8	42.5	104.5	262.9	569.4	-238.5	-129.3	394.8	-8.7	-4.7	-5.3	-5.2	-2.9	-4.3	-5.3	-5.4
332.0	153.2	4.8	-5.1	355.9	565.9	-189.8	-173.9	463.5	-7.2	-5.7	-6.5	-6.8	-2.6	-2.3	-4.3	-4.6
341.8	180.2	20.0	-63.8	351.8	549.1	-144.7	-174.6	461.2	-10.9	-12.6	-13.7	-12.1	-9.5	-6.3	-8.1	-9.4

Table 18: Dynamic Stiffness Real and Imaginary Parts at 6800 rpm and 783 kPa (MN/m)

f (Hz)	$R(H_{xx})$	$R(H_{xy})$	$R(H_{yx})$	$R(H_{yy})$	$I(H_{xx})$	$I(H_{xy})$	$I(H_{yx})$	$I(H_{yy})$	$\Delta R(H_{xx})$	$\Delta R(H_{xy})$	$\Delta R(H_{yx})$	$\Delta R(H_{yy})$	$\Delta I(H_{xx})$	$\Delta I(H_{xy})$	$\Delta I(H_{yx})$	$\Delta I(H_{yy})$
9.8	109.0	-9.5	-14.4	255.9	15.5	0.8	-2.4	65.5	-0.2	-1.7	-0.2	-1.8	-0.1	-1.4	-0.1	-1.2
19.5	110.9	-9.4	-12.7	235.7	31.1	-0.3	0.4	23.4	-0.2	-1.4	-0.1	-1.6	-0.1	-0.7	-0.1	-1.0
29.3	110.1	-10.5	-13.8	276.6	46.3	1.6	0.3	41.9	-0.1	-0.7	-0.2	-1.6	-0.1	-0.3	-0.1	-1.0
39.1	110.0	-10.8	-12.5	264.8	60.0	2.8	-1.2	74.1	-0.1	-0.5	-0.1	-1.5	-0.2	-0.4	-0.1	-0.9
48.8	119.8	-10.3	-7.7	257.1	76.1	3.9	-3.6	109.1	-0.2	-0.4	-0.1	-1.3	-0.2	-0.5	-0.2	-1.0
58.6	119.6	-7.8	-7.3	272.6	88.8	4.6	-5.9	123.2	-0.1	-0.4	-0.1	-1.4	-0.2	-0.4	-0.2	-1.0
68.4	119.7	-6.2	-9.1	281.9	104.7	8.3	-0.9	134.4	-0.1	-0.4	-0.3	-1.4	-0.2	-0.3	-0.1	-1.0
78.1	124.6	-1.2	-1.8	266.6	114.7	6.4	-7.4	145.9	-0.2	-0.4	-0.2	-1.4	-0.2	-0.2	-0.3	-0.8
87.9	121.6	-1.9	-6.0	289.7	131.0	4.6	-7.0	178.5	-0.1	-0.3	-0.2	-1.6	-0.3	-0.3	-0.2	-0.8
97.7	129.1	1.6	-2.2	284.5	135.9	4.6	-12.3	177.7	-0.2	-0.4	-0.3	-1.6	-0.1	-0.3	-0.2	-1.1
107.4	128.1	3.1	-0.9	290.5	154.8	5.3	-13.2	199.5	-0.4	-0.5	-0.5	-2.3	-0.4	-0.5	-0.6	-1.2
117.2	130.4	3.9	-0.4	289.8	158.5	5.5	-19.0	217.7	-0.9	-0.8	-1.1	-3.0	-0.7	-1.2	-1.7	-2.2
127.0	131.0	6.2	2.2	273.2	172.6	6.1	-20.0	233.0	-0.3	-0.5	-0.4	-1.6	-0.2	-0.3	-0.4	-1.3
136.7	127.3	8.9	1.6	274.4	180.8	6.9	-23.9	238.5	-0.2	-0.4	-0.3	-1.4	-0.3	-0.3	-0.2	-1.0
146.5	139.5	14.8	5.6	271.2	196.6	9.5	-25.9	246.8	-0.2	-0.4	-0.3	-1.5	-0.2	-0.3	-0.2	-0.8
156.3	134.6	25.0	-1.4	250.0	212.7	17.2	-24.4	268.4	-0.2	-0.3	-0.3	-1.4	-0.2	-0.3	-0.2	-1.1
166.0	128.8	22.9	-1.0	304.8	219.9	11.1	-34.4	315.7	-0.2	-0.3	-0.2	-1.6	-0.3	-0.3	-0.1	-0.9
175.8	118.6	27.1	-4.3	290.0	238.2	12.0	-33.3	327.6	-0.3	-0.3	-0.1	-1.5	-0.2	-0.2	-0.2	-1.0
185.5	136.7	36.8	-4.0	305.0	265.4	14.4	-29.8	333.0	-0.2	-0.3	-0.2	-1.3	-0.5	-0.3	-0.2	-0.9
195.3	137.3	42.5	-6.8	292.4	259.9	11.5	-34.9	345.1	-0.1	-0.2	-0.2	-1.5	-0.2	-0.3	-0.2	-0.9
205.1	129.2	48.0	-13.5	316.3	283.3	15.8	-27.1	375.9	-0.4	-0.2	-0.1	-1.5	-0.2	-0.2	-0.2	-0.9
214.8	121.8	52.0	-15.9	306.5	294.1	18.5	-29.4	372.0	-0.1	-0.2	-0.1	-1.4	-0.3	-0.3	-0.2	-0.8
224.6	121.2	83.3	-16.6	161.4	327.9	33.5	-23.6	400.1	-0.2	-0.3	-0.5	-1.7	-0.5	-0.5	-0.2	-1.6
234.4	108.8	64.6	-37.0	331.5	346.8	8.3	-18.3	435.5	-0.4	-0.4	-0.4	-1.6	-0.7	-0.4	-0.8	-0.9
244.1	125.8	69.1	-29.6	336.0	347.5	4.7	-13.6	442.3	-0.3	-0.3	-0.1	-1.4	-0.2	-0.2	-0.2	-0.9
253.9	124.4	70.7	-29.5	355.3	353.6	6.3	-5.0	452.9	-0.2	-0.3	-0.2	-1.6	-0.3	-0.2	-0.2	-0.9
263.7	122.6	73.0	-30.8	310.7	367.6	8.6	4.6	439.9	-0.2	-0.3	-0.2	-1.5	-0.1	-0.3	-0.3	-0.9
273.4	116.1	95.1	-34.3	172.2	394.9	31.5	19.8	438.0	-0.2	-0.4	-0.3	-1.8	-0.4	-0.3	-0.2	-1.3
283.2	108.7	72.6	-33.9	309.8	409.0	3.9	21.6	464.3	-0.2	-0.3	-0.2	-1.4	-0.2	-0.3	-0.3	-0.9
293.0	103.9	128.2	-33.0	282.5	429.1	1.0	65.7	676.5	-0.3	-1.0	-0.5	-3.4	-0.4	-0.7	-1.0	-3.5
302.7	98.7	143.1	-57.7	414.1	490.3	-22.2	121.6	732.9	-0.7	-1.3	-1.3	-2.6	-0.7	-0.4	-0.7	-4.0
312.5	74.3	228.5	-265.2	15.1	613.3	167.1	171.0	864.6	-2.8	-3.4	-4.3	-4.6	-3.3	-1.9	-5.4	-8.5
322.3	167.0	277.5	51.7	360.2	629.6	40.4	440.0	875.9	-2.4	-3.2	-8.1	-9.8	-2.6	-3.4	-6.0	-5.1
332.0	625.2	161.6	553.6	478.7	331.1	-119.8	96.2	439.0	-9.3	-2.7	-5.1	-3.9	-4.6	-2.4	-6.2	-1.9
341.8	392.5	156.3	284.5	381.0	455.8	-10.2	43.0	456.8	-7.5	-4.0	-4.9	-3.1	-11.2	-3.5	-6.9	-3.3

Table 19: Dynamic Stiffness Real and Imaginary Parts at 6800 rpm and 1567 kPa (MN/m)

f (Hz)	$R(H_{xx})$	$R(H_{xy})$	$R(H_{yx})$	$R(H_{yy})$	$I(H_{xx})$	$I(H_{xy})$	$I(H_{yx})$	$I(H_{yy})$	$\Delta R(H_{xx})$	$\Delta R(H_{xy})$	$\Delta R(H_{yx})$	$\Delta R(H_{yy})$	$\Delta I(H_{xx})$	$\Delta I(H_{xy})$	$\Delta I(H_{yx})$	$\Delta I(H_{yy})$
9.8	127.7	-12.6	-16.0	428.4	15.5	3.3	-3.2	121.6	-0.3	-1.5	-0.3	-2.5	-0.1	-0.8	-0.3	-1.5
19.5	129.3	-9.5	-13.2	387.6	31.1	4.4	0.2	39.0	-0.4	-0.8	-0.2	-2.1	-0.1	-0.5	-0.1	-1.3
29.3	128.1	-12.8	-14.1	441.5	47.8	4.8	-0.3	35.1	-0.3	-0.4	-0.2	-1.8	0.0	-0.5	-0.1	-1.1
39.1	128.0	-12.2	-12.5	421.2	61.6	4.6	-1.9	62.9	-0.2	-0.4	-0.2	-1.6	-0.2	-0.4	-0.1	-0.9
48.8	138.2	-11.0	-6.8	392.8	76.9	7.5	-3.2	112.3	-0.3	-0.5	-0.2	-1.9	-0.1	-0.3	-0.1	-1.1
58.6	137.2	-7.5	-6.9	412.0	90.7	8.8	-6.2	109.3	-0.2	-0.3	-0.1	-1.6	-0.2	-0.4	-0.2	-1.2
68.4	137.0	-8.3	-9.5	418.7	103.5	10.7	-8.9	112.7	-0.4	-0.4	-0.2	-1.6	-0.2	-0.2	-0.3	-1.2
78.1	142.7	0.5	-3.1	402.9	117.8	13.2	-8.8	139.2	-0.3	-0.3	-0.2	-1.7	-0.3	-0.3	-0.3	-0.9
87.9	139.3	-0.3	-6.8	427.7	135.8	11.1	-9.4	180.6	-0.3	-0.4	-0.2	-1.4	-0.3	-0.3	-0.2	-1.1
97.7	146.4	4.0	-5.1	422.5	141.4	11.3	-15.1	169.1	-0.3	-0.4	-0.3	-1.6	-0.2	-0.3	-0.3	-1.1
107.4	145.9	6.6	-4.3	430.9	159.9	12.1	-13.0	192.1	-0.5	-0.2	-0.5	-2.1	-0.4	-0.6	-0.9	-1.2
117.2	122.0	8.4	61.0	435.5	186.8	15.9	16.7	212.4	-17.8	-4.8	-65.6	-8.3	-25.1	-3.8	-21.2	-12.0
127.0	149.8	11.3	-3.3	403.5	180.4	12.4	-20.7	233.7	-0.4	-0.6	-0.4	-2.1	-0.2	-0.5	-0.6	-1.5
136.7	146.1	15.7	-3.6	394.0	189.1	12.7	-23.3	252.0	-0.3	-0.3	-0.3	-2.1	-0.2	-0.5	-0.3	-1.0
146.5	160.9	20.0	0.5	392.7	204.9	14.7	-24.0	254.3	-0.2	-0.4	-0.5	-1.6	-0.4	-0.3	-0.3	-1.0
156.3	154.5	27.3	-3.7	396.6	223.5	19.0	-25.0	255.5	-0.3	-0.2	-0.3	-1.6	-0.4	-0.4	-0.2	-0.9
166.0	150.6	25.1	-5.5	430.1	228.9	13.8	-29.3	315.8	-0.3	-0.3	-0.2	-1.7	-0.5	-0.4	-0.2	-1.0
175.8	138.8	29.5	-6.5	416.3	249.7	16.9	-28.7	327.3	-0.4	-0.3	-0.2	-1.6	-0.4	-0.3	-0.1	-1.0
185.5	159.4	38.7	-8.0	429.9	275.6	18.7	-28.4	330.0	-0.3	-0.2	-0.4	-1.6	-0.7	-0.4	-0.4	-0.8
195.3	160.4	44.5	-9.5	419.6	268.7	16.1	-30.1	343.1	-0.2	-0.3	-0.2	-1.4	-0.5	-0.3	-0.4	-0.9
205.1	152.8	47.3	-14.1	455.2	297.2	19.5	-25.9	378.8	-0.3	-0.3	-0.1	-1.7	-0.5	-0.2	-0.4	-0.9
214.8	145.7	52.6	-16.4	438.4	306.5	24.4	-26.6	366.9	-0.2	-0.2	-0.1	-1.6	-0.5	-0.3	-0.5	-0.9
224.6	148.0	68.7	-16.4	340.4	343.5	35.0	-16.7	363.7	-0.2	-0.3	-0.6	-1.6	-0.5	-0.3	-0.7	-0.9
234.4	130.9	64.8	-45.7	465.5	369.3	13.1	-3.4	438.1	-3.8	-1.7	-21.4	-2.9	-14.5	-1.7	-22.8	-5.0
244.1	155.7	69.4	-21.3	475.4	361.3	5.4	-16.0	461.0	-0.4	-0.4	-0.3	-1.9	-0.6	-0.5	-0.4	-1.4
253.9	154.1	70.4	-20.3	464.1	364.6	19.1	-11.4	447.7	-0.2	-0.2	-0.1	-1.8	-0.4	-0.2	-0.3	-0.8
263.7	155.4	73.5	-21.9	438.6	381.9	17.9	-6.8	444.6	-0.1	-0.3	-0.3	-1.8	-0.4	-0.4	-0.4	-0.9
273.4	158.7	84.9	-22.1	343.9	404.8	32.9	4.0	417.1	-0.3	-0.3	-0.2	-1.8	-0.7	-0.3	-0.4	-0.9
283.2	152.9	73.1	-23.3	439.0	418.8	10.1	-1.9	457.1	-0.5	-0.3	-0.4	-1.8	-0.5	-0.3	-0.4	-0.9
293.0	151.5	82.3	-28.1	392.0	434.7	39.7	11.4	477.3	-0.5	-0.2	-0.4	-1.7	-0.5	-0.3	-0.3	-0.8
302.7	153.6	133.3	-49.2	253.2	469.6	74.2	19.1	588.3	-0.4	-0.5	-0.6	-2.0	-1.2	-0.4	-0.5	-0.9
312.5	132.8	117.2	-53.5	296.7	490.0	98.5	23.7	546.7	-0.7	-0.4	-1.4	-2.1	-0.8	-0.5	-0.5	-1.7
322.3	146.6	111.9	-49.9	343.1	507.2	85.4	54.2	536.7	-0.8	-0.5	-1.3	-2.2	-1.2	-0.7	-0.4	-1.1
332.0	159.5	114.9	-13.4	607.6	558.4	3.3	119.7	660.0	-2.0	-1.0	-2.7	-2.7	-2.4	-0.6	-1.5	-1.7
341.8	154.9	136.3	-35.4	532.2	672.1	97.4	176.8	585.1	-1.9	-1.2	-1.2	-2.0	-2.2	-0.9	-3.1	-2.0

Table 20: Dynamic Stiffness Real and Imaginary Parts at 6800 rpm and 2350 kPa (MN/m)

f (Hz)	$R(H_{xx})$	$R(H_{xy})$	$R(H_{yx})$	$R(H_{yy})$	$I(H_{xx})$	$I(H_{xy})$	$I(H_{yx})$	$I(H_{yy})$	$\Delta R(H_{xx})$	$\Delta R(H_{xy})$	$\Delta R(H_{yx})$	$\Delta R(H_{yy})$	$\Delta I(H_{xx})$	$\Delta I(H_{xy})$	$\Delta I(H_{yx})$	$\Delta I(H_{yy})$
9.8	146.5	-7.1	-16.3	602.6	16.1	5.4	-3.0	142.1	-0.2	-1.6	-0.3	-2.7	-0.2	-3.3	-0.3	-2.0
19.5	148.4	-7.9	-14.2	549.7	32.4	4.1	-0.8	54.4	-0.2	-1.1	-0.2	-1.8	-0.3	-0.9	-0.2	-1.2
29.3	147.1	-9.7	-14.0	579.1	51.1	5.5	-1.5	43.8	-0.1	-1.0	-0.2	-1.8	-0.2	-0.5	-0.2	-1.2
39.1	147.2	-8.6	-13.0	564.1	65.6	6.7	-3.2	70.6	-0.1	-0.6	-0.2	-1.4	-0.2	-0.6	-0.1	-1.1
48.8	157.3	-6.7	-7.8	541.9	80.3	8.8	-4.3	115.1	-0.2	-0.6	-0.1	-1.7	-0.2	-0.5	-0.2	-0.9
58.6	156.3	-4.2	-8.0	563.9	96.0	8.2	-7.8	97.9	-0.1	-0.6	-0.3	-1.5	-0.3	-0.4	-0.4	-1.0
68.4	156.4	-3.1	-9.5	569.4	109.8	9.5	-10.7	105.9	-0.2	-0.4	-0.3	-1.7	-0.2	-0.3	-0.2	-0.9
78.1	161.6	6.1	-5.3	550.8	125.4	15.6	-8.2	139.5	-0.1	-0.3	-0.1	-1.5	0.0	-0.3	-0.3	-0.9
87.9	159.5	4.8	-8.6	576.7	144.6	11.7	-11.5	182.0	-0.2	-0.3	-0.4	-1.6	-0.2	-0.4	-0.2	-1.0
97.7	166.2	8.3	-8.7	567.0	150.5	11.4	-16.1	166.2	-0.2	-0.3	-0.3	-1.5	-0.2	-0.3	-0.4	-1.2
107.4	166.7	12.6	-7.3	580.4	171.4	11.3	-15.4	190.3	-0.4	-0.5	-0.9	-2.4	-0.6	-0.4	-1.0	-1.5
117.2	166.8	14.2	-4.7	572.0	177.9	11.0	-20.4	213.5	-1.1	-0.3	-2.4	-3.5	-1.0	-1.0	-2.3	-2.0
127.0	169.6	16.9	-7.4	550.4	192.4	12.7	-20.1	233.3	-0.2	-0.4	-0.7	-1.6	-0.4	-0.4	-0.6	-1.5
136.7	166.5	20.5	-7.7	545.5	202.4	12.6	-23.1	252.7	-0.3	-0.3	-0.4	-1.7	-0.2	-0.4	-0.4	-1.0
146.5	183.4	25.7	-5.9	536.7	218.6	13.1	-24.5	258.5	-0.5	-0.3	-0.4	-1.7	-0.2	-0.4	-0.3	-1.0
156.3	177.6	31.9	-8.7	544.9	239.2	16.4	-25.0	246.6	-0.2	-0.3	-0.4	-1.5	-0.3	-0.3	-0.4	-0.9
166.0	174.2	28.0	-11.1	577.3	245.2	9.3	-27.9	313.3	-0.2	-0.3	-0.2	-1.6	-0.2	-0.3	-0.2	-0.9
175.8	163.3	32.3	-11.1	568.9	268.1	13.2	-26.8	325.5	-0.2	-0.3	-0.2	-1.6	-0.2	-0.3	-0.2	-0.9
185.5	186.8	40.3	-12.9	577.9	294.6	15.3	-27.0	323.2	-0.2	-0.2	-0.3	-1.6	-0.5	-0.3	-0.5	-0.9
195.3	186.7	43.4	-13.1	568.5	285.8	14.1	-26.5	327.4	-0.3	-0.3	-0.2	-1.5	-0.3	-0.3	-0.3	-0.8
205.1	181.5	46.9	-15.7	592.5	317.2	18.1	-22.9	365.0	-0.4	-0.3	-0.4	-1.6	-0.2	-0.3	-0.3	-0.8
214.8	174.4	52.1	-16.7	581.7	327.7	24.1	-24.3	354.2	-0.3	-0.4	-0.4	-1.7	-0.3	-0.4	-0.3	-0.8
224.6	179.9	72.0	-18.3	499.6	367.7	25.4	-19.0	381.5	-0.3	-0.3	-1.2	-1.8	-0.8	-0.5	-0.8	-1.2
234.4	167.9	57.9	-24.5	614.6	380.3	12.3	-19.5	417.2	-0.4	-0.3	-0.8	-1.7	-0.9	-0.3	-1.2	-1.4
244.1	192.2	65.4	-20.5	593.9	385.0	14.7	-14.6	424.0	-0.4	-0.2	-0.3	-1.7	-0.2	-0.2	-0.2	-0.8
253.9	190.0	65.0	-17.9	609.2	386.5	22.1	-10.1	423.3	-0.2	-0.3	-0.2	-1.4	-0.3	-0.3	-0.2	-0.9
263.7	192.4	73.7	-17.1	560.3	403.5	27.9	-6.3	426.1	-0.3	-0.2	-0.3	-1.5	-0.2	-0.2	-0.3	-1.0
273.4	203.3	83.2	-18.7	484.5	428.1	39.7	0.2	397.0	-0.3	-0.3	-0.2	-1.5	-0.3	-0.3	-0.1	-0.9
283.2	193.9	67.6	-19.4	592.7	438.5	13.6	-8.8	443.0	-0.3	-0.3	-0.2	-1.6	-0.4	-0.3	-0.4	-1.0
293.0	197.1	79.7	-20.5	541.3	455.0	44.4	2.8	457.1	-0.2	-0.3	-0.3	-1.6	-0.5	-0.2	-0.2	-0.9
302.7	202.8	106.7	-18.1	449.7	475.5	74.9	12.6	478.1	-0.3	-0.2	-0.3	-1.5	-0.5	-0.4	-0.2	-1.0
312.5	187.4	110.3	-31.0	475.0	501.2	96.7	8.3	482.1	-0.3	-0.3	-0.2	-1.5	-0.7	-0.3	-0.3	-0.9
322.3	201.6	105.8	-34.5	515.6	509.7	77.1	29.2	504.6	-0.5	-0.4	-0.4	-1.6	-0.6	-0.3	-0.3	-1.0
332.0	227.9	159.0	1.3	870.6	516.9	-106.0	137.7	939.5	-0.2	-0.9	-1.3	-3.2	-1.0	-0.8	-0.8	-1.4
341.8	205.0	101.0	-13.8	688.0	595.6	60.5	76.5	574.7	-1.4	-13.6	-6.4	-12.9	-6.8	-3.3	-5.0	-13.0

Table 21: Dynamic Stiffness Real and Imaginary Parts at 6800 rpm and 3134 kPa (MN/m)

f (Hz)	$R(H_{xx})$	$R(H_{xy})$	$R(H_{yx})$	$R(H_{yy})$	$I(H_{xx})$	$I(H_{xy})$	$I(H_{yx})$	$I(H_{yy})$	$\Delta R(H_{xx})$	$\Delta R(H_{xy})$	$\Delta R(H_{yx})$	$\Delta R(H_{yy})$	$\Delta I(H_{xx})$	$\Delta I(H_{xy})$	$\Delta I(H_{yx})$	$\Delta I(H_{yy})$
9.8	171.7	-10.7	-16.6	731.8	17.6	7.3	-2.4	138.8	-0.1	-0.8	-0.3	-3.5	-0.2	-3.0	-0.2	-2.5
19.5	173.3	-5.8	-14.7	676.0	34.9	5.1	-1.8	57.3	-0.1	-1.5	-0.2	-2.8	-0.1	-1.5	-0.2	-2.8
29.3	171.8	-6.6	-14.6	698.4	55.0	6.2	-3.0	33.1	-0.2	-0.7	-0.3	-1.7	-0.1	-0.3	-0.1	-1.6
39.1	172.4	-7.2	-13.6	676.7	71.4	7.6	-4.9	72.0	-0.3	-0.7	-0.2	-1.7	-0.2	-0.6	-0.2	-1.5
48.8	183.8	-4.0	-8.9	663.5	85.5	9.9	-5.8	116.9	-0.2	-0.5	-0.3	-1.7	-0.3	-0.5	-0.3	-1.5
58.6	182.3	-0.8	-9.6	689.8	103.1	8.3	-9.4	92.1	-0.1	-0.2	-0.2	-1.5	-0.3	-0.6	-0.3	-1.2
68.4	183.3	0.4	-11.3	700.8	118.5	9.7	-12.9	101.4	-0.2	-0.4	-0.3	-1.6	-0.2	-0.5	-0.2	-1.0
78.1	186.6	7.1	-11.5	672.7	134.4	19.5	-9.7	146.5	-0.1	-0.5	-0.4	-1.8	-0.3	-0.4	-0.1	-1.1
87.9	187.4	7.7	-11.3	707.3	156.8	11.7	-13.4	181.4	-0.3	-0.4	-0.5	-1.5	-0.2	-0.3	-0.3	-1.4
97.7	193.7	11.3	-11.9	692.7	161.9	10.8	-18.3	160.8	-0.3	-0.5	-0.5	-1.7	-0.1	-0.3	-0.4	-1.2
107.4	196.0	15.8	-10.9	708.0	183.7	11.3	-17.5	180.9	-0.6	-0.4	-1.8	-3.0	-0.5	-0.7	-0.9	-1.8
117.2	194.8	16.0	-5.4	692.1	192.5	8.8	-23.5	210.6	-3.7	-2.1	-8.7	-3.4	-1.7	-1.4	-6.5	-6.8
127.0	199.0	20.1	-11.2	672.4	207.2	11.6	-21.3	225.2	-0.1	-0.5	-1.2	-2.3	-0.5	-0.5	-0.4	-1.6
136.7	194.4	24.7	-12.2	671.0	217.7	10.9	-24.4	246.6	-0.3	-0.4	-0.7	-1.7	-0.4	-0.5	-0.6	-1.3
146.5	215.2	31.1	-10.1	666.4	233.5	8.2	-26.8	264.8	-0.4	-0.4	-0.2	-1.7	-0.3	-0.4	-0.8	-1.7
156.3	211.3	35.8	-12.5	675.8	256.7	13.4	-25.5	236.5	-0.2	-0.3	-0.1	-1.6	-0.3	-0.2	-0.4	-1.1
166.0	206.8	29.3	-15.6	702.5	261.7	6.9	-28.0	297.2	-0.3	-0.3	-0.2	-1.5	-0.3	-0.4	-0.4	-1.1
175.8	197.8	34.5	-15.3	694.2	288.2	10.8	-26.8	317.5	-0.2	-0.3	-0.1	-1.4	-0.2	-0.2	-0.2	-1.0
185.5	226.0	42.0	-16.6	699.0	313.0	12.2	-26.8	304.2	-0.2	-0.3	-0.5	-1.6	-0.4	-0.3	-0.4	-0.9
195.3	222.2	43.9	-17.1	692.1	302.2	12.2	-26.1	307.8	-0.3	-0.3	-0.3	-1.4	-0.3	-0.4	-0.4	-1.0
205.1	220.4	48.5	-17.9	707.3	338.1	17.6	-22.3	340.0	-0.4	-0.3	-0.3	-1.5	-0.4	-0.2	-0.4	-1.0
214.8	211.5	55.5	-18.4	690.2	347.9	23.9	-24.7	335.3	-0.3	-0.2	-0.3	-1.4	-0.3	-0.3	-0.3	-1.0
224.6	221.6	67.3	-19.8	621.4	392.6	31.8	-18.1	329.1	-0.2	-0.2	-0.3	-1.7	-0.6	-0.3	-0.5	-1.4
234.4	208.0	55.9	-25.6	743.7	405.1	10.0	-19.3	400.5	-0.9	-0.4	-1.7	-2.1	-0.7	-0.6	-2.6	-1.6
244.1	235.6	66.1	-20.6	713.9	409.4	13.4	-14.3	403.5	-0.4	-0.3	-0.4	-1.5	-0.2	-0.3	-0.4	-1.1
253.9	232.9	66.6	-17.8	722.4	410.3	24.0	-10.2	396.7	-0.2	-0.2	-0.2	-1.5	-0.3	-0.3	-0.4	-1.0
263.7	238.1	74.9	-15.1	676.6	427.8	29.9	-6.1	397.2	-0.2	-0.2	-0.1	-1.5	-0.1	-0.3	-0.3	-1.0
273.4	255.1	88.5	-18.5	597.2	454.0	43.3	-0.6	368.0	-0.2	-0.4	-0.2	-1.6	-0.3	-0.2	-0.3	-1.1
283.2	246.0	69.0	-15.7	724.0	462.4	8.2	-14.0	429.7	-0.4	-0.4	-0.3	-1.9	-0.5	-0.4	-0.2	-1.2
293.0	251.2	95.9	-14.0	644.2	476.6	40.5	-0.9	463.1	-0.5	-0.3	-0.6	-1.6	-0.3	-0.4	-0.2	-1.0
302.7	260.1	115.5	-10.4	611.3	492.8	54.7	9.3	487.4	-0.4	-0.3	-0.3	-2.4	-0.5	-0.7	-0.3	-1.2
312.5	249.0	108.6	-25.9	679.0	522.4	69.5	4.8	465.8	-0.3	-0.4	-0.5	-2.5	-0.6	-0.9	-0.4	-2.9
322.3	262.2	174.8	-28.2	494.1	525.5	83.8	17.9	570.1	-0.7	-1.0	-1.2	-7.5	-0.6	-4.1	-0.4	-9.2
332.0	289.4	373.5	-33.9	636.8	540.1	-166.6	84.5	1416.3	-0.9	-10.9	-1.9	-33.1	-1.0	-7.0	-2.1	-7.9
341.8	285.9	119.1	-36.6	831.8	606.2	30.8	59.4	561.6	-1.3	-0.9	-1.6	-6.3	-0.7	-2.4	-1.4	-4.7

Table 22: Dynamic Stiffness Real and Imaginary Parts at 9000 rpm and 0 kPa (MN/m)

f (Hz)	$R(H_{xx})$	$R(H_{xy})$	$R(H_{yx})$	$R(H_{yy})$	$I(H_{xx})$	$I(H_{xy})$	$I(H_{yx})$	$I(H_{yy})$	$\Delta R(H_{xx})$	$\Delta R(H_{xy})$	$\Delta R(H_{yx})$	$\Delta R(H_{yy})$	$\Delta I(H_{xx})$	$\Delta I(H_{xy})$	$\Delta I(H_{yx})$	$\Delta I(H_{yy})$
9.8	133.3	-13.7	-15.6	219.5	10.7	13.3	4.4	-52.0	-0.3	-1.4	-0.4	-4.6	-0.4	-1.0	-0.2	-1.8
19.5	131.9	-16.5	-17.8	197.8	25.2	-0.7	-2.4	34.1	-0.2	-1.3	-0.1	-4.2	-0.2	-1.0	-0.3	-3.6
29.3	130.9	-20.8	-18.5	227.2	57.8	5.0	3.2	38.2	-0.1	-0.9	-0.2	-4.0	-0.1	-0.6	-0.1	-2.1
39.1	127.4	-20.4	-20.4	250.2	70.1	3.6	-2.0	80.3	-0.1	-1.4	-0.1	-3.5	-0.2	-0.5	-0.2	-2.4
48.8	137.3	-21.0	-18.1	280.1	69.9	7.0	-0.7	110.5	-0.1	-0.9	-0.1	-3.4	-0.2	-0.4	-0.4	-1.8
58.6	142.1	-15.8	-13.6	290.0	94.8	4.8	-0.7	129.8	-0.3	-1.1	-0.2	-3.4	-0.2	-0.5	-0.2	-2.0
68.4	147.2	-13.2	-13.3	292.8	106.4	3.0	-3.5	133.9	-0.1	-0.9	-0.2	-3.2	-0.2	-0.4	-0.2	-1.9
78.1	144.1	-12.3	-8.2	303.4	119.2	3.2	-10.1	149.6	-0.1	-0.8	-0.1	-3.4	-0.1	-0.3	-0.2	-1.6
87.9	154.6	-9.8	-5.2	319.9	137.9	2.9	-4.9	169.0	-0.1	-0.9	-0.1	-3.6	-0.2	-0.4	-0.1	-2.1
97.7	148.7	-6.3	-6.4	302.6	143.8	1.4	-15.0	172.1	-0.1	-0.9	-0.1	-3.2	-0.1	-0.4	-0.2	-1.7
107.4	158.4	-3.5	-5.0	299.2	159.1	1.2	-8.7	181.7	-0.1	-0.9	-0.2	-3.2	-0.2	-0.5	-0.2	-1.7
117.2	152.2	-4.6	-5.2	325.6	174.1	0.2	-13.4	214.4	-0.1	-0.8	-0.2	-3.2	-0.2	-0.4	-0.3	-1.8
127.0	151.9	-0.8	-3.4	330.3	185.1	-2.7	-15.1	192.8	-0.2	-1.0	-0.2	-3.4	-0.2	-0.3	-0.4	-1.9
136.7	146.0	-0.1	1.5	332.4	197.1	-3.3	-17.7	186.7	-0.1	-0.8	-0.5	-3.5	-0.3	-0.5	-0.4	-1.9
146.5	170.8	3.5	6.4	338.2	200.4	-5.2	-14.3	204.5	-0.7	-2.0	-1.7	-4.7	-0.9	-1.4	-1.2	-4.4
156.3	170.3	5.9	7.9	289.3	216.1	3.7	-18.1	320.6	-0.4	-1.1	-1.0	-3.8	-0.5	-0.4	-0.8	-1.9
166.0	162.3	9.5	5.8	332.6	225.1	1.3	-21.1	272.5	-0.4	-0.8	-0.3	-3.9	-0.3	-0.5	-0.3	-1.6
175.8	146.0	10.2	6.9	379.7	251.6	4.4	-18.0	313.2	-0.3	-1.0	-0.3	-3.6	-0.3	-0.3	-0.4	-2.0
185.5	166.8	18.5	9.2	363.9	246.4	6.8	-27.0	282.9	-0.1	-0.9	-0.3	-3.4	-0.3	-0.4	-0.3	-1.7
195.3	171.0	25.7	18.0	390.8	251.0	3.1	-26.8	339.1	-0.2	-0.9	-0.4	-3.5	-0.3	-0.5	-0.6	-1.7
205.1	158.0	28.8	7.2	375.3	279.9	17.0	-26.0	349.6	-0.4	-0.8	-0.1	-3.6	-0.2	-0.4	-0.2	-2.2
214.8	140.1	33.2	2.3	360.0	302.3	21.6	-27.2	383.5	-0.4	-1.0	-0.2	-4.0	-0.4	-0.5	-0.2	-1.8
224.6	152.4	53.7	9.0	354.6	341.2	13.8	-18.1	374.8	-0.4	-1.4	-0.4	-3.9	-0.5	-0.6	-0.3	-2.7
234.4	139.5	61.0	6.6	381.1	345.4	14.8	-17.1	386.1	-0.2	-1.2	-0.2	-4.2	-0.2	-0.6	-0.6	-2.0
244.1	128.7	77.8	-0.2	425.2	358.1	36.0	0.3	432.4	-0.3	-1.2	-0.3	-5.7	-0.2	-1.3	-0.4	-4.1
253.9	135.0	100.6	-4.4	490.1	368.6	38.0	20.1	426.4	-0.1	-1.2	-0.7	-6.4	-0.5	-2.3	-0.3	-4.7
263.7	145.5	93.0	0.2	429.7	393.5	18.4	28.6	432.9	-0.5	-1.2	-0.8	-4.5	-0.4	-2.1	-0.8	-4.5
273.4	202.4	150.0	99.0	497.7	428.6	30.1	-32.5	406.1	-1.0	-1.8	-1.1	-4.4	-1.1	-1.0	-1.3	-4.1
283.2	221.1	229.2	167.2	673.3	445.0	17.7	34.0	341.3	-1.5	-4.3	-3.4	-7.1	-1.4	-1.9	-1.7	-9.8
293.0	238.1	104.6	207.4	388.7	328.5	-119.9	-162.9	198.0	-0.9	-2.1	-1.4	-8.7	-2.0	-2.3	-5.1	-7.4
302.7	184.0	212.7	11.8	458.1	375.2	-108.2	-121.0	360.1	-1.1	-2.6	-0.9	-4.1	-0.7	-2.1	-1.0	-3.4
312.5	203.2	97.5	32.1	467.3	436.2	-95.7	-40.2	314.0	-0.8	-6.7	-0.8	-5.2	-3.1	-2.9	-2.0	-3.2
322.3	153.5	90.4	37.4	377.3	402.9	-47.2	-42.2	387.5	-0.7	-1.8	-0.9	-3.8	-0.6	-0.5	-0.5	-1.9
332.0	165.9	101.6	28.1	399.6	384.7	-85.3	-64.1	354.2	-0.6	-1.0	-1.0	-3.8	-0.4	-0.7	-1.1	-2.6
341.8	88.6	96.4	100.7	420.9	392.6	-62.2	-31.0	338.1	-1.2	-1.3	-2.9	-5.0	-2.8	-2.2	-2.2	-2.1

Table 23: Dynamic Stiffness Real and Imaginary Parts at 9000 rpm and 783 kPa (MN/m)

f (Hz)	$R(H_{xx})$	$R(H_{xy})$	$R(H_{yx})$	$R(H_{yy})$	$I(H_{xx})$	$I(H_{xy})$	$I(H_{yx})$	$I(H_{yy})$	$\Delta R(H_{xx})$	$\Delta R(H_{xy})$	$\Delta R(H_{yx})$	$\Delta R(H_{yy})$	$\Delta I(H_{xx})$	$\Delta I(H_{xy})$	$\Delta I(H_{yx})$	$\Delta I(H_{yy})$
9.8	145.3	-27.5	-19.1	335.7	13.4	5.0	-3.8	103.2	-0.4	-1.5	-0.2	-2.8	-0.3	-1.3	-0.4	-2.5
19.5	142.8	-23.5	-15.8	326.8	25.7	5.9	1.5	23.2	-0.2	-0.8	-0.2	-2.0	-0.1	-0.6	-0.2	-1.5
29.3	140.9	-25.6	-18.1	366.1	57.5	5.1	3.0	26.8	-0.1	-0.4	-0.3	-1.7	-0.1	-0.6	-0.1	-1.1
39.1	140.4	-23.8	-17.1	356.7	69.5	7.6	-0.1	73.9	-0.2	-0.6	-0.1	-1.4	-0.2	-0.6	-0.2	-1.2
48.8	152.7	-22.0	-12.6	340.6	74.9	8.9	-2.8	120.6	-0.1	-0.3	-0.1	-1.5	-0.2	-0.5	-0.2	-1.3
58.6	152.1	-20.0	-11.4	361.5	96.4	9.8	-4.4	128.5	-0.1	-0.5	-0.1	-1.4	-0.2	-0.4	-0.2	-1.0
68.4	155.1	-16.2	-9.7	375.3	112.4	16.0	0.1	132.4	-0.2	-0.5	-0.1	-1.4	-0.2	-0.4	-0.2	-1.0
78.1	156.9	-10.6	-6.9	362.3	122.8	13.9	-5.0	150.6	-0.2	-0.5	-0.3	-1.4	-0.2	-0.4	-0.1	-0.9
87.9	163.6	-10.0	-7.0	389.2	141.1	12.7	-7.1	186.2	-0.2	-0.4	-0.1	-1.5	-0.2	-0.4	-0.1	-0.8
97.7	162.6	-5.0	-6.4	383.9	148.1	13.0	-10.3	172.9	-0.3	-0.3	-0.3	-1.4	-0.1	-0.3	-0.1	-0.9
107.4	170.2	-1.2	-4.4	394.0	161.9	13.8	-11.9	190.7	-0.2	-0.5	-0.2	-1.5	-0.2	-0.3	-0.1	-0.9
117.2	161.7	0.0	-5.8	396.7	177.2	12.6	-14.7	214.4	-0.2	-0.3	-0.2	-1.5	-0.2	-0.3	-0.1	-0.9
127.0	167.8	3.5	-4.6	379.6	187.2	12.6	-16.9	226.1	-0.2	-0.3	-0.2	-1.6	-0.2	-0.3	-0.2	-1.1
136.7	162.6	6.3	-3.4	380.3	202.4	11.3	-18.2	235.8	-0.3	-0.5	-0.5	-1.5	-0.4	-0.4	-0.2	-1.1
146.5	180.2	12.3	-0.4	377.4	204.7	11.8	-16.9	233.8	-0.6	-0.7	-0.9	-2.8	-0.6	-1.1	-1.0	-1.6
156.3	186.5	22.1	-4.8	360.9	220.1	15.4	-15.6	251.2	-0.7	-0.7	-0.7	-1.9	-0.5	-0.7	-1.0	-1.9
166.0	176.4	17.7	0.4	407.5	231.2	12.2	-22.6	285.9	-0.5	-0.5	-0.4	-1.7	-0.4	-0.4	-0.5	-1.1
175.8	169.3	19.1	-1.3	392.3	259.4	15.3	-22.6	301.8	-0.4	-0.3	-0.3	-1.7	-0.2	-0.4	-0.3	-1.2
185.5	182.0	25.9	1.9	402.7	257.7	15.8	-25.4	303.5	-0.2	-0.3	-0.1	-1.8	-0.3	-0.3	-0.2	-1.1
195.3	189.1	33.6	0.9	384.7	265.6	16.1	-29.0	312.1	-0.2	-0.3	-0.3	-1.6	-0.2	-0.4	-0.1	-0.9
205.1	177.7	38.8	-4.9	406.9	292.1	24.5	-27.5	352.1	-0.5	-0.2	-0.3	-1.7	-0.3	-0.3	-0.2	-1.0
214.8	157.9	44.3	-4.5	387.1	307.0	29.5	-31.9	343.6	-0.3	-0.3	-0.2	-1.5	-0.3	-0.4	-0.1	-1.1
224.6	176.3	68.5	-17.6	277.1	336.8	32.7	-29.5	386.6	-0.3	-0.3	-0.2	-1.7	-0.5	-0.3	-0.3	-0.8
234.4	158.1	58.6	-20.3	411.7	348.7	20.9	-31.4	407.0	-0.5	-0.3	-0.2	-1.6	-0.3	-0.4	-0.2	-1.1
244.1	151.7	66.3	-21.0	416.3	352.1	20.0	-32.5	419.7	-0.3	-0.2	-0.2	-1.5	-0.2	-0.4	-0.1	-0.9
253.9	160.1	70.5	-28.8	436.7	364.1	20.5	-23.3	436.2	-0.3	-0.3	-0.4	-1.9	-0.4	-0.4	-0.3	-1.1
263.7	169.0	78.0	-32.4	387.8	382.6	22.9	-15.1	422.4	-0.3	-0.3	-0.2	-1.4	-0.2	-0.3	-0.2	-1.0
273.4	162.8	99.0	-47.3	268.5	413.6	38.5	-2.2	443.9	-0.3	-0.3	-0.6	-1.6	-0.3	-0.3	-0.3	-1.6
283.2	179.5	83.0	-35.2	381.5	417.6	22.3	6.2	448.0	-0.3	-0.2	-0.5	-1.5	-0.3	-0.3	-0.2	-1.0
293.0	178.9	133.0	-39.9	384.7	419.8	12.1	54.1	656.4	-0.4	-1.1	-0.6	-7.4	-0.3	-1.1	-0.9	-3.3
302.7	175.6	137.0	-48.8	492.1	457.9	-2.4	84.6	682.2	-1.1	-2.2	-2.1	-6.7	-0.9	-1.5	-3.6	-9.2
312.5	153.7	186.3	-176.2	286.9	538.9	92.6	88.5	748.9	-0.9	-1.5	-2.9	-3.0	-1.1	-0.6	-2.6	-4.3
322.3	187.8	194.8	-53.8	498.7	484.8	-6.0	277.6	836.6	-0.6	-4.0	-5.2	-13.1	-2.3	-2.8	-2.5	-7.9
332.0	244.7	196.7	-9.7	532.3	595.0	48.8	260.3	623.5	-1.7	-1.3	-1.3	-3.0	-1.6	-1.0	-2.5	-2.0
341.8	301.7	247.8	133.0	593.0	651.2	52.2	322.6	581.1	-1.7	-1.0	-4.0	-3.9	-1.4	-1.2	-3.3	-3.1

Table 24: Dynamic Stiffness Real and Imaginary Parts at 9000 rpm and 1567 kPa (MN/m)

f (Hz)	$R(H_{xx})$	$R(H_{xy})$	$R(H_{yx})$	$R(H_{yy})$	$I(H_{xx})$	$I(H_{xy})$	$I(H_{yx})$	$I(H_{yy})$	$\Delta R(H_{xx})$	$\Delta R(H_{xy})$	$\Delta R(H_{yx})$	$\Delta R(H_{yy})$	$\Delta I(H_{xx})$	$\Delta I(H_{xy})$	$\Delta I(H_{yx})$	$\Delta I(H_{yy})$
9.8	165.7	-26.5	-21.3	478.4	14.8	5.9	-4.4	148.0	-0.1	-1.2	-0.3	-2.7	-0.5	-2.9	-0.4	-2.7
19.5	163.9	-26.1	-20.1	476.5	28.4	8.1	0.3	51.5	-0.2	-1.6	-0.2	-1.9	-0.3	-1.1	-0.2	-2.2
29.3	161.9	-23.5	-19.8	524.1	57.6	5.9	2.3	26.7	-0.4	-0.9	-0.3	-2.2	-0.2	-0.3	-0.2	-1.3
39.1	161.4	-22.2	-17.4	491.6	68.6	9.6	0.2	58.4	-0.2	-0.5	-0.2	-1.9	-0.2	-0.5	-0.2	-0.8
48.8	172.9	-20.1	-12.7	466.0	76.4	11.5	-2.5	112.8	-0.3	-0.3	-0.1	-1.5	-0.2	-0.5	-0.2	-1.2
58.6	172.4	-18.9	-11.6	492.2	97.3	12.3	-3.7	102.2	-0.2	-0.6	-0.1	-2.1	-0.3	-0.3	-0.2	-1.1
68.4	175.7	-16.9	-12.3	497.8	109.4	13.8	-6.0	103.1	-0.2	-0.5	-0.1	-1.4	-0.3	-0.5	-0.2	-1.3
78.1	177.9	-8.3	-7.6	481.5	125.1	18.3	-4.6	130.2	-0.1	-0.3	-0.1	-1.6	-0.1	-0.2	-0.1	-1.0
87.9	183.2	-7.7	-8.6	505.0	144.1	17.2	-8.2	173.3	-0.2	-0.3	-0.1	-1.7	-0.2	-0.5	-0.1	-1.1
97.7	183.0	-3.7	-8.1	502.4	152.0	16.8	-11.9	153.1	-0.3	-0.4	-0.2	-1.6	-0.2	-0.4	-0.2	-1.1
107.4	190.9	0.3	-8.2	515.4	166.2	17.1	-13.6	172.5	-0.3	-0.3	-0.2	-1.8	-0.2	-0.4	-0.2	-0.9
117.2	182.6	3.5	-8.8	509.2	179.8	16.5	-16.7	195.1	-0.1	-0.5	-0.2	-1.3	-0.2	-0.2	-0.2	-1.2
127.0	189.0	7.6	-6.7	486.5	193.3	18.0	-17.9	212.7	-0.2	-0.4	-0.3	-1.9	-0.2	-0.4	-0.5	-1.2
136.7	183.2	12.8	-7.2	472.2	208.0	18.1	-19.5	230.6	-0.2	-0.5	-0.3	-1.9	-0.2	-0.5	-0.3	-1.1
146.5	202.4	18.5	-5.6	472.4	210.5	16.9	-18.5	232.3	-0.6	-1.0	-0.6	-3.4	-0.4	-1.5	-1.0	-3.0
156.3	207.4	26.6	-4.3	476.7	230.6	18.0	-20.9	229.1	-0.4	-1.1	-0.6	-2.9	-0.3	-0.5	-0.8	-2.7
166.0	199.4	22.1	-4.8	511.5	237.5	15.4	-23.0	275.5	-0.1	-0.4	-0.4	-1.8	-0.3	-0.5	-0.3	-0.9
175.8	190.8	26.9	-4.7	498.5	264.7	17.0	-26.0	296.0	-0.2	-0.4	-0.3	-1.6	-0.3	-0.4	-0.3	-1.4
185.5	205.4	33.7	-2.9	498.9	264.1	16.3	-27.2	293.8	-0.3	-0.4	-0.2	-2.3	-0.3	-0.2	-0.2	-1.4
195.3	210.1	38.7	-4.9	492.1	275.1	15.9	-28.8	295.9	-0.3	-0.4	-0.1	-1.7	-0.2	-0.5	-0.3	-1.0
205.1	204.4	42.0	-8.9	522.9	296.7	19.4	-28.5	332.5	-0.5	-0.3	-0.1	-1.7	-0.5	-0.4	-0.2	-1.4
214.8	184.6	48.6	-9.8	502.0	309.5	23.7	-31.6	329.4	-0.2	-0.4	-0.1	-2.2	-0.4	-0.4	-0.3	-1.3
224.6	200.3	61.0	-14.1	422.3	340.9	26.1	-26.4	337.5	-0.4	-0.5	-0.2	-2.6	-0.7	-0.5	-0.2	-0.9
234.4	185.7	57.0	-18.7	523.8	348.9	14.6	-33.2	386.2	-0.5	-0.3	-0.2	-1.6	-0.5	-0.3	-0.1	-1.1
244.1	180.5	66.9	-20.4	526.9	356.9	11.1	-31.1	417.6	-0.3	-0.3	-0.2	-1.7	-0.3	-0.3	-0.1	-1.5
253.9	188.3	70.0	-24.2	515.8	367.5	19.6	-28.6	417.7	-0.2	-0.4	-0.1	-1.7	-0.4	-0.2	-0.2	-0.9
263.7	196.2	74.9	-27.8	491.1	387.4	19.7	-22.4	407.0	-0.3	-0.2	-0.2	-2.0	-0.3	-0.3	-0.1	-1.2
273.4	198.0	86.5	-31.5	403.8	412.0	30.0	-14.6	390.0	-0.3	-0.3	-0.2	-2.4	-0.4	-0.5	-0.1	-1.1
283.2	208.8	82.0	-33.3	481.3	420.6	13.9	-11.4	419.9	-0.3	-0.3	-0.2	-1.8	-0.4	-0.3	-0.1	-1.3
293.0	202.7	91.3	-37.6	449.3	422.3	28.9	-3.3	452.6	-0.2	-0.3	-0.2	-2.3	-0.4	-0.5	-0.2	-1.1
302.7	202.1	129.7	-56.1	365.9	458.2	41.2	0.8	577.9	-0.6	-0.5	-1.0	-3.9	-0.9	-0.7	-0.8	-1.2
312.5	193.6	121.2	-61.2	424.0	489.5	52.1	7.1	539.4	-0.4	-1.0	-0.6	-5.4	-0.7	-1.0	-0.7	-1.3
322.3	186.3	119.4	-55.2	423.6	477.1	45.4	31.5	533.0	-0.6	-0.4	-0.5	-3.7	-0.4	-0.7	-0.5	-1.0
332.0	208.8	109.1	-46.8	610.5	514.1	9.0	76.1	577.4	-0.2	-0.4	-0.2	-1.7	-0.3	-0.4	-0.4	-1.3
341.8	190.1	123.7	-57.2	553.1	553.4	47.7	104.5	547.2	-0.6	-0.4	-0.7	-2.2	-0.9	-0.6	-0.5	-1.4

Table 25: Dynamic Stiffness Real and Imaginary Parts at 9000 rpm and 2350 kPa (MN/m)

f (Hz)	$R(H_{xx})$	$R(H_{xy})$	$R(H_{yx})$	$R(H_{yy})$	$I(H_{xx})$	$I(H_{xy})$	$I(H_{yx})$	$I(H_{yy})$	$\Delta R(H_{xx})$	$\Delta R(H_{xy})$	$\Delta R(H_{yx})$	$\Delta R(H_{yy})$	$\Delta I(H_{xx})$	$\Delta I(H_{xy})$	$\Delta I(H_{yx})$	$\Delta I(H_{yy})$
9.8	191.9	-24.2	-24.1	617.0	14.5	11.8	-3.6	151.1	-0.7	-3.9	-0.3	-2.0	-0.5	-3.4	-0.3	-2.9
19.5	191.0	-18.3	-22.6	608.6	29.7	7.9	-0.1	61.0	-0.4	-1.4	-0.3	-5.1	-0.2	-1.8	-0.2	-1.9
29.3	189.5	-20.1	-20.8	616.2	58.8	5.0	1.1	37.3	-0.3	-1.5	-0.3	-2.6	-0.2	-0.6	-0.3	-2.1
39.1	188.3	-19.3	-19.4	592.7	69.9	8.9	0.7	55.8	-0.2	-0.6	-0.3	-2.4	-0.3	-1.2	-0.4	-1.2
48.8	199.4	-17.6	-14.9	574.8	78.7	10.8	-2.0	98.6	-0.2	-0.4	-0.2	-1.8	-0.2	-0.6	-0.3	-1.3
58.6	198.8	-14.4	-13.7	613.0	99.5	10.1	-3.6	93.2	-0.2	-0.9	-0.1	-2.4	-0.2	-0.3	-0.2	-1.6
68.4	203.8	-12.4	-14.4	617.2	112.5	12.5	-6.1	97.6	-0.2	-0.3	-0.2	-1.5	-0.1	-0.5	-0.3	-1.1
78.1	204.9	-3.0	-11.0	595.7	129.9	18.1	-3.8	133.3	-0.3	-0.3	-0.2	-1.6	-0.1	-0.4	-0.2	-1.1
87.9	210.2	-4.8	-11.4	617.9	148.5	15.7	-9.2	173.6	-0.2	-0.3	-0.1	-1.7	-0.3	-0.4	-0.2	-1.1
97.7	210.4	-1.2	-11.3	611.9	156.6	15.1	-12.0	149.2	-0.2	-0.5	-0.3	-1.8	-0.2	-0.5	-0.2	-1.2
107.4	217.0	2.7	-11.7	631.1	171.0	14.7	-13.7	167.1	-0.1	-0.3	-0.1	-2.0	-0.3	-0.2	-0.3	-1.0
117.2	210.9	5.7	-12.0	619.0	185.3	15.6	-17.6	188.4	-0.2	-0.3	-0.1	-1.5	-0.2	-0.4	-0.2	-1.1
127.0	216.3	10.2	-11.8	595.0	199.3	16.9	-18.6	208.3	-0.3	-0.4	-0.2	-1.7	-0.3	-0.3	-0.6	-1.4
136.7	211.0	15.0	-11.8	581.2	214.0	17.9	-19.8	220.8	-0.4	-0.4	-0.4	-2.0	-0.2	-0.4	-0.6	-0.9
146.5	230.0	21.7	-9.1	580.0	218.7	16.2	-19.3	229.9	-0.8	-1.1	-1.4	-2.4	-0.6	-0.5	-1.1	-2.6
156.3	234.1	28.2	-9.7	583.4	238.8	16.2	-20.6	221.3	-0.5	-1.2	-2.1	-3.4	-0.8	-1.0	-0.6	-1.9
166.0	227.8	23.7	-10.8	617.1	246.2	11.6	-22.8	269.4	-0.2	-0.5	-0.7	-2.2	-0.7	-0.4	-0.6	-1.1
175.8	219.6	28.5	-10.7	609.0	272.7	13.1	-25.0	296.8	-0.2	-0.4	-0.4	-1.5	-0.4	-0.4	-0.1	-1.3
185.5	236.4	33.7	-9.8	613.4	274.3	12.8	-24.9	280.0	-0.1	-0.6	-0.3	-1.9	-0.4	-0.3	-0.4	-1.6
195.3	238.3	36.6	-10.8	604.9	283.9	12.2	-27.0	284.9	-0.3	-0.5	-0.3	-1.7	-0.6	-0.3	-0.3	-1.3
205.1	234.0	41.6	-13.1	625.1	306.4	16.5	-26.3	324.1	-0.5	-0.5	-0.1	-2.1	-0.3	-0.6	-0.2	-1.4
214.8	217.8	46.6	-13.0	618.3	318.0	19.3	-28.5	323.7	-0.3	-0.5	-0.3	-1.8	-0.5	-0.4	-0.4	-1.2
224.6	230.3	58.3	-16.2	544.4	350.4	19.3	-26.1	338.8	-0.4	-0.4	-0.2	-1.5	-0.7	-0.3	-0.3	-1.1
234.4	220.4	52.0	-19.1	637.2	358.4	12.5	-28.1	373.9	-0.3	-0.5	-0.3	-1.7	-0.3	-0.4	-0.2	-1.3
244.1	214.1	59.6	-20.2	618.8	367.8	15.2	-28.0	374.6	-0.3	-0.4	-0.2	-1.7	-0.5	-0.5	-0.1	-1.8
253.9	222.4	63.3	-25.6	624.7	380.8	21.0	-24.0	386.3	-0.3	-0.2	-0.3	-1.8	-0.6	-0.5	-0.3	-1.1
263.7	229.6	71.5	-26.0	587.0	400.0	22.8	-21.0	390.6	-0.4	-0.2	-0.2	-2.0	-0.5	-0.5	-0.3	-1.2
273.4	237.2	80.5	-30.0	510.7	424.2	32.6	-15.9	364.7	-0.2	-0.3	-0.2	-1.9	-0.5	-0.5	-0.2	-1.4
283.2	244.6	74.0	-30.9	594.9	433.2	14.2	-15.4	399.9	-0.2	-0.3	-0.2	-2.0	-0.5	-0.4	-0.2	-1.8
293.0	242.7	88.0	-31.4	544.9	433.4	33.1	-6.4	430.8	-0.2	-0.4	-0.4	-2.2	-0.5	-0.6	-0.3	-1.1
302.7	242.1	105.0	-39.0	490.0	470.5	35.8	7.7	448.6	-10.4	-9.4	-16.7	-7.4	-4.2	-12.4	-2.6	-15.6
312.5	240.7	92.2	-42.2	722.5	495.8	7.4	8.6	518.9	-0.4	-0.4	-0.3	-2.0	-0.9	-0.6	-0.5	-1.5
322.3	231.4	125.8	-42.6	460.6	488.8	63.4	7.9	506.2	-0.4	-0.5	-0.5	-2.7	-0.7	-0.9	-0.4	-2.4
332.0	272.9	132.6	-57.4	786.6	504.8	-51.1	113.5	744.2	-0.2	-0.3	-0.4	-2.4	-0.5	-0.4	-0.7	-1.3
341.8	243.2	115.4	-53.2	669.8	549.9	36.0	61.7	529.2	-0.5	-0.3	-0.2	-1.5	-0.8	-0.6	-0.5	-1.2

Table 26: Dynamic Stiffness Real and Imaginary Parts at 9000 rpm and 3134 kPa (MN/m)

f (Hz)	$R(H_{xx})$	$R(H_{xy})$	$R(H_{yx})$	$R(H_{yy})$	$I(H_{xx})$	$I(H_{xy})$	$I(H_{yx})$	$I(H_{yy})$	$\Delta R(H_{xx})$	$\Delta R(H_{xy})$	$\Delta R(H_{yx})$	$\Delta R(H_{yy})$	$\Delta I(H_{xx})$	$\Delta I(H_{xy})$	$\Delta I(H_{yx})$	$\Delta I(H_{yy})$
9.8	219.2	-19.8	-25.4	749.3	15.1	13.9	-4.1	153.6	-0.9	-2.0	-0.4	-3.9	-0.5	-3.2	-1.1	-1.7
19.5	217.8	-17.1	-22.9	719.7	31.7	10.3	-1.2	85.0	-0.2	-2.6	-0.5	-2.5	-0.5	-2.2	-0.4	-2.0
29.3	216.7	-19.1	-22.7	738.1	61.7	5.2	0.4	31.5	-0.4	-2.1	-0.3	-1.8	-0.4	-1.4	-0.3	-1.9
39.1	216.9	-16.9	-21.1	716.4	74.2	8.6	-0.8	51.4	-0.3	-0.7	-0.3	-1.8	-0.3	-1.1	-0.2	-1.4
48.8	227.5	-14.3	-16.3	708.3	82.2	11.2	-3.3	94.8	-0.3	-0.7	-0.2	-1.5	-0.2	-0.9	-0.2	-1.1
58.6	227.3	-11.5	-15.0	740.7	104.6	9.7	-5.2	82.1	-0.2	-0.4	-0.2	-1.8	-0.2	-0.4	-0.4	-0.9
68.4	232.4	-8.6	-16.2	737.5	118.6	12.5	-8.2	87.5	-0.3	-0.5	-0.4	-1.6	-0.2	-0.4	-0.2	-0.9
78.1	231.6	-1.8	-18.0	705.0	137.8	23.3	-3.1	133.0	-0.2	-0.3	-0.2	-1.7	-0.2	-0.5	-0.2	-0.8
87.9	240.1	-1.5	-14.2	735.9	156.1	14.8	-11.3	163.6	-0.2	-0.3	-0.2	-1.5	-0.2	-0.5	-0.2	-1.0
97.7	240.3	2.4	-14.7	720.9	165.4	14.4	-14.6	135.9	-0.2	-0.5	-0.4	-1.7	-0.3	-0.3	-0.1	-1.0
107.4	247.2	7.0	-14.8	743.0	179.9	14.9	-15.6	155.2	-0.2	-0.3	-0.2	-1.5	-0.4	-0.5	-0.1	-1.2
117.2	241.6	10.7	-15.8	731.8	196.1	15.2	-19.1	173.9	-0.1	-0.3	-0.3	-1.7	-0.3	-0.3	-0.3	-1.0
127.0	246.8	15.4	-15.2	705.0	210.4	17.0	-20.5	195.4	-0.4	-0.3	-0.4	-1.8	-0.1	-0.5	-0.5	-1.1
136.7	243.6	21.1	-16.1	692.0	225.8	16.7	-22.3	215.5	-0.5	-0.7	-0.7	-2.0	-0.4	-0.6	-0.8	-1.4
146.5	261.0	28.8	-13.8	690.7	231.5	13.3	-20.1	236.2	-1.2	-1.3	-1.6	-3.2	-0.8	-1.2	-2.4	-2.7
156.3	266.9	31.4	-14.5	704.9	252.5	11.3	-22.9	207.9	-1.1	-0.9	-1.7	-3.1	-0.8	-1.0	-2.1	-2.4
166.0	261.2	27.2	-16.8	729.5	259.6	8.1	-24.5	256.9	-0.4	-0.6	-0.9	-1.9	-0.4	-0.4	-0.8	-1.2
175.8	254.8	31.8	-16.1	721.8	286.2	9.5	-25.8	284.2	-0.6	-0.5	-0.7	-1.5	-0.3	-0.5	-0.4	-1.0
185.5	270.3	37.5	-14.9	726.3	290.0	10.5	-26.4	268.4	-0.3	-0.6	-0.4	-1.7	-0.5	-0.3	-0.3	-1.1
195.3	273.8	41.3	-16.3	707.4	298.9	10.9	-25.7	268.1	-0.3	-0.6	-0.4	-1.7	-0.4	-0.4	-0.4	-1.1
205.1	270.2	44.2	-17.0	734.4	322.5	12.6	-25.9	305.2	-0.4	-0.4	-0.4	-1.5	-0.3	-0.4	-0.2	-1.1
214.8	256.3	50.9	-17.1	714.0	335.5	18.0	-27.3	298.7	-0.3	-0.5	-0.3	-1.5	-0.4	-0.3	-0.4	-1.2
224.6	268.8	58.7	-19.4	655.2	367.3	17.9	-24.0	303.1	-0.3	-0.4	-0.4	-1.8	-0.5	-0.5	-0.2	-0.8
234.4	260.1	52.2	-23.1	747.4	376.8	7.4	-26.4	352.6	-0.3	-0.4	-0.2	-1.5	-0.1	-0.4	-0.2	-1.0
244.1	255.4	62.5	-22.5	716.4	387.1	11.2	-26.7	358.1	-0.3	-0.3	-0.2	-1.5	-0.2	-0.3	-0.2	-1.0
253.9	261.9	63.1	-26.4	728.6	399.5	17.4	-23.5	363.2	-0.3	-0.4	-0.2	-1.5	-0.5	-0.3	-0.3	-0.8
263.7	271.1	70.4	-25.2	688.6	418.6	22.8	-19.5	359.0	-0.2	-0.3	-0.1	-1.5	-0.4	-0.4	-0.2	-0.9
273.4	282.3	81.8	-29.1	621.9	444.6	29.2	-15.0	346.9	-0.4	-0.3	-0.1	-1.5	-0.4	-0.3	-0.3	-0.9
283.2	289.9	75.9	-30.0	708.9	452.0	6.6	-15.3	402.3	-0.2	-0.4	-0.2	-1.4	-0.4	-0.4	-0.1	-0.9
293.0	290.4	86.7	-29.9	644.1	454.0	35.1	-6.2	394.6	-0.3	-0.6	-0.4	-1.6	-0.3	-0.4	-0.3	-1.1
302.7	293.3	104.1	-30.8	607.9	484.3	43.7	1.7	431.8	-1.5	-1.0	-2.0	-2.3	-2.0	-1.6	-3.7	-3.5
312.5	295.8	184.3	-56.1	608.2	521.0	14.3	-7.0	721.1	-0.4	-0.9	-0.5	-2.0	-0.6	-0.8	-0.8	-3.1
322.3	286.0	118.2	-33.8	589.6	509.1	61.7	9.0	450.5	-0.4	-0.6	-0.3	-2.0	-0.6	-0.4	-0.1	-1.1
332.0	302.5	268.3	-91.8	428.8	558.1	14.4	-37.9	888.8	-0.5	-1.1	-1.2	-5.9	-0.3	-1.8	-0.7	-3.6
341.8	299.0	108.4	-39.2	827.5	564.2	10.4	37.9	527.5	-0.5	-0.5	-0.2	-1.5	-0.6	-0.4	-0.5	-1.2

Table 27: Dynamic Stiffness Real and Imaginary Parts at 10800 rpm and 0 kPa (MN/m)

f (Hz)	$R(H_{xx})$	$R(H_{xy})$	$R(H_{yx})$	$R(H_{yy})$	$I(H_{xx})$	$I(H_{xy})$	$I(H_{yx})$	$I(H_{yy})$	$\Delta R(H_{xx})$	$\Delta R(H_{xy})$	$\Delta R(H_{yx})$	$\Delta R(H_{yy})$	$\Delta I(H_{xx})$	$\Delta I(H_{xy})$	$\Delta I(H_{yx})$	$\Delta I(H_{yy})$
9.8	163.2	-19.2	-21.6	267.1	12.0	6.9	0.6	-4.8	-0.4	-2.5	-0.8	-4.8	-0.3	-1.9	-0.5	-3.5
19.5	162.2	-17.2	-22.8	245.7	28.1	-0.4	-3.4	9.4	-0.3	-2.5	-0.2	-4.0	-0.4	-1.8	-0.4	-2.5
29.3	160.9	-24.8	-22.6	294.1	57.5	-2.4	0.8	56.4	-0.3	-1.6	-0.3	-3.8	-0.2	-1.3	-0.3	-2.3
39.1	157.2	-25.9	-22.2	294.6	71.6	-0.3	-3.6	72.4	-0.2	-1.7	-0.7	-3.9	-0.4	-1.6	-0.3	-2.7
48.8	165.7	-24.0	-22.7	291.1	74.4	4.8	-1.6	100.4	-0.2	-1.2	-0.3	-3.5	-0.3	-0.5	-0.3	-2.7
58.6	173.8	-16.5	-16.3	309.8	97.4	0.0	-3.0	129.2	-0.2	-1.0	-0.2	-3.6	-0.2	-0.4	-0.2	-2.2
68.4	176.4	-17.5	-15.9	314.5	110.1	-0.7	-4.7	129.7	-0.1	-1.1	-0.3	-3.7	-0.2	-0.5	-0.2	-1.8
78.1	175.9	-17.6	-11.0	318.6	124.6	-0.7	-12.4	142.3	-0.1	-1.5	-0.2	-3.4	-0.3	-0.4	-0.2	-2.1
87.9	185.8	-15.0	-8.7	338.2	144.0	0.0	-10.9	157.9	-0.1	-0.9	-0.6	-3.6	-0.2	-0.5	-0.2	-2.8
97.7	181.7	-10.1	-11.3	330.3	150.6	-1.5	-17.2	173.4	-0.3	-1.1	-0.3	-3.4	-0.2	-0.4	-0.2	-1.7
107.4	190.5	-5.6	-8.0	327.9	165.6	-1.9	-12.2	187.8	-0.2	-0.9	-0.3	-3.1	-0.2	-0.6	-0.1	-1.7
117.2	187.1	-7.0	-12.3	343.0	180.6	-2.9	-16.4	214.8	-0.1	-1.2	-0.3	-3.4	-0.2	-0.6	-0.4	-1.7
127.0	189.6	-2.2	-10.4	359.9	192.9	-7.0	-14.3	191.2	-0.3	-1.5	-0.3	-3.7	-0.3	-0.5	-0.3	-2.0
136.7	187.5	0.2	-8.3	363.3	205.1	-9.6	-18.5	191.7	-0.2	-1.0	-0.3	-3.5	-0.3	-0.5	-0.6	-2.0
146.5	210.3	3.9	0.0	380.7	209.3	-15.7	-12.3	205.5	-0.3	-1.5	-0.4	-3.3	-0.2	-0.9	-0.3	-2.1
156.3	209.2	3.9	1.2	329.2	221.7	-7.4	-14.6	328.4	-0.2	-1.0	-0.7	-3.2	-0.4	-0.5	-0.9	-1.7
166.0	205.2	4.9	-1.2	371.2	229.7	-10.4	-15.8	275.6	-0.5	-1.0	-0.7	-4.2	-0.4	-0.9	-0.2	-2.5
175.8	193.2	5.0	3.6	427.1	253.7	-9.6	-8.3	311.9	-0.4	-2.1	-1.8	-5.0	-1.1	-0.8	-0.9	-3.8
185.5	212.0	9.9	6.1	397.8	249.6	-6.4	-21.6	273.2	-1.0	-1.8	-2.1	-6.6	-1.2	-2.0	-1.1	-3.3
195.3	217.1	16.8	29.6	432.9	252.5	-10.1	-12.7	329.8	-0.7	-1.2	-1.1	-4.1	-0.7	-0.5	-0.3	-2.6
205.1	207.0	16.4	25.6	411.0	276.7	3.8	-13.1	337.7	-0.6	-1.2	-0.4	-3.8	-0.3	-0.6	-0.6	-1.7
214.8	190.9	15.7	8.0	394.7	297.7	7.0	-11.6	362.1	-0.5	-1.0	-0.5	-3.2	-0.3	-0.5	-0.4	-2.4
224.6	205.5	36.0	24.9	408.0	328.7	6.2	-9.9	357.0	-0.3	-1.2	-0.7	-3.9	-0.4	-0.4	-0.3	-1.8
234.4	197.2	31.8	41.0	405.8	332.6	5.5	-16.3	359.6	-0.2	-0.8	-0.7	-3.3	-0.1	-0.8	-0.5	-2.6
244.1	185.1	49.4	37.5	447.1	348.7	22.5	16.7	416.7	-0.3	-1.2	-0.3	-4.0	-0.8	-0.7	-1.6	-2.9
253.9	201.8	77.0	57.6	501.1	361.7	7.4	32.1	349.0	-0.3	-1.9	-0.5	-5.0	-0.9	-0.5	-2.0	-2.4
263.7	197.9	84.2	43.9	476.4	379.4	18.3	22.9	397.2	-0.9	-1.2	-0.9	-3.8	-0.5	-1.0	-2.3	-3.3
273.4	224.5	122.5	64.3	500.1	376.9	-4.9	-78.8	296.2	-1.5	-2.1	-3.2	-5.4	-0.9	-1.2	-2.8	-4.1
283.2	280.5	185.5	210.5	625.0	393.7	-60.0	-25.8	192.5	-3.7	-2.1	-7.0	-5.2	-5.0	-5.6	-10.9	-13.1
293.0	271.8	115.3	289.5	523.3	307.8	-69.6	-211.6	211.8	-2.5	-3.3	-3.5	-7.5	-3.3	-1.6	-7.9	-6.3
302.7	197.0	107.6	-10.0	361.9	386.1	-35.3	-134.8	342.5	-1.1	-2.2	-1.2	-6.3	-1.7	-1.3	-4.8	-4.9
312.5	253.1	97.3	48.3	413.0	425.9	-54.9	-77.4	362.6	-1.8	-2.6	-1.4	-4.0	-2.6	-1.3	-1.8	-3.0
322.3	192.7	109.4	42.0	422.8	385.7	-25.2	-96.8	411.8	-1.1	-1.5	-1.1	-4.1	-0.6	-1.2	-1.3	-2.9
332.0	174.6	85.6	-3.8	385.7	390.5	-23.6	-114.8	380.2	-0.7	-1.6	-0.9	-4.5	-1.2	-0.7	-2.2	-1.9
341.8	163.4	126.8	24.3	420.3	411.7	-20.8	-90.7	389.3	-2.4	-1.3	-2.5	-3.6	-1.1	-1.9	-1.0	-2.7

Table 28: Dynamic Stiffness Real and Imaginary Parts at 10800 rpm and 783 kPa (MN/m)

f (Hz)	$R(H_{xx})$	$R(H_{xy})$	$R(H_{yx})$	$R(H_{yy})$	$I(H_{xx})$	$I(H_{xy})$	$I(H_{yx})$	$I(H_{yy})$	$\Delta R(H_{xx})$	$\Delta R(H_{xy})$	$\Delta R(H_{yx})$	$\Delta R(H_{yy})$	$\Delta I(H_{xx})$	$\Delta I(H_{xy})$	$\Delta I(H_{yx})$	$\Delta I(H_{yy})$
9.8	174.1	-25.4	-20.9	349.8	14.8	4.1	-5.9	90.8	-0.6	-2.4	-0.8	-3.8	-0.5	-1.1	-0.4	-1.6
19.5	171.4	-23.0	-17.9	348.6	28.5	1.1	1.4	16.5	-0.4	-1.4	-0.3	-3.1	-0.4	-0.6	-0.4	-2.6
29.3	170.4	-25.7	-21.1	386.4	57.1	4.3	1.9	32.5	-0.3	-1.5	-0.3	-2.7	-0.4	-0.9	-0.1	-1.8
39.1	169.7	-26.2	-20.7	375.0	70.6	5.9	-1.1	73.8	-0.2	-0.7	-0.1	-1.4	-0.2	-0.6	-0.5	-1.5
48.8	180.9	-25.1	-16.2	361.9	78.0	4.7	-3.9	112.9	-0.4	-0.8	-0.2	-2.1	-0.2	-0.5	-0.2	-1.0
58.6	181.9	-24.0	-15.2	378.6	99.2	5.7	-5.3	121.4	-0.1	-0.5	-0.1	-1.9	-0.2	-0.7	-0.2	-1.1
68.4	185.6	-19.2	-13.6	389.9	116.5	12.2	-0.4	128.0	-0.3	-0.5	-0.3	-1.6	-0.3	-0.3	-0.4	-1.6
78.1	187.2	-14.2	-10.4	379.0	127.3	9.4	-5.9	145.2	-0.1	-0.5	-0.2	-1.5	-0.1	-0.3	-0.3	-1.0
87.9	194.4	-14.4	-11.0	405.6	145.4	7.7	-8.0	178.0	-0.2	-0.6	-0.1	-1.7	-0.3	-0.6	-0.2	-1.2
97.7	193.9	-8.8	-10.0	400.2	154.2	7.2	-9.9	169.9	-0.4	-0.3	-0.2	-1.7	-0.1	-0.4	-0.2	-1.1
107.4	201.4	-5.4	-8.3	410.4	166.1	8.0	-11.9	188.5	-0.4	-0.4	-0.4	-1.4	-0.3	-0.3	-0.3	-1.0
117.2	196.5	-3.6	-9.9	416.9	183.0	6.3	-16.1	208.3	-0.1	-0.4	-0.2	-1.7	-0.3	-0.4	-0.3	-0.9
127.0	203.6	-1.1	-8.7	402.3	193.2	5.4	-16.9	221.3	-0.2	-0.5	-0.3	-1.5	-0.3	-0.6	-0.4	-1.3
136.7	201.6	1.5	-7.8	404.3	209.2	3.2	-18.6	229.8	-0.3	-0.5	-0.2	-1.6	-0.4	-0.4	-0.3	-1.2
146.5	216.5	6.1	-5.0	401.6	210.4	3.3	-17.7	227.3	-0.2	-0.3	-0.2	-1.8	-0.4	-0.6	-0.3	-1.2
156.3	226.7	15.9	-10.5	379.7	223.4	6.6	-11.2	237.9	-0.2	-0.4	-0.2	-1.5	-0.3	-0.6	-0.4	-1.2
166.0	217.5	9.3	-4.1	433.2	235.8	2.7	-19.6	273.3	-0.5	-0.6	-0.4	-1.9	-0.3	-0.6	-0.3	-1.6
175.8	212.1	9.6	-2.2	423.0	257.3	3.0	-17.0	285.0	-1.0	-1.6	-0.6	-3.5	-0.5	-1.4	-1.3	-2.9
185.5	223.9	13.0	1.7	429.9	257.5	4.0	-18.7	284.7	-0.7	-1.0	-0.6	-3.1	-0.6	-1.6	-1.2	-2.4
195.3	232.8	17.3	3.5	412.6	261.4	5.0	-21.3	291.4	-0.3	-0.8	-0.4	-1.7	-0.4	-0.5	-0.3	-1.6
205.1	222.9	20.5	3.1	427.9	283.8	12.9	-20.9	318.7	-0.6	-0.4	-0.2	-1.8	-0.3	-0.3	-0.2	-1.2
214.8	203.9	23.9	3.7	411.1	297.9	19.7	-26.8	310.6	-0.3	-0.4	-0.3	-1.6	-0.2	-0.4	-0.2	-1.1
224.6	218.8	47.9	-5.3	280.3	321.9	26.0	-25.2	358.9	-0.3	-0.5	-0.3	-2.6	-0.6	-0.5	-0.2	-1.4
234.4	200.6	32.0	-3.8	427.2	332.8	17.9	-29.6	365.6	-0.3	-0.4	-0.2	-1.7	-0.3	-0.4	-0.2	-1.1
244.1	193.9	40.1	-2.7	424.0	337.1	21.2	-35.3	376.4	-0.3	-0.2	-0.2	-1.4	-0.2	-0.4	-0.2	-1.0
253.9	198.7	45.2	-9.2	437.6	349.3	26.6	-30.9	394.1	-0.3	-0.4	-0.1	-1.7	-0.3	-0.5	-0.2	-0.9
263.7	204.8	53.1	-14.5	390.1	368.7	34.6	-25.1	381.0	-0.2	-0.4	-0.3	-1.4	-0.3	-0.3	-0.3	-1.0
273.4	197.2	76.7	-27.8	254.5	395.3	54.4	-14.7	404.5	-0.3	-0.3	-0.2	-1.7	-0.3	-0.5	-0.2	-1.4
283.2	208.6	60.2	-21.2	381.1	404.6	40.2	-15.4	414.6	-0.3	-0.4	-0.2	-1.4	-0.3	-0.2	-0.3	-0.9
293.0	207.1	122.3	-19.0	363.5	408.4	30.0	32.1	659.8	-0.4	-1.0	-0.7	-3.6	-0.3	-0.4	-0.7	-3.8
302.7	195.8	121.6	-40.5	491.3	451.2	19.6	34.9	662.5	-0.5	-1.1	-0.3	-2.2	-0.5	-0.5	-0.5	-3.8
312.5	193.4	199.0	-157.5	242.7	523.4	122.0	81.1	755.0	-0.8	-0.9	-1.2	-2.8	-0.8	-1.1	-1.1	-2.7
322.3	209.3	208.2	-45.0	427.0	483.5	34.6	208.2	843.3	-1.3	-1.9	-1.8	-6.8	-1.1	-1.8	-2.8	-3.8
332.0	288.1	214.1	-37.3	513.5	632.3	102.1	258.5	633.5	-0.8	-0.7	-0.8	-2.3	-1.2	-0.8	-1.5	-1.6
341.8	390.8	291.0	163.2	613.6	660.0	86.8	326.5	587.3	-5.1	-1.7	-7.7	-5.1	-4.7	-3.8	-1.9	-3.7

Table 29: Dynamic Stiffness Real and Imaginary Parts at 10800 rpm and 1567 kPa (MN/m)

f (Hz)	$R(H_{xx})$	$R(H_{xy})$	$R(H_{yx})$	$R(H_{yy})$	$I(H_{xx})$	$I(H_{xy})$	$I(H_{yx})$	$I(H_{yy})$	$\Delta R(H_{xx})$	$\Delta R(H_{xy})$	$\Delta R(H_{yx})$	$\Delta R(H_{yy})$	$\Delta I(H_{xx})$	$\Delta I(H_{xy})$	$\Delta I(H_{yx})$	$\Delta I(H_{yy})$
9.8	196.3	-33.3	-22.7	475.8	15.4	7.4	-4.3	117.3	-0.3	-3.4	-0.4	-2.7	-0.4	-2.6	-0.6	-4.5
19.5	194.7	-28.4	-24.4	483.5	28.8	6.9	-1.2	50.8	-0.5	-1.7	-0.4	-3.2	-0.6	-2.6	-0.5	-2.3
29.3	194.3	-27.6	-23.0	524.0	57.6	7.5	0.7	40.3	-0.4	-1.4	-0.3	-2.4	-0.5	-1.1	-0.3	-1.8
39.1	192.9	-26.2	-22.4	503.6	68.4	7.0	-0.2	58.5	-0.3	-1.6	-0.5	-2.1	-0.3	-1.0	-0.2	-2.1
48.8	203.2	-26.7	-17.3	473.4	77.9	8.8	-2.7	102.2	-0.4	-0.9	-0.1	-1.6	-0.3	-0.6	-0.3	-1.1
58.6	204.4	-23.7	-15.8	491.9	99.2	10.1	-3.3	96.6	-0.2	-0.7	-0.2	-1.9	-0.2	-1.1	-0.4	-1.2
68.4	207.7	-22.9	-16.7	498.7	110.7	11.6	-6.1	99.7	-0.1	-0.8	-0.2	-2.1	-0.3	-0.6	-0.7	-1.4
78.1	210.7	-14.5	-11.3	486.3	127.2	14.5	-4.0	123.6	-0.3	-0.5	-0.1	-1.9	-0.2	-0.6	-0.4	-1.4
87.9	217.1	-14.1	-12.3	508.7	145.6	13.1	-7.3	162.2	-0.2	-0.3	-0.2	-1.8	-0.4	-0.7	-0.3	-1.1
97.7	216.2	-10.4	-11.6	505.5	154.5	13.4	-9.8	149.4	-0.2	-0.4	-0.3	-1.6	-0.2	-0.7	-0.3	-1.3
107.4	223.6	-6.2	-11.2	514.9	166.9	13.3	-13.0	169.4	-0.2	-0.6	-0.2	-1.4	-0.2	-0.5	-0.4	-1.2
117.2	217.6	-3.8	-10.9	512.3	181.3	12.4	-15.4	188.5	-0.2	-0.5	-0.1	-1.5	-0.2	-0.5	-0.3	-1.0
127.0	224.7	-0.7	-9.6	496.2	194.0	14.5	-15.7	207.3	-0.3	-0.4	-0.2	-1.5	-0.4	-0.4	-0.1	-1.0
136.7	221.3	4.3	-9.7	484.5	210.9	14.7	-18.9	221.1	-0.4	-0.6	-0.3	-1.8	-0.4	-0.3	-0.1	-1.2
146.5	238.1	8.8	-7.4	489.7	212.0	15.0	-18.9	223.3	-0.2	-0.3	-0.2	-1.5	-0.2	-0.6	-0.4	-1.1
156.3	247.0	17.1	-8.6	483.1	229.8	15.1	-18.5	215.2	-0.3	-0.4	-0.6	-1.6	-0.3	-0.4	-0.3	-1.3
166.0	238.6	10.9	-7.5	524.3	237.2	11.6	-19.6	266.4	-0.5	-0.6	-0.8	-2.3	-0.7	-0.5	-0.4	-1.1
175.8	231.7	16.0	-6.1	512.2	260.9	13.9	-21.4	276.0	-0.6	-1.3	-2.3	-2.5	-1.6	-1.5	-1.2	-3.3
185.5	246.1	19.5	-1.7	509.9	260.5	12.7	-23.0	275.8	-0.6	-1.5	-2.0	-2.6	-1.5	-0.7	-1.1	-3.0
195.3	251.0	24.5	-2.3	502.6	270.5	13.6	-24.4	280.6	-0.2	-0.3	-0.9	-2.3	-0.9	-0.7	-0.4	-1.0
205.1	245.5	25.9	-3.1	524.4	286.4	18.1	-23.9	306.9	-0.6	-0.6	-0.4	-1.6	-0.7	-0.5	-0.6	-1.4
214.8	227.6	32.0	-3.2	505.5	298.6	24.0	-28.5	299.8	-0.2	-0.3	-0.3	-1.5	-0.4	-0.4	-0.6	-1.1
224.6	242.3	43.5	-3.9	420.3	325.6	29.0	-24.6	308.5	-0.5	-0.3	-0.3	-1.7	-0.6	-0.6	-0.3	-1.0
234.4	227.4	39.4	-6.8	522.4	333.4	19.7	-33.8	352.0	-0.6	-0.4	-0.3	-1.6	-0.2	-0.4	-0.1	-1.2
244.1	221.0	47.1	-6.6	527.6	340.4	18.6	-36.3	371.9	-0.3	-0.5	-0.3	-1.9	-0.2	-0.6	-0.5	-1.2
253.9	226.8	56.6	-10.2	501.1	351.4	30.3	-35.7	384.4	-0.2	-0.4	-0.5	-1.4	-0.2	-0.4	-0.2	-1.3
263.7	231.6	59.8	-14.9	484.1	371.0	34.0	-31.9	370.2	-0.3	-0.3	-0.5	-1.7	-0.3	-0.4	-0.2	-0.9
273.4	230.6	72.8	-19.3	389.4	391.6	47.0	-27.3	357.3	-0.4	-0.3	-0.2	-1.8	-0.6	-0.4	-0.5	-0.9
283.2	238.9	68.3	-24.8	476.4	402.7	32.8	-28.5	391.2	-0.3	-0.3	-0.5	-1.4	-0.7	-0.3	-0.3	-1.0
293.0	231.1	83.2	-29.3	427.5	407.8	51.2	-21.6	421.4	-0.3	-0.3	-0.4	-1.5	-0.6	-0.4	-0.3	-1.2
302.7	228.8	132.0	-51.2	323.8	447.5	66.8	-22.0	558.7	-0.5	-0.6	-0.6	-2.1	-0.8	-0.6	-0.6	-1.3
312.5	216.9	129.9	-54.9	353.0	475.4	86.6	-19.7	514.5	-1.0	-0.4	-0.5	-1.7	-0.8	-0.4	-0.6	-1.4
322.3	216.0	126.9	-55.9	387.2	466.9	74.9	6.4	510.5	-0.7	-0.2	-0.4	-1.7	-0.8	-0.6	-0.2	-1.1
332.0	234.9	118.1	-58.1	599.7	512.3	31.7	52.8	565.1	-0.9	-0.6	-0.3	-1.7	-0.5	-0.4	-0.3	-1.2
341.8	226.6	139.0	-69.5	536.9	548.1	71.7	87.1	534.6	-1.5	-0.9	-1.3	-2.1	-1.1	-0.6	-1.6	-1.5

Table 30: Dynamic Stiffness Real and Imaginary Parts at 10800 rpm and 2350 kPa (MN/m)

f (Hz)	$R(H_{xx})$	$R(H_{xy})$	$R(H_{yx})$	$R(H_{yy})$	$I(H_{xx})$	$I(H_{xy})$	$I(H_{yx})$	$I(H_{yy})$	$\Delta R(H_{xx})$	$\Delta R(H_{xy})$	$\Delta R(H_{yx})$	$\Delta R(H_{yy})$	$\Delta I(H_{xx})$	$\Delta I(H_{xy})$	$\Delta I(H_{yx})$	$\Delta I(H_{yy})$
9.8	222.3	-33.3	-26.4	574.0	15.3	14.1	-6.6	147.8	-0.7	-2.6	-1.0	-4.7	-0.8	-4.2	-0.8	-3.5
19.5	221.1	-22.3	-27.1	611.1	29.0	10.8	-0.7	50.4	-0.3	-2.5	-0.5	-4.2	-0.6	-4.2	-0.5	-4.3
29.3	219.0	-26.2	-25.1	627.3	58.9	4.8	1.3	38.9	-0.5	-1.3	-0.5	-3.9	-0.4	-1.3	-0.3	-2.9
39.1	218.0	-26.8	-25.0	604.1	69.2	7.1	0.6	57.7	-0.2	-1.3	-0.6	-3.9	-0.3	-1.4	-0.4	-1.8
48.8	228.8	-24.4	-19.3	581.1	78.2	8.6	-1.7	99.3	-0.3	-0.9	-0.1	-1.7	-0.4	-1.3	-0.2	-2.3
58.6	229.6	-22.3	-17.3	610.3	99.6	8.9	-3.1	88.8	-0.4	-1.3	-0.2	-3.7	-0.4	-0.8	-0.5	-1.9
68.4	234.8	-19.0	-18.2	615.4	111.7	9.9	-4.9	91.4	-0.3	-0.8	-0.2	-2.0	-0.6	-0.5	-0.4	-1.7
78.1	236.2	-10.7	-13.6	600.6	130.3	16.0	-2.0	127.0	-0.2	-0.5	-0.4	-2.2	-0.2	-0.7	-0.5	-1.0
87.9	241.3	-11.9	-14.1	618.9	147.5	14.4	-7.9	161.5	-0.4	-0.3	-0.2	-1.9	-0.4	-0.6	-0.2	-1.9
97.7	242.7	-8.7	-14.1	610.8	157.1	14.5	-10.5	141.1	-0.3	-0.5	-0.2	-2.6	-0.2	-0.4	-0.5	-1.4
107.4	248.6	-5.5	-13.5	624.3	169.3	14.5	-13.3	161.5	-0.3	-0.5	-0.3	-1.4	-0.4	-0.3	-0.4	-1.4
117.2	243.6	-1.7	-13.5	617.8	184.5	15.5	-16.4	182.7	-0.1	-0.4	-0.4	-1.9	-0.3	-0.6	-0.3	-1.6
127.0	249.6	1.2	-13.5	597.9	198.5	17.6	-17.8	201.8	-0.2	-0.6	-0.3	-1.8	-0.2	-0.4	-0.4	-1.2
136.7	246.1	6.1	-13.6	587.2	214.0	18.7	-19.2	213.3	-0.3	-0.4	-0.3	-2.4	-0.2	-0.5	-0.4	-1.7
146.5	263.5	12.9	-11.0	588.0	216.8	17.6	-18.4	220.0	-0.3	-0.5	-0.4	-1.7	-0.1	-0.6	-0.5	-1.1
156.3	269.7	21.3	-11.7	583.5	234.3	17.8	-18.7	206.4	-0.4	-0.6	-0.3	-1.7	-0.3	-0.5	-0.5	-1.5
166.0	263.1	15.1	-11.5	624.7	243.0	14.2	-20.1	259.3	-0.5	-0.7	-0.9	-1.4	-0.4	-0.4	-0.8	-2.2
175.8	255.8	22.0	-9.0	611.4	266.2	15.8	-20.6	274.2	-1.5	-1.6	-2.0	-5.0	-1.0	-1.6	-1.8	-2.5
185.5	270.9	25.8	-5.9	613.9	268.0	16.9	-21.7	265.9	-1.5	-1.2	-1.3	-4.2	-0.9	-2.2	-2.6	-3.6
195.3	274.4	28.1	-6.5	604.3	277.1	16.4	-24.3	272.9	-0.6	-1.2	-1.1	-2.6	-0.8	-0.5	-0.6	-2.1
205.1	271.3	34.4	-7.3	615.6	295.0	21.1	-25.1	302.2	-0.9	-0.4	-0.5	-2.3	-0.8	-0.7	-0.3	-1.4
214.8	256.4	40.2	-7.4	609.3	306.3	24.1	-27.7	301.2	-0.3	-0.3	-0.4	-3.2	-0.8	-0.6	-0.4	-1.2
224.6	267.8	52.5	-8.3	537.9	334.2	23.8	-27.4	323.3	-0.3	-0.8	-0.4	-2.2	-0.4	-0.3	-0.3	-2.1
234.4	257.8	45.8	-10.6	628.5	342.4	18.4	-31.7	348.1	-0.3	-0.5	-0.3	-2.1	-0.2	-0.3	-0.5	-1.2
244.1	251.4	54.7	-12.2	609.2	350.2	20.9	-33.1	352.3	-0.2	-0.5	-0.2	-2.0	-0.2	-0.5	-0.4	-1.9
253.9	257.4	60.2	-16.1	610.7	363.0	26.4	-31.9	367.3	-0.5	-0.4	-0.1	-2.0	-0.7	-0.9	-0.4	-1.4
263.7	263.1	68.2	-18.8	574.7	382.3	31.1	-31.6	372.5	-0.2	-0.3	-0.3	-2.3	-0.7	-0.8	-0.4	-1.6
273.4	266.0	77.3	-22.2	495.5	401.4	42.1	-26.3	346.1	-0.4	-0.4	-0.3	-2.3	-0.9	-0.7	-0.4	-1.2
283.2	272.3	69.9	-27.7	587.2	412.8	26.3	-28.3	382.7	-1.0	-0.5	-0.3	-1.9	-0.4	-0.4	-0.4	-1.0
293.0	269.0	87.0	-28.4	536.5	415.0	43.6	-20.5	412.8	-0.5	-0.5	-0.3	-1.7	-0.8	-0.4	-0.4	-2.7
302.7	266.3	111.8	-32.3	464.6	448.7	62.5	-15.8	447.6	-0.2	-0.9	-0.3	-4.1	-1.1	-0.6	-0.7	-1.2
312.5	262.3	106.5	-36.0	592.5	478.1	52.1	-13.3	462.9	-0.7	-0.3	-0.4	-2.1	-1.4	-0.5	-0.6	-1.7
322.3	256.6	158.4	-51.2	419.1	476.8	67.7	-16.4	564.2	-0.6	-1.0	-1.4	-6.5	-0.9	-2.4	-0.4	-6.3
332.0	290.6	133.4	-43.8	794.7	490.0	-42.7	84.3	710.7	-0.4	-1.4	-0.9	-3.6	-0.4	-0.9	-0.4	-3.1
341.8	273.1	130.6	-61.6	656.1	536.2	43.4	48.1	521.2	-0.9	-0.6	-0.5	-2.2	-0.9	-0.5	-0.6	-1.5

Table 31: Dynamic Stiffness Real and Imaginary Parts at 10800 rpm and 3134 kPa (MN/m)

f (Hz)	$R(H_{xx})$	$R(H_{xy})$	$R(H_{yx})$	$R(H_{yy})$	$I(H_{xx})$	$I(H_{xy})$	$I(H_{yx})$	$I(H_{yy})$	$\Delta R(H_{xx})$	$\Delta R(H_{xy})$	$\Delta R(H_{yx})$	$\Delta R(H_{yy})$	$\Delta I(H_{xx})$	$\Delta I(H_{xy})$	$\Delta I(H_{yx})$	$\Delta I(H_{yy})$
9.8	249.4	-28.7	-28.4	746.7	17.7	11.6	-5.5	148.6	-1.1	-2.5	-0.9	-4.4	-0.9	-2.5	-1.5	-2.6
19.5	248.7	-20.3	-26.2	731.5	33.0	5.3	-1.8	88.8	-0.4	-3.3	-0.5	-2.4	-0.3	-3.2	-0.9	-3.8
29.3	247.8	-23.8	-26.1	735.8	61.7	9.2	-0.5	32.7	-0.5	-0.6	-0.4	-2.5	-0.8	-1.6	-0.3	-3.1
39.1	246.9	-25.6	-24.7	720.4	72.4	8.8	-0.9	46.8	-0.4	-0.9	-0.4	-2.5	-0.2	-1.5	-0.7	-2.1
48.8	257.1	-21.6	-20.6	708.5	81.9	11.2	-2.4	84.7	-0.2	-0.7	-0.3	-3.0	-0.2	-0.7	-0.2	-1.6
58.6	258.7	-18.7	-18.9	737.7	104.1	9.3	-4.4	72.4	-0.2	-0.7	-0.3	-3.2	-0.3	-0.3	-0.2	-1.4
68.4	263.8	-16.7	-18.8	737.3	117.8	12.6	-7.0	80.8	-0.4	-0.5	-0.4	-2.0	-0.3	-0.4	-0.2	-0.9
78.1	263.2	-8.5	-19.6	707.6	137.8	24.3	-0.4	124.8	-0.2	-0.4	-0.2	-2.3	-0.1	-0.4	-0.3	-1.4
87.9	271.2	-9.5	-15.7	733.5	154.6	16.9	-9.7	154.1	-0.3	-0.5	-0.1	-2.7	-0.4	-0.8	-0.3	-0.9
97.7	272.5	-4.2	-15.9	719.7	164.8	17.3	-12.5	127.3	-0.5	-0.3	-0.2	-2.2	-0.4	-0.4	-0.5	-1.4
107.4	278.8	0.4	-16.0	740.3	177.1	16.5	-15.4	145.3	-0.1	-0.5	-0.1	-3.2	-0.3	-0.5	-0.2	-0.9
117.2	274.3	3.2	-15.9	729.2	193.9	17.3	-18.5	163.4	-0.2	-0.5	-0.3	-2.5	-0.3	-0.3	-0.4	-0.9
127.0	280.5	8.3	-15.8	704.2	207.5	19.4	-20.4	184.6	-0.5	-0.5	-0.3	-2.9	-0.3	-0.5	-0.2	-1.3
136.7	277.5	14.1	-16.2	690.6	223.4	19.4	-21.5	203.3	-0.3	-0.4	-0.5	-2.7	-0.4	-0.3	-0.2	-1.5
146.5	295.1	20.9	-14.8	693.4	227.4	16.7	-21.8	220.1	-0.2	-0.5	-0.3	-2.0	-0.3	-0.5	-0.3	-1.3
156.3	301.0	26.9	-14.9	701.0	245.5	16.6	-21.5	189.4	-0.3	-0.6	-0.4	-2.5	-0.6	-0.4	-0.6	-1.3
166.0	295.9	21.5	-16.2	727.9	254.5	13.5	-23.9	239.1	-0.8	-0.6	-0.8	-3.0	-0.6	-0.8	-0.9	-1.8
175.8	290.2	27.8	-13.5	716.3	277.8	15.5	-25.6	261.3	-2.0	-2.5	-3.0	-3.5	-1.9	-1.7	-3.9	-4.9
185.5	305.5	33.2	-11.0	720.4	282.2	14.9	-27.2	248.7	-1.0	-0.9	-1.9	-4.6	-1.2	-1.0	-1.9	-2.4
195.3	308.5	37.9	-12.6	700.1	290.2	16.5	-27.4	249.0	-0.8	-0.7	-0.6	-3.0	-0.5	-0.7	-1.2	-1.8
205.1	305.6	42.5	-13.3	721.2	309.8	18.6	-28.0	282.8	-0.6	-0.6	-0.5	-3.7	-0.5	-0.4	-0.5	-1.0
214.8	293.4	51.0	-13.0	700.6	322.5	23.6	-29.5	279.5	-0.4	-0.4	-0.5	-3.5	-0.5	-0.4	-0.4	-1.2
224.6	305.8	59.4	-13.1	637.8	349.0	23.6	-27.5	282.2	-0.3	-0.9	-0.6	-4.7	-0.5	-0.4	-0.2	-1.5
234.4	296.1	52.4	-16.4	732.9	358.5	12.8	-31.6	331.7	-0.4	-0.3	-0.3	-2.3	-0.5	-0.5	-0.2	-1.3
244.1	290.4	63.5	-16.5	702.3	367.4	15.1	-34.5	335.2	-0.7	-0.5	-0.3	-2.5	-0.5	-0.3	-0.2	-1.4
253.9	295.5	66.2	-20.7	708.5	379.8	21.2	-33.0	341.9	-0.2	-0.4	-0.3	-3.1	-0.4	-0.7	-0.4	-1.0
263.7	302.0	73.4	-21.0	669.4	398.2	27.5	-29.6	337.4	-0.3	-0.3	-0.1	-3.1	-0.3	-0.6	-0.4	-1.8
273.4	309.1	84.6	-26.6	598.7	419.9	33.5	-27.3	324.2	-0.4	-0.7	-0.3	-4.4	-0.4	-0.5	-0.4	-1.1
283.2	315.4	76.3	-30.6	693.6	429.4	12.1	-29.4	379.2	-0.3	-0.5	-0.3	-2.5	-0.4	-0.6	-0.3	-1.1
293.0	314.8	92.8	-31.1	618.9	432.7	40.3	-18.9	376.9	-0.4	-0.3	-0.3	-3.8	-0.4	-0.7	-0.3	-1.6
302.7	315.6	113.9	-33.4	578.8	463.7	50.4	-14.6	416.1	-0.2	-0.9	-0.4	-5.5	-0.7	-1.1	-0.4	-1.5
312.5	320.5	191.5	-60.7	642.1	498.9	-7.9	-8.3	752.1	-0.5	-1.2	-1.4	-9.3	-0.9	-4.0	-0.6	-11.2
322.3	309.8	134.0	-39.1	552.8	490.2	66.6	-3.6	437.0	-0.6	-1.0	-0.6	-6.1	-0.6	-1.1	-0.5	-1.2
332.0	340.2	298.1	-146.5	470.9	550.2	-38.7	-38.9	1015.7	-1.4	-4.9	-6.4	-11.2	-1.8	-9.6	-1.6	-31.8
341.8	325.9	122.4	-53.9	803.4	547.8	10.2	27.2	515.2	-0.6	-0.2	-0.4	-2.4	-0.6	-0.7	-0.5	-1.1

Table 32: Dynamic Stiffness Real and Imaginary Parts at 13200 rpm and 0 kPa (MN/m)

f (Hz)	$R(H_{xx})$	$R(H_{xy})$	$R(H_{yx})$	$R(H_{yy})$	$I(H_{xx})$	$I(H_{xy})$	$I(H_{yx})$	$I(H_{yy})$	$\Delta R(H_{xx})$	$\Delta R(H_{xy})$	$\Delta R(H_{yx})$	$\Delta R(H_{yy})$	$\Delta I(H_{xx})$	$\Delta I(H_{xy})$	$\Delta I(H_{yx})$	$\Delta I(H_{yy})$
9.8	202.8	-3.5	-25.9	307.0	10.7	9.5	8.3	-59.4	-1.3	-4.4	-1.7	-10.1	-1.2	-4.1	-1.1	-5.3
19.5	202.2	-0.8	-30.5	255.2	25.3	-2.6	-10.2	34.0	-0.9	-4.6	-0.4	-6.5	-0.6	-3.4	-0.7	-4.8
29.3	203.3	-8.7	-33.6	303.7	49.8	0.7	-2.0	35.7	-0.4	-2.3	-0.8	-7.2	-0.9	-0.5	-1.1	-3.6
39.1	197.5	-8.8	-36.7	307.2	59.8	-5.3	-0.2	45.6	-0.9	-2.4	-0.4	-4.4	-0.6	-2.9	-0.3	-2.5
48.8	203.9	-4.3	-39.0	313.8	65.9	-1.4	-0.8	78.0	-0.9	-2.3	-0.5	-3.8	-0.4	-1.2	-1.0	-3.8
58.6	210.8	2.5	-31.0	327.0	86.3	-5.8	-2.2	106.8	-0.3	-1.8	-0.7	-4.7	-0.5	-1.3	-1.0	-2.1
68.4	212.8	2.2	-34.6	328.0	95.9	-10.2	-4.5	101.9	-0.5	-1.5	-0.7	-3.4	-0.4	-0.8	-0.9	-3.0
78.1	210.7	1.3	-29.0	324.2	111.0	-13.2	-6.7	115.2	-0.3	-1.2	-0.5	-3.6	-0.5	-0.6	-0.5	-2.5
87.9	220.4	9.1	-19.9	374.7	127.0	-19.9	8.9	148.7	-0.5	-1.9	-0.3	-4.2	-0.5	-1.8	-0.5	-2.5
97.7	214.7	6.6	-27.7	333.2	136.4	-19.6	-8.3	147.5	-0.7	-1.5	-0.8	-4.4	-0.5	-0.9	-0.8	-2.6
107.4	220.7	8.0	-25.0	326.6	150.0	-24.5	-3.5	162.9	-0.7	-1.9	-0.8	-4.6	-0.8	-0.9	-0.6	-2.1
117.2	220.2	9.0	-22.6	339.3	163.8	-26.7	0.0	192.4	-0.7	-1.1	-0.4	-3.6	-0.4	-1.0	-0.8	-2.2
127.0	220.2	10.2	-21.8	349.7	177.2	-32.1	4.1	175.7	-0.6	-1.7	-0.6	-3.7	-0.4	-0.6	-0.5	-2.0
136.7	222.4	10.7	-15.8	358.6	190.7	-38.4	2.2	175.6	-0.2	-1.1	-0.5	-3.7	-0.4	-1.6	-0.9	-2.2
146.5	238.0	9.2	-11.0	374.3	192.8	-45.9	2.8	185.8	-0.6	-1.1	-0.5	-3.6	-0.5	-0.7	-0.9	-2.7
156.3	236.9	5.4	-11.9	320.4	203.0	-38.8	3.9	306.8	-0.3	-1.3	-1.0	-3.9	-0.4	-0.7	-1.0	-2.2
166.0	237.3	6.8	-4.5	364.3	217.2	-44.7	-2.5	249.5	-0.9	-1.6	-0.8	-3.3	-0.6	-0.8	-0.8	-2.5
175.8	228.6	11.0	6.9	413.5	236.8	-46.8	3.1	288.9	-0.8	-1.4	-0.8	-4.7	-0.5	-0.8	-0.7	-2.2
185.5	244.5	10.1	-7.5	386.9	233.6	-42.0	-2.0	263.6	-0.5	-1.4	-0.5	-4.0	-0.6	-1.3	-0.7	-3.1
195.3	250.8	9.2	18.8	427.3	234.5	-46.4	4.4	313.3	-0.5	-0.9	-0.4	-3.7	-0.8	-0.8	-0.7	-2.0
205.1	238.2	10.1	12.9	416.5	256.1	-32.3	12.5	332.4	-1.2	-1.5	-0.7	-3.7	-0.7	-0.6	-0.9	-2.4
214.8	233.0	13.0	2.1	399.9	275.6	-32.4	14.4	338.5	-0.6	-2.1	-1.0	-4.4	-1.0	-1.0	-0.6	-4.1
224.6	251.5	23.3	25.0	418.9	297.9	-42.8	14.3	337.8	-0.7	-1.5	-1.9	-6.1	-1.6	-1.5	-1.8	-2.6
234.4	245.0	25.4	47.5	433.3	303.4	-24.5	19.6	357.9	-0.3	-1.5	-0.9	-4.0	-0.5	-0.7	-1.5	-1.6
244.1	234.4	44.0	37.1	476.6	322.5	-18.6	64.2	395.7	-0.8	-1.9	-0.3	-4.3	-0.7	-1.2	-1.0	-2.8
253.9	249.8	47.4	85.8	517.7	339.6	-22.7	80.0	353.5	-0.5	-1.6	-2.1	-6.4	-0.6	-1.2	-1.8	-3.4
263.7	265.2	62.9	131.0	524.1	343.5	-48.1	76.5	329.9	-0.5	-1.7	-1.2	-5.6	-1.1	-1.4	-3.6	-3.2
273.4	268.9	77.9	110.6	495.1	336.1	-47.2	-17.2	278.7	-1.5	-1.5	-3.5	-4.7	-0.8	-0.8	-1.6	-3.3
283.2	337.5	104.4	271.6	539.6	294.2	-115.7	-136.0	103.7	-3.6	-5.6	-6.0	-11.8	-6.6	-2.5	-12.1	-6.2
293.0	284.2	47.3	240.2	460.3	237.9	-92.5	-298.3	179.2	-2.8	-2.1	-5.2	-7.4	-1.5	-1.1	-4.9	-6.2
302.7	196.7	40.3	-5.9	357.7	323.6	-64.8	-119.6	311.3	-0.7	-1.1	-0.7	-3.9	-0.6	-1.4	-1.3	-2.6
312.5	236.3	21.5	41.9	413.3	394.5	-54.8	-52.2	332.1	-1.5	-2.6	-2.1	-4.1	-2.2	-1.2	-1.9	-2.4
322.3	232.3	50.2	95.2	398.4	334.3	-28.1	-110.6	372.4	-0.7	-1.2	-1.1	-4.1	-1.0	-0.8	-2.6	-2.7
332.0	209.6	21.8	41.7	367.6	324.7	-40.3	-119.3	330.9	-0.6	-1.3	-1.6	-4.7	-0.7	-0.6	-1.6	-2.3
341.8	195.6	55.6	85.6	405.8	344.5	-40.5	-86.5	323.0	-1.5	-1.7	-2.2	-4.2	-1.0	-1.2	-1.6	-2.6

Table 33: Dynamic Stiffness Real and Imaginary Parts at 13200 rpm and 783 kPa (MN/m)

f (Hz)	$R(H_{xx})$	$R(H_{xy})$	$R(H_{yx})$	$R(H_{yy})$	$I(H_{xx})$	$I(H_{xy})$	$I(H_{yx})$	$I(H_{yy})$	$\Delta R(H_{xx})$	$\Delta R(H_{xy})$	$\Delta R(H_{yx})$	$\Delta R(H_{yy})$	$\Delta I(H_{xx})$	$\Delta I(H_{xy})$	$\Delta I(H_{yx})$	$\Delta I(H_{yy})$
9.8	213.6	-9.0	-26.6	364.2	15.2	-6.0	-8.0	62.0	-1.0	-3.7	-0.7	-4.2	-1.0	-1.0	-1.7	-6.9
19.5	208.9	1.5	-28.6	373.4	23.6	5.7	-3.4	12.2	-1.1	-3.7	-0.7	-8.2	-1.0	-2.9	-0.4	-3.7
29.3	209.9	-7.3	-33.1	389.0	50.4	-0.8	1.5	29.8	-0.7	-2.3	-1.2	-2.8	-1.0	-1.6	-1.1	-3.9
39.1	205.8	-5.0	-36.2	379.0	62.4	-1.9	0.8	61.1	-0.6	-1.3	-0.6	-4.3	-0.7	-2.3	-0.7	-2.3
48.8	214.5	-4.2	-32.0	367.5	67.7	-8.3	-4.1	89.5	-0.6	-1.2	-0.6	-2.1	-0.3	-1.6	-0.5	-3.5
58.6	217.5	-4.9	-32.4	380.7	86.8	-6.3	-5.4	101.1	-0.4	-1.5	-0.9	-2.3	-0.5	-1.4	-0.7	-1.3
68.4	220.4	-3.3	-30.5	386.6	103.6	-1.3	2.6	110.7	-0.5	-1.2	-0.7	-2.5	-0.4	-1.3	-0.2	-2.1
78.1	219.4	1.0	-27.6	373.3	114.6	-7.4	-2.0	124.1	-0.6	-1.1	-0.5	-1.8	-0.8	-0.6	-0.6	-1.8
87.9	225.8	0.4	-28.3	397.4	131.4	-10.1	-0.6	154.5	-0.6	-1.2	-0.3	-2.2	-0.4	-0.9	-0.6	-1.3
97.7	223.5	4.3	-28.0	389.1	140.7	-11.1	0.6	152.9	-0.3	-0.6	-0.5	-2.6	-0.1	-1.1	-0.3	-1.5
107.4	229.2	4.3	-26.7	399.5	152.0	-13.9	1.0	174.2	-0.8	-0.9	-0.6	-1.8	-0.5	-0.8	-0.6	-1.3
117.2	225.2	5.5	-22.9	402.7	167.9	-15.6	1.2	188.5	-0.5	-0.7	-0.3	-2.3	-0.3	-0.9	-0.4	-1.7
127.0	232.8	7.2	-21.8	391.4	178.7	-19.5	-0.6	203.7	-0.3	-1.0	-0.3	-1.6	-0.6	-1.0	-0.5	-1.4
136.7	231.9	7.1	-16.2	396.8	194.8	-23.7	0.9	212.1	-0.2	-0.6	-0.4	-2.1	-0.4	-0.8	-0.4	-1.4
146.5	242.5	7.9	-15.4	393.5	195.8	-25.5	-0.5	213.9	-0.4	-0.4	-0.5	-2.2	-0.3	-0.8	-0.5	-1.7
156.3	255.7	14.9	-21.4	367.8	205.4	-23.7	4.5	223.6	-0.7	-0.8	-0.4	-1.4	-0.3	-1.1	-0.9	-1.4
166.0	245.4	7.1	-8.8	419.7	221.5	-26.3	-1.9	260.6	-0.4	-0.5	-1.0	-1.7	-0.4	-0.4	-0.5	-1.7
175.8	243.8	5.3	-9.5	414.8	238.8	-30.2	0.0	269.9	-0.4	-1.2	-0.3	-2.1	-0.3	-1.1	-0.4	-1.9
185.5	255.1	6.5	-7.1	421.1	239.3	-28.5	-1.4	270.8	-0.4	-0.6	-0.7	-1.6	-0.8	-0.7	-1.0	-2.1
195.3	262.7	8.8	-4.6	406.6	245.6	-28.8	-0.5	279.3	-0.8	-0.9	-0.6	-2.3	-0.6	-1.1	-0.3	-1.6
205.1	254.0	9.9	-2.5	422.1	261.9	-21.4	2.4	301.4	-0.7	-0.7	-1.0	-1.7	-0.7	-0.9	-0.6	-1.4
214.8	239.6	11.7	1.2	409.0	277.9	-18.7	-2.8	295.0	-1.0	-0.8	-0.8	-1.8	-0.9	-0.6	-1.3	-1.8
224.6	256.4	27.9	-10.3	286.9	299.1	-18.1	3.0	341.0	-1.1	-1.4	-0.7	-5.0	-1.0	-3.1	-1.3	-1.9
234.4	241.8	8.4	0.6	429.1	309.1	-22.2	1.2	343.0	-1.0	-1.2	-0.3	-1.7	-0.5	-0.8	-0.3	-1.5
244.1	237.0	13.8	5.6	427.2	310.8	-17.7	0.9	350.9	-0.2	-0.5	-0.3	-2.3	-0.6	-0.6	-0.4	-1.8
253.9	239.8	13.8	4.9	443.5	321.1	-10.7	5.8	366.0	-0.6	-0.9	-0.5	-1.9	-0.6	-0.8	-0.1	-1.2
263.7	243.9	15.1	3.9	400.3	332.0	-3.1	9.9	352.0	-0.3	-0.7	-0.3	-1.8	-0.8	-0.4	-0.3	-1.3
273.4	240.5	32.8	-5.9	284.9	353.9	9.2	19.7	374.5	-0.4	-0.3	-0.4	-1.8	-0.4	-0.4	-0.3	-1.0
283.2	243.4	13.1	11.1	392.1	362.0	5.9	18.6	376.1	-0.3	-0.6	-0.5	-1.8	-0.5	-0.4	-0.2	-1.0
293.0	244.1	55.8	21.9	395.6	364.2	-2.8	75.3	579.2	-0.6	-1.3	-1.2	-3.1	-0.5	-0.7	-0.2	-3.0
302.7	234.4	61.8	15.6	469.8	394.6	-0.7	88.6	599.6	-0.4	-1.4	-0.7	-4.3	-0.6	-0.9	-0.5	-2.0
312.5	225.2	99.9	-84.0	281.7	454.7	80.9	117.8	614.4	-0.6	-0.6	-0.8	-2.4	-0.8	-0.7	-2.2	-2.8
322.3	258.6	127.9	30.1	390.5	423.8	27.8	269.2	730.6	-1.8	-2.3	-3.2	-4.7	-1.7	-1.7	-1.0	-1.7
332.0	290.0	107.7	68.0	480.8	599.7	117.0	266.4	552.7	-4.0	-2.1	-1.5	-2.4	-2.1	-1.4	-1.4	-1.5
341.8	438.6	191.2	308.0	573.9	535.9	70.7	192.0	472.1	-1.1	-1.1	-1.0	-2.1	-5.7	-2.8	-5.0	-3.2

Table 34: Dynamic Stiffness Real and Imaginary Parts at 13200 rpm and 1567 kPa (MN/m)

f (Hz)	$R(H_{xx})$	$R(H_{xy})$	$R(H_{yx})$	$R(H_{yy})$	$I(H_{xx})$	$I(H_{xy})$	$I(H_{yx})$	$I(H_{yy})$	$\Delta R(H_{xx})$	$\Delta R(H_{xy})$	$\Delta R(H_{yx})$	$\Delta R(H_{yy})$	$\Delta I(H_{xx})$	$\Delta I(H_{xy})$	$\Delta I(H_{yx})$	$\Delta I(H_{yy})$
9.8	233.3	-23.5	-32.1	469.3	16.8	4.7	-9.8	134.1	-0.9	-3.6	-0.8	-9.4	-1.2	-2.8	-1.8	-4.9
19.5	233.2	-17.3	-30.1	462.8	24.8	-0.2	-3.4	51.9	-0.5	-6.1	-0.9	-6.6	-1.0	-2.4	-1.2	-5.6
29.3	231.6	-18.3	-35.2	504.4	52.1	-1.5	1.0	25.8	-1.6	-2.6	-1.1	-2.8	-1.1	-3.1	-1.5	-5.2
39.1	226.6	-22.3	-36.3	484.5	62.5	2.0	-0.7	57.2	-0.3	-1.6	-0.6	-3.7	-0.4	-0.8	-0.7	-3.0
48.8	237.3	-21.8	-32.6	455.0	69.8	-1.2	-4.7	99.6	-0.5	-0.8	-0.3	-2.6	-0.6	-1.1	-1.0	-1.8
58.6	238.5	-16.0	-30.9	474.1	89.9	0.3	-4.2	91.1	-0.5	-0.6	-0.6	-2.0	-0.7	-0.7	-0.5	-1.0
68.4	238.2	-19.0	-36.3	482.8	100.8	3.5	-4.4	95.5	-0.5	-0.6	-1.1	-1.9	-0.5	-0.6	-0.5	-1.2
78.1	241.9	-11.8	-28.6	466.7	115.9	3.3	-1.8	116.7	-0.2	-0.5	-0.4	-1.8	-0.2	-0.7	-0.5	-1.2
87.9	247.1	-14.9	-28.2	486.8	134.4	1.6	-1.2	157.9	-0.4	-0.5	-0.1	-1.6	-0.3	-1.4	-0.2	-1.2
97.7	246.6	-9.9	-27.6	486.9	143.8	2.1	-0.6	142.3	-0.3	-0.7	-0.3	-1.9	-0.4	-0.5	-0.7	-1.9
107.4	251.4	-6.3	-26.6	493.3	155.2	2.2	-0.9	164.7	-0.1	-0.6	-0.4	-2.4	-0.2	-0.7	-0.4	-1.3
117.2	246.1	-5.0	-24.2	493.0	171.2	1.2	0.0	180.9	-0.2	-0.7	-0.3	-2.1	-0.4	-0.8	-0.3	-1.3
127.0	253.3	-1.5	-20.5	474.3	183.2	0.2	-0.7	199.8	-0.5	-0.9	-0.3	-1.5	-0.6	-0.5	-0.5	-1.3
136.7	252.0	2.8	-18.3	466.4	201.3	-0.8	-2.2	214.0	-0.3	-1.0	-0.4	-1.6	-0.5	-0.5	-0.2	-1.3
146.5	264.4	5.3	-16.5	469.0	200.2	-1.4	-2.0	214.0	-0.3	-0.8	-0.6	-1.9	-0.4	-0.6	-0.4	-1.1
156.3	276.7	12.6	-16.9	465.4	216.2	1.4	-3.3	207.5	-0.3	-0.5	-0.4	-1.5	-0.7	-0.5	-0.2	-1.7
166.0	266.5	5.2	-11.9	505.0	227.6	-1.4	-1.9	255.1	-0.4	-0.8	-0.5	-1.7	-0.7	-0.6	-0.4	-1.2
175.8	262.5	8.2	-8.6	492.3	247.9	-1.9	-5.0	267.4	-0.7	-0.7	-0.4	-2.2	-0.4	-0.6	-0.6	-1.3
185.5	276.1	13.5	-8.1	493.9	246.7	-1.8	-4.0	263.8	-0.5	-0.6	-0.8	-1.7	-0.5	-0.9	-0.3	-2.0
195.3	282.2	17.8	-6.5	484.4	257.7	-3.0	-6.0	269.6	-0.5	-0.3	-0.4	-1.9	-0.8	-0.7	-0.4	-1.7
205.1	277.9	18.6	-6.7	511.2	268.9	3.1	-0.2	295.7	-1.0	-1.0	-0.3	-2.2	-0.6	-0.6	-1.4	-1.5
214.8	262.6	25.8	-4.6	490.7	282.0	3.7	-3.5	288.2	-0.9	-1.4	-1.0	-3.1	-0.6	-1.2	-1.9	-2.4
224.6	280.3	32.3	-0.5	406.5	306.8	3.4	-0.5	298.5	-2.4	-1.7	-1.2	-3.3	-1.1	-1.5	-2.5	-2.2
234.4	267.2	24.3	-0.5	511.9	314.1	-0.8	-5.5	339.5	-1.0	-0.8	-0.6	-1.9	-1.0	-0.5	-0.7	-1.7
244.1	263.0	32.2	3.4	514.4	318.7	-4.2	-5.2	375.0	-0.3	-0.5	-0.2	-2.2	-0.5	-0.8	-0.3	-1.5
253.9	265.3	33.6	5.0	503.1	325.8	9.3	-3.5	361.6	-0.6	-0.5	-0.5	-2.2	-0.4	-0.4	-0.4	-1.1
263.7	270.8	34.2	4.5	482.2	338.9	11.6	-1.1	353.3	-0.4	-0.3	-0.2	-1.9	-0.3	-0.7	-0.5	-2.1
273.4	267.7	44.0	4.2	393.0	354.7	21.4	-0.5	336.8	-0.4	-0.7	-0.3	-2.5	-0.6	-0.6	-0.3	-1.8
283.2	272.4	34.8	7.1	474.0	363.0	13.1	-0.4	362.9	-0.5	-0.3	-0.4	-1.5	-0.5	-0.8	-0.3	-1.6
293.0	264.5	49.7	5.3	430.1	370.1	33.8	4.2	391.9	-0.4	-0.6	-0.4	-2.4	-0.3	-0.7	-0.2	-1.7
302.7	259.2	84.8	-3.5	345.6	398.8	47.3	6.9	505.4	-0.4	-0.5	-0.6	-3.7	-0.7	-1.0	-0.5	-1.4
312.5	246.2	83.6	-2.5	375.5	419.9	66.1	6.5	474.7	-0.6	-0.6	-0.8	-6.6	-0.7	-1.6	-0.6	-3.0
322.3	242.3	83.9	0.6	392.8	415.1	63.2	21.4	469.8	-0.5	-0.4	-0.7	-3.8	-0.7	-1.1	-0.4	-2.7
332.0	249.0	75.3	18.9	592.9	460.4	30.6	64.7	536.5	-0.8	-1.2	-0.3	-1.9	-0.7	-0.9	-0.9	-1.5
341.8	241.9	89.2	11.6	534.1	494.4	71.6	78.8	480.5	-1.3	-0.8	-0.8	-1.9	-0.6	-0.4	-1.6	-1.8

Table 35: Dynamic Stiffness Real and Imaginary Parts at 13200 rpm and 2350 kPa (MN/m)

f (Hz)	$R(H_{xx})$	$R(H_{xy})$	$R(H_{yx})$	$R(H_{yy})$	$I(H_{xx})$	$I(H_{xy})$	$I(H_{yx})$	$I(H_{yy})$	$\Delta R(H_{xx})$	$\Delta R(H_{xy})$	$\Delta R(H_{yx})$	$\Delta R(H_{yy})$	$\Delta I(H_{xx})$	$\Delta I(H_{xy})$	$\Delta I(H_{yx})$	$\Delta I(H_{yy})$
9.8	263.1	-21.9	-35.5	576.0	15.7	4.6	-12.4	147.2	-1.5	-5.2	-1.2	-6.8	-1.3	-9.1	-2.3	-3.8
19.5	261.8	-19.4	-35.0	582.0	26.5	5.6	-4.7	46.8	-1.0	-3.3	-1.3	-9.3	-1.2	-5.6	-1.2	-9.6
29.3	259.1	-29.7	-38.1	596.1	54.3	1.2	2.2	35.2	-1.2	-2.3	-2.3	-3.2	-0.6	-1.5	-1.4	-4.7
39.1	254.7	-24.6	-37.2	588.5	62.8	6.2	-0.1	60.2	-0.8	-2.1	-1.6	-2.5	-1.2	-3.1	-1.0	-2.6
48.8	263.7	-22.5	-34.3	560.0	71.3	3.4	-2.9	97.4	-0.4	-1.2	-1.1	-2.6	-0.3	-1.3	-0.6	-1.7
58.6	265.8	-24.8	-34.5	589.0	90.7	3.4	-2.8	84.2	-0.6	-1.5	-0.3	-2.6	-0.6	-0.9	-0.8	-2.3
68.4	267.8	-19.9	-35.6	591.9	100.4	6.3	-2.0	82.2	-0.5	-0.6	-0.3	-1.8	-0.4	-0.4	-0.3	-1.3
78.1	269.5	-13.1	-29.8	572.0	120.3	9.0	3.2	118.0	-0.6	-0.5	-0.4	-1.9	-0.3	-0.6	-0.5	-1.2
87.9	274.1	-16.2	-31.0	593.9	135.5	7.4	0.3	151.9	-0.4	-0.7	-0.3	-1.7	-0.7	-0.7	-0.4	-1.2
97.7	274.5	-12.7	-30.3	588.7	147.3	6.9	0.0	135.0	-0.8	-0.6	-0.3	-2.4	-0.1	-0.4	-0.5	-1.3
107.4	278.5	-7.1	-29.5	600.6	156.6	7.9	0.7	156.1	-0.2	-0.3	-0.3	-2.0	-0.2	-0.6	-0.5	-1.1
117.2	274.0	-5.9	-27.3	595.1	173.0	8.1	0.2	175.3	-0.4	-0.3	-0.5	-1.6	-0.4	-0.5	-0.3	-1.4
127.0	280.3	-2.4	-23.8	572.2	186.8	8.4	-1.5	195.6	-0.3	-0.6	-0.8	-2.6	-0.4	-0.5	-0.5	-1.1
136.7	275.9	0.5	-23.1	564.5	204.1	7.1	-1.1	206.3	-0.8	-0.6	-0.4	-1.8	-0.4	-0.6	-0.5	-1.8
146.5	292.0	5.4	-19.6	559.1	204.2	7.0	-3.4	211.1	-0.6	-0.4	-0.7	-1.4	-0.3	-0.3	-0.5	-1.3
156.3	301.4	14.2	-17.7	560.6	222.3	9.8	-3.8	194.4	-0.5	-0.4	-0.6	-1.8	-0.6	-0.3	-0.4	-1.0
166.0	293.4	6.3	-17.1	596.0	232.4	5.6	-2.6	248.0	-0.2	-0.6	-0.3	-1.5	-0.7	-0.4	-0.6	-1.3
175.8	288.3	11.7	-13.2	586.5	252.8	6.7	-3.4	267.3	-0.4	-0.5	-0.3	-1.6	-0.8	-0.5	-0.3	-0.9
185.5	303.2	17.0	-12.2	587.2	251.9	7.9	-4.2	258.2	-0.3	-0.5	-0.5	-1.5	-0.8	-0.7	-0.7	-1.3
195.3	306.6	21.5	-9.9	578.9	263.4	7.5	-6.5	260.6	-0.4	-0.5	-0.5	-1.8	-0.4	-0.6	-0.3	-1.0
205.1	305.9	26.3	-9.6	600.1	277.2	11.1	-3.5	295.3	-0.7	-0.6	-0.7	-2.3	-0.5	-1.0	-0.7	-1.4
214.8	291.3	32.6	-4.8	581.9	289.8	13.4	-6.4	290.3	-1.4	-1.6	-0.4	-2.2	-0.5	-1.1	-1.7	-2.6
224.6	306.3	40.6	-4.8	516.3	314.2	9.1	-1.5	307.6	-2.6	-1.2	-0.8	-3.8	-0.9	-1.5	-3.6	-1.9
234.4	297.8	31.4	-3.5	606.0	321.1	6.5	-5.6	337.8	-1.0	-0.8	-0.5	-1.7	-0.5	-0.9	-1.0	-2.0
244.1	291.6	39.4	-0.1	588.8	326.9	8.8	-6.8	337.7	-0.6	-0.4	-0.2	-1.8	-0.4	-0.5	-0.8	-1.4
253.9	297.7	42.3	-1.1	600.5	335.4	15.3	-6.0	350.1	-0.5	-0.4	-0.5	-1.6	-0.6	-0.6	-0.5	-1.0
263.7	303.1	48.0	0.2	558.2	350.0	18.8	-4.5	354.0	-0.7	-0.6	-0.6	-1.7	-0.5	-0.4	-0.3	-1.1
273.4	303.1	55.1	1.4	482.9	363.3	28.3	-4.8	327.4	-0.7	-0.6	-0.4	-1.9	-0.6	-0.3	-0.2	-1.0
283.2	307.5	44.0	2.3	573.9	372.4	15.9	-7.2	359.9	-0.6	-0.4	-0.3	-2.0	-0.5	-0.5	-0.3	-0.9
293.0	300.2	60.3	4.8	528.7	375.3	34.5	-3.3	386.8	-0.3	-0.4	-0.4	-1.7	-0.5	-0.5	-0.5	-0.8
302.7	295.4	84.0	3.5	456.7	400.6	51.8	0.2	419.8	-0.2	-0.3	-0.3	-2.0	-0.6	-0.3	-0.2	-1.2
312.5	288.3	83.7	-2.4	540.2	425.0	53.5	0.0	430.5	-0.5	-0.3	-0.5	-3.1	-0.9	-0.4	-0.4	-1.3
322.3	284.0	91.3	-7.1	546.9	421.6	39.0	5.3	489.5	-0.7	-0.9	-0.4	-1.7	-0.9	-0.5	-0.3	-2.1
332.0	311.0	103.0	-23.2	761.7	445.5	-34.0	93.7	698.8	-0.7	-1.0	-1.3	-3.4	-0.3	-1.5	-0.8	-2.7
341.8	284.5	97.4	-1.7	640.9	479.1	46.5	32.6	480.3	-0.4	-0.4	-0.9	-2.2	-0.7	-0.4	-0.8	-1.6

Table 36: Dynamic Stiffness Real and Imaginary Parts at 13200 rpm and 3134 kPa (MN/m)

f (Hz)	$R(H_{xx})$	$R(H_{xy})$	$R(H_{yx})$	$R(H_{yy})$	$I(H_{xx})$	$I(H_{xy})$	$I(H_{yx})$	$I(H_{yy})$	$\Delta R(H_{xx})$	$\Delta R(H_{xy})$	$\Delta R(H_{yx})$	$\Delta R(H_{yy})$	$\Delta I(H_{xx})$	$\Delta I(H_{xy})$	$\Delta I(H_{yx})$	$\Delta I(H_{yy})$
9.8	288.6	-27.9	-39.4	701.1	18.6	-1.6	-14.4	165.0	-3.1	-5.8	-0.7	-6.4	-1.4	-3.3	-1.5	-7.6
19.5	288.0	-23.9	-41.1	716.4	28.4	0.6	-5.4	90.7	-1.2	-3.3	-1.6	-7.8	-1.1	-4.1	-1.2	-4.2
29.3	286.3	-26.8	-39.5	712.2	55.9	7.2	2.1	34.9	-0.9	-1.9	-0.6	-4.1	-0.9	-4.2	-0.8	-3.3
39.1	284.5	-24.5	-40.2	703.7	65.9	6.7	-0.3	45.2	-0.6	-2.0	-1.0	-1.7	-0.6	-1.6	-1.1	-2.6
48.8	293.2	-24.4	-36.5	692.0	74.6	7.4	-2.3	83.2	-0.6	-1.2	-1.1	-2.9	-0.4	-1.1	-0.7	-2.1
58.6	293.5	-24.4	-36.0	713.4	95.8	6.8	0.1	72.3	-0.6	-0.9	-0.9	-2.8	-0.4	-1.0	-0.9	-1.5
68.4	299.6	-20.6	-36.3	717.2	107.5	9.3	-2.2	77.2	-0.2	-0.7	-0.7	-2.1	-0.6	-0.9	-0.6	-1.8
78.1	297.0	-15.4	-35.7	687.2	128.5	16.7	8.4	114.7	-0.4	-0.7	-0.3	-2.2	-0.4	-0.8	-0.4	-1.2
87.9	305.1	-16.3	-32.0	713.1	142.4	11.2	-1.5	147.8	-0.4	-0.7	-0.6	-2.6	-0.4	-0.6	-0.6	-1.5
97.7	304.6	-11.9	-31.4	699.6	153.1	10.9	-2.4	121.6	-0.5	-0.6	-0.6	-1.8	-0.6	-0.6	-0.5	-1.3
107.4	310.1	-7.1	-30.4	718.4	163.7	12.3	-2.2	139.4	-0.4	-0.4	-0.4	-2.2	-0.2	-0.9	-0.4	-1.5
117.2	304.5	-5.1	-28.7	710.4	181.0	12.8	-3.5	156.6	-0.3	-0.4	-0.4	-1.7	-0.4	-0.4	-0.6	-0.9
127.0	311.3	-0.3	-26.0	686.6	194.3	15.6	-3.8	174.7	-0.5	-0.3	-0.5	-1.8	-0.4	-0.6	-0.9	-1.3
136.7	307.4	5.3	-24.7	672.1	211.5	14.2	-4.5	193.5	-0.2	-0.5	-0.4	-1.9	-0.4	-0.3	-0.2	-1.2
146.5	324.0	12.1	-22.8	672.2	213.7	10.8	-6.5	212.1	-0.4	-0.4	-0.6	-1.7	-0.6	-0.5	-0.5	-1.3
156.3	332.6	18.4	-21.2	677.6	231.3	13.4	-5.9	181.7	-0.5	-0.6	-0.5	-2.2	-0.6	-0.6	-0.3	-1.2
166.0	327.4	11.8	-20.8	705.0	241.1	10.6	-5.5	228.3	-0.4	-0.5	-0.5	-1.5	-0.7	-0.6	-0.6	-1.0
175.8	321.0	16.6	-16.3	694.6	263.0	12.0	-6.0	254.5	-0.4	-0.7	-0.7	-2.1	-0.2	-0.6	-0.5	-1.2
185.5	336.0	23.6	-15.5	700.3	264.1	13.1	-6.9	236.7	-0.6	-0.5	-0.2	-1.7	-0.4	-0.5	-0.7	-1.5
195.3	339.5	30.2	-13.2	680.9	274.8	13.1	-7.5	236.7	-0.2	-0.6	-0.6	-1.7	-0.6	-0.4	-1.1	-1.6
205.1	337.8	34.7	-12.5	701.3	289.3	15.1	-6.2	271.1	-0.9	-0.8	-0.6	-2.2	-0.5	-1.0	-1.1	-1.3
214.8	324.6	43.0	-10.1	677.8	302.5	16.9	-7.3	268.0	-1.9	-1.4	-2.2	-3.1	-1.3	-1.7	-2.7	-3.8
224.6	342.1	47.6	-7.6	621.3	329.3	15.8	-7.8	271.3	-2.1	-1.4	-2.4	-3.9	-1.7	-1.5	-2.4	-2.4
234.4	334.9	39.0	-6.6	715.5	335.6	7.1	-8.5	319.7	-0.8	-0.7	-1.2	-2.5	-0.8	-0.9	-0.5	-1.7
244.1	329.4	51.5	-2.9	687.7	341.2	9.3	-11.1	322.6	-0.5	-0.5	-0.9	-2.0	-0.4	-0.4	-0.6	-1.9
253.9	332.8	53.9	-3.9	694.7	351.5	16.8	-10.1	329.1	-0.1	-0.4	-0.8	-1.5	-0.9	-0.6	-0.4	-1.2
263.7	338.7	59.6	-1.8	656.9	364.0	21.5	-8.4	319.9	-0.2	-0.5	-0.7	-1.6	-0.2	-0.5	-0.7	-1.2
273.4	343.3	68.7	-1.6	589.0	380.2	26.3	-9.4	306.9	-0.4	-0.7	-0.4	-1.9	-0.6	-0.3	-0.6	-0.9
283.2	346.1	56.5	-0.3	683.5	387.7	8.9	-12.8	353.0	-0.6	-0.6	-0.2	-1.8	-0.4	-0.6	-0.4	-1.0
293.0	342.6	76.8	0.5	610.5	389.0	34.4	-8.4	357.0	-0.3	-0.4	-0.6	-1.8	-0.6	-0.4	-0.7	-1.3
302.7	340.1	97.6	0.8	569.0	413.9	42.6	-5.3	398.9	-0.6	-0.6	-0.1	-1.6	-0.8	-0.5	-0.9	-1.8
312.5	335.4	155.1	-14.8	660.5	442.2	-15.0	-12.5	717.7	-1.1	-1.7	-0.7	-4.5	-0.7	-1.0	-0.6	-3.7
322.3	327.7	112.7	0.7	541.7	436.3	60.9	-3.7	407.8	-0.7	-0.3	-0.4	-2.0	-0.9	-0.4	-0.2	-1.2
332.0	337.6	247.0	-49.3	432.6	485.5	-13.9	-50.1	899.8	-0.6	-2.7	-0.6	-8.7	-0.5	-1.6	-1.3	-5.1
341.8	333.3	99.9	-2.1	795.3	489.4	12.3	12.6	482.9	-0.7	-0.5	-0.6	-2.5	-1.0	-0.7	-0.4	-1.2

Load In-between Pad

Table 37: Dynamic Stiffness Real and Imaginary Parts at 6800 rpm and 0 kPa (MN/m)

f (Hz)	$R(H_{xx})$	$R(H_{xy})$	$R(H_{yx})$	$R(H_{yy})$	$I(H_{xx})$	$I(H_{xy})$	$I(H_{yx})$	$I(H_{yy})$	$\Delta R(H_{xx})$	$\Delta R(H_{xy})$	$\Delta R(H_{yx})$	$\Delta R(H_{yy})$	$\Delta I(H_{xx})$	$\Delta I(H_{xy})$	$\Delta I(H_{yx})$	$\Delta I(H_{yy})$
9.8	166.1	-52.4	-69.8	196.9	15.9	1.0	-8.2	61.6	-0.5	-1.7	-1.5	-6.8	-0.3	-0.6	-1.9	-4.4
19.5	165.5	-42.9	-75.1	152.9	33.6	-2.5	-17.9	24.1	-0.2	-0.9	-1.9	-7.3	-0.1	-0.4	-3.0	-5.7
29.3	169.8	-48.6	-48.5	159.6	52.5	1.2	10.5	51.7	-0.2	-1.0	-0.8	-4.9	-0.2	-0.5	-2.0	-3.5
39.1	173.3	-50.4	-29.3	131.2	67.4	-2.5	11.9	66.1	-0.1	-0.9	-2.4	-4.2	-0.1	-0.4	-2.4	-2.6
48.8	178.7	-49.0	-58.6	155.1	79.3	-2.9	-9.2	80.6	-0.2	-0.8	-2.3	-4.3	-0.2	-0.3	-1.0	-1.8
58.6	185.3	-44.6	-46.3	172.8	96.3	-2.1	-19.2	98.6	-0.2	-0.8	-1.4	-4.0	-0.2	-0.3	-1.2	-2.5
68.4	189.2	-44.4	-50.1	185.4	109.1	-5.0	-17.4	102.9	-0.1	-0.8	-0.7	-3.8	-0.1	-0.4	-1.8	-2.1
78.1	192.6	-41.7	-43.3	191.8	123.3	-6.2	-1.9	113.5	-0.2	-0.8	-0.3	-3.6	-0.1	-0.3	-0.9	-2.2
87.9	197.4	-38.1	-46.8	204.6	134.8	-8.2	-4.7	138.4	-0.1	-0.9	-0.6	-4.1	-0.2	-0.4	-0.8	-2.4
97.7	201.2	-37.7	-41.0	192.7	147.4	-8.4	-22.9	141.2	-0.1	-0.9	-0.8	-4.0	-0.2	-0.5	-0.5	-2.3
107.4	207.0	-37.0	-47.4	193.5	158.2	-7.7	-27.1	158.9	-0.3	-1.6	-0.8	-3.6	-0.5	-0.6	-0.8	-2.3
117.2	209.2	-31.7	-24.9	199.0	170.4	-10.2	-16.9	168.1	-0.7	-1.6	-1.3	-4.5	-0.8	-1.3	-0.8	-2.7
127.0	213.5	-27.0	-32.0	209.1	183.4	-10.1	-28.1	162.9	-0.3	-0.9	-1.3	-3.3	-0.3	-0.6	-1.8	-2.2
136.7	217.3	-24.5	-24.7	209.5	197.8	-15.1	-25.8	184.2	-0.2	-1.0	-1.3	-3.7	-0.3	-0.3	-0.7	-2.5
146.5	222.8	-21.9	-32.8	231.3	208.3	-13.5	-40.2	199.9	-0.2	-0.8	-1.5	-3.4	-0.1	-0.5	-0.7	-2.4
156.3	225.4	-17.8	-34.1	167.4	220.8	-9.0	-40.0	288.5	-0.2	-0.8	-1.0	-3.3	-0.2	-0.3	-1.5	-2.0
166.0	229.0	-10.9	-39.7	230.2	234.3	-13.5	-43.9	247.1	-0.3	-0.9	-1.8	-3.4	-0.2	-0.3	-0.8	-2.3
175.8	238.0	-4.3	-44.2	282.0	251.3	-18.8	-50.0	292.4	-0.2	-0.7	-1.2	-4.5	-0.2	-0.4	-1.0	-3.0
185.5	238.5	5.1	-35.0	249.2	263.0	-20.9	-44.2	247.8	-0.1	-0.8	-1.4	-3.4	-0.3	-0.3	-0.6	-2.0
195.3	246.6	12.2	-42.0	293.5	274.0	-24.9	-42.0	313.3	-0.1	-0.9	-1.8	-3.9	-0.3	-0.3	-0.9	-2.0
205.1	250.5	17.1	-30.7	273.1	290.7	-28.4	-27.6	301.8	-0.5	-0.9	-2.1	-4.0	-0.2	-0.3	-1.3	-2.1
214.8	265.9	22.0	-34.1	245.1	320.3	-33.1	-35.5	325.6	-0.3	-0.9	-1.8	-4.2	-0.3	-0.3	-1.9	-2.3
224.6	287.9	18.8	-47.4	257.2	327.0	-42.0	-39.7	342.7	-0.6	-1.0	-2.0	-3.9	-0.5	-0.7	-1.1	-2.2
234.4	289.1	24.3	-34.7	286.2	345.5	-52.9	-31.5	336.1	-0.2	-0.8	-0.6	-3.9	-0.3	-0.3	-1.3	-2.4
244.1	287.4	42.5	-20.3	271.8	366.8	-56.2	-21.3	355.1	-0.2	-1.1	-1.7	-5.0	-0.2	-0.3	-2.4	-2.6
253.9	302.9	55.3	-65.7	295.0	376.0	-60.4	-40.6	386.3	-0.5	-1.1	-2.0	-4.2	-0.6	-0.5	-2.2	-2.9
263.7	295.0	25.5	-25.7	299.2	382.0	-47.9	-10.0	400.1	-0.3	-1.0	-4.0	-5.0	-0.3	-0.7	-3.0	-2.1
273.4	301.0	36.9	11.5	300.2	412.1	-57.0	9.7	389.2	-0.2	-0.9	-1.8	-3.9	-0.6	-0.4	-2.6	-2.4
283.2	309.2	59.8	-13.3	299.5	439.7	-42.9	18.8	431.2	-0.5	-1.0	-0.4	-4.5	-1.3	-0.8	-2.3	-2.6
293.0	278.4	55.9	13.1	328.9	492.0	-11.0	28.3	492.5	-0.6	-0.9	-1.6	-4.5	-0.9	-1.5	-5.0	-2.6
302.7	372.5	61.5	51.0	351.8	531.6	-31.0	77.0	590.3	-0.7	-1.3	-3.0	-6.0	-1.4	-1.8	-6.8	-4.3
312.5	586.8	110.1	163.9	571.4	826.9	129.5	345.5	910.3	-4.6	-9.4	-14.3	-10.5	-10.2	-4.6	-17.5	-17.0
322.3	626.5	324.3	210.0	541.9	1068.2	167.3	469.2	826.3	-11.7	-8.5	-14.0	-7.5	-21.3	-10.6	-14.7	-14.1
332.0	1346.1	438.4	2021.1	1882.6	-461.2	-1544.8	-735.4	-1191.1	-217.7	-277.1	-205.4	-328.2	-118.5	-46.0	-262.2	-190.2
341.8	213.4	29.3	244.4	764.8	37.8	-288.4	-708.8	-0.4	-42.9	-47.1	-36.1	-26.6	-76.3	-27.0	-37.6	-25.0

Table 38: Dynamic Stiffness Real and Imaginary Parts at 6800 rpm and 783 kPa (MN/m)

f (Hz)	$R(H_{xx})$	$R(H_{xy})$	$R(H_{yx})$	$R(H_{yy})$	$I(H_{xx})$	$I(H_{xy})$	$I(H_{yx})$	$I(H_{yy})$	$\Delta R(H_{xx})$	$\Delta R(H_{xy})$	$\Delta R(H_{yx})$	$\Delta R(H_{yy})$	$\Delta I(H_{xx})$	$\Delta I(H_{xy})$	$\Delta I(H_{yx})$	$\Delta I(H_{yy})$
9.8	202.9	-50.8	-59.2	194.4	15.1	-4.4	-17.4	49.8	-0.5	-1.4	-3.2	-10.3	-0.4	-1.4	-3.3	-5.7
19.5	206.8	-58.0	-60.9	213.6	30.9	-4.7	5.9	-0.6	-0.2	-1.0	-11.3	-10.2	-0.2	-0.6	-6.2	-8.9
29.3	207.7	-55.7	-68.4	250.9	44.6	-6.4	1.7	12.2	-0.2	-0.4	-2.9	-5.0	-0.1	-0.4	-2.8	-8.9
39.1	211.3	-56.7	-61.3	207.2	57.4	-6.5	1.4	65.8	-0.3	-0.4	-7.7	-11.5	-0.3	-0.5	-4.0	-4.3
48.8	216.3	-55.2	-63.6	225.5	73.6	-8.6	-6.1	66.3	-0.2	-0.4	-2.8	-6.1	-0.1	-0.3	-1.2	-4.7
58.6	218.4	-54.4	-52.9	228.3	85.2	-6.7	-13.7	89.1	-0.2	-0.4	-1.5	-2.9	-0.2	-0.4	-2.3	-3.1
68.4	220.0	-55.5	-67.2	240.4	104.8	-4.8	-0.5	97.7	-0.2	-0.4	-2.5	-4.4	-0.2	-0.3	-0.8	-2.1
78.1	227.7	-50.3	-48.4	224.2	112.3	-6.8	-8.5	98.8	-0.1	-0.4	-0.5	-3.9	-0.1	-0.3	-0.9	-2.0
87.9	229.0	-50.5	-58.0	243.3	123.5	-9.2	-21.2	126.3	-0.2	-0.2	-0.5	-3.1	-0.2	-0.4	-1.5	-1.6
97.7	233.5	-47.9	-55.1	245.6	133.6	-8.4	-24.9	128.4	-0.2	-0.4	-1.4	-4.5	-0.1	-0.4	-1.0	-2.8
107.4	236.7	-46.5	-58.1	250.4	144.8	-9.9	-22.1	148.8	-0.6	-1.0	-1.0	-3.4	-0.3	-0.4	-2.2	-4.3
117.2	242.1	-43.2	-52.8	265.2	155.3	-11.5	-28.2	154.1	-0.7	-0.6	-2.2	-1.7	-1.0	-1.5	-0.8	-2.6
127.0	246.3	-40.2	-55.1	249.6	168.7	-11.9	-28.1	178.4	-0.1	-0.5	-0.7	-1.5	-0.4	-0.4	-4.0	-2.6
136.7	249.2	-35.0	-52.9	260.5	180.9	-13.4	-32.5	181.2	-0.2	-0.4	-2.3	-2.7	-0.3	-0.3	-1.9	-2.0
146.5	252.9	-28.4	-66.4	253.4	192.7	-14.0	-44.2	188.9	-0.1	-0.2	-5.0	-3.0	-0.2	-0.3	-2.3	-3.8
156.3	256.7	-17.8	-75.1	233.6	205.9	-13.8	-22.9	192.1	-0.1	-0.3	-6.0	-3.2	-0.2	-0.2	-1.1	-0.9
166.0	260.8	-21.8	-65.6	281.0	219.0	-23.0	-10.1	246.4	-0.1	-0.3	-4.2	-1.9	-0.2	-0.3	-5.7	-2.0
175.8	261.8	-16.9	-51.8	291.1	233.8	-24.8	-30.0	231.0	-0.2	-0.2	-1.5	-3.7	-0.2	-0.2	-5.6	-2.4
185.5	269.8	-12.5	-51.4	293.7	246.9	-25.7	-38.6	251.6	-0.2	-0.3	-3.0	-5.6	-0.3	-0.2	-1.1	-1.6
195.3	275.7	-8.9	-55.7	299.5	261.7	-27.7	-28.5	259.4	-0.2	-0.2	-1.2	-2.6	-0.2	-0.3	-2.5	-5.2
205.1	279.7	-7.0	-62.7	307.3	274.3	-30.6	-33.5	283.6	-0.3	-0.2	-2.0	-3.4	-0.2	-0.3	-1.4	-2.5
214.8	288.8	-1.3	-67.3	314.3	293.0	-27.7	-36.8	270.7	-0.1	-0.3	-5.5	-4.9	-0.3	-0.3	-3.3	-4.9
224.6	295.7	33.7	-77.0	198.5	308.9	-20.7	-49.2	328.6	-0.2	-0.3	-6.0	-2.9	-0.5	-0.3	-2.8	-1.8
234.4	306.8	1.4	-80.0	340.4	318.9	-42.9	-39.4	320.9	-0.3	-0.3	-6.9	-2.8	-0.2	-0.3	-3.8	-4.2
244.1	308.1	7.7	-83.2	329.6	336.5	-37.1	-21.6	323.2	-0.2	-0.4	-7.9	-3.3	-0.2	-0.3	-2.2	-5.2
253.9	319.2	6.8	-97.3	342.7	357.8	-40.5	-39.1	326.7	-0.2	-0.4	-9.7	-2.3	-0.4	-0.3	-7.2	-3.0
263.7	328.8	18.8	-105.8	344.8	375.1	-33.9	-15.6	342.5	-0.1	-0.3	-11.7	-5.2	-0.2	-0.4	-6.3	-2.3
273.4	340.2	50.5	-115.8	232.3	406.8	-8.9	26.4	373.3	-0.3	-0.5	-16.3	-5.6	-0.5	-0.5	-5.3	-3.2
283.2	342.8	13.9	-114.4	331.1	425.7	-22.6	27.2	356.3	-0.3	-0.3	-16.0	-4.6	-0.4	-0.6	-2.8	-2.6
293.0	363.4	75.8	-154.2	259.7	485.0	13.5	81.7	457.2	-0.4	-1.6	-19.9	-7.3	-0.9	-0.4	-2.8	-3.2
302.7	480.0	288.3	-249.8	403.5	544.8	-82.6	362.1	952.9	-2.9	-4.3	-22.6	-11.3	-1.8	-5.2	-10.8	-11.3
312.5	432.9	159.3	-188.9	399.1	685.0	40.9	305.7	559.4	-1.6	-3.2	-27.7	-13.5	-2.6	-0.9	-15.7	-25.9
322.3	598.9	204.8	223.1	701.2	813.6	-30.9	721.3	619.8	-2.9	-2.1	-32.9	-25.7	-6.3	-2.2	-26.5	-18.1
332.0	1138.6	349.8	620.4	787.8	1053.0	11.2	1055.8	604.1	-17.2	-5.6	-44.9	-24.7	-4.8	-3.6	-42.4	-14.2
341.8	616.3	50.1	545.1	564.1	-208.2	-312.6	-465.4	185.3	-40.9	-28.5	-24.8	-20.7	-53.1	-22.1	-68.7	-24.3

Table 39: Dynamic Stiffness Real and Imaginary Parts at 6800 rpm and 1567 kPa (MN/m)

f (Hz)	$R(H_{xx})$	$R(H_{xy})$	$R(H_{yx})$	$R(H_{yy})$	$I(H_{xx})$	$I(H_{xy})$	$I(H_{yx})$	$I(H_{yy})$	$\Delta R(H_{xx})$	$\Delta R(H_{xy})$	$\Delta R(H_{yx})$	$\Delta R(H_{yy})$	$\Delta I(H_{xx})$	$\Delta I(H_{xy})$	$\Delta I(H_{yx})$	$\Delta I(H_{yy})$
9.8	247.5	-58.1	-72.9	285.7	13.2	-4.9	-31.4	37.0	-0.4	-0.5	-1.0	-5.3	-0.4	-0.6	-8.0	-2.6
19.5	248.8	-60.8	-115.9	314.1	25.0	-6.1	-27.9	-6.6	-0.2	-1.0	-8.7	-8.0	-0.2	-0.8	-10.6	-4.4
29.3	251.5	-59.5	-61.1	283.3	38.8	-7.4	-14.0	23.5	-0.2	-0.7	-2.1	-2.3	-0.2	-0.5	-1.3	-2.2
39.1	255.2	-60.9	-42.4	290.9	51.7	-8.7	20.5	43.8	-0.2	-0.3	-4.4	-2.8	-0.3	-0.4	-7.9	-2.9
48.8	259.1	-59.1	-59.9	289.2	64.9	-10.4	-2.9	58.8	-0.2	-0.5	-2.5	-2.1	-0.1	-0.4	-3.4	-1.6
58.6	261.0	-58.7	-53.3	295.3	74.8	-9.9	-17.7	74.5	-0.1	-0.3	-3.5	-2.0	-0.3	-0.4	-1.1	-1.6
68.4	260.6	-58.2	-71.8	303.4	85.8	-11.1	-13.6	70.5	-0.3	-0.4	-1.9	-1.7	-0.2	-0.3	-2.6	-1.5
78.1	268.7	-55.0	-49.6	290.4	100.0	-11.1	-16.9	81.4	-0.2	-0.4	-2.9	-1.9	-0.2	-0.3	-2.8	-1.2
87.9	269.2	-55.9	-64.0	311.7	108.1	-13.8	-28.8	116.0	-0.2	-0.3	-1.3	-1.6	-0.2	-0.4	-1.0	-1.1
97.7	272.8	-52.8	-67.5	303.2	116.1	-13.8	-20.9	107.9	-0.5	-0.4	-2.8	-1.8	-0.3	-0.4	-1.4	-1.1
107.4	275.6	-51.0	-65.7	313.5	126.9	-15.8	-14.5	126.6	-0.5	-0.7	-1.2	-2.0	-0.4	-0.3	-1.3	-1.2
117.2	281.3	-53.6	-59.9	321.7	134.6	-15.1	-40.9	140.6	-4.9	-4.4	-8.1	-11.6	-5.8	-8.2	-4.8	-4.3
127.0	283.3	-45.8	-59.9	310.1	146.6	-18.3	-30.3	151.1	-0.5	-0.5	-1.1	-1.6	-0.5	-0.6	-0.8	-1.3
136.7	286.1	-41.6	-64.5	312.7	157.3	-20.1	-42.2	159.6	-0.3	-0.4	-2.0	-1.8	-0.3	-0.2	-1.4	-1.4
146.5	289.0	-36.4	-51.1	315.7	168.0	-22.4	-26.4	166.2	-0.1	-0.2	-1.3	-2.1	-0.2	-0.4	-1.5	-1.1
156.3	289.0	-29.3	-51.8	306.7	179.2	-23.5	-22.0	157.4	-0.1	-0.3	-3.6	-2.1	-0.2	-0.2	-1.9	-1.2
166.0	293.9	-33.5	-57.6	337.8	189.0	-30.2	-33.6	200.1	-0.2	-0.3	-0.7	-1.8	-0.2	-0.3	-2.1	-2.0
175.8	293.3	-28.0	-59.0	339.8	200.1	-32.5	-42.5	208.1	-0.3	-0.3	-1.3	-1.5	-0.2	-0.3	-2.3	-1.3
185.5	299.6	-26.0	-55.4	344.4	213.5	-33.9	-30.7	211.8	-0.2	-0.3	-1.6	-1.8	-0.4	-0.2	-0.9	-1.3
195.3	303.0	-20.7	-56.2	343.4	228.6	-38.0	-30.1	222.3	-0.2	-0.2	-2.6	-1.7	-0.3	-0.2	-2.7	-1.4
205.1	305.6	-18.3	-52.1	363.8	237.3	-42.6	-24.4	245.3	-0.4	-0.3	-1.8	-2.0	-0.2	-0.3	-2.7	-1.0
214.8	313.9	-13.3	-34.9	367.2	251.3	-42.1	-40.9	234.6	-0.3	-0.3	-1.2	-1.5	-0.3	-0.2	-2.8	-1.3
224.6	320.8	-1.8	-54.9	310.6	262.0	-41.7	-27.0	249.7	-0.3	-0.2	-1.9	-1.5	-0.4	-0.3	-2.0	-1.3
234.4	329.9	-15.6	-51.8	393.5	275.0	-56.4	-29.2	268.7	-0.7	-0.6	-2.2	-1.9	-0.2	-0.4	-2.8	-1.6
244.1	332.1	-12.5	-38.6	389.4	288.1	-54.6	-23.9	275.1	-0.5	-0.2	-2.9	-1.9	-0.2	-0.3	-5.1	-1.3
253.9	335.0	-6.9	-47.6	406.6	300.6	-55.8	-1.6	291.9	-0.5	-0.3	-3.7	-2.0	-0.3	-0.3	-6.8	-1.5
263.7	344.2	-0.9	-28.0	398.3	317.2	-52.1	10.4	286.9	-0.5	-0.2	-6.7	-2.2	-0.4	-0.2	-8.7	-1.7
273.4	349.7	11.2	-37.6	337.3	333.5	-42.6	-13.1	281.4	-0.7	-0.3	-5.5	-2.2	-0.4	-0.2	-3.0	-1.0
283.2	354.9	-6.0	-39.9	406.1	352.6	-56.2	10.1	302.6	-0.7	-0.3	-5.7	-2.4	-0.5	-0.2	-5.2	-1.6
293.0	363.8	11.8	-27.6	388.4	368.0	-38.4	26.6	324.6	-0.8	-0.3	-2.8	-2.9	-0.7	-0.2	-6.7	-1.6
302.7	369.2	50.2	-21.2	344.5	399.9	-18.3	35.2	383.8	-0.9	-0.3	-3.7	-3.1	-0.9	-0.6	-3.0	-1.4
312.5	377.2	13.1	-20.0	497.5	426.7	-53.0	67.1	331.8	-0.9	-0.3	-4.8	-4.2	-1.2	-0.4	-9.2	-2.9
322.3	389.1	104.3	-15.7	364.6	484.1	8.2	113.3	444.6	-1.4	-0.7	-7.5	-7.4	-1.5	-0.9	-11.5	-8.5
332.0	418.3	42.5	78.6	557.0	506.0	-86.5	171.7	391.1	-0.6	-0.4	-3.9	-6.5	-1.4	-0.5	-9.6	-5.0
341.8	522.4	96.1	158.9	568.9	596.6	-44.0	225.3	390.4	-1.6	-0.6	-12.5	-6.7	-1.8	-1.0	-16.5	-5.7

Table 40: Dynamic Stiffness Real and Imaginary Parts at 6800 rpm and 2350 kPa (MN/m)

f (Hz)	$R(H_{xx})$	$R(H_{xy})$	$R(H_{yx})$	$R(H_{yy})$	$I(H_{xx})$	$I(H_{xy})$	$I(H_{yx})$	$I(H_{yy})$	$\Delta R(H_{xx})$	$\Delta R(H_{xy})$	$\Delta R(H_{yx})$	$\Delta R(H_{yy})$	$\Delta I(H_{xx})$	$\Delta I(H_{xy})$	$\Delta I(H_{yx})$	$\Delta I(H_{yy})$
9.8	285.5	-63.7	-66.5	281.0	12.0	-3.1	-61.5	149.7	-0.8	-0.7	-3.1	-12.7	-0.6	-1.0	-13.1	-11.0
19.5	285.6	-65.5	-109.4	405.7	23.0	-8.2	-22.5	-40.5	-0.2	-0.6	-4.9	-8.2	-0.2	-0.5	-17.6	-8.7
29.3	289.3	-64.5	-53.6	328.1	34.4	-6.6	-28.4	67.7	-0.3	-0.5	-3.3	-4.2	-0.2	-0.6	-3.5	-5.3
39.1	293.4	-63.6	-46.8	340.8	46.4	-8.8	24.6	36.7	-0.3	-0.3	-2.0	-2.2	-0.3	-0.4	-18.8	-4.3
48.8	296.4	-63.3	-82.6	361.3	58.5	-10.8	0.9	48.5	-0.1	-0.2	-5.3	-3.0	-0.1	-0.4	-4.3	-1.9
58.6	299.3	-63.5	-66.3	365.3	67.0	-10.6	-22.1	59.0	-0.2	-0.5	-2.2	-1.7	-0.3	-0.4	-3.6	-1.5
68.4	298.2	-62.3	-78.4	366.1	77.2	-12.7	-5.4	62.7	-0.2	-0.3	-5.2	-2.3	-0.2	-0.2	-6.8	-2.0
78.1	306.3	-57.2	-61.0	348.9	92.9	-12.2	-14.6	71.5	-0.2	-0.3	-0.3	-2.1	-0.1	-0.3	-4.4	-1.6
87.9	306.2	-60.4	-71.5	366.5	97.3	-17.4	-24.0	99.6	-0.2	-0.3	-1.3	-1.6	-0.3	-0.3	-0.5	-1.6
97.7	309.3	-57.5	-62.0	356.2	104.4	-18.0	-22.3	89.0	-0.3	-0.3	-4.6	-2.1	-0.4	-0.5	-1.1	-1.0
107.4	311.6	-56.5	-67.4	367.4	113.6	-20.7	-29.2	117.9	-0.5	-0.6	-3.6	-2.0	-0.8	-0.8	-3.2	-1.9
117.2	316.1	-54.8	-61.8	370.1	121.2	-24.1	-43.2	121.6	-1.7	-2.7	-7.0	-3.6	-1.3	-1.0	-4.5	-3.5
127.0	318.4	-51.6	-69.3	370.9	131.3	-25.2	-40.3	139.0	-0.5	-0.5	-0.8	-2.1	-0.4	-0.7	-4.8	-2.1
136.7	320.3	-47.2	-64.8	367.7	140.2	-27.6	-33.1	148.7	-0.3	-0.4	-0.4	-2.0	-0.3	-0.4	-3.4	-1.7
146.5	322.4	-43.7	-49.1	369.5	149.1	-30.9	-32.1	152.2	-0.2	-0.3	-1.8	-1.9	-0.2	-0.2	-2.4	-1.6
156.3	322.3	-38.7	-48.6	361.1	158.7	-32.6	-29.5	136.2	-0.1	-0.3	-2.6	-2.4	-0.3	-0.3	-2.8	-1.3
166.0	326.2	-43.3	-64.1	388.3	167.7	-37.4	-50.5	181.1	-0.1	-0.3	-3.1	-1.9	-0.4	-0.3	-5.1	-3.0
175.8	326.6	-39.5	-59.9	397.7	177.3	-41.3	-51.9	196.2	-0.3	-0.2	-2.6	-2.2	-0.2	-0.2	-7.1	-2.5
185.5	329.8	-37.0	-57.7	398.4	189.7	-43.5	-34.8	190.7	-0.2	-0.2	-0.9	-2.4	-0.3	-0.2	-1.6	-1.5
195.3	332.8	-33.1	-53.9	401.7	203.4	-46.2	-40.7	196.9	-0.2	-0.4	-3.1	-2.4	-0.2	-0.3	-2.9	-1.3
205.1	333.9	-31.1	-53.6	413.4	211.2	-49.2	-31.4	218.1	-0.4	-0.3	-2.9	-2.1	-0.3	-0.2	-1.8	-1.0
214.8	342.9	-27.9	-40.4	428.1	223.5	-51.7	-53.7	214.0	-0.2	-0.3	-3.3	-2.3	-0.3	-0.3	-3.8	-1.3
224.6	346.7	-18.8	-43.3	374.7	232.9	-52.8	-36.7	221.1	-0.3	-0.4	-5.1	-2.1	-0.5	-0.3	-0.9	-1.4
234.4	354.7	-30.5	-50.5	444.7	244.1	-62.3	-40.7	236.3	-0.5	-0.3	-6.1	-2.6	-0.2	-0.3	-5.2	-1.9
244.1	356.8	-26.5	-39.8	444.9	256.5	-62.1	-38.8	247.9	-0.4	-0.3	-2.9	-2.2	-0.2	-0.2	-1.3	-1.6
253.9	360.1	-22.5	-31.6	454.5	266.2	-60.5	-25.1	250.5	-0.7	-0.4	-5.0	-2.1	-0.4	-0.2	-1.1	-1.6
263.7	365.1	-16.6	-18.3	452.7	279.9	-60.1	-30.6	253.5	-0.5	-0.3	-4.4	-2.2	-0.2	-0.3	-4.6	-2.2
273.4	370.9	-8.5	-25.9	408.5	293.8	-57.9	-35.8	244.3	-0.7	-0.4	-1.7	-1.9	-0.4	-0.3	-2.8	-2.9
283.2	375.3	-20.2	-22.0	464.6	308.9	-68.9	-28.5	269.3	-1.0	-0.4	-2.7	-2.0	-0.4	-0.3	-5.4	-2.3
293.0	384.1	-5.4	-15.3	449.8	319.9	-54.3	-15.6	288.7	-0.9	-0.4	-7.0	-2.7	-0.4	-0.3	-2.6	-2.9
302.7	384.1	11.5	-7.7	438.9	340.7	-44.1	-20.1	317.6	-1.2	-0.3	-6.8	-3.7	-0.8	-0.2	-6.6	-4.0
312.5	392.7	-12.7	-4.7	584.3	360.7	-83.4	-9.5	315.5	-1.0	-0.8	-2.4	-3.9	-1.2	-0.4	-1.8	-3.8
322.3	403.5	32.8	28.4	459.4	381.8	-34.3	20.5	320.9	-1.5	-0.5	-3.5	-3.9	-1.2	-0.5	-3.6	-5.9
332.0	435.9	25.0	50.7	609.7	385.7	-165.9	83.1	423.0	-1.5	-0.9	-3.1	-10.7	-0.9	-0.8	-5.0	-3.7
341.8	437.5	32.1	105.2	601.8	422.6	-84.9	34.8	335.7	-16.7	-2.6	-21.8	-10.5	-24.1	-4.0	-22.6	-2.7

Table 41: Dynamic Stiffness Real and Imaginary Parts at 6800 rpm and 3134 kPa (MN/m)

f (Hz)	$R(H_{xx})$	$R(H_{xy})$	$R(H_{yx})$	$R(H_{yy})$	$I(H_{xx})$	$I(H_{xy})$	$I(H_{yx})$	$I(H_{yy})$	$\Delta R(H_{xx})$	$\Delta R(H_{xy})$	$\Delta R(H_{yx})$	$\Delta R(H_{yy})$	$\Delta I(H_{xx})$	$\Delta I(H_{xy})$	$\Delta I(H_{yx})$	$\Delta I(H_{yy})$
9.8	317.1	-67.0	-103.3	402.2	11.3	-4.9	-18.4	85.4	-0.4	-1.6	-3.2	-6.6	-0.5	-1.5	-8.5	-7.1
19.5	314.9	-68.1	-67.2	367.5	20.3	-5.7	24.6	5.8	-0.3	-1.2	-8.2	-3.8	-0.5	-0.9	-14.5	-4.5
29.3	318.5	-67.7	-80.1	385.6	30.3	-7.1	-29.2	43.2	-0.2	-0.5	-3.0	-3.0	-0.1	-0.8	-2.7	-3.7
39.1	322.2	-68.5	-89.9	408.7	42.7	-9.8	-7.6	36.1	-0.2	-0.7	-3.2	-5.3	-0.2	-0.6	-14.9	-4.3
48.8	324.6	-67.8	-83.6	406.9	52.6	-12.0	-8.2	48.1	-0.1	-0.4	-5.2	-3.1	-0.1	-0.4	-3.4	-1.9
58.6	328.3	-68.1	-83.1	409.8	60.9	-13.3	-28.9	55.8	-0.2	-0.4	-3.9	-2.6	-0.2	-0.3	-3.6	-2.5
68.4	326.3	-66.9	-67.3	407.3	69.3	-15.7	-31.3	58.3	-0.2	-0.3	-5.1	-2.4	-0.3	-0.3	-3.6	-1.8
78.1	324.6	-64.8	-79.2	394.1	88.1	-13.4	-13.1	66.2	-0.2	-0.3	-1.8	-1.8	-0.2	-0.4	-4.1	-1.7
87.9	333.9	-65.5	-83.0	418.3	88.4	-21.0	-27.0	94.1	-0.2	-0.4	-1.2	-1.9	-0.4	-0.4	-1.2	-1.4
97.7	336.6	-62.7	-65.8	400.3	95.0	-21.8	-23.1	83.5	-0.5	-0.5	-3.9	-2.0	-0.6	-0.3	-0.9	-1.3
107.4	337.5	-61.5	-69.8	411.4	102.6	-24.2	-17.9	104.8	-0.4	-0.6	-4.9	-3.2	-1.5	-1.3	-2.7	-1.2
117.2	341.6	-60.4	-96.1	419.3	110.3	-27.4	-35.8	110.1	-1.2	-0.9	-4.8	-2.5	-0.9	-0.7	-2.0	-1.6
127.0	343.9	-58.3	-64.4	414.6	119.0	-28.9	-41.8	125.9	-0.5	-0.4	-1.1	-2.0	-0.3	-0.4	-5.1	-1.7
136.7	345.5	-53.8	-71.7	412.6	128.5	-32.8	-29.9	134.1	-0.4	-0.3	-1.2	-1.8	-0.2	-0.4	-4.1	-1.5
146.5	346.9	-47.1	-47.4	401.4	134.8	-36.3	-42.8	148.7	-0.3	-0.3	-3.1	-2.2	-0.1	-0.2	-1.5	-1.5
156.3	347.2	-48.8	-43.8	407.2	143.5	-38.2	-45.3	130.0	-0.3	-0.2	-3.5	-2.4	-0.2	-0.3	-1.9	-1.4
166.0	350.3	-53.5	-63.8	440.7	151.5	-41.8	-47.4	175.0	-0.2	-0.2	-1.1	-2.3	-0.3	-0.3	-3.6	-1.6
175.8	350.5	-49.6	-69.7	441.4	161.0	-45.9	-49.8	180.3	-0.3	-0.3	-2.5	-1.8	-0.4	-0.2	-5.4	-2.2
185.5	352.5	-47.4	-77.4	449.7	171.9	-46.8	-43.8	178.7	-0.2	-0.2	-1.6	-1.7	-0.3	-0.3	-1.1	-1.5
195.3	354.6	-42.4	-32.9	438.1	183.4	-49.2	-50.4	180.0	-0.3	-0.2	-4.4	-2.4	-0.3	-0.2	-3.5	-2.1
205.1	354.8	-42.2	-55.1	458.6	190.7	-52.3	-42.1	202.0	-0.5	-0.2	-1.0	-2.3	-0.3	-0.3	-2.3	-1.4
214.8	363.3	-37.1	-56.7	462.5	202.9	-51.5	-76.3	194.2	-0.3	-0.3	-3.4	-2.1	-0.4	-0.3	-4.6	-2.0
224.6	366.9	-37.3	-30.5	429.2	208.3	-57.1	-42.7	194.4	-0.6	-0.6	-4.6	-2.3	-3.1	-0.8	-0.9	-1.6
234.4	374.0	-44.0	-34.6	486.7	221.1	-65.2	-34.1	214.2	-0.4	-0.3	-5.0	-2.1	-0.2	-0.3	-2.1	-2.1
244.1	374.4	-37.9	-32.2	480.0	232.5	-64.3	-41.8	227.3	-0.4	-0.2	-1.4	-2.1	-0.3	-0.2	-1.7	-1.3
253.9	375.3	-34.1	-35.9	499.0	241.1	-62.4	-28.3	229.4	-0.4	-0.2	-2.5	-1.7	-0.5	-0.3	-3.5	-1.6
263.7	379.4	-29.5	-3.0	490.1	252.3	-62.6	-44.5	226.1	-0.4	-0.3	-5.8	-2.1	-0.3	-0.2	-2.0	-1.4
273.4	384.9	-21.1	-19.5	443.2	264.3	-60.3	-56.7	214.7	-0.5	-0.3	-1.3	-1.9	-0.6	-0.3	-2.6	-1.3
283.2	389.9	-35.7	-8.7	507.3	279.0	-71.2	-51.4	243.3	-0.7	-0.2	-3.5	-2.3	-0.5	-0.3	-2.1	-1.3
293.0	396.7	-18.4	-12.7	486.3	288.4	-59.9	-26.6	263.5	-0.7	-0.3	-1.4	-2.8	-0.5	-0.3	-2.5	-2.3
302.7	396.1	-4.0	-5.4	474.6	304.5	-55.1	-51.1	284.2	-0.9	-0.3	-2.3	-1.7	-0.9	-0.4	-4.7	-1.8
312.5	408.6	-0.7	-24.0	705.5	319.3	-183.5	-16.7	460.3	-1.1	-0.8	-2.5	-5.6	-0.9	-1.2	-2.9	-4.0
322.3	410.2	10.3	26.8	497.9	333.0	-49.2	-6.9	300.0	-1.4	-0.4	-3.8	-2.1	-0.8	-0.3	-2.8	-3.1
332.0	429.6	127.6	0.7	527.7	377.9	-136.3	-1.0	519.2	-1.6	-1.2	-2.6	-8.4	-1.0	-2.1	-1.6	-9.2
341.8	430.5	-13.0	57.1	682.7	383.5	-109.6	0.3	310.0	-1.9	-1.0	-5.0	-2.7	-1.0	-0.4	-3.0	-3.0

Table 42: Dynamic Stiffness Real and Imaginary Parts at 9000 rpm and 0 kPa (MN/m)

f (Hz)	$R(H_{xx})$	$R(H_{xy})$	$R(H_{yx})$	$R(H_{yy})$	$I(H_{xx})$	$I(H_{xy})$	$I(H_{yx})$	$I(H_{yy})$	$\Delta R(H_{xx})$	$\Delta R(H_{xy})$	$\Delta R(H_{yx})$	$\Delta R(H_{yy})$	$\Delta I(H_{xx})$	$\Delta I(H_{xy})$	$\Delta I(H_{yx})$	$\Delta I(H_{yy})$
9.8	212.3	-68.4	-50.5	177.3	7.4	11.2	59.8	-59.1	-0.6	-2.1	-3.1	-9.7	-0.9	-1.9	-7.3	-5.8
19.5	211.3	-57.0	-42.4	149.8	36.2	-4.5	-23.5	60.6	-0.3	-1.5	-2.6	-8.0	-0.4	-0.7	-2.4	-4.3
29.3	215.0	-60.1	-65.5	169.4	49.4	5.8	-1.6	30.7	-0.2	-0.9	-3.0	-11.3	-0.3	-0.5	-2.1	-2.9
39.1	217.2	-65.4	-55.8	175.9	63.5	-1.4	-13.2	72.0	-0.2	-0.8	-1.9	-4.7	-0.5	-0.6	-2.2	-2.7
48.8	224.3	-68.1	-72.0	200.3	75.8	-1.5	3.6	77.2	-0.2	-1.0	-1.5	-6.6	-0.2	-0.7	-1.0	-3.7
58.6	231.7	-61.4	-64.9	225.0	93.4	-2.0	2.1	98.3	-0.2	-1.1	-1.0	-3.7	-0.2	-0.2	-1.6	-2.5
68.4	235.9	-58.0	-62.7	222.4	104.8	-2.5	-10.5	106.3	-0.3	-1.0	-1.1	-3.4	-0.2	-0.4	-0.4	-2.6
78.1	239.3	-57.0	-60.9	229.0	121.0	-6.1	-15.2	121.3	-0.1	-0.9	-0.8	-4.3	-0.3	-0.3	-0.9	-2.7
87.9	242.4	-54.1	-58.3	250.5	129.8	-5.6	-14.3	147.5	-0.1	-0.9	-0.5	-3.6	-0.3	-0.5	-0.6	-2.5
97.7	248.9	-52.8	-54.3	244.2	140.9	-4.4	-15.2	141.0	-0.3	-0.9	-0.8	-3.5	-0.2	-0.4	-1.4	-2.3
107.4	254.1	-48.9	-46.1	227.8	147.8	-0.1	-10.4	154.2	-0.2	-0.9	-0.9	-3.8	-0.3	-0.3	-1.1	-2.9
117.2	259.8	-45.1	-49.1	264.9	161.7	-10.3	-19.7	176.6	-0.1	-1.0	-2.2	-3.7	-0.2	-0.3	-1.2	-2.0
127.0	264.3	-40.8	-47.7	266.1	173.8	-10.0	-14.3	155.0	-0.2	-0.9	-1.4	-3.9	-0.3	-0.6	-1.2	-1.9
136.7	270.9	-45.5	-51.0	270.9	186.2	-13.0	-21.4	160.7	-0.3	-1.2	-1.1	-3.5	-0.2	-0.4	-1.7	-3.0
146.5	275.7	-39.3	-46.0	283.6	192.7	-8.0	-15.1	174.2	-0.5	-2.5	-1.2	-4.5	-0.3	-0.9	-2.3	-2.8
156.3	274.5	-34.7	-37.9	226.8	205.6	-6.1	-22.1	278.0	-0.4	-0.9	-1.4	-4.1	-0.3	-1.5	-1.3	-2.8
166.0	280.1	-29.7	-28.9	274.7	213.8	-2.5	-32.1	219.3	-0.4	-1.1	-1.8	-3.5	-0.3	-0.4	-1.0	-2.3
175.8	283.5	-22.9	-38.0	335.1	227.5	-9.1	-22.9	269.6	-0.3	-1.0	-0.7	-5.4	-0.4	-0.6	-1.7	-2.5
185.5	278.0	-13.2	-41.5	297.3	241.1	-5.4	-40.0	227.4	-0.4	-0.9	-1.6	-3.8	-0.4	-0.8	-0.7	-1.7
195.3	287.4	-5.3	-25.1	336.1	246.6	-1.1	-29.4	289.7	-0.4	-0.9	-1.2	-3.2	-0.2	-0.4	-1.6	-1.8
205.1	286.8	8.6	-46.0	317.4	274.2	-10.9	-33.9	296.4	-0.4	-1.1	-1.2	-3.9	-0.2	-0.4	-1.4	-2.2
214.8	323.4	7.1	-31.8	304.8	303.7	1.4	-22.7	320.8	-1.0	-1.1	-2.0	-3.7	-0.4	-0.6	-4.1	-2.9
224.6	334.0	-2.3	-35.3	296.1	298.9	-10.2	-27.3	326.4	-0.6	-1.1	-2.3	-3.6	-0.3	-0.6	-2.3	-2.2
234.4	334.0	23.1	-33.5	353.1	330.5	-31.2	-10.2	320.3	-0.4	-1.1	-2.1	-4.0	-1.2	-0.4	-2.9	-2.1
244.1	353.5	66.6	-38.8	347.3	377.6	-34.4	6.7	351.1	-0.5	-1.1	-1.1	-3.8	-1.0	-0.7	-2.5	-3.2
253.9	321.8	112.6	-69.3	369.1	407.8	-11.8	11.7	400.7	-1.3	-1.7	-2.1	-3.9	-4.0	-1.2	-5.2	-3.6
263.7	316.1	82.6	-71.1	391.5	438.6	7.2	37.7	434.2	-1.9	-1.4	-6.4	-5.1	-2.7	-0.8	-3.0	-3.3
273.4	424.3	144.2	49.3	428.6	511.5	23.7	92.3	496.9	-8.8	-2.7	-4.7	-6.1	-4.3	-2.0	-6.0	-3.9
283.2	539.1	414.8	183.9	727.7	543.6	72.4	187.6	642.3	-6.8	-11.2	-4.7	-11.4	-5.9	-5.5	-7.0	-8.2
293.0	726.4	397.3	630.4	1055.0	236.9	-586.5	-209.8	-255.9	-23.0	-34.8	-37.4	-59.6	-21.0	-10.1	-37.2	-23.1
302.7	628.4	708.7	658.7	1233.6	-67.2	70.8	-509.1	1324.1	-26.4	-121.2	-78.5	-106.5	-105.3	-73.6	-128.6	-172.2
312.5	289.7	-35.7	-243.7	389.8	437.7	-311.2	-74.9	21.3	-6.1	-6.1	-11.7	-12.8	-6.6	-7.3	-7.0	-10.7
322.3	522.0	-95.3	139.0	304.1	269.3	-313.8	-198.9	149.7	-11.3	-6.2	-7.5	-11.5	-5.5	-8.1	-10.7	-7.6
332.0	383.8	-15.8	62.5	383.8	407.2	-226.0	-205.8	242.2	-2.3	-2.5	-5.8	-6.3	-1.8	-1.9	-8.5	-10.3
341.8	393.5	-26.9	-12.6	438.7	357.4	-153.4	-149.7	213.3	-3.1	-3.6	-3.4	-6.1	-5.9	-1.7	-8.2	-4.5

Table 43: Dynamic Stiffness Real and Imaginary Parts at 9000 rpm and 783 kPa (MN/m)

f (Hz)	$R(H_{xx})$	$R(H_{xy})$	$R(H_{yx})$	$R(H_{yy})$	$I(H_{xx})$	$I(H_{xy})$	$I(H_{yx})$	$I(H_{yy})$	$\Delta R(H_{xx})$	$\Delta R(H_{xy})$	$\Delta R(H_{yx})$	$\Delta R(H_{yy})$	$\Delta I(H_{xx})$	$\Delta I(H_{xy})$	$\Delta I(H_{yx})$	$\Delta I(H_{yy})$
9.8	238.0	-61.9	-74.9	239.8	14.4	-4.4	-11.9	26.3	-0.6	-1.7	-1.4	-5.7	-0.6	-1.6	-2.7	-8.6
19.5	241.8	-67.6	-54.0	219.1	31.7	-8.8	11.8	16.2	-0.3	-1.3	-4.6	-6.4	-0.5	-1.2	-6.2	-7.7
29.3	242.4	-66.0	-71.9	259.1	43.8	-7.4	-16.7	34.4	-0.3	-1.3	-2.9	-4.3	-0.3	-0.3	-2.7	-4.3
39.1	245.6	-67.6	-76.4	256.1	55.0	-7.6	-12.7	65.2	-0.3	-0.9	-1.6	-3.0	-0.2	-0.6	-3.8	-2.2
48.8	251.3	-65.7	-60.8	249.0	70.8	-9.6	1.8	74.1	-0.3	-0.3	-0.5	-2.0	-0.2	-0.5	-0.5	-1.7
58.6	253.6	-65.9	-73.3	263.1	83.5	-8.2	-12.1	89.8	-0.2	-0.4	-1.6	-2.3	-0.5	-0.7	-0.9	-1.8
68.4	258.6	-66.6	-66.9	265.3	102.2	-6.6	-3.7	98.3	-0.4	-0.4	-0.9	-1.9	-0.3	-0.4	-2.0	-1.7
78.1	263.7	-62.1	-59.3	257.0	108.6	-7.8	-8.2	101.3	-0.2	-0.4	-1.0	-1.8	-0.2	-0.5	-0.5	-1.2
87.9	266.4	-63.6	-62.5	282.8	119.2	-9.6	-16.8	128.9	-0.2	-0.4	-0.5	-1.4	-0.2	-0.3	-1.3	-1.6
97.7	271.0	-60.6	-61.3	276.5	128.2	-8.5	-20.4	128.8	-0.3	-0.3	-0.8	-1.9	-0.3	-0.3	-2.8	-1.8
107.4	274.1	-59.1	-65.5	285.5	138.8	-9.6	-16.4	147.6	-0.1	-0.4	-0.3	-1.5	-0.3	-0.5	-0.4	-1.1
117.2	280.5	-56.3	-64.8	294.5	147.7	-10.4	-24.1	155.1	-0.2	-0.3	-0.8	-2.3	-0.2	-0.3	-1.1	-1.3
127.0	284.7	-53.9	-61.6	290.8	158.4	-10.4	-20.3	164.6	-0.3	-0.4	-0.9	-2.1	-0.2	-0.3	-1.5	-1.2
136.7	288.0	-49.5	-60.2	299.0	170.2	-10.1	-28.6	169.4	-0.5	-0.3	-1.8	-1.7	-0.2	-0.4	-0.6	-1.1
146.5	290.0	-43.9	-51.0	298.3	179.8	-12.1	-18.2	172.0	-1.4	-1.1	-1.9	-2.0	-0.3	-0.6	-1.7	-2.4
156.3	294.9	-33.7	-47.0	274.8	189.6	-10.3	-18.9	171.0	-1.4	-0.6	-3.8	-2.7	-0.7	-0.8	-1.1	-1.4
166.0	298.4	-40.1	-47.9	317.3	200.9	-16.1	-30.7	210.1	-0.4	-0.4	-1.7	-1.7	-0.6	-0.5	-3.1	-2.2
175.8	298.7	-34.5	-54.1	319.2	212.9	-17.1	-27.6	211.7	-0.4	-0.3	-1.7	-2.0	-0.6	-0.3	-2.0	-1.4
185.5	302.5	-30.2	-51.0	323.3	224.5	-15.1	-23.1	215.2	-0.4	-0.3	-1.5	-1.6	-0.5	-0.4	-1.0	-1.4
195.3	305.0	-22.3	-48.9	315.2	240.0	-14.7	-30.3	231.3	-0.2	-0.3	-1.9	-1.5	-0.3	-0.3	-1.5	-1.4
205.1	306.5	-17.7	-51.4	326.4	249.2	-14.3	-19.3	250.3	-0.5	-0.3	-1.2	-2.0	-0.4	-0.4	-0.4	-1.5
214.8	313.1	-7.7	-44.7	325.8	271.1	-11.1	-25.0	247.8	-0.2	-0.2	-1.8	-1.6	-0.4	-0.4	-2.1	-1.6
224.6	319.4	28.5	-54.9	227.1	287.7	-3.9	-25.4	298.9	-0.3	-0.4	-2.2	-2.1	-0.4	-0.4	-2.4	-1.2
234.4	328.7	1.0	-54.7	351.0	299.2	-24.9	-31.7	286.8	-0.4	-0.4	-2.6	-2.2	-0.3	-0.3	-0.8	-1.2
244.1	327.2	7.2	-47.5	351.4	321.0	-23.9	-22.9	296.7	-0.4	-0.3	-3.3	-2.2	-0.2	-0.3	-1.4	-1.9
253.9	340.1	13.0	-52.7	370.5	344.5	-25.8	15.0	312.5	-0.2	-0.3	-3.8	-2.1	-0.4	-0.3	-3.1	-1.9
263.7	349.0	31.1	-51.7	356.1	363.2	-18.5	20.5	320.1	-0.2	-0.3	-4.9	-2.7	-0.2	-0.6	-2.7	-1.2
273.4	370.5	72.4	-42.2	268.3	394.4	0.0	29.2	362.7	-0.3	-1.0	-4.4	-4.1	-0.6	-0.7	-3.2	-3.0
283.2	368.9	34.6	-47.9	362.7	423.0	-5.4	51.6	358.8	-0.3	-0.3	-7.5	-3.8	-0.4	-0.8	-2.3	-2.3
293.0	404.5	159.3	-29.4	400.6	454.3	-51.2	141.1	579.9	-1.5	-0.9	-6.1	-6.0	-0.7	-1.8	-4.8	-4.9
302.7	397.4	76.8	4.5	568.8	495.8	-102.6	171.2	465.9	-7.0	-9.1	-13.9	-13.3	-6.6	-3.6	-15.8	-26.9
312.5	553.8	163.7	215.3	747.2	438.3	-268.9	302.6	436.1	-2.7	-1.4	-6.3	-9.6	-2.0	-2.7	-13.4	-10.2
322.3	772.5	315.1	334.7	760.5	870.3	-58.4	924.8	646.5	-8.6	-4.9	-13.6	-18.0	-12.2	-3.1	-35.1	-14.7
332.0	1747.3	479.7	1441.2	936.0	244.7	-367.2	240.3	188.3	-35.9	-10.1	-45.1	-23.5	-29.6	-14.5	-33.4	-14.7
341.8	510.5	19.7	355.6	456.5	-156.9	-281.7	-526.4	137.7	-6.4	-3.2	-9.9	-7.6	-4.9	-1.6	-15.2	-7.2

Table 44: Dynamic Stiffness Real and Imaginary Parts at 9000 rpm and 1567 kPa (MN/m)

f (Hz)	$R(H_{xx})$	$R(H_{xy})$	$R(H_{yx})$	$R(H_{yy})$	$I(H_{xx})$	$I(H_{xy})$	$I(H_{yx})$	$I(H_{yy})$	$\Delta R(H_{xx})$	$\Delta R(H_{xy})$	$\Delta R(H_{yx})$	$\Delta R(H_{yy})$	$\Delta I(H_{xx})$	$\Delta I(H_{xy})$	$\Delta I(H_{yx})$	$\Delta I(H_{yy})$
9.8	274.4	-65.0	-72.2	317.6	13.5	-5.4	-10.1	34.4	-0.5	-2.3	-0.8	-2.1	-0.3	-1.3	-2.7	-3.7
19.5	276.1	-71.9	-62.4	286.6	25.3	-6.5	10.5	9.0	-0.4	-1.7	-4.2	-3.3	-0.4	-0.8	-4.4	-6.4
29.3	278.9	-68.4	-75.6	335.9	38.9	-10.5	-13.1	18.8	-0.3	-0.9	-1.8	-5.5	-0.4	-0.7	-1.0	-3.1
39.1	282.5	-68.6	-71.9	322.1	50.2	-11.4	-17.3	41.3	-0.3	-0.7	-3.5	-2.9	-0.1	-0.2	-3.0	-2.1
48.8	286.8	-68.2	-65.1	313.2	63.1	-12.9	-13.5	60.0	-0.2	-0.4	-0.4	-1.7	-0.2	-0.3	-1.2	-1.2
58.6	289.2	-68.8	-71.6	323.0	73.5	-12.5	-22.9	70.6	-0.5	-0.5	-1.3	-2.0	-0.2	-0.3	-1.0	-1.7
68.4	289.1	-69.6	-68.6	318.6	84.1	-13.7	-19.8	64.7	-0.4	-0.6	-0.5	-1.9	-0.3	-0.4	-1.0	-1.4
78.1	297.0	-66.1	-64.5	311.4	98.0	-13.5	-20.8	76.7	-0.2	-0.3	-0.7	-1.6	-0.2	-0.2	-0.6	-1.4
87.9	298.7	-68.8	-73.6	336.0	105.5	-15.1	-24.0	103.5	-0.2	-0.4	-0.3	-1.6	-0.3	-0.3	-0.6	-1.5
97.7	301.8	-66.2	-70.9	324.9	113.0	-15.0	-18.8	105.4	-0.3	-0.5	-0.5	-1.5	-0.1	-0.4	-1.0	-1.0
107.4	305.2	-64.8	-70.8	335.6	122.9	-16.6	-23.0	121.5	-0.1	-0.3	-0.6	-2.0	-0.2	-0.4	-0.6	-1.4
117.2	310.5	-63.0	-73.6	339.0	130.9	-16.9	-35.3	129.0	-0.2	-0.3	-0.6	-1.5	-0.4	-0.3	-0.6	-1.2
127.0	312.7	-59.6	-69.2	334.2	140.8	-17.1	-28.7	141.9	-0.3	-0.4	-0.8	-1.8	-0.2	-0.3	-0.5	-1.0
136.7	315.7	-54.6	-73.7	339.5	149.9	-17.1	-30.8	149.2	-0.4	-0.5	-0.6	-1.8	-0.3	-0.7	-0.4	-1.5
146.5	317.9	-50.7	-59.9	340.7	159.8	-20.2	-28.4	152.0	-1.2	-1.3	-0.8	-2.7	-0.4	-1.2	-1.3	-1.8
156.3	317.8	-43.1	-59.6	324.9	169.0	-20.1	-25.4	142.3	-0.7	-1.2	-1.9	-3.0	-0.4	-1.1	-0.6	-2.1
166.0	322.2	-48.6	-64.7	360.0	178.2	-24.0	-33.5	183.4	-0.3	-0.4	-0.5	-2.9	-0.6	-0.6	-1.4	-1.3
175.8	321.4	-41.9	-65.4	358.2	187.3	-25.6	-38.6	187.2	-0.3	-0.4	-0.3	-1.9	-0.3	-0.5	-1.1	-1.2
185.5	325.1	-38.2	-56.9	361.4	200.5	-25.4	-36.0	192.5	-0.2	-0.4	-0.2	-1.8	-0.3	-0.3	-0.7	-1.2
195.3	326.5	-31.3	-61.3	355.3	213.7	-26.2	-32.5	203.0	-0.2	-0.3	-1.2	-2.3	-0.2	-0.4	-0.9	-1.2
205.1	326.6	-27.8	-57.7	372.7	222.5	-30.2	-37.4	226.3	-0.4	-0.3	-0.9	-1.9	-0.3	-0.3	-0.9	-1.2
214.8	334.5	-19.2	-51.0	374.1	236.5	-29.5	-41.3	218.1	-0.2	-0.4	-1.6	-2.5	-0.3	-0.5	-0.7	-1.6
224.6	337.6	-8.8	-55.2	320.6	248.0	-30.1	-34.6	231.5	-0.1	-0.3	-1.1	-2.3	-0.4	-0.6	-0.4	-1.0
234.4	344.7	-16.1	-62.2	388.3	261.8	-43.4	-37.7	256.0	-0.3	-0.4	-1.3	-2.0	-0.2	-0.3	-0.8	-1.2
244.1	346.2	-10.0	-51.4	385.7	277.2	-43.8	-39.5	265.4	-0.3	-0.3	-0.9	-2.4	-0.2	-0.2	-0.6	-1.3
253.9	348.5	-5.1	-55.2	411.6	293.0	-48.0	-32.2	281.7	-0.2	-0.3	-2.2	-2.0	-0.3	-0.3	-2.0	-1.5
263.7	356.6	1.8	-44.7	403.8	309.0	-45.1	-21.1	275.3	-0.1	-0.3	-2.2	-2.4	-0.2	-0.4	-1.2	-1.4
273.4	361.2	16.1	-44.4	336.9	327.7	-37.9	-22.1	270.6	-0.2	-0.3	-0.8	-2.7	-0.3	-0.7	-1.6	-1.9
283.2	369.2	2.6	-46.5	408.2	349.3	-50.9	-8.8	301.5	-0.2	-0.3	-1.0	-2.4	-0.3	-0.3	-0.8	-1.3
293.0	377.1	22.7	-41.4	384.1	364.7	-38.4	-0.6	323.9	-0.3	-0.3	-1.7	-2.3	-0.3	-0.7	-0.7	-2.5
302.7	384.4	63.6	-31.3	333.5	397.2	-19.9	14.9	375.6	-0.4	-1.0	-1.2	-2.1	-0.5	-1.3	-1.3	-4.6
312.5	396.8	38.7	-27.7	447.4	426.9	-40.8	30.6	346.7	-0.4	-0.4	-2.3	-2.0	-0.6	-0.7	-1.1	-3.6
322.3	418.3	54.0	14.3	488.3	438.7	-74.5	103.2	412.1	-1.8	-0.9	-2.6	-2.7	-1.9	-1.6	-3.8	-5.3
332.0	439.1	41.4	38.5	560.1	512.0	-74.3	146.0	373.5	-0.3	-0.4	-2.6	-6.0	-0.4	-0.3	-1.9	-3.7
341.8	551.2	108.3	165.8	583.0	575.6	-55.8	197.4	377.1	-1.5	-0.6	-3.8	-8.5	-1.2	-0.9	-5.6	-2.1

Table 45: Dynamic Stiffness Real and Imaginary Parts at 9000 rpm and 2350 kPa (MN/m)

f (Hz)	$R(H_{xx})$	$R(H_{xy})$	$R(H_{yx})$	$R(H_{yy})$	$I(H_{xx})$	$I(H_{xy})$	$I(H_{yx})$	$I(H_{yy})$	$\Delta R(H_{xx})$	$\Delta R(H_{xy})$	$\Delta R(H_{yx})$	$\Delta R(H_{yy})$	$\Delta I(H_{xx})$	$\Delta I(H_{xy})$	$\Delta I(H_{yx})$	$\Delta I(H_{yy})$
9.8	306.9	-71.4	-85.3	411.8	11.6	-5.4	-16.1	5.1	-1.2	-1.1	-5.2	-5.0	-0.7	-2.3	-5.4	-15.4
19.5	305.2	-73.0	-69.2	256.9	24.7	-10.0	-20.5	55.3	-0.5	-1.5	-7.1	-19.9	-0.5	-1.2	-17.3	-11.8
29.3	308.7	-70.5	-76.8	404.6	34.8	-10.1	-10.4	-8.7	-0.6	-1.0	-9.3	-5.8	-0.2	-0.6	-3.8	-8.2
39.1	311.9	-71.4	-61.4	361.0	45.8	-10.9	-9.1	32.0	-0.4	-0.8	-6.6	-3.3	-0.3	-0.8	-11.4	-4.2
48.8	315.9	-71.9	-70.8	356.6	57.9	-13.2	-8.6	52.1	-0.3	-0.8	-1.5	-2.9	-0.1	-0.5	-0.8	-2.0
58.6	317.9	-71.7	-72.8	374.7	67.9	-12.9	-23.7	59.5	-0.7	-0.5	-8.6	-3.6	-0.5	-0.5	-1.1	-2.4
68.4	318.7	-71.8	-77.7	363.7	77.4	-15.3	-16.7	46.8	-0.4	-0.5	-2.5	-2.4	-0.3	-0.4	-5.3	-2.8
78.1	326.4	-68.0	-68.9	355.4	92.9	-14.5	-14.9	62.9	-0.1	-0.4	-1.7	-2.3	-0.2	-0.3	-1.9	-2.0
87.9	326.7	-71.9	-78.4	378.5	96.4	-18.1	-27.5	91.5	-0.1	-0.2	-0.3	-1.7	-0.2	-0.4	-2.1	-1.5
97.7	329.6	-69.7	-74.1	366.1	103.2	-18.4	-27.4	94.3	-0.3	-0.4	-2.4	-2.8	-0.3	-0.3	-1.1	-1.8
107.4	332.6	-68.5	-79.2	380.1	111.8	-19.5	-29.6	107.5	-0.2	-0.3	-2.0	-2.8	-0.3	-0.3	-2.8	-1.6
117.2	336.8	-66.5	-78.5	375.1	119.2	-20.6	-35.3	119.9	-0.1	-0.3	-4.1	-2.9	-0.3	-0.3	-1.5	-1.8
127.0	339.6	-63.1	-73.9	372.8	127.8	-20.6	-34.7	125.1	-0.3	-0.4	-1.3	-2.4	-0.4	-0.5	-2.5	-1.6
136.7	341.5	-58.6	-74.9	384.9	136.9	-23.1	-33.4	129.6	-0.4	-0.5	-1.6	-3.4	-0.6	-0.4	-2.2	-1.9
146.5	343.3	-53.4	-67.9	392.3	143.4	-25.0	-30.2	132.2	-1.1	-1.1	-1.3	-3.3	-1.4	-1.4	-2.1	-2.0
156.3	343.3	-49.0	-60.1	370.3	153.5	-26.2	-32.6	131.9	-1.1	-0.9	-4.1	-2.5	-1.0	-0.8	-3.1	-3.1
166.0	347.2	-53.6	-75.5	401.6	160.8	-30.3	-35.3	162.0	-0.6	-0.5	-2.6	-2.0	-0.6	-0.4	-1.5	-2.4
175.8	347.2	-48.3	-78.0	402.8	168.7	-32.7	-40.9	169.0	-0.4	-0.3	-2.7	-3.2	-0.5	-0.4	-4.5	-2.2
185.5	348.6	-44.5	-69.1	402.1	180.8	-33.2	-32.2	173.6	-0.2	-0.4	-3.3	-2.7	-0.3	-0.3	-0.6	-1.6
195.3	349.5	-39.0	-62.6	387.7	192.1	-35.8	-37.1	184.5	-0.2	-0.4	-4.3	-2.8	-0.3	-0.3	-5.1	-2.0
205.1	349.4	-33.8	-61.8	399.7	200.0	-37.9	-37.6	211.0	-0.4	-0.3	-2.4	-2.7	-0.2	-0.3	-2.5	-2.7
214.8	357.1	-28.0	-56.6	411.0	213.0	-40.1	-50.4	209.8	-0.1	-0.3	-4.9	-3.1	-0.3	-0.4	-5.5	-2.5
224.6	357.5	-16.4	-55.2	357.9	223.1	-44.9	-45.2	220.2	-0.3	-0.3	-2.1	-3.5	-0.4	-0.3	-2.5	-3.4
234.4	364.8	-28.0	-57.1	419.1	234.7	-55.0	-47.2	239.1	-0.4	-0.3	-1.9	-2.6	-0.2	-0.4	-1.4	-1.2
244.1	364.7	-22.8	-52.9	420.8	247.9	-55.4	-41.3	247.8	-0.2	-0.3	-3.4	-3.1	-0.3	-0.3	-2.9	-2.7
253.9	366.6	-17.9	-51.5	440.8	259.6	-55.1	-34.0	262.0	-0.3	-0.3	-2.4	-2.3	-0.3	-0.2	-3.0	-3.6
263.7	370.4	-11.0	-48.4	437.0	275.0	-57.9	-32.2	262.5	-0.3	-0.3	-1.0	-3.1	-0.2	-0.3	-4.1	-3.4
273.4	376.3	-2.5	-45.8	378.7	290.2	-52.9	-36.8	247.7	-0.3	-0.3	-2.9	-2.8	-0.4	-0.4	-3.7	-2.4
283.2	383.5	-16.5	-45.7	451.8	307.3	-67.5	-32.7	294.8	-0.2	-0.2	-2.7	-2.8	-0.3	-0.3	-3.3	-3.5
293.0	391.0	2.8	-28.4	414.2	318.2	-54.2	-18.4	295.8	-0.4	-0.3	-3.1	-5.1	-0.4	-0.3	-5.0	-4.1
302.7	392.0	24.2	-28.5	390.3	339.3	-43.8	-11.2	321.0	-0.4	-0.4	-4.1	-5.2	-0.7	-0.3	-3.9	-6.8
312.5	400.8	-10.1	-38.8	556.6	358.3	-95.2	-1.9	327.5	-0.4	-0.4	-4.5	-3.8	-0.7	-0.5	-4.5	-9.4
322.3	407.6	56.8	-7.9	404.1	379.1	-34.4	15.7	370.6	-0.4	-0.5	-3.3	-6.2	-0.6	-0.3	-5.0	-11.6
332.0	413.8	-2.4	35.0	617.8	395.5	-125.7	57.6	350.5	-0.2	-0.6	-4.3	-9.6	-0.4	-0.5	-3.2	-9.4
341.8	457.8	34.4	58.3	581.1	445.4	-76.8	87.6	343.1	-0.6	-0.4	-3.0	-10.0	-0.6	-0.3	-5.9	-7.7

Table 46: Dynamic Stiffness Real and Imaginary Parts at 9000 rpm and 3134 kPa (MN/m)

f (Hz)	$R(H_{xx})$	$R(H_{xy})$	$R(H_{yx})$	$R(H_{yy})$	$I(H_{xx})$	$I(H_{xy})$	$I(H_{yx})$	$I(H_{yy})$	$\Delta R(H_{xx})$	$\Delta R(H_{xy})$	$\Delta R(H_{yx})$	$\Delta R(H_{yy})$	$\Delta I(H_{xx})$	$\Delta I(H_{xy})$	$\Delta I(H_{yx})$	$\Delta I(H_{yy})$
9.8	331.6	-75.3	-95.8	461.0	11.2	-6.0	-40.3	76.2	-1.6	-1.4	-3.1	-6.5	-1.6	-4.2	-7.8	-10.1
19.5	327.8	-74.0	-120.0	402.4	21.1	-10.3	-38.9	40.3	-0.5	-0.7	-4.1	-4.9	-0.4	-1.6	-4.5	-5.8
29.3	332.6	-74.1	-67.3	420.1	30.0	-8.7	-8.8	21.9	-0.7	-1.0	-1.8	-2.4	-0.4	-0.8	-1.3	-2.4
39.1	335.3	-75.9	-75.2	411.5	42.8	-11.6	21.9	18.9	-0.5	-0.9	-2.3	-2.7	-0.6	-0.7	-5.4	-2.6
48.8	338.7	-74.9	-87.7	409.3	53.6	-13.6	-9.3	39.7	-0.2	-0.6	-2.5	-2.1	-0.3	-0.8	-1.3	-1.7
58.6	343.0	-75.1	-77.8	414.8	61.6	-14.5	-25.5	52.7	-0.3	-0.4	-2.3	-2.0	-0.3	-0.8	-1.5	-1.7
68.4	340.0	-74.4	-84.5	410.4	70.4	-17.8	-15.8	46.6	-0.3	-0.4	-1.4	-1.6	-0.2	-0.3	-0.8	-1.2
78.1	339.6	-72.6	-93.0	398.9	90.6	-15.3	-3.3	58.8	-0.2	-0.4	-1.9	-2.0	-0.1	-0.4	-1.8	-1.3
87.9	348.6	-75.3	-80.8	421.0	88.0	-20.9	-26.5	84.5	-0.3	-0.5	-0.3	-1.7	-0.3	-0.2	-1.7	-1.2
97.7	352.4	-73.1	-74.8	408.9	95.9	-21.7	-21.5	78.5	-0.2	-0.4	-0.4	-2.0	-0.1	-0.3	-2.7	-1.3
107.4	353.6	-72.0	-75.8	417.6	103.3	-22.7	-30.1	96.7	-0.2	-0.3	-1.3	-1.8	-0.2	-0.3	-2.0	-1.2
117.2	358.0	-70.7	-82.5	420.7	108.3	-23.9	-39.3	101.2	-0.4	-0.3	-0.8	-1.9	-0.3	-0.4	-1.8	-1.2
127.0	360.6	-67.3	-77.0	415.8	117.1	-24.5	-43.9	116.7	-0.4	-0.6	-1.6	-1.9	-0.3	-0.3	-1.5	-1.3
136.7	362.2	-62.5	-72.7	422.3	126.3	-27.2	-37.7	121.3	-0.6	-0.4	-1.1	-1.8	-0.2	-0.5	-1.1	-1.0
146.5	362.4	-55.2	-59.6	415.5	133.1	-28.9	-35.8	124.1	-1.4	-1.4	-1.2	-2.2	-0.6	-1.3	-0.6	-2.5
156.3	363.2	-56.3	-60.4	416.5	141.0	-31.9	-39.8	110.2	-1.1	-1.2	-2.2	-2.5	-1.0	-0.9	-0.8	-2.1
166.0	366.3	-60.0	-77.6	433.4	147.6	-35.1	-50.3	152.5	-0.2	-0.5	-1.0	-2.6	-0.6	-0.7	-0.8	-2.3
175.8	366.2	-55.0	-68.8	435.9	156.0	-38.3	-52.2	158.5	-0.4	-0.4	-1.6	-1.6	-0.6	-0.4	-1.8	-1.6
185.5	368.3	-51.5	-72.0	441.2	166.8	-38.7	-46.8	155.9	-0.2	-0.5	-0.9	-1.7	-0.4	-0.4	-1.7	-1.1
195.3	368.5	-46.2	-66.3	431.4	177.3	-41.4	-44.3	167.1	-0.2	-0.3	-2.4	-1.8	-0.4	-0.4	-0.7	-1.4
205.1	367.5	-43.0	-63.8	446.1	184.4	-44.8	-41.4	186.4	-0.5	-0.3	-0.9	-1.7	-0.3	-0.3	-2.5	-1.2
214.8	375.4	-35.7	-55.5	449.1	194.9	-44.8	-58.9	185.1	-0.2	-0.3	-0.9	-1.6	-0.5	-0.4	-4.9	-1.5
224.6	375.3	-34.1	-55.6	415.8	203.9	-49.8	-44.7	182.6	-0.3	-0.3	-2.2	-2.2	-0.4	-0.3	-2.9	-1.3
234.4	381.5	-41.2	-55.9	473.7	214.6	-59.6	-45.6	212.6	-0.4	-0.3	-1.7	-2.3	-0.2	-0.4	-2.3	-1.1
244.1	381.1	-34.0	-53.1	470.5	227.3	-60.6	-45.5	220.1	-0.2	-0.2	-0.4	-1.9	-0.1	-0.4	-2.2	-1.2
253.9	381.8	-30.4	-44.4	483.0	237.7	-60.1	-37.0	227.4	-0.2	-0.3	-3.1	-1.9	-0.5	-0.4	-2.6	-1.7
263.7	385.3	-25.2	-37.3	478.6	250.4	-60.0	-44.6	220.7	-0.3	-0.2	-2.2	-2.0	-0.2	-0.3	-2.5	-1.5
273.4	390.2	-15.9	-38.2	431.4	263.9	-58.6	-42.1	210.7	-0.2	-0.2	-1.6	-2.0	-0.3	-0.3	-2.6	-1.4
283.2	397.1	-27.7	-34.0	489.9	279.1	-69.9	-43.4	247.2	-0.2	-0.3	-2.2	-1.8	-0.3	-0.3	-2.3	-1.3
293.0	403.8	-12.9	-26.4	470.3	287.9	-58.2	-36.2	250.2	-0.3	-0.3	-1.2	-3.2	-0.3	-0.3	-1.2	-1.1
302.7	403.2	4.4	-15.7	461.0	305.8	-56.1	-43.4	273.7	-0.4	-0.6	-1.9	-2.1	-0.8	-0.8	-3.3	-1.7
312.5	406.9	22.6	-19.7	602.6	315.5	-154.5	-33.2	415.6	-0.5	-2.5	-1.8	-8.8	-0.8	-2.7	-2.3	-2.1
322.3	417.8	22.4	1.1	472.9	332.7	-47.8	-14.3	287.9	-0.4	-0.5	-1.9	-2.9	-0.4	-0.2	-2.3	-3.8
332.0	450.3	28.1	-7.9	630.3	337.1	-219.7	33.9	474.5	-0.6	-0.3	-1.7	-11.7	-0.3	-0.9	-2.5	-5.2
341.8	442.3	2.2	34.6	631.5	386.1	-98.4	7.8	309.4	-0.4	-0.4	-4.0	-4.6	-0.4	-0.5	-4.2	-1.6

Table 47: Dynamic Stiffness Real and Imaginary Parts at 10800 rpm and 0 kPa (MN/m)

f (Hz)	$R(H_{xx})$	$R(H_{xy})$	$R(H_{yx})$	$R(H_{yy})$	$I(H_{xx})$	$I(H_{xy})$	$I(H_{yx})$	$I(H_{yy})$	$\Delta R(H_{xx})$	$\Delta R(H_{xy})$	$\Delta R(H_{yx})$	$\Delta R(H_{yy})$	$\Delta I(H_{xx})$	$\Delta I(H_{xy})$	$\Delta I(H_{yx})$	$\Delta I(H_{yy})$
9.8	239.1	-57.9	-75.2	244.3	0.3	32.5	11.8	-37.9	-0.6	-1.1	-3.0	-5.9	-1.5	-3.7	-1.6	-5.0
19.5	248.8	-64.8	-74.6	222.1	33.2	3.1	-5.5	26.9	-1.1	-3.1	-1.3	-6.5	-0.5	-1.2	-2.1	-4.5
29.3	249.1	-62.2	-72.4	239.4	44.7	17.8	1.4	15.3	-0.4	-2.0	-0.6	-4.5	-1.0	-1.1	-1.6	-3.4
39.1	248.9	-67.6	-67.2	207.1	60.0	3.2	-4.4	52.7	-0.3	-1.6	-0.9	-3.8	-0.3	-1.2	-0.9	-2.7
48.8	258.3	-75.7	-80.4	231.3	73.2	2.2	0.6	77.1	-0.5	-0.9	-0.5	-3.7	-0.3	-1.0	-1.4	-2.5
58.6	269.8	-72.4	-66.9	255.0	86.3	-3.2	-9.3	103.7	-0.6	-1.2	-0.8	-4.3	-0.6	-0.7	-1.1	-2.4
68.4	270.8	-66.4	-72.9	256.8	102.3	-4.0	-10.4	106.4	-0.4	-0.9	-0.8	-3.5	-0.4	-0.5	-0.9	-2.2
78.1	276.1	-65.8	-75.0	263.4	117.4	-7.1	-13.4	118.4	-0.7	-1.0	-0.7	-4.0	-0.3	-0.5	-0.9	-2.0
87.9	280.4	-67.8	-70.8	288.7	123.6	-4.1	-3.3	131.3	-0.2	-1.1	-1.2	-4.3	-0.3	-0.6	-0.3	-2.5
97.7	285.1	-58.7	-69.5	273.9	137.4	-8.7	-18.8	139.2	-0.3	-1.3	-1.2	-3.8	-0.3	-0.4	-0.9	-1.8
107.4	286.8	-53.8	-60.3	264.9	144.3	-5.7	-8.3	155.5	-0.3	-0.8	-1.1	-4.0	-0.3	-0.8	-0.8	-1.8
117.2	297.0	-51.4	-62.8	296.0	155.6	-10.0	-13.0	169.5	-0.4	-0.9	-1.1	-3.8	-0.1	-0.3	-1.2	-2.1
127.0	304.2	-48.6	-56.6	307.7	172.9	-15.3	-7.7	157.7	-0.3	-1.1	-0.7	-4.2	-0.3	-0.4	-0.9	-3.0
136.7	313.8	-57.5	-50.3	303.8	183.6	-13.5	-6.9	150.0	-0.3	-1.1	-0.6	-4.5	-0.6	-0.5	-0.7	-2.3
146.5	312.1	-47.8	-46.3	311.9	185.7	-8.3	-12.7	172.0	-0.3	-0.8	-0.9	-3.9	-0.2	-0.6	-0.7	-2.2
156.3	316.1	-41.3	-42.7	264.5	203.5	-13.9	-19.7	269.9	-0.2	-1.0	-2.1	-3.6	-0.3	-0.5	-0.5	-1.9
166.0	321.9	-29.0	-42.5	326.5	202.5	-11.4	-19.5	222.2	-0.6	-1.0	-1.0	-4.8	-0.6	-0.5	-0.7	-2.1
175.8	324.0	-31.4	-49.0	377.1	218.9	-19.3	-17.2	254.3	-1.0	-1.5	-1.8	-4.2	-1.9	-0.9	-2.0	-3.5
185.5	319.4	-18.3	-41.0	349.5	238.4	-13.0	-14.3	222.6	-0.7	-2.1	-1.4	-5.8	-2.0	-1.7	-1.4	-3.9
195.3	322.8	-12.6	-28.0	384.4	235.3	6.3	-19.1	296.6	-0.6	-1.6	-1.9	-4.5	-0.6	-0.8	-2.1	-2.5
205.1	348.0	3.1	-7.2	375.6	262.7	-32.4	-17.4	276.0	-1.4	-1.6	-0.5	-4.2	-0.5	-0.5	-1.5	-3.2
214.8	359.0	-7.4	-19.1	365.6	286.0	16.3	-22.8	317.7	-0.7	-1.0	-0.7	-3.9	-0.6	-0.7	-3.4	-3.9
224.6	367.3	1.4	-35.1	350.3	297.6	4.7	-18.8	323.3	-0.5	-1.9	-2.8	-3.7	-1.5	-0.5	-2.0	-3.4
234.4	466.0	10.4	115.4	427.6	312.5	-91.8	40.3	259.1	-1.1	-3.4	-4.2	-3.7	-1.7	-1.4	-1.2	-3.6
244.1	484.6	9.0	143.8	385.5	298.1	-68.9	-30.5	309.1	-1.0	-3.8	-3.1	-4.1	-1.3	-2.6	-1.3	-3.2
253.9	469.6	137.7	169.7	562.0	260.8	-75.7	-102.4	332.2	-3.0	-3.3	-4.8	-5.6	-3.2	-2.7	-4.2	-4.5
263.7	480.3	92.2	242.9	505.1	321.6	-128.2	-115.0	267.4	-2.1	-1.8	-5.8	-5.4	-2.5	-2.1	-5.3	-6.0
273.4	715.6	224.3	344.8	600.8	338.2	-17.4	-113.4	504.4	-5.3	-6.0	-11.2	-9.1	-11.6	-7.2	-13.0	-7.1
283.2	276.8	67.8	-50.0	578.6	192.3	-500.2	-428.2	-143.6	-3.6	-6.4	-3.2	-11.7	-5.7	-10.8	-6.7	-11.2
293.0	405.8	89.3	59.8	421.8	392.3	-209.9	-339.6	163.1	-3.3	-3.7	-7.6	-4.6	-2.3	-1.7	-2.2	-5.5
302.7	403.6	-164.4	-107.7	108.4	421.3	-128.9	-14.5	216.5	-3.5	-3.3	-3.8	-14.5	-2.2	-7.8	-6.8	-7.2
312.5	576.9	-69.2	-54.7	378.6	407.4	-205.5	84.2	209.5	-2.4	-1.8	-3.2	-6.7	-2.2	-1.8	-8.3	-4.0
322.3	591.6	22.6	4.0	441.4	497.0	-235.2	-87.0	231.4	-4.3	-3.2	-10.3	-5.6	-3.8	-1.8	-5.3	-5.9
332.0	396.1	50.6	-45.2	477.8	546.2	-166.3	-160.9	158.9	-2.8	-3.7	-3.6	-4.9	-1.3	-2.4	-3.2	-5.4
341.8	504.0	-44.5	-25.2	449.8	437.0	-120.1	-53.4	182.0	-2.3	-4.5	-4.2	-6.4	-2.0	-2.0	-4.2	-3.6

Table 48: Dynamic Stiffness Real and Imaginary Parts at 10800 rpm and 783 kPa (MN/m)

f (Hz)	$R(H_{xx})$	$R(H_{xy})$	$R(H_{yx})$	$R(H_{yy})$	$I(H_{xx})$	$I(H_{xy})$	$I(H_{yx})$	$I(H_{yy})$	$\Delta R(H_{xx})$	$\Delta R(H_{xy})$	$\Delta R(H_{yx})$	$\Delta R(H_{yy})$	$\Delta I(H_{xx})$	$\Delta I(H_{xy})$	$\Delta I(H_{yx})$	$\Delta I(H_{yy})$
9.8	263.9	-67.2	-69.7	272.8	14.3	-1.0	-19.2	61.4	-1.0	-2.4	-3.6	-7.1	-1.2	-1.9	-1.4	-4.7
19.5	267.4	-66.8	-62.1	250.2	31.4	-5.3	22.7	9.2	-0.6	-1.7	-5.9	-7.1	-1.0	-1.7	-3.7	-2.2
29.3	268.1	-69.9	-82.9	281.3	43.7	-9.8	-7.2	37.2	-1.0	-1.0	-2.8	-3.2	-0.8	-1.1	-2.4	-3.2
39.1	271.6	-70.7	-75.8	268.6	54.1	-8.1	-12.2	66.9	-0.7	-1.1	-2.3	-2.8	-0.3	-0.4	-2.5	-2.1
48.8	277.9	-70.8	-68.7	271.0	68.3	-10.8	-3.9	77.4	-0.4	-0.5	-0.8	-2.1	-0.5	-0.6	-1.2	-1.7
58.6	279.9	-69.8	-81.6	281.7	81.3	-9.2	-6.6	89.2	-0.3	-0.3	-1.9	-2.0	-0.5	-1.1	-1.6	-1.6
68.4	284.6	-71.7	-75.2	280.7	100.9	-8.2	-1.0	93.3	-0.6	-1.1	-0.5	-1.8	-0.5	-0.9	-0.9	-2.1
78.1	291.7	-67.2	-68.6	279.7	106.3	-10.5	-8.6	98.8	-0.4	-0.6	-0.5	-1.8	-0.4	-0.5	-1.3	-1.3
87.9	294.2	-69.0	-71.2	306.5	117.2	-12.0	-10.0	125.7	-0.3	-0.7	-1.3	-1.6	-0.3	-0.4	-0.8	-1.2
97.7	299.9	-67.0	-66.9	301.4	126.6	-12.5	-13.5	128.8	-0.5	-0.7	-1.3	-1.7	-0.2	-0.3	-1.7	-1.4
107.4	302.7	-65.1	-75.1	311.3	136.7	-12.8	-13.7	146.0	-0.3	-0.5	-1.1	-1.6	-0.5	-0.3	-1.2	-1.2
117.2	309.1	-62.7	-72.6	319.7	144.7	-13.3	-18.1	150.8	-0.4	-0.5	-1.6	-2.4	-0.4	-0.4	-2.4	-1.7
127.0	315.2	-59.4	-66.1	316.6	155.0	-13.1	-19.1	163.3	-0.3	-0.5	-0.8	-1.9	-0.2	-0.2	-1.6	-1.3
136.7	318.9	-55.5	-60.8	330.4	166.7	-14.8	-18.6	166.1	-0.2	-0.5	-1.9	-1.9	-0.3	-0.5	-1.0	-1.4
146.5	322.1	-50.5	-59.5	329.0	174.8	-15.7	-13.8	166.7	-0.3	-0.3	-0.6	-2.3	-0.2	-0.6	-1.5	-1.6
156.3	327.3	-41.2	-51.0	304.9	181.5	-15.2	-21.5	165.1	-0.1	-0.5	-2.6	-1.8	-0.4	-0.4	-1.5	-1.2
166.0	331.0	-49.1	-56.8	345.5	193.8	-21.1	-20.9	198.9	-0.5	-0.6	-0.6	-2.1	-0.7	-0.7	-2.2	-1.4
175.8	331.8	-43.6	-53.0	345.1	204.2	-23.1	-13.9	199.0	-0.8	-0.7	-1.9	-2.7	-1.0	-2.1	-1.7	-2.1
185.5	334.2	-40.7	-45.0	353.3	214.8	-19.2	-15.1	206.4	-0.9	-3.0	-2.4	-2.1	-1.2	-1.1	-2.4	-4.1
195.3	338.6	-35.4	-43.0	343.4	229.0	-18.5	-14.2	218.3	-0.5	-0.7	-1.4	-2.6	-0.5	-0.9	-1.2	-1.1
205.1	340.2	-32.2	-44.7	354.5	236.9	-17.8	-19.8	236.7	-0.4	-0.3	-1.0	-1.7	-0.4	-0.5	-1.2	-1.5
214.8	350.0	-21.9	-40.7	355.1	260.9	-10.6	-20.5	230.9	-0.4	-0.7	-2.8	-1.7	-0.4	-0.4	-1.7	-1.3
224.6	356.0	9.7	-44.9	266.9	274.8	-5.1	-18.6	274.8	-0.2	-0.4	-2.7	-2.1	-0.5	-0.4	-1.9	-1.2
234.4	360.3	-15.0	-42.2	377.1	285.6	-19.2	-21.1	267.8	-0.4	-0.3	-2.5	-1.8	-0.5	-0.6	-1.2	-1.6
244.1	357.9	-8.8	-40.4	379.0	309.9	-16.8	-20.1	280.6	-0.3	-0.4	-2.2	-1.8	-0.4	-0.4	-2.5	-1.9
253.9	370.5	0.4	-33.8	390.1	330.2	-13.7	-0.9	299.2	-0.4	-0.3	-3.4	-1.6	-0.6	-0.4	-4.0	-1.3
263.7	379.2	17.5	-32.3	373.1	348.9	-0.8	5.6	304.7	-0.4	-0.4	-4.4	-1.6	-0.5	-0.6	-3.4	-1.3
273.4	405.1	62.2	-45.6	285.9	398.7	25.6	33.6	351.8	-0.6	-0.6	-2.9	-1.8	-0.5	-0.7	-5.1	-1.5
283.2	401.5	30.7	-26.1	377.4	420.9	31.7	33.2	366.0	-0.5	-0.4	-5.2	-2.5	-0.4	-0.6	-3.1	-3.3
293.0	485.5	194.0	-11.3	426.5	477.3	-20.7	200.4	585.5	-0.8	-1.1	-5.7	-4.0	-1.1	-2.0	-3.1	-5.8
302.7	461.4	90.9	81.1	639.7	500.4	-117.8	222.1	416.3	-1.1	-1.1	-2.5	-6.0	-1.6	-0.7	-5.0	-3.7
312.5	627.7	91.3	387.0	686.0	275.1	-331.2	175.6	286.4	-3.4	-2.5	-9.2	-9.8	-3.3	-2.1	-3.3	-5.1
322.3	923.6	33.1	1249.4	627.1	-299.1	-418.6	-596.6	-29.7	-13.0	-2.5	-20.7	-10.8	-4.5	-4.1	-26.3	-8.8
332.0	884.0	53.9	692.1	535.7	-617.0	-431.1	-864.5	-7.9	-11.5	-2.2	-21.0	-8.2	-12.6	-5.6	-15.8	-8.6
341.8	404.9	8.7	151.5	441.4	-89.3	-211.6	-458.9	195.2	-2.0	-0.7	-3.9	-3.8	-2.2	-1.3	-14.3	-7.0

Table 49: Dynamic Stiffness Real and Imaginary Parts at 10800 rpm and 1567 kPa (MN/m)

f (Hz)	$R(H_{xx})$	$R(H_{xy})$	$R(H_{yx})$	$R(H_{yy})$	$I(H_{xx})$	$I(H_{xy})$	$I(H_{yx})$	$I(H_{yy})$	$\Delta R(H_{xx})$	$\Delta R(H_{xy})$	$\Delta R(H_{yx})$	$\Delta R(H_{yy})$	$\Delta I(H_{xx})$	$\Delta I(H_{xy})$	$\Delta I(H_{yx})$	$\Delta I(H_{yy})$
9.8	293.8	-69.7	-83.3	330.9	12.7	-1.6	-25.9	72.5	-1.4	-1.8	-3.1	-6.7	-0.7	-1.9	-2.4	-3.5
19.5	293.7	-68.9	-107.8	343.4	25.0	-6.6	-4.1	18.5	-0.9	-2.8	-5.7	-8.1	-0.9	-0.9	-4.2	-5.2
29.3	298.4	-71.4	-73.6	337.8	38.6	-11.9	-12.7	31.6	-0.7	-1.9	-1.6	-5.5	-0.3	-1.4	-1.0	-1.6
39.1	301.5	-73.5	-61.8	326.8	48.0	-12.1	-5.5	45.6	-1.1	-1.2	-2.6	-4.4	-0.2	-0.7	-2.5	-2.3
48.8	305.9	-73.0	-71.8	324.5	61.9	-15.2	-9.9	61.3	-0.5	-0.7	-0.6	-2.1	-0.3	-0.4	-1.0	-2.3
58.6	307.6	-73.0	-78.3	330.5	72.8	-13.0	-16.2	65.6	-0.6	-0.9	-2.4	-1.8	-0.4	-0.6	-0.9	-1.4
68.4	308.7	-74.0	-77.9	331.8	83.8	-16.0	-21.7	68.0	-0.4	-0.8	-1.2	-1.7	-0.5	-0.5	-0.9	-1.5
78.1	317.2	-71.3	-68.3	323.7	97.7	-15.5	-12.5	73.3	-0.3	-0.5	-0.8	-1.9	-0.4	-0.6	-1.3	-1.1
87.9	318.9	-74.6	-75.8	345.4	105.5	-17.3	-19.2	105.3	-0.2	-0.5	-1.4	-1.6	-0.3	-0.4	-0.5	-1.3
97.7	321.8	-73.4	-74.6	339.1	112.3	-17.6	-18.3	102.2	-0.3	-0.6	-1.5	-1.6	-0.3	-0.4	-0.7	-1.2
107.4	325.1	-72.0	-75.4	347.2	122.0	-18.6	-20.5	122.9	-0.3	-0.5	-0.6	-1.6	-0.4	-0.4	-0.8	-1.3
117.2	331.2	-70.4	-73.6	352.7	130.1	-18.3	-30.3	125.6	-0.3	-0.3	-1.3	-1.9	-0.2	-0.3	-0.7	-0.9
127.0	334.6	-67.0	-70.3	348.4	139.6	-17.8	-30.0	142.8	-0.3	-0.5	-0.5	-1.5	-0.5	-0.2	-0.2	-1.2
136.7	337.3	-62.6	-67.7	351.5	149.5	-18.5	-28.7	146.1	-0.4	-0.5	-0.7	-1.6	-0.4	-0.5	-0.7	-1.0
146.5	341.0	-57.6	-58.0	355.7	157.0	-20.5	-27.3	150.6	-0.3	-0.4	-0.8	-2.1	-0.1	-0.3	-1.0	-1.2
156.3	342.3	-50.9	-51.9	339.2	166.2	-21.5	-30.0	140.0	-0.3	-0.4	-2.7	-1.8	-0.6	-0.4	-1.5	-1.0
166.0	346.3	-57.0	-68.6	374.9	174.5	-25.0	-39.2	180.4	-0.3	-0.4	-1.8	-2.2	-0.6	-0.5	-2.2	-1.5
175.8	345.2	-50.5	-66.6	374.7	182.0	-27.3	-36.8	179.9	-0.9	-1.2	-1.9	-1.9	-1.2	-0.5	-1.3	-2.1
185.5	348.9	-48.5	-57.9	376.7	193.0	-25.3	-29.5	186.0	-0.5	-1.2	-2.2	-3.1	-1.5	-1.4	-1.4	-1.6
195.3	351.4	-43.3	-57.9	371.9	207.2	-28.3	-26.0	195.0	-0.3	-0.6	-2.5	-1.7	-0.6	-0.5	-2.0	-1.4
205.1	351.0	-41.1	-57.6	384.9	213.5	-26.9	-29.8	208.5	-0.5	-0.5	-1.0	-1.6	-0.3	-0.4	-2.6	-1.2
214.8	358.4	-34.2	-44.9	388.4	229.0	-26.3	-34.9	202.3	-0.4	-0.4	-0.9	-1.6	-0.3	-0.4	-1.5	-1.3
224.6	361.2	-23.0	-40.4	332.6	237.3	-24.7	-29.3	212.0	-0.2	-0.3	-3.0	-1.9	-0.4	-0.3	-2.0	-1.2
234.4	366.7	-30.0	-47.8	402.0	251.4	-35.6	-36.8	236.1	-0.3	-0.4	-2.1	-1.7	-0.2	-0.3	-1.8	-1.2
244.1	366.1	-17.6	-36.1	385.5	266.2	-32.4	-34.4	252.4	-0.3	-0.4	-2.6	-1.6	-0.4	-0.3	-1.6	-1.2
253.9	366.8	-13.9	-35.4	404.4	281.2	-31.9	-24.4	259.2	-0.3	-0.4	-4.4	-1.6	-0.4	-0.3	-1.2	-1.1
263.7	373.5	-7.7	-29.0	408.4	301.1	-32.4	-19.0	257.7	-0.3	-0.4	-4.9	-1.7	-0.5	-0.3	-1.9	-1.0
273.4	378.7	6.8	-26.1	348.5	321.1	-23.9	-24.4	253.5	-0.3	-0.4	-1.6	-1.5	-0.5	-0.3	-3.3	-1.1
283.2	385.2	-4.3	-26.3	410.9	343.9	-35.1	-12.3	281.2	-0.2	-0.4	-2.8	-2.1	-0.4	-0.5	-3.8	-1.3
293.0	391.9	17.5	-21.4	391.7	362.1	-21.6	-8.8	308.2	-0.4	-0.4	-1.4	-2.0	-0.3	-0.5	-2.6	-1.3
302.7	394.5	74.8	-23.0	326.2	403.7	3.7	-4.2	374.1	-0.5	-1.0	-1.8	-2.3	-0.6	-0.8	-6.2	-1.9
312.5	407.4	82.8	-31.4	402.2	443.9	1.2	13.4	372.2	-0.9	-0.9	-1.9	-2.3	-1.0	-0.8	-3.8	-2.0
322.3	426.1	77.8	-4.6	417.2	490.2	2.3	81.4	387.5	-1.3	-0.8	-2.6	-2.4	-0.8	-0.8	-4.5	-1.6
332.0	459.7	53.0	57.6	559.6	544.2	-64.7	149.9	368.3	-0.8	-0.7	-1.9	-2.8	-0.6	-0.5	-5.4	-1.9
341.8	628.1	130.4	209.7	593.2	659.5	-26.1	246.0	371.5	-1.9	-0.6	-7.0	-3.2	-2.2	-0.9	-2.0	-2.0

Table 50: Dynamic Stiffness Real and Imaginary Parts at 10800 rpm and 2350 kPa (MN/m)

f (Hz)	$R(H_{xx})$	$R(H_{xy})$	$R(H_{yx})$	$R(H_{yy})$	$I(H_{xx})$	$I(H_{xy})$	$I(H_{yx})$	$I(H_{yy})$	$\Delta R(H_{xx})$	$\Delta R(H_{xy})$	$\Delta R(H_{yx})$	$\Delta R(H_{yy})$	$\Delta I(H_{xx})$	$\Delta I(H_{xy})$	$\Delta I(H_{yx})$	$\Delta I(H_{yy})$
9.8	321.2	-73.6	-92.5	405.7	12.2	-6.1	-33.4	69.2	-1.4	-1.2	-2.1	-4.5	-1.6	-3.9	-5.2	-3.5
19.5	320.1	-77.9	-110.6	363.9	21.8	-4.2	-8.3	13.5	-1.5	-1.3	-6.5	-4.8	-0.9	-2.8	-11.1	-3.6
29.3	325.7	-76.6	-80.5	390.7	32.6	-7.7	-18.4	30.3	-0.9	-1.5	-3.1	-3.3	-0.8	-1.2	-2.1	-3.0
39.1	327.3	-76.6	-71.6	373.6	44.8	-10.1	3.2	35.7	-0.6	-1.6	-1.1	-2.9	-1.1	-0.8	-8.1	-3.2
48.8	331.2	-76.2	-83.0	370.5	56.3	-14.1	-9.3	55.7	-0.6	-0.8	-1.9	-2.1	-0.7	-1.2	-0.9	-2.0
58.6	334.0	-76.6	-80.8	378.0	65.7	-14.3	-18.4	51.5	-0.3	-0.7	-3.8	-2.1	-0.7	-0.7	-2.1	-1.9
68.4	332.1	-77.0	-81.6	379.0	76.9	-18.4	-14.9	53.4	-0.4	-0.5	-2.4	-1.8	-0.4	-0.8	-1.9	-1.5
78.1	341.9	-72.9	-73.9	366.9	91.7	-17.4	-7.7	61.0	-0.2	-0.5	-1.4	-1.6	-0.2	-0.3	-0.7	-1.4
87.9	342.1	-78.2	-84.0	387.9	95.0	-20.2	-21.7	92.0	-0.4	-0.6	-1.1	-1.6	-0.4	-0.7	-2.5	-1.3
97.7	346.4	-77.4	-74.0	377.3	102.6	-20.7	-20.6	86.8	-0.4	-0.5	-1.4	-1.7	-0.4	-0.7	-1.1	-1.1
107.4	348.0	-75.7	-84.5	390.1	110.5	-21.3	-26.0	105.4	-0.3	-0.3	-2.2	-1.8	-0.3	-0.5	-1.2	-1.1
117.2	352.7	-74.6	-79.6	388.3	118.1	-22.3	-34.3	112.6	-0.2	-0.4	-1.5	-1.7	-0.3	-0.5	-1.0	-1.1
127.0	356.5	-72.3	-80.9	386.6	128.1	-23.3	-37.9	126.1	-0.2	-0.6	-0.8	-1.7	-0.2	-0.5	-1.7	-1.1
136.7	358.9	-67.7	-76.5	389.8	136.2	-23.5	-38.4	129.2	-0.3	-0.3	-0.4	-1.4	-0.3	-0.5	-2.2	-1.1
146.5	361.6	-63.9	-69.5	393.5	144.0	-26.6	-32.0	133.6	-0.3	-0.6	-1.0	-1.6	-0.3	-0.5	-1.2	-1.1
156.3	362.1	-58.1	-69.8	380.3	151.6	-27.1	-26.6	120.0	-0.5	-0.4	-0.8	-1.5	-0.3	-0.4	-1.6	-1.0
166.0	365.9	-63.6	-77.2	407.8	158.2	-30.2	-35.9	162.8	-0.4	-0.3	-0.8	-1.5	-0.4	-0.5	-1.0	-1.4
175.8	365.6	-58.4	-79.0	410.0	165.3	-32.5	-37.3	165.3	-0.9	-1.0	-2.8	-1.9	-1.5	-0.7	-2.8	-1.9
185.5	367.8	-56.1	-66.6	411.2	177.3	-32.6	-34.0	166.8	-0.9	-1.5	-2.5	-2.6	-1.7	-1.4	-1.4	-1.6
195.3	370.2	-52.1	-66.4	408.2	188.6	-33.5	-28.8	171.7	-0.4	-0.5	-1.6	-1.8	-0.5	-0.7	-2.6	-1.4
205.1	369.4	-47.4	-67.9	417.0	194.7	-35.4	-32.5	193.4	-0.6	-0.5	-1.3	-1.6	-0.5	-0.3	-1.6	-1.2
214.8	376.8	-41.6	-61.9	425.8	207.0	-35.5	-44.9	187.8	-0.6	-0.3	-3.0	-1.9	-0.3	-0.4	-4.4	-1.4
224.6	376.9	-31.8	-63.3	372.9	216.3	-38.8	-39.9	199.8	-0.3	-0.4	-1.5	-1.9	-0.5	-0.3	-2.0	-1.4
234.4	382.4	-40.4	-61.1	435.5	227.1	-45.1	-43.6	215.6	-0.5	-0.3	-1.2	-1.8	-0.3	-0.5	-3.2	-1.7
244.1	382.1	-33.9	-60.1	432.5	241.2	-44.6	-42.9	224.4	-0.3	-0.3	-1.8	-1.7	-0.4	-0.2	-0.8	-1.1
253.9	382.5	-28.3	-62.5	447.9	253.1	-44.4	-37.4	235.0	-0.5	-0.3	-2.5	-1.6	-0.5	-0.3	-2.7	-1.2
263.7	386.9	-18.1	-50.6	437.8	269.4	-45.0	-32.3	238.4	-0.3	-0.3	-1.0	-2.2	-0.4	-0.4	-3.0	-1.5
273.4	392.6	-10.5	-47.7	387.7	284.4	-40.0	-37.6	225.6	-0.4	-0.3	-1.4	-2.2	-0.4	-0.5	-1.8	-1.1
283.2	397.5	-22.2	-54.6	452.7	302.9	-51.1	-32.1	258.7	-0.2	-0.4	-1.9	-1.7	-0.5	-0.4	-2.6	-1.5
293.0	404.4	-3.2	-46.7	429.8	316.7	-43.0	-20.7	278.5	-0.3	-0.5	-1.4	-2.5	-0.6	-0.6	-1.1	-1.1
302.7	404.3	21.8	-44.2	402.0	339.9	-33.6	-13.2	306.9	-0.2	-0.6	-1.8	-2.7	-0.6	-0.4	-1.5	-1.2
312.5	413.4	18.5	-51.9	477.8	364.0	-41.8	-0.6	303.8	-0.3	-0.4	-1.9	-3.4	-0.7	-0.6	-1.8	-2.7
322.3	428.2	50.3	-44.0	499.7	396.7	-83.8	23.5	404.4	-0.5	-2.1	-2.9	-2.7	-0.8	-0.9	-2.7	-3.0
332.0	432.4	3.7	14.8	631.3	411.8	-128.7	68.7	358.6	-0.3	-0.3	-2.3	-3.1	-0.5	-0.6	-3.5	-1.7
341.8	485.8	40.5	39.9	589.3	473.5	-65.9	85.5	325.5	-0.6	-0.4	-5.0	-3.1	-0.8	-0.5	-5.0	-1.7

Table 51: Dynamic Stiffness Real and Imaginary Parts at 10800 rpm and 3134 kPa (MN/m)

f (Hz)	$R(H_{xx})$	$R(H_{xy})$	$R(H_{yx})$	$R(H_{yy})$	$I(H_{xx})$	$I(H_{xy})$	$I(H_{yx})$	$I(H_{yy})$	$\Delta R(H_{xx})$	$\Delta R(H_{xy})$	$\Delta R(H_{yx})$	$\Delta R(H_{yy})$	$\Delta I(H_{xx})$	$\Delta I(H_{xy})$	$\Delta I(H_{yx})$	$\Delta I(H_{yy})$
9.8	343.9	-85.7	-94.8	440.7	9.7	-1.9	-34.4	64.5	-1.8	-4.8	-1.3	-5.5	-2.0	-6.4	-3.3	-4.7
19.5	343.9	-79.0	-106.0	418.4	21.1	-12.2	-16.6	32.6	-1.3	-3.6	-2.4	-7.2	-1.8	-3.4	-3.9	-4.8
29.3	345.2	-81.7	-82.5	425.5	28.9	-6.3	-14.3	26.8	-0.4	-1.0	-2.4	-5.0	-0.9	-0.8	-3.7	-2.1
39.1	349.5	-80.4	-83.4	422.3	42.7	-11.6	1.7	31.8	-0.4	-0.8	-2.3	-2.4	-1.3	-0.7	-3.5	-1.6
48.8	352.7	-82.0	-90.5	427.6	53.4	-14.9	-10.7	42.5	-0.2	-0.6	-1.0	-2.1	-0.7	-0.5	-1.0	-2.0
58.6	355.3	-82.2	-85.1	427.3	60.5	-14.6	-19.6	46.0	-1.2	-0.6	-2.7	-2.7	-0.7	-0.7	-1.4	-1.3
68.4	354.2	-80.8	-86.8	427.1	70.7	-17.2	-15.3	45.6	-0.5	-0.4	-1.4	-2.7	-0.6	-0.4	-0.5	-1.1
78.1	355.8	-80.9	-89.7	409.9	91.9	-18.2	-4.6	55.4	-0.4	-0.5	-0.9	-2.2	-0.5	-0.5	-0.9	-1.5
87.9	362.8	-82.7	-86.8	433.5	88.2	-21.6	-24.1	82.5	-0.3	-0.3	-0.5	-2.0	-0.4	-0.5	-1.2	-1.5
97.7	367.2	-81.4	-81.6	422.4	95.5	-22.2	-22.3	72.6	-0.4	-0.6	-0.8	-2.2	-0.5	-0.5	-0.4	-1.1
107.4	367.8	-80.1	-86.0	433.7	104.1	-23.6	-28.1	93.1	-0.1	-0.3	-1.9	-2.6	-0.3	-0.4	-0.6	-1.2
117.2	372.0	-78.8	-85.7	433.5	110.2	-24.3	-33.5	96.0	-0.5	-0.4	-0.9	-1.9	-0.4	-0.4	-1.7	-1.1
127.0	375.1	-76.0	-85.9	427.8	118.1	-24.6	-34.2	112.4	-0.4	-0.6	-0.5	-2.0	-0.5	-0.3	-1.0	-1.4
136.7	378.0	-71.7	-81.0	431.8	128.3	-27.9	-39.3	118.7	-0.2	-0.4	-1.2	-2.5	-0.3	-0.3	-0.7	-1.0
146.5	380.7	-65.7	-73.3	425.0	133.8	-28.8	-33.8	122.8	-0.3	-0.5	-1.1	-2.9	-0.2	-0.4	-0.5	-2.5
156.3	380.5	-64.9	-76.6	427.6	142.0	-32.0	-30.9	104.4	-0.5	-0.5	-1.9	-2.5	-0.4	-0.3	-1.3	-1.4
166.0	383.7	-68.8	-81.6	448.0	147.7	-33.9	-40.7	150.1	-0.4	-0.4	-0.7	-2.3	-0.7	-0.8	-0.8	-1.4
175.8	383.7	-63.0	-82.9	453.1	154.5	-35.3	-42.0	148.5	-1.7	-2.7	-1.5	-2.9	-1.1	-2.1	-2.9	-5.1
185.5	384.7	-61.2	-74.1	451.5	166.2	-38.5	-36.3	151.9	-1.2	-0.9	-2.3	-2.7	-1.2	-0.6	-1.8	-1.1
195.3	386.6	-56.5	-69.1	444.9	175.9	-38.8	-38.4	155.2	-0.5	-0.4	-0.9	-1.9	-0.4	-0.8	-2.5	-1.3
205.1	386.2	-53.6	-71.6	457.4	182.6	-42.4	-37.2	175.0	-0.5	-0.5	-1.6	-2.3	-0.4	-0.5	-1.9	-1.1
214.8	394.3	-47.6	-64.0	461.4	192.1	-40.7	-50.5	168.3	-0.3	-0.5	-1.6	-2.3	-0.8	-0.6	-2.6	-1.3
224.6	393.9	-46.1	-66.3	429.3	201.2	-45.0	-44.1	168.1	-0.5	-0.6	-2.7	-2.9	-0.4	-0.5	-1.1	-1.0
234.4	398.4	-49.8	-65.2	480.5	211.2	-53.7	-49.1	201.6	-0.5	-0.6	-1.6	-2.5	-0.2	-0.7	-0.5	-1.1
244.1	397.0	-40.8	-62.4	472.6	223.8	-54.0	-46.7	211.1	-0.6	-0.3	-1.3	-2.3	-0.2	-0.5	-1.7	-1.0
253.9	397.4	-37.3	-64.3	487.0	235.4	-54.0	-44.9	216.9	-0.5	-0.4	-3.2	-2.4	-0.3	-0.5	-0.5	-1.1
263.7	401.4	-31.1	-55.6	481.3	248.1	-53.0	-41.9	210.5	-0.3	-0.5	-2.3	-2.7	-0.5	-0.7	-2.1	-1.2
273.4	404.5	-24.0	-54.9	441.9	262.9	-53.8	-44.0	202.8	-0.3	-0.4	-1.1	-2.3	-0.4	-0.5	-1.4	-1.1
283.2	409.5	-32.4	-54.1	494.1	279.8	-64.9	-44.0	238.6	-0.4	-0.6	-2.4	-2.3	-0.2	-0.2	-2.1	-1.8
293.0	417.9	-16.4	-47.4	472.9	290.1	-53.1	-30.2	249.7	-0.4	-0.6	-1.3	-2.5	-0.4	-0.7	-1.4	-1.8
302.7	416.8	2.0	-45.3	462.7	311.5	-52.1	-31.8	276.7	-0.4	-1.1	-1.8	-3.0	-0.5	-0.2	-1.8	-2.6
312.5	416.2	68.2	-27.4	463.0	324.4	-76.8	-25.8	375.7	-0.6	-3.5	-2.7	-5.6	-1.2	-6.0	-2.7	-13.9
322.3	435.6	17.9	-25.0	481.7	344.2	-46.4	-1.4	284.1	-0.6	-1.3	-3.4	-3.6	-0.5	-0.9	-2.6	-2.4
332.0	474.8	132.0	-31.7	518.2	368.1	-180.3	49.4	518.1	-1.5	-6.5	-3.5	-15.7	-1.5	-6.7	-4.5	-7.2
341.8	467.3	-4.7	26.0	650.4	404.9	-110.0	21.8	310.4	-0.7	-1.0	-1.3	-4.7	-0.7	-1.7	-1.9	-2.0

Table 52: Dynamic Stiffness Real and Imaginary Parts at 13200 rpm and 0 kPa (MN/m)

f (Hz)	$R(H_{xx})$	$R(H_{xy})$	$R(H_{yx})$	$R(H_{yy})$	$I(H_{xx})$	$I(H_{xy})$	$I(H_{yx})$	$I(H_{yy})$	$\Delta R(H_{xx})$	$\Delta R(H_{xy})$	$\Delta R(H_{yx})$	$\Delta R(H_{yy})$	$\Delta I(H_{xx})$	$\Delta I(H_{xy})$	$\Delta I(H_{yx})$	$\Delta I(H_{yy})$
9.8	279.6	-62.3	-111.2	277.2	9.8	-13.3	2.4	64.9	-3.0	-3.1	-5.4	-9.5	-3.0	-1.6	-2.6	-7.5
19.5	283.5	-62.7	-103.2	281.7	22.4	-0.6	-10.8	35.2	-1.6	-2.1	-3.4	-8.7	-0.9	-2.4	-4.0	-3.6
29.3	286.8	-60.1	-92.8	293.7	34.7	-8.3	1.1	70.0	-1.3	-1.7	-6.4	-8.4	-1.5	-0.9	-3.7	-5.2
39.1	286.3	-62.6	-70.8	241.5	45.6	-10.4	3.5	32.1	-1.2	-1.8	-2.3	-9.1	-1.2	-1.2	-2.3	-3.8
48.8	287.9	-58.5	-89.4	265.4	57.2	-16.4	-15.7	56.1	-0.6	-1.4	-2.3	-3.9	-0.4	-0.7	-1.5	-2.3
58.6	292.4	-57.4	-79.2	278.8	73.4	-19.7	1.9	64.4	-0.6	-1.3	-1.5	-4.9	-1.7	-1.0	-2.8	-3.9
68.4	295.0	-58.1	-87.2	292.8	81.2	-22.6	-15.9	71.9	-0.8	-1.2	-2.4	-5.0	-1.2	-0.6	-2.2	-3.2
78.1	298.8	-59.1	-88.9	283.8	93.7	-28.3	-9.0	84.3	-0.8	-1.0	-2.4	-3.8	-0.7	-0.5	-2.3	-3.2
87.9	300.6	-57.2	-87.1	296.6	103.8	-31.7	-15.1	116.7	-0.5	-1.2	-1.3	-4.2	-1.0	-0.5	-1.6	-3.3
97.7	303.2	-58.7	-87.8	288.6	113.2	-36.7	-23.2	114.7	-0.7	-1.2	-0.8	-4.3	-1.1	-0.9	-2.5	-2.1
107.4	307.0	-60.7	-89.5	288.8	122.1	-39.6	-16.2	129.4	-0.7	-1.2	-1.0	-3.8	-1.0	-0.7	-0.9	-1.8
117.2	311.8	-62.4	-81.5	293.8	133.1	-44.0	-14.5	146.7	-0.3	-1.3	-1.3	-3.9	-0.6	-0.7	-2.0	-4.0
127.0	315.1	-62.5	-90.6	313.2	142.5	-46.6	-24.4	138.7	-1.0	-1.1	-1.8	-4.2	-0.2	-0.7	-1.1	-2.2
136.7	319.6	-63.4	-89.0	311.1	152.7	-48.3	-19.2	146.3	-0.5	-1.3	-1.7	-5.4	-0.5	-0.5	-0.7	-2.7
146.5	324.7	-63.4	-83.5	332.0	161.7	-49.9	-16.4	162.1	-0.6	-1.0	-1.4	-3.9	-0.3	-0.8	-0.9	-3.8
156.3	327.0	-67.6	-87.4	277.8	170.4	-48.6	-13.7	245.0	-0.5	-1.0	-3.3	-5.0	-0.7	-0.4	-2.2	-2.5
166.0	330.0	-67.4	-80.4	327.0	178.1	-51.5	-6.4	194.6	-0.6	-1.1	-1.8	-4.7	-0.8	-0.6	-2.8	-3.1
175.8	331.6	-63.8	-74.9	375.8	191.2	-50.7	-10.5	242.8	-0.8	-0.8	-0.5	-4.8	-0.4	-0.9	-0.9	-3.4
185.5	334.7	-62.3	-73.8	349.1	200.8	-51.0	-14.6	198.3	-0.5	-0.9	-2.9	-5.1	-0.9	-0.6	-1.7	-2.5
195.3	337.3	-58.7	-73.7	384.4	211.8	-52.7	-22.3	251.1	-0.4	-0.8	-3.1	-3.8	-0.4	-0.3	-3.1	-2.5
205.1	344.4	-66.2	-61.2	358.1	219.9	-52.5	-17.1	241.6	-0.9	-1.1	-2.7	-5.6	-1.1	-0.7	-2.5	-3.1
214.8	350.2	-61.3	-60.2	342.1	236.4	-48.7	-28.8	255.3	-0.5	-1.6	-2.0	-4.5	-1.2	-1.1	-1.5	-3.3
224.6	360.3	-62.7	-60.0	340.1	245.5	-47.4	-37.3	273.3	-2.8	-2.1	-2.2	-6.5	-4.8	-1.7	-3.3	-3.4
234.4	362.0	-61.6	-52.8	367.0	250.1	-43.5	-45.1	274.4	-0.8	-1.0	-1.3	-4.4	-1.2	-0.7	-1.0	-3.2
244.1	365.1	-57.4	-65.2	370.0	269.8	-45.1	-35.4	286.6	-0.5	-1.1	-2.4	-4.8	-0.4	-0.4	-2.8	-2.8
253.9	366.8	-50.9	-65.4	378.1	286.1	-40.7	-29.1	296.1	-0.7	-0.9	-3.6	-4.7	-0.4	-0.5	-2.8	-4.2
263.7	376.9	-52.3	-84.0	365.9	302.6	-34.1	-13.7	324.3	-0.8	-0.9	-9.3	-5.3	-0.4	-0.5	-1.2	-3.2
273.4	389.8	-47.9	-50.3	381.0	307.7	-31.2	-17.2	312.6	-0.5	-1.1	-5.8	-4.7	-0.6	-0.7	-4.6	-3.3
283.2	389.7	-35.6	-73.6	384.9	334.0	-7.0	0.5	349.0	-0.5	-1.2	-8.4	-4.5	-0.5	-0.6	-3.2	-4.1
293.0	392.9	-30.0	-83.6	386.9	366.8	-5.2	21.4	393.4	-0.6	-0.9	-8.9	-4.6	-0.6	-0.5	-2.5	-4.9
302.7	412.1	-20.4	-80.1	384.6	413.2	31.3	82.9	445.3	-0.6	-1.1	-11.4	-6.1	-0.6	-1.1	-5.1	-6.6
312.5	470.1	35.6	-55.3	458.6	512.3	78.9	240.5	516.7	-1.4	-1.6	-12.3	-11.6	-1.2	-1.4	-14.5	-10.1
322.3	550.3	126.2	22.0	464.0	605.3	234.1	372.6	779.7	-1.5	-2.5	-12.3	-13.3	-2.9	-2.7	-5.4	-8.5
332.0	1481.6	1191.8	1262.4	2072.8	534.3	-203.6	731.8	720.7	-40.3	-31.1	-59.9	-48.0	-35.9	-57.6	-71.9	-98.7
341.8	407.7	30.6	148.1	675.9	-37.8	-472.5	-557.9	-199.7	-2.7	-4.9	-16.0	-22.8	-3.4	-3.4	-15.5	-15.3

Table 53: Dynamic Stiffness Real and Imaginary Parts at 13200 rpm and 783 kPa (MN/m)

f (Hz)	$R(H_{xx})$	$R(H_{xy})$	$R(H_{yx})$	$R(H_{yy})$	$I(H_{xx})$	$I(H_{xy})$	$I(H_{yx})$	$I(H_{yy})$	$\Delta R(H_{xx})$	$\Delta R(H_{xy})$	$\Delta R(H_{yx})$	$\Delta R(H_{yy})$	$\Delta I(H_{xx})$	$\Delta I(H_{xy})$	$\Delta I(H_{yx})$	$\Delta I(H_{yy})$
9.8	305.0	-65.7	-95.6	302.0	13.0	-15.0	-7.7	36.6	-3.2	-2.3	-3.8	-3.9	-1.9	-2.6	-3.4	-2.1
19.5	303.3	-70.8	-95.5	302.8	25.2	-13.3	1.3	12.8	-1.8	-1.3	-4.0	-2.8	-1.2	-1.9	-3.1	-2.8
29.3	306.5	-75.8	-98.5	314.8	30.5	-8.2	-7.0	31.9	-3.8	-1.6	-2.3	-3.5	-2.4	-3.6	-1.6	-3.3
39.1	306.1	-72.0	-93.4	304.6	43.0	-13.3	-12.7	45.5	-0.9	-1.8	-2.0	-2.9	-1.7	-0.9	-3.3	-1.9
48.8	306.4	-69.9	-96.7	306.0	55.4	-21.0	-9.4	61.2	-0.8	-1.5	-0.4	-1.7	-0.7	-1.0	-1.5	-1.4
58.6	309.8	-71.1	-95.7	314.0	66.8	-20.0	-14.3	71.5	-1.1	-0.6	-1.3	-1.8	-1.5	-1.1	-0.9	-1.4
68.4	317.1	-73.4	-83.7	316.6	82.3	-24.0	-4.0	72.4	-0.5	-1.2	-1.9	-2.4	-0.7	-0.8	-0.8	-1.4
78.1	317.7	-70.4	-89.6	305.3	89.0	-27.8	-11.8	80.8	-0.4	-0.7	-2.3	-2.1	-0.5	-0.6	-1.6	-1.1
87.9	320.4	-74.5	-98.6	329.4	97.2	-30.5	-14.4	108.8	-0.7	-0.6	-1.1	-1.9	-1.1	-1.2	-2.9	-1.6
97.7	325.2	-74.4	-94.6	320.8	105.9	-33.6	-16.6	112.0	-0.3	-0.5	-2.8	-1.8	-0.5	-0.5	-2.6	-1.5
107.4	324.8	-75.5	-98.7	330.3	114.7	-34.4	-12.5	126.6	-1.0	-0.6	-0.9	-2.2	-0.7	-0.6	-1.4	-1.2
117.2	329.7	-77.5	-96.9	334.6	123.9	-36.6	-18.6	133.5	-0.4	-0.6	-0.9	-1.8	-0.5	-0.3	-1.3	-1.4
127.0	332.4	-77.2	-92.8	330.5	131.4	-38.2	-19.4	150.5	-0.6	-0.8	-0.9	-1.7	-0.5	-0.7	-2.0	-1.4
136.7	336.2	-75.0	-90.8	342.0	144.2	-39.9	-18.1	154.0	-0.5	-0.8	-1.1	-1.7	-0.5	-0.5	-1.5	-1.6
146.5	339.1	-73.3	-90.2	345.8	151.5	-42.3	-21.1	158.3	-0.8	-0.6	-1.4	-1.6	-0.5	-0.7	-1.8	-1.6
156.3	339.5	-68.8	-83.2	324.3	159.5	-43.8	-24.2	164.8	-0.4	-0.9	-2.0	-1.9	-0.9	-0.4	-1.5	-1.6
166.0	345.2	-80.1	-87.9	362.1	167.8	-42.6	-19.1	189.4	-0.9	-0.5	-0.4	-1.8	-0.6	-0.7	-1.9	-1.3
175.8	344.8	-77.0	-86.8	369.1	178.7	-45.4	-20.2	189.9	-0.4	-0.4	-1.0	-1.7	-0.6	-0.5	-1.1	-1.4
185.5	346.0	-75.0	-81.3	368.8	186.9	-42.1	-17.1	189.2	-0.6	-0.4	-0.6	-1.5	-0.7	-0.5	-1.1	-1.7
195.3	349.1	-70.7	-71.9	357.8	198.2	-41.2	-14.7	196.2	-0.8	-0.8	-1.4	-1.7	-0.6	-0.5	-3.2	-1.6
205.1	350.7	-72.0	-72.3	368.2	205.1	-38.2	-17.0	216.0	-1.0	-0.6	-0.8	-1.9	-1.0	-0.4	-2.1	-1.3
214.8	357.5	-67.0	-67.5	372.3	218.9	-36.3	-23.9	209.4	-1.0	-0.9	-1.1	-2.3	-1.1	-0.4	-2.7	-1.8
224.6	360.3	-42.7	-56.2	284.2	230.9	-36.8	-35.6	265.9	-2.3	-0.7	-3.5	-2.3	-2.8	-1.2	-1.1	-1.9
234.4	369.0	-68.8	-68.8	389.4	239.6	-39.6	-32.8	243.1	-0.6	-0.5	-1.3	-1.7	-1.1	-0.4	-3.0	-1.9
244.1	366.1	-64.3	-65.7	391.7	253.6	-35.5	-25.0	249.9	-0.6	-0.5	-1.9	-1.9	-0.3	-0.3	-2.4	-1.4
253.9	368.5	-60.3	-65.1	405.1	265.7	-31.3	-22.1	261.8	-0.5	-0.3	-2.0	-2.1	-0.4	-0.4	-1.9	-1.7
263.7	375.0	-51.8	-61.0	380.7	281.6	-25.5	-16.8	257.1	-0.4	-0.4	-1.4	-1.8	-0.5	-0.6	-3.9	-1.5
273.4	381.7	-22.9	-57.5	291.4	294.2	-12.4	-15.2	288.1	-0.4	-0.4	-2.4	-1.7	-0.8	-0.5	-1.6	-1.7
283.2	380.9	-48.3	-58.3	378.0	313.0	-17.8	-12.8	286.5	-0.7	-0.4	-2.2	-1.8	-0.7	-0.4	-3.4	-1.8
293.0	388.3	21.6	-49.6	352.8	322.9	-33.6	5.3	467.0	-0.5	-1.4	-2.1	-4.2	-0.3	-1.3	-2.7	-1.4
302.7	386.3	-25.9	-46.5	506.3	352.1	-67.8	21.3	422.5	-0.5	-1.0	-2.7	-3.7	-1.1	-1.2	-3.2	-3.0
312.5	424.2	63.0	-43.4	528.8	369.9	-73.2	103.6	549.2	-0.8	-0.7	-3.4	-5.2	-0.9	-2.7	-2.6	-2.4
322.3	417.2	61.1	-48.9	427.2	425.0	5.4	97.7	538.6	-0.5	-1.5	-3.5	-3.0	-1.0	-0.7	-4.9	-4.2
332.0	445.8	29.0	-42.0	463.0	524.1	58.6	164.8	436.9	-0.7	-0.5	-3.9	-4.8	-0.7	-1.0	-6.0	-4.1
341.8	700.1	191.6	142.5	552.6	660.5	145.0	356.9	553.9	-3.7	-2.2	-4.9	-5.0	-2.4	-1.9	-9.9	-6.7

Table 54: Dynamic Stiffness Real and Imaginary Parts at 13200 rpm and 1567 kPa (MN/m)

f (Hz)	$R(H_{xx})$	$R(H_{xy})$	$R(H_{yx})$	$R(H_{yy})$	$I(H_{xx})$	$I(H_{xy})$	$I(H_{yx})$	$I(H_{yy})$	$\Delta R(H_{xx})$	$\Delta R(H_{xy})$	$\Delta R(H_{yx})$	$\Delta R(H_{yy})$	$\Delta I(H_{xx})$	$\Delta I(H_{xy})$	$\Delta I(H_{yx})$	$\Delta I(H_{yy})$
9.8	331.6	-83.4	-91.4	351.3	22.6	-19.5	3.1	41.5	-6.0	-5.4	-5.4	-5.9	-5.0	-2.7	-5.2	-4.9
19.5	330.7	-85.4	-96.4	352.9	23.7	-14.8	-3.8	26.8	-1.3	-4.1	-1.9	-7.0	-1.3	-3.7	-1.3	-4.7
29.3	336.1	-83.8	-109.4	359.9	29.7	-14.1	-12.4	23.4	-2.1	-3.3	-1.7	-2.3	-2.4	-2.1	-3.7	-2.9
39.1	334.7	-84.9	-96.4	345.2	39.3	-12.8	-20.7	43.3	-1.2	-1.9	-2.0	-2.9	-1.5	-1.5	-2.9	-1.8
48.8	335.2	-81.7	-98.1	344.3	52.6	-19.4	-12.5	57.9	-1.4	-1.4	-1.8	-1.9	-0.5	-0.7	-1.2	-1.2
58.6	334.3	-82.3	-99.9	353.5	59.9	-20.7	-18.7	59.9	-1.0	-0.9	-2.1	-2.1	-1.2	-0.8	-2.0	-1.8
68.4	332.8	-81.5	-102.4	356.2	71.3	-22.1	-20.4	62.5	-0.7	-1.1	-0.9	-1.7	-0.9	-0.9	-1.0	-2.2
78.1	344.3	-83.3	-94.0	345.7	83.8	-25.1	-8.0	65.7	-0.8	-0.5	-0.7	-1.9	-0.9	-0.8	-1.1	-1.2
87.9	346.3	-86.9	-100.3	364.3	90.1	-27.8	-16.5	95.1	-1.0	-0.6	-1.4	-1.6	-0.5	-0.5	-2.2	-1.6
97.7	347.8	-86.7	-94.0	355.2	98.1	-30.3	-20.3	94.6	-0.7	-0.6	-1.0	-1.6	-1.2	-0.8	-1.1	-1.3
107.4	348.8	-87.6	-103.7	365.0	105.5	-30.8	-20.9	114.5	-0.7	-1.0	-1.5	-2.0	-0.3	-0.7	-1.4	-1.2
117.2	352.9	-87.4	-103.1	369.1	113.0	-31.7	-20.7	118.0	-0.5	-0.6	-0.8	-1.7	-0.4	-0.6	-0.6	-1.5
127.0	355.6	-86.3	-96.6	363.4	122.4	-33.2	-22.5	133.6	-0.2	-0.4	-0.9	-1.8	-0.5	-0.7	-0.5	-1.7
136.7	356.4	-83.9	-94.4	367.8	132.2	-33.9	-24.0	141.4	-0.4	-0.7	-0.7	-2.3	-0.4	-0.6	-1.1	-1.4
146.5	360.7	-83.5	-92.2	372.2	138.1	-34.2	-23.5	144.2	-0.5	-0.5	-0.7	-1.6	-0.5	-0.5	-2.2	-1.3
156.3	361.0	-78.1	-85.8	356.6	146.6	-34.5	-26.7	134.7	-1.0	-0.5	-1.4	-1.7	-0.6	-0.6	-1.9	-1.5
166.0	363.8	-86.2	-94.8	391.7	153.5	-38.0	-22.3	175.2	-0.5	-0.4	-0.7	-2.0	-0.7	-0.9	-0.8	-1.2
175.8	364.5	-83.4	-92.1	389.6	163.8	-39.1	-28.5	177.1	-0.7	-0.4	-1.2	-2.1	-0.5	-0.8	-0.6	-1.5
185.5	367.8	-82.7	-93.3	396.2	172.7	-37.4	-20.0	175.0	-0.8	-0.4	-0.8	-2.0	-0.8	-0.5	-1.3	-2.1
195.3	369.3	-78.8	-86.4	389.4	181.2	-36.1	-17.4	183.1	-0.7	-0.5	-0.7	-1.9	-0.9	-0.7	-1.9	-1.6
205.1	368.8	-76.5	-84.7	402.1	188.3	-34.6	-20.6	198.8	-1.0	-1.0	-1.3	-1.6	-0.8	-0.5	-2.1	-1.6
214.8	374.5	-71.4	-77.7	407.3	199.7	-32.5	-25.2	190.9	-1.3	-1.0	-2.6	-2.9	-1.0	-1.8	-1.2	-1.4
224.6	378.5	-63.9	-72.1	344.6	209.0	-31.2	-32.7	201.0	-4.3	-1.7	-4.7	-2.6	-4.1	-1.4	-3.8	-2.5
234.4	382.3	-73.6	-75.3	420.3	221.3	-39.9	-37.3	224.8	-0.7	-0.5	-1.6	-2.3	-1.2	-0.5	-2.4	-1.4
244.1	380.8	-62.4	-74.6	407.8	232.7	-36.4	-27.9	239.4	-0.3	-0.4	-1.1	-2.3	-0.5	-0.5	-1.6	-1.7
253.9	380.7	-59.5	-70.7	417.9	242.5	-31.3	-27.0	242.3	-0.5	-0.6	-1.1	-1.6	-0.9	-0.5	-1.6	-1.5
263.7	385.2	-55.8	-75.6	423.1	255.9	-30.1	-23.3	237.1	-0.4	-0.4	-3.5	-1.8	-0.4	-0.4	-1.8	-1.5
273.4	389.1	-42.6	-61.0	353.8	266.7	-21.6	-15.2	231.1	-0.7	-0.3	-1.2	-1.8	-0.6	-0.3	-2.8	-1.7
283.2	392.7	-54.6	-73.1	420.9	282.2	-30.8	-15.9	256.5	-0.4	-0.4	-2.1	-1.7	-0.6	-0.4	-0.9	-1.5
293.0	397.0	-38.1	-57.1	389.8	294.6	-14.9	-13.7	281.2	-0.4	-0.3	-1.2	-2.1	-0.7	-0.7	-1.4	-1.5
302.7	389.1	19.0	-49.5	302.3	317.7	4.2	-17.8	364.5	-0.3	-0.7	-1.7	-2.5	-0.7	-0.5	-1.3	-1.9
312.5	396.4	18.2	-55.6	367.2	339.2	9.3	-12.4	350.4	-0.6	-0.5	-2.0	-3.0	-0.6	-0.4	-3.0	-2.6
322.3	405.7	10.5	-55.3	375.4	357.9	9.6	7.2	359.3	-0.6	-0.8	-3.5	-1.8	-0.6	-0.5	-1.4	-3.0
332.0	413.0	-16.2	-40.0	525.0	390.0	-38.9	39.4	361.5	-0.4	-0.4	-3.1	-2.2	-0.6	-0.9	-3.0	-2.7
341.8	447.6	14.1	-6.0	508.1	434.4	7.5	69.6	359.5	-1.0	-0.5	-1.9	-2.3	-1.2	-0.9	-2.7	-2.1

Table 55: Dynamic Stiffness Real and Imaginary Parts at 13200 rpm and 2350 kPa (MN/m)

f (Hz)	$R(H_{xx})$	$R(H_{xy})$	$R(H_{yx})$	$R(H_{yy})$	$I(H_{xx})$	$I(H_{xy})$	$I(H_{yx})$	$I(H_{yy})$	$\Delta R(H_{xx})$	$\Delta R(H_{xy})$	$\Delta R(H_{yx})$	$\Delta R(H_{yy})$	$\Delta I(H_{xx})$	$\Delta I(H_{xy})$	$\Delta I(H_{yx})$	$\Delta I(H_{yy})$
9.8	315.9	-70.9	-94.2	384.6	11.2	-9.3	-8.8	51.0	-1.6	-6.1	-4.8	-14.5	-1.5	-3.7	-2.2	-7.1
19.5	314.3	-62.8	-42.9	302.6	26.1	-10.0	40.4	4.7	-1.7	-0.7	-7.2	-4.5	-1.1	-4.1	-12.5	-7.8
29.3	318.8	-66.3	-110.4	373.6	30.6	-9.1	-28.8	34.2	-1.1	-2.8	-6.5	-7.5	-1.3	-2.2	-1.9	-7.3
39.1	323.0	-69.5	-93.7	346.5	41.6	-16.3	-43.4	42.9	-0.7	-1.7	-2.7	-1.9	-1.1	-2.4	-5.0	-3.5
48.8	326.1	-68.4	-81.6	340.4	53.8	-18.2	-5.5	53.5	-0.6	-1.4	-1.3	-2.8	-0.7	-1.7	-1.6	-2.9
58.6	326.8	-68.4	-88.9	350.7	64.5	-20.9	-10.1	59.1	-0.5	-1.2	-1.9	-3.2	-0.7	-1.4	-1.5	-1.5
68.4	325.6	-69.4	-88.2	346.9	73.5	-23.4	-18.6	62.1	-0.9	-0.5	-1.8	-2.7	-0.6	-0.5	-1.4	-2.2
78.1	332.6	-66.7	-62.6	336.6	86.5	-24.1	-21.5	67.5	-0.4	-0.7	-3.7	-2.1	-0.4	-1.1	-2.2	-1.9
87.9	334.3	-71.4	-78.2	358.5	93.0	-29.1	-15.5	92.9	-0.5	-0.9	-2.5	-3.1	-0.6	-0.7	-1.1	-1.3
97.7	338.7	-71.8	-76.7	350.4	100.2	-30.4	-24.2	95.7	-0.6	-1.0	-2.7	-2.0	-0.2	-0.4	-1.7	-1.7
107.4	339.4	-71.7	-91.1	360.7	109.3	-32.5	-19.3	113.6	-0.5	-0.6	-2.1	-2.7	-0.4	-1.3	-1.3	-1.1
117.2	344.9	-72.9	-78.8	360.7	115.7	-31.8	-25.0	116.9	-0.5	-0.6	-1.4	-1.7	-0.4	-0.6	-1.1	-1.3
127.0	346.4	-71.8	-77.4	356.7	124.1	-33.6	-20.2	128.3	-0.8	-0.5	-1.9	-3.2	-0.2	-0.6	-1.4	-1.4
136.7	350.8	-69.8	-89.1	366.8	132.2	-32.5	-29.6	138.5	-0.2	-0.6	-1.2	-3.1	-0.2	-0.5	-2.5	-1.5
146.5	350.2	-65.5	-81.3	368.5	142.2	-34.8	-15.2	145.3	-0.3	-0.4	-3.4	-2.4	-0.5	-1.0	-1.5	-2.3
156.3	349.5	-61.9	-78.4	354.4	149.6	-37.3	-23.1	133.3	-0.6	-0.8	-2.5	-1.8	-0.3	-0.6	-1.2	-3.7
166.0	356.6	-71.5	-77.3	387.8	157.9	-38.7	-13.9	169.4	-0.6	-0.9	-2.8	-5.1	-0.4	-0.5	-2.6	-3.2
175.8	357.1	-68.1	-81.4	389.0	165.7	-40.1	-19.3	167.9	-0.5	-0.6	-1.9	-3.2	-0.3	-0.7	-2.4	-1.7
185.5	357.8	-67.0	-88.1	388.8	176.5	-36.0	-23.6	174.6	-0.6	-0.5	-3.1	-2.2	-0.6	-0.6	-1.6	-1.3
195.3	360.8	-61.7	-60.9	374.2	187.2	-37.0	-11.8	180.7	-0.3	-0.5	-2.6	-2.7	-0.4	-0.5	-2.6	-2.2
205.1	356.1	-57.9	-78.4	392.3	191.1	-36.4	-15.9	201.2	-0.5	-0.4	-3.1	-2.1	-0.7	-0.5	-2.9	-1.4
214.8	364.0	-52.5	-77.1	393.8	203.6	-35.0	-19.6	189.7	-1.0	-2.0	-3.5	-3.2	-1.5	-1.9	-4.6	-2.3
224.6	362.9	-44.3	-74.5	341.3	210.6	-34.8	-27.6	204.9	-1.0	-1.0	-3.3	-3.1	-1.0	-0.9	-2.2	-2.0
234.4	370.0	-53.7	-80.8	409.5	222.3	-39.7	-40.3	224.2	-0.9	-0.7	-2.8	-2.1	-0.4	-0.6	-4.8	-2.1
244.1	368.3	-48.1	-62.8	401.8	237.4	-38.3	-28.9	235.3	-0.6	-0.4	-3.8	-3.0	-0.3	-0.4	-3.4	-2.4
253.9	365.3	-35.8	-60.2	409.7	249.0	-39.1	-26.5	266.5	-0.5	-0.5	-3.2	-4.2	-0.3	-0.9	-2.7	-2.1
263.7	370.1	-33.6	-67.7	405.6	264.9	-32.4	-20.5	243.2	-0.3	-0.6	-4.1	-3.3	-0.3	-0.5	-4.3	-2.3
273.4	372.1	-21.0	-60.0	342.7	279.0	-24.6	-16.6	235.3	-0.6	-0.5	-5.6	-3.3	-0.3	-0.3	-1.9	-3.2
283.2	377.1	-32.3	-72.5	414.0	299.8	-36.8	-18.1	268.9	-0.5	-0.4	-5.9	-2.8	-0.5	-0.5	-3.7	-3.2
293.0	382.0	-10.4	-61.5	375.4	312.9	-20.8	-3.2	291.3	-0.5	-0.4	-3.2	-4.9	-0.4	-0.4	-1.5	-4.9
302.7	376.9	23.8	-47.7	326.4	337.8	-3.1	10.8	339.0	-0.5	-0.4	-5.2	-3.8	-0.5	-0.4	-3.2	-6.9
312.5	387.6	3.2	-55.6	450.3	363.8	-24.0	12.6	316.2	-0.5	-0.5	-4.2	-2.6	-1.0	-0.7	-3.4	-10.5
322.3	399.6	113.6	-68.6	384.5	391.9	-45.8	57.6	524.2	-1.7	-1.2	-7.0	-4.2	-1.3	-3.1	-4.8	-16.4
332.0	406.6	14.0	-57.6	532.5	451.5	-60.2	90.2	356.6	-0.8	-0.2	-6.8	-11.4	-0.9	-1.3	-4.8	-5.9
341.8	466.1	59.4	-15.8	514.6	498.2	-28.1	122.5	368.1	-1.2	-0.9	-9.8	-7.5	-1.2	-1.0	-6.5	-4.9

Table 56: Dynamic Stiffness Real and Imaginary Parts at 13200 rpm and 3134 kPa (MN/m)

f (Hz)	$R(H_{xx})$	$R(H_{xy})$	$R(H_{yx})$	$R(H_{yy})$	$I(H_{xx})$	$I(H_{xy})$	$I(H_{yx})$	$I(H_{yy})$	$\Delta R(H_{xx})$	$\Delta R(H_{xy})$	$\Delta R(H_{yx})$	$\Delta R(H_{yy})$	$\Delta I(H_{xx})$	$\Delta I(H_{xy})$	$\Delta I(H_{yx})$	$\Delta I(H_{yy})$
9.8	342.1	-81.8	-100.4	391.3	9.4	-5.7	-16.7	54.3	-1.8	-5.9	-1.9	-7.8	-2.2	-6.3	-1.8	-4.5
19.5	340.0	-78.7	-99.0	383.0	19.7	-2.1	-17.1	30.9	-1.5	-5.2	-2.6	-6.2	-0.9	-2.7	-2.7	-5.8
29.3	344.6	-78.4	-95.5	392.8	29.8	-12.0	-16.8	32.5	-1.7	-4.5	-1.4	-6.3	-1.0	-2.8	-1.2	-4.6
39.1	347.4	-75.6	-85.3	374.7	36.4	-9.3	-6.6	37.5	-1.3	-1.9	-2.0	-3.9	-1.1	-2.5	-2.0	-2.1
48.8	347.5	-78.1	-83.6	371.2	50.8	-16.5	-1.0	45.9	-0.7	-1.1	-0.9	-3.2	-1.3	-1.7	-0.4	-1.4
58.6	347.7	-76.1	-82.8	382.2	60.1	-17.1	-16.6	52.7	-0.8	-1.6	-0.6	-2.1	-0.4	-1.5	-1.4	-1.8
68.4	349.6	-78.0	-86.8	381.1	67.5	-21.4	-11.8	51.4	-0.5	-0.7	-0.8	-2.4	-1.0	-2.0	-1.3	-1.2
78.1	354.6	-74.4	-84.4	375.0	82.4	-20.7	-6.2	61.7	-0.8	-0.9	-0.8	-1.5	-0.9	-1.0	-1.4	-1.1
87.9	357.4	-79.7	-92.5	394.8	87.0	-28.1	-20.4	87.2	-0.9	-1.4	-0.8	-2.1	-0.6	-1.3	-0.5	-1.2
97.7	360.3	-80.7	-90.7	386.6	93.5	-28.8	-23.4	86.7	-0.6	-1.0	-1.4	-2.7	-0.5	-0.6	-0.3	-1.6
107.4	360.8	-79.9	-89.5	391.1	102.2	-30.5	-21.6	105.1	-0.6	-0.5	-0.6	-1.9	-0.4	-0.6	-0.7	-1.2
117.2	365.7	-80.4	-84.7	394.8	108.7	-31.5	-26.4	108.0	-0.6	-0.7	-0.7	-1.9	-0.4	-1.1	-0.7	-1.5
127.0	367.6	-78.2	-86.9	389.7	116.6	-30.5	-26.4	120.1	-0.8	-0.7	-0.5	-1.4	-0.6	-0.4	-0.4	-1.0
136.7	370.5	-76.8	-83.1	396.7	125.9	-31.0	-35.9	127.4	-0.4	-1.0	-0.8	-1.5	-0.6	-0.9	-1.1	-1.2
146.5	369.7	-72.9	-81.4	401.4	133.3	-34.2	-30.2	132.0	-0.4	-0.7	-1.0	-1.9	-0.7	-0.6	-0.9	-1.9
156.3	369.9	-69.0	-82.4	386.3	141.0	-33.8	-26.2	115.3	-0.3	-0.4	-0.3	-2.0	-0.5	-0.9	-0.5	-1.5
166.0	375.4	-76.6	-82.3	408.6	148.7	-36.4	-31.9	157.8	-0.2	-0.4	-0.6	-1.7	-0.3	-0.6	-0.6	-1.2
175.8	375.2	-72.6	-80.5	411.0	156.2	-38.3	-34.8	161.4	-0.3	-0.4	-0.5	-1.6	-0.5	-0.5	-0.6	-1.5
185.5	376.1	-71.1	-78.1	416.4	170.0	-39.4	-30.7	165.0	-0.8	-0.7	-1.7	-1.8	-0.5	-0.7	-1.6	-1.9
195.3	379.8	-66.8	-73.7	411.0	175.1	-36.2	-27.9	169.3	-0.3	-0.3	-1.2	-2.1	-0.3	-0.7	-0.5	-1.6
205.1	375.8	-62.5	-78.7	417.3	181.0	-36.3	-27.6	184.2	-0.4	-0.5	-0.8	-2.2	-0.4	-0.7	-0.3	-1.5
214.8	385.2	-59.1	-75.0	428.8	194.7	-37.9	-35.3	182.7	-1.0	-0.8	-1.0	-2.4	-0.8	-1.0	-1.2	-1.9
224.6	381.7	-48.2	-69.9	376.8	199.5	-39.3	-36.7	198.3	-2.0	-1.7	-1.7	-3.1	-1.7	-1.5	-2.2	-2.1
234.4	388.5	-59.5	-71.9	437.7	211.1	-43.5	-39.7	212.3	-0.8	-0.8	-1.1	-1.8	-0.8	-0.5	-2.0	-2.0
244.1	388.1	-52.4	-64.2	430.7	223.7	-41.7	-36.5	219.2	-0.6	-0.4	-1.3	-1.7	-0.6	-0.3	-0.7	-1.2
253.9	387.2	-45.2	-65.7	438.8	233.5	-37.3	-38.5	228.0	-0.3	-0.7	-1.0	-2.1	-0.5	-0.7	-0.5	-1.1
263.7	390.0	-38.0	-58.5	433.4	248.1	-37.6	-33.5	227.8	-0.2	-0.4	-0.9	-1.6	-0.3	-0.4	-0.3	-1.3
273.4	393.3	-28.0	-53.6	383.5	261.1	-33.4	-30.0	216.6	-0.5	-0.3	-0.9	-1.6	-0.5	-0.5	-0.8	-1.4
283.2	399.4	-39.6	-57.3	451.3	278.4	-47.0	-35.0	250.9	-0.7	-0.6	-0.9	-2.1	-0.7	-0.4	-0.7	-1.4
293.0	404.0	-18.9	-46.8	411.9	288.6	-30.2	-27.1	267.6	-0.5	-0.7	-1.5	-1.5	-0.3	-0.4	-1.4	-1.6
302.7	399.3	4.1	-44.1	379.9	309.2	-17.8	-18.0	289.5	-0.4	-0.2	-1.2	-1.9	-0.6	-0.4	-1.5	-2.7
312.5	407.0	-20.1	-48.1	530.2	330.1	-59.6	-20.2	293.2	-0.5	-0.6	-1.3	-3.1	-0.6	-0.5	-1.2	-2.7
322.3	412.0	37.1	-35.1	373.9	346.9	-5.3	-2.5	328.6	-0.7	-0.5	-1.6	-3.0	-0.7	-0.7	-1.8	-1.6
332.0	416.1	-12.0	-18.4	589.1	383.5	-104.9	17.7	351.5	-0.4	-0.8	-1.1	-2.7	-0.3	-0.7	-1.9	-1.8
341.8	453.4	22.3	9.5	551.7	419.3	-54.6	38.1	335.1	-0.7	-0.6	-1.6	-1.9	-0.7	-0.7	-2.0	-2.8